CARBON NANOPARTICLES AS INDUCERS OF PULMONARY FIBROSIS- STUDY ON CELL-MATERIAL INTERACTIONS

AMALU NAVAS

Ph.D. THESIS

2023

SREE CHITRA TIRUNAL INSTITUTE FOR MEDICAL SCIENCES AND TECHNOLOGY, TRIVANDRUM

An Institution of National Importance established by an Act of the Indian Parliament
(Act No.52 of 1980)

Dept. of Science and Technology, Govt. of India
www.sctimst.ac.in

CARBON NANOPARTICLES AS INDUCERS OF PULMONARY FIBROSIS- STUDY ON CELL-MATERIAL INTERACTIONS

A THESIS SUBMITTED BY

AMALU NAVAS

TO

SREE CHITRA TIRUNAL INSTITUTE FOR MEDICAL SCIENCES AND TECHNOLOGY, TRIVANDRUM.

IN PARTIAL FULFILMENT OF THE REQUIREMENTS

FOR THE AWARD OF

DOCTOR OF PHILOSOPHY

2023

DECLARATION BY THE STUDENT

CERTIFICATE

I, **Amalu Navas**, hereby certify that I had personally carried out the work depicted in the thesis titled, "**Carbon Nanoparticles as Inducers of Pulmonary Fibrosis- Study on Cell-Material Interactions**." No part of this thesis has been submitted for the award of any other degree or diploma prior to this date.

Amalu Navas

Date: 05-10-23

CERTIFICATE OF THE GUIDE

Dr. A. Maya Nandkumar

Division of Microbial Technology

Sree Chitra Tirunal Institute for Medical Sciences and Technology

This is to certify that **Ms. Amalu Navas, in the Division of Microbial Technology,** BMT wing of this institute has fulfilled the requirements prescribed for the Ph.D. degree of the Sree Chitra Tirunal Institute for Medical Sciences and Technology, Trivandrum. The thesis entitled: **"Carbon Nanoparticles as Inducers of Pulmonary Fibrosis-A Study on Cell-Material Interactions"** was carried out under my direct supervision. No part of the thesis was submitted for the award of any degree or diploma prior to this date.

10/11/2022

Dr. A. Maya Nandkumar
Research supervisor
Scientist 'G' and Head
Division of Microbial Technology
SCTIMST, TVM

Date 11th Nov. 2022

APPROVAL OF THE THESIS

The thesis entitled

CARBON NANOPARTICLES AS INDUCERS OF PULMONARY FIBROSIS- STUDY ON CELL-MATERIAL INTERACTIONS

Submitted by

AMALU NAVAS

for the degree of

Doctor of Philosophy

of

SREE CHITRA TIRUNAL INSTITUTE FOR MEDICAL SCIENCES AND TECHNOLOGY, TRIVANDRUM

is evaluated and approved by

Dr. A. Maya Nandkumar

(Name & Signature of the Guide)

Prof. Kavita Shah

(Name & Signature of thesis examiner)

ACKNOWLEDGEMENT

I consider myself privileged to have had the opportunity to carry out my doctoral studies in the Division of Microbial Technology, Sree Chitra Tirunal Institute for Medical Sciences and Technology, Trivandrum, India. I take this opportunity to express my heartfelt gratitude to all those who made this possible.

I am deeply indebted to my esteemed mentor Dr. A. Maya Nandkumar, for her continuous support through all these years and valuable guidance, encouragement, suggestions, and motivation, which have helped me greatly in the successful completion of my studies. I am truly thankful for her dedication and critical thinking which have contributed to my academic development. I am thankful to her for all her efforts to nurture me as a person and as a researcher.

I would like to thank all my Doctoral advisory committee members- Dr. R.S. Jayasree (Division of Biophotonics and Imaging, SCTIMST), Dr. Anil Kumar P.R (Division of Tissue Culture, SCTIMST), and Dr. Anugya Bhatt (Division of Thrombosis Research, SCTIMST) for their support and critical reviews.

I am grateful to the Director, SCTIMST, and Head BMT wing for their support and the excellent facilities at the Institute. I express my gratitude to the Registrar, Deputy Registrar, and all the staff of the academic division for their support during the period.

I acknowledge SAIF-CUSAT for the HRTEM analysis of samples. I extend my gratitude to Dr Ramesh. P, Scientist G, Division of Polymeric Medical Devices, SCTIMST for providing the Carbon black nanoparticle used in the study. I also thank Dr. Rekha M. R (Division of Bio Surface Technology-SCTIMST) for the DLS analysis.

I would like to thank my beloved Senior Dr. Keerthi S. for all the support and time spent together on discussions and interpretations of the data. I appreciate the goodwill extended to me by my junior Ms. Moon Moon Baglari. I thank my lab members Mr.

Pradeep Kumar S.S., Ms. Sreeja, Ms. Ashtami, Ms. Anjali Krishna, and Ms. Sugalya B for their support and friendship.

I would like to thank the Department of Science and Technology for the DST-INSPIRE fellowship and DBT (BT/PR11281/MED/32/82/2008) for the financial assistance.

I owe a lot to my Parents, husband, and kids for their love, support, and encouragement. I am very much indebted to my brother, and my in-laws who supported me in every possible way with the completion of this work. This would not have happened without your sacrifices. Above all, I owe it to the Lord Almighty for enabling me to achieve this goal

Amalu Navas

CONTENTS

LIST OF FIGURES

LIST OF TABLES

ABBREVIATIONS

2D	Two-dimension
3D	Three-dimension
ALI	Air-liquid interface
ANOVA	Analysis of variance
AO	Acridine orange
ATCC	American-type culture collection
ATRA	All trans-retinoic acid
CBNP	Carbon black nanoparticle
cDNA	Complementary Deoxyribonucleic Acid
COPD	Chronic obstructive pulmonary disease
COX	Cyclooxygenase
CV	Crystal Violet
DCFDA	Dichloro-fluorescein diacetate
DEP	Diesel exhaust particle
DMSO	Dimethyl sulfoxide
ECIS	Electric cell-substrate impedance sensing
EDTA	Ethylene diamine-tetra acetate
ELISA	Enzyme-linked immune sorbent assay
EMT	Epithelial-Mesenchymal Transition
FBS	Fetal bovine serum
FITC	Fluorescein isothiocyanate
HRTEM	High-resolution transmission electron microscopy

IFN	Interferon
IL	Interleukin
LDH	Lactate dehydrogenase
MCP	Monocyte chemoattractant protein
MMP	Matrix metalloproteases
MOI	Multiplicity of infection
MTT	3-(4,5-Dimethylthiazol-2-Yl)-2,5-Diphenyltetrazolium Bromide
OD	Optical density
PBS	Phosphate buffered saline.
PCR	Polymerase chain reaction
PFA	Paraformaldehyde
ROS	Reactive oxygen species
RT-PCR	Real time-Polymerase chain reaction
RNA	Ribonucleic acid
TEM	Transmission electron microscopy
TGFβ	Transforming growth factor
TIMP	Tissue inhibitors of metalloproteases
TNF	Tumor necrosis factor
WHO	World health organization
µg	Microgram
µL	Microlitre
pg	Picogram
Hz	Hertz

Ω	Ohm
M	molar

SYNOPSIS

Air pollution leads to over 6.5 million deaths each year globally. Industrialization, uncontrolled urbanization, population growth, and fossil fuel combustion contribute to air pollution. In 2019 alone, nearly 17.8% of all deaths in India were due to air pollution, which is the most significant number of air pollution deaths in any country (The Lancet Plenary health-2019). Carbon Black nanoparticle (CBNP) is one of the top 50 most produced chemicals worldwide. Applications include electronics, plastics, coatings, ink, and green technology. The development of nanotechnology and the comprehensive chemical, electronic and medical applications of nanoparticles have raised concerns about the inhalation risk of these particles. These pollutants, which are fine and ultrafine particulate matter, are major risk factors. When the concentration of these particles increases in the atmosphere, the general population is increasingly exposed to these particles, and there is increased inhalation and concentration of CBNP in the different regions of the respiratory system. They deposit in various regions of the lower respiratory tract based on their size. Particles of nano-size (less than 100nm in one dimension) can reach as far as the gas exchange regions of our respiratory system and elicit unpredictable responses.

We hypothesize that sustained exposure and the inability to clear nanoparticles from the lungs via muco-ciliary clearance or phagocytosis may drive an exaggerated inflammatory response that leads to irregular tissue remodelling and fibrosis. The interaction of these particles with various cellular components of the lung, the alveolar macrophages, epithelial cells, and interstitial fibroblasts would elicit several responses

that could be inflammatory and could lead to cellular remodelling. Against this backdrop, this study sought to understand the interactions of CBNP with major cell populations in the alveolar region- the alveolar epithelial cells, the fibroblasts, and the monocytes and their impact on respiratory infections. Our findings indicate that short-term exposure to high concentrations of CBNP nanoparticles induced inflammatory responses. On the other hand, prolonged exposure to low concentrations of CBNP induced pro-fibrotic responses in all the cell types studied through mechanisms like activation of TGF-dependent -smad3-Wnt signalling, PI3k signalling, and M2 polarization. In addition, the anti-fibrotic potential of All trans-retinoic acid (ATRA), the active metabolite of vitamin A was assessed as a possible therapeutic molecule. All assessments were done using suitable *in vitro* systems. Importantly, our work provides laboratory evidence for the first time that carbon black nanoparticle exposure predisposes humans to bacterial infections and a greater risk of fibrosis development.

The objectives of the study were:

- Understand the responses of alveolar cells to CBNP exposure.
- Study the effect of All-Trans Retinoic Acid (ATRA) as an anti-fibrotic molecule
- Understand the effect of CBNP on bacterial pathogenesis.
- Establishment of an *in vitro* cellular system suitable to study fibrosis.

Methodology

High-resolution transmission electron microscopy and Dynamic light scattering were used to characterize the nanoparticle CBNP.

Representatives of cell types in the alveolar region used in our study are as follows:

- A549 cells - alveolar epithelial cells as they form an innate functional barrier - epithelial responses.
- WI38- Lung fibroblast cells responsible for repair - effectors of fibrosis
- THP1- monocytes - immune cells - effector for phagocytosis.

A549 and WI38 cells were cultured in F12K: DMEM and THP1 cells in RPMI 1640 supplemented with 10% fetal bovine serum.

Biochemical, morphological, and molecular changes in these cells were analyzed on exposure to CBNP at varying concentrations. MTT {3-(4,5-dimethylthiazol-2-yl)-2,5-diphenyl tetrazolium bromide}, LDH (Lactate Dehydrogenase), and NRU (Neutral Red Uptake) assays were done. Reactive oxygen species (ROS) were assessed by the Dichloro-dihydro-fluorescein diacetate (H2DCFDA) method. Sybr green quantitative real-time PCR analysis for assessing gene expression (IL-6, IL-8, TNFα, MCP, TGFβ1, PGE2, iNOS, E-cadherin, Collagen 1, αSMA, SP-C, Caspase-3, TIMP). Immunocytochemistry for the detection and visualization of specific proteins (SP-C, psmad3, αSMA, β-catenin) and enzyme-linked immunosorbent assay (ELISA) for quantification of expressed protein of interest (IL-6, IL-8, TNF-α, TGFβ1, prostaglandin E2, IL-10) were performed following standard protocols.

Electric cell-substrate impedance sensing (ECIS) was used to assess alveolar epithelial cell behaviour to carbon black nanoparticles and assess infection dynamics on a challenge with a known respiratory pathogen – *Pseudomonas.*

Different models were tried and an *invitro* system – the ALI (Air liquid interface)-trans well - heterocellular co-culture system was developed as a suitable model system to study fibrosis. TEER (Trans epithelial electrical resistance) and permeability assays in the system along with actin staining by rhodamine-phalloidin for cytoskeletal intactness were done for evaluating the suitability of the system.

Canonical TGFβ signalling pathways were assessed in alveolar epithelial cells through pSmad3, βcatenin immunostaining, and Epithelial-mesenchymal transition was assessed by αSmooth muscle actin (α SMA) immunostaining**.**

The effect of CBNP on bacterial pathogenesis was assessed at different levels. First, the Direct effect of particles on *Pseudomonas* virulence was analyzed by Biofilm formation (Crystal violet assay), virulence factors – Rhamnolipid, Pyocyanin, and Protease estimation assays by following standard protocols like Quantification by methylene blue, Chloroform-HCl and Skim-milk assay respectively

Then the effect of the CBNP on susceptibility to *Pseudomonas* infection of A549 was assessed by ECIS. Finally, the effect of infection on CBNP pre-exposed epithelial cells was also studied.

Statistical significance was assessed using ANOVA, and student's t-test, and $p \leq 0.05$ was considered significant.

Results

Prolonged exposure to low doses of CBNP induced pro-fibrotic responses in alveolar cells.

We analyzed the short-term (24, 48 h) and prolonged exposure (120 h) effects of various concentrations of carbon black nanoparticle (1-160 µg/mL) on alveolar epithelial cells (A549), fibroblast cells (WI38) and monocytes (THP1). High doses of CBNP on short-term exposure caused cytotoxicity as well as genotoxicity (dose >80 µg/mL), whereas low doses(1-20 µg/mL) induced pro-inflammatory responses. High-dose treatments induced cytotoxicity by enhanced reactive oxygen species generation, loss of lysosomal membrane integrity, and mitochondrial depolarisation in alveolar epithelial cells (A549). There was upregulation of caspase 3 gene expression. High doses of CBNP induced apoptotic cell death in alveolar epithelial and fibroblast cells. But in the case of monocytes pyroptotic cell death was observed on exposure to CBNP evidenced by upregulation in inflammasome markers (Caspase1, IL-1β) both at the level of gene and protein expression (Caspase 1- Glo assay kit).

Prolonged and repeated exposure (up to 120 h) of low doses of CBNP, induced mesenchymal transition in alveolar epithelial cells evidenced by morphological changes from cuboidal epithelial to spindle-shaped fibroblast cells. Upregulation of EMT (epithelial to mesenchymal) marker genes (TGFβ, αSMA, Collagen1, MMP) and downregulation of epithelial markers (E-cadherin, Tissue inhibitors of metalloproteinases, and prostaglandin E2) also pointed towards EMT transition. Collagen synthesis and increased contractility, both characteristic features of fibroblast cells, were also observed in prolonged CBNP-exposed epithelial cells.

The mechanism of EMT on CBNP exposure was delineated. The hypothesis here was the activation of TGF β –Smad3-Wnt signalling by repeated and prolonged exposure to low doses of CBNP. Phosphorylation of Smad3 and nuclear translocation of β-catenin are required for the transcription of EMT-related genes. The presence of *psmad3* on CBNP-exposed epithelial cells pointed towards CBNP-induced EMT through smad3 dependent pathway. Nuclear translocation of β-catenin was evident in CBNP-exposed cells from immunocytochemistry. Sustained nuclear accumulation of β-catenin and exogenous overexpression of WNT ligands suggest that canonical smad-WNT signalling systems were activated and triggered the fibrogenic conversion. In conclusion, TGF-β, smad3, and WNT signals converge and modulate the nuclear accumulation of β-catenin, and transcription of downstream effectors was activated.

Activation of fibroblasts to myofibroblasts is also a hallmark of fibrosis. Prolonged exposure of CBNP in WI38, induced proliferation and activation of fibroblasts. Alpha smooth muscle actin and collagen 1, markers of myofibroblast phenotype were upregulated pointing towards myofibroblast conversion. The phosphoinositide 3-kinase (PI3K) pathway involved in cell proliferation and survival was upregulated in WI38 on exposure to low doses of CBNP.

Another interesting observation was the polarisation of monocytes to M2 phenotype on prolonged exposure. Monocytes can be differentiated and polarised into M1 and M2 phenotypes. M1 is involved in inflammatory responses, whereas M2 is involved in wound healing responses and fibrosis. Prolonged exposure of CBNP-induced polarisation to the M2 phenotype characterized by downregulation of pro-inflammatory cytokines.

All trans-retinoic acid has anti-fibrotic potential

(ATRA)-an active metabolite of vitamin A, can regulate the proliferation and differentiation of various cell types. Initially, we assessed the cytotoxic activity of ATRA in all the cell types used in this study. We observed that pre-treatment of 1µM ATRA was optimal and non-cytotoxic. Retinoic acid (RA) regulates normal lung development, maturation, homeostasis, and repair. The effect of ATRA 1 µm (derivative of Vitamin A) on ROS and surfactant protein C(SPC) expression, for functional integrity upon CBNP exposure, was analyzed. CBNP induced a marked reduction in ROS production. Upregulation of SPC expression indicated protection and upregulation of epithelial function on treatment with ATRA. Pre-treatment of ATRA also has down-regulated the EMT marker gene expression in alveolar epithelial cells and fibroblasts. Fibroblast proliferation, activation, and migration were also effectively controlled by ATRA pre-treatment. These observations lead to the conclusion that ATRA could be an effective anti-fibrotic therapeutic molecule.

Direct exposure to CBNP can induce biofilm production in Pseudomonas aeruginosa- a known respiratory pathogen.

We evaluated the effect of CBNP on *Pseudomonas aeruginosa*- the ubiquitously distributed opportunistic pathogen. Due to a range of mechanisms for adaptation, survival, and resistance to multiple classes of antibiotics, infections by the gram-negative *P. aeruginosa* strains can be life-threatening, and it is emerging as a global public health threat. First, we assessed the direct effect of CBNP on *P. aeruginosa* virulence factors at various time points. It was observed that direct exposure to low concentrations **(1-20 µg/mL)** of CBNP induced increased biofilm

production in *Pseudomonas* ATCC 27853 by 48 h, whereas higher concentrations (40-160 µg/mL) did not. We observed an increase in biofilm components in the presence of low doses of CBNP. Increased expression of the virulence factors like rhamnolipids, pyocyanin, and protease in *Pseudomonas* after low-dose CBNP exposure was observed. These virulence factors play a vital role in the biofilm formation and pathogenesis of Pseudomonas. Bacteria can switch from their motile nature to sessile forms in a biofilm. The induction of stress responses usually results in the transition from single cells to biofilm and the loss of flagellar motility. Here we observed a reduction in the motility of *Pseudomonas* on CBNP exposure which correlates with our earlier observation of increased biofilm formation under the influence of low doses of CBNP.

CBNP exposure enhances bacterial infection susceptibility to respiratory pathogen and also accentuates EMT

Bacterial pathogens breach the epithelial lining to gain access to a wide range of nutrients and escape immune mechanisms like phagocytosis, complement fixation, etc. and disseminate deeper into tissues. In defense against these pathogens, the epithelium has multiple layers of microbial sensing and intrinsic defense systems built in that act as countermeasures against microbial intruders. The epithelial barrier integrity was significantly compromised with CBNP exposure. The ECIS data showed that the impedance of CBNP-treated A549 (type 11 pneumocytes) was lowered. The impedance was further lowered and was equivalent to cell-free impedance when infected with *Pseudomonas* (ATCC 27853). Our result suggests that CBNP exposures

lead to dysfunction of the epithelial junction, resulting in loss of epithelial barrier integrity and increased susceptibility to bacterial infections.

On **direct bacterial lysate** treatment, we observed an upregulation of pro-inflammatory cytokine expression in epithelial cells whereas on the treatment of *P. **aeruginosa*** **lysate-treated monocyte conditioned media** on CBNP pre-exposed epithelial cells we observed a further upregulation of EMT markers which implies that bacterial lysate challenged monocyte conditioned medium accentuated EMT induced by CBNP. The bacterial lysate-challenged monocyte-conditioned medium is a reservoir of cytokines and stimulates the *in vivo* innate immune response to a bacterial infection. Exposure of A549 monolayers to this conditioned medium significantly upregulated EMT markers, pointing to the significance and complexity of cell-cell interactions.

Air liquid interface (ALI) co-cultures of epithelial-fibroblast cells improves barrier integrity, making it a suitable in-vitro culture system for prolonged particle exposure studies.

Studies on understanding the various aspects of cell-material-microbial interactions led to the development of *in vitro* co-culture system which could better represent *in vivo* conditions and were suitable for endpoint analyses. The *in vitro* system detailed here is superior to submerged cell culture systems which are technologically simple and non-physiologic. Here type 2 epithelial lung cells (represented by A549 cells) were seeded on the apical (air) side of a porous/perforated membrane in a transwell insert and fibroblast cells (represented by WI38 cells) were seeded on the basolateral side of the membrane. For evaluation, the transepithelial electrical resistance (TEER) of

epithelial cells in air-liquid interface(ALI) co-cultures for 15 days was analyzed. Higher TEER values were obtained for the co-culture system vis~a~vis the submerged co-culture as well as air-liquid interface systems of single cell type. The highest TEER value reported till now was obtained in the A549-WI38 ALI co-culture system. The increased TEER values were maintained for 11 days followed by a slight reduction in TEER values. The structural and functional integrity of the co-culture system was also assessed. Time course permeability measurement experiments showed that the permeability of sodium fluorescein across the ALI Coculture system was lower compared to the A549 monolayer system in the apical-to-basolateral direction. From these observations, it can be inferred that ALI co-culture forms a tighter and less permeable epithelial layer than the submerged monoculture system.

ECIS (**Electric cell-substrate impedance sensing)** is an *in vitro* model of adherent monolayers for multiparametric analysis of cell attachment, morphology, and behavior on a challenge with various stimuli, including nanoparticles, pathogens, and drugs in real-time. The system was evaluated to understand the effect of diesel exhaust nanoparticles on A549 monolayers. The study analyzed whether fluctuations in the electrical properties of cell-covered microelectrodes reflected dynamic changes in cell morphology on exposure to diesel exhaust particles- another type of particulate carbon nanoparticle which forms a significant component of vehicular pollution. Our findings indicate that ECIS provides many benefits as an alternative method to quantify, automate, and measure the effect of pollutants or particles in real-time when compared to traditional endpoint methods MTT, LDH, and NRU assays.

Significance of the study

Investigations on the impact of nanoparticles on human health are important for safety from unintentional health hazards. Since the respiratory system connects directly the external environment to the blood in the human body through the alveolar gas exchange surfaces, the effect elicited by these particles on the respiratory system is of prime importance. The study provides evidence for the first time that repeated exposure to low doses of carbon black nanoparticles can induce fibrotic responses and predispose a person to respiratory diseases. Delineating the molecular mechanisms of these interactions and their consequences is the highlight of the work. Our work is also the first to study the triagonal interactions between the cell-the nanomaterial and the microbe. The study expands our understanding of the implications of dose and time of exposure of nanoparticles in respiratory pathobiology. In addition, it provides a new paradigm for understanding the pathogenesis of respiratory diseases in association with nanoparticle exposure.

1. INTRODUCTION

Nanoscience and nanotechnology is the fastest-growing area of material science that has reached the public pushing all the boundaries of research. The impact of the development of nanotechnology can be seen in the products of daily usage extending from computer chips to beauty products. The improved or renewed properties of nanoparticles are attributed not only to their composition but also to physicochemical characteristics like size which differ from the bulk material (Porto et al., 2019). Among the nanomaterials, Carbon nanomaterials gain the most attention owing to their versatility. Carbon nanomaterials which are composed of pure carbon have improved chemical, electrical, thermal, and mechanical characteristics. Since the discovery of new carbon nanoparticles like fullerenes (in 1985), carbon nanotubes (1991), and graphene (2004) in addition to diamond and graphite, industrial applications and thereby production of carbon nanoparticles have increased worldwide. The discovery of fullerenes and graphene isolation gained Nobel prizes in chemistry (1996-Harold Kroto, Robert Curl, Richard Smalley) and Physics (2010- Andre Geim, Konstantin Novoselov) respectively. Carbon nanoparticles exhibit high stability, and good conductivity and were considered to be environmentally friendly. Carbon nanoparticles are often termed "wonder materials "in scientific publications (Zaytseva and Neumann, 2016)). The applications are not restricted to commercial products but also they are used in biomedical fields for imaging and therapy. Researchers are trying to develop carbon nanoparticles that could be used in gene therapies or tracing genes for an improved understanding of diseases.

Carbon black is a type of carbon-based material. Carbon black (CB; CAS No. 1333-86-4) is a type of elemental carbon produced by incomplete combustion or thermal

decomposition of heavy petroleum raw materials like ethylene cracking tar, and coal tar under controlled conditions. The global carbon black market was valued at approximately 12.61 billion US dollars (USD) which are predicted to reach 18.09 billion by 2029. Asia Pacific dominates the global market. Carbon black is mainly used as a filler (in automotive, electronics construction, etc), as a reinforcing agent, as a colouring agent, and as an ultraviolet absorber. Carbon black is a preferred choice in the rubber industry. Based on the process of synthesizing different grades of Carbon black are available in the market.

Among the engineered carbon nanoparticles, Carbon black ranks as one of the top fifty industrial chemicals produced around the world. The increasing production and demand lead to the release of these nanoparticles into the atmosphere. Despite the economic and industrial importance, CB raises concern as an ultrafine particle (UFP) of the particulate matter (PM) by the interactions of released nanomaterials with living organisms. As a component of PM, carbon nanoparticles can be readily inhaled. Hence, the Respiratory system serves as the prime target of carbon black exposure. In general, PM induces systemic inflammation, but ultra-fine particles like CB can escape the innate immune defenses and reach as far as the gas-exchange regions of the lung - the alveoli and can even enter the circulatory system.

Several reports(Nikota et al., 2017)) suggested that multi-walled carbon nanotubes (MWCNTs) a form of carbon nanoparticles can act as inducers of lung fibrosis in mice. It is noteworthy that despite sharing the same chemical composition CB was used as a negative control in toxicological studies (Martinon et al.,2006). Zhang et al., reported that nanoCB exposure positively relates to the secretion of pro-inflammatory cytokines

and might contribute to reducing lung function(Zhang et al., 2014). CB was identified as a trigger for systemic inflammation in chronic obstructive pulmonary disease (COPD) patients (Garshick et al.,2018).

Diesel exhaust emission from road traffic also releases fine particles of diameter less than 100nm. Diesel engine emissions are one of the largest sources of nanoparticles in urban areas. Diesel exhaust particles (DEP) are a product of incomplete combustion of diesel fuel composed of a central elemental carbon core and adsorbed compounds like poly aromatic hydrocarbons (PAH), nitro-PAHs, trace amounts of sulphates, nitrates, and other trace elements (Wichmann, 2007). The effect of DEP on the lower respiratory tract also needs to be understood.

Environmental, occupational, and medication-related exposures often lead to exaggerated inflammation and interstitial lung diseases (ILD). Idiopathic Pulmonary fibrosis is considered the most common and important type of ILD because of its unknown aetiology, poor prognosis, and modest response to therapeutic interventions (Raghu et al., 2015). To date, medicines have only been developed to ease the symptoms of the disease. The lack of a suitable system to study fibrosis is also a major impediment to a clear understanding of the disease Persistent inflammation is considered an important initiator of progressive Lung fibrosis. The pathological hallmarks of pulmonary fibrosis include the increased proliferation of fibroblasts, deposition of extracellular matrix leading to irreversible destruction of lung architecture, and loss of organ function. The lung is a complex organ containing resident as well as recruited immune cells and stromal cells. Previous reports suggest that lung epithelium stimulated by injury or insult resulting in abnormal epithelium

expresses numerous mediators that can lead to the activation of mesenchymal cells and lung remodelling initiating the fibrotic cascade (Rc and Pf, 2015), (Sakai and Tager, 2013). The key molecular events involved in this include activation of transforming growth factor β (TGF-β), expression of ECM molecules, epithelial-mesenchymal transition (EMT), and activating pro-fibrotic cascade (Willis and Borok, 2007). To date, rarely have studies been conducted focussing on the fibrotic effect of nanoparticles in lungs however those results were inconsistent (Dong and Ma, 2016). The economically and industrially important nanoparticle Carbon black should be assessed for its respiratory toxicity in particular its fibrotic potential.

The epithelium is the first line of defence in the respiratory tract extending from the proximal to the distal region of the lungs. Epithelial injury is triggered not only by environmental exposures. Microbial infections can contribute to epithelial injury and also to repeated innate immune system activation. Borthwick et al.,2010 (Rajak and Chattopadhyay, 2020) reported that a pro-inflammatory microenvironment may play a role in airway remodelling. However, the role of activated immune cells in a pre-activated fibrotic cascade is not understood to date despite the fact that fibrosis is an end result of multicellular interactions.

Scientific studies reveal a significant correlation between ambient air pollution and respiratory illnesses and mortality (Rajak & Chattopadhyay, 2020). The current Coronavirus disease (COVID-19) could be taken as a prominent example. Most polluted and populated cities were hit worse by COVID-19. Major cities in India -like Delhi, Mumbai, and Bengaluru experiencing poor air quality (IQAir, 2020) reported higher case numbers and mortality rates. Similar observations were made in different

countries (Khadka et al., 2020). Manoj et al.,2020 reported that particulate matter and aerosol can support a platform of virus transmission. The trend is often followed in bacterial infections. Despite ambient air pollution being a leading cause of morbidity and increasing susceptibility to an infectious agent, very few studies investigated the association of particulate matter with specific bacterial pathogens.

Aerosol can act as the carrier of microbes where they will interact with the fine particulate matter. The changes in the microbiome caused by these interactions are also the least studied. Physico-chemical changes in the atmosphere, the presence of new aerosol materials (by vehicular and industrial emissions), etc, can significantly affect the environmental microbiome (Archer and Pointing 2020: For example, the presence of high concentrations of carbon can lead to specific selection in a heterotrophic organism like *Pseudomonas* (Vaïtilingom et al., 2010) as they represent a source of nutrition for the microbe. This warrants further investigation of the effect of these aerosol components like nanoparticles on prevalent environmental pathogens.

We hypothesize that sustained exposure to carbon nanoparticles may lead to tissue remodelling and fibrosis. The interaction of these particles with the alveolar cells can lead to cellular remodelling. Further, these interactions can pre-dispose the alveolar epithelium to infection susceptibility as well as accentuate fibrotic response. We also hypothesized that microbial-particle interaction may bring about changes in the virulence factors of the pathogen.

The current study aimed to understand the cell-material and the triagonal cell-material-microbial interactions and delineate the molecular mechanisms underlying these interactions. The lack of *in-vitro* systems to study cellular and multicellular responses

in fibrosis also hamper the research on understanding the molecular mechanisms which are also addressed in the study. All-trans retinoic acid (ATRA), the vitamin A metabolite is assessed for its therapeutic possibility in fibrosis treatment. Briefly. the current study aimed at understanding cell-material as well as cell-material microbial interactions that drive the nanoparticle-induced fibrotic responses in alveolar cells (Fig 1.1).

To address the hypothesis following objectives were formulated

- Establishment of an *in vitro* cellular system to study fibrosis
- Understand the responses of alveolar cells on CBNP exposure.
- Study the effect of All-Trans Retinoic Acid (ATRA) as a therapeutic, antifibrotic molecule
- Understand the effect of CBNP on bacterial pathogenesis

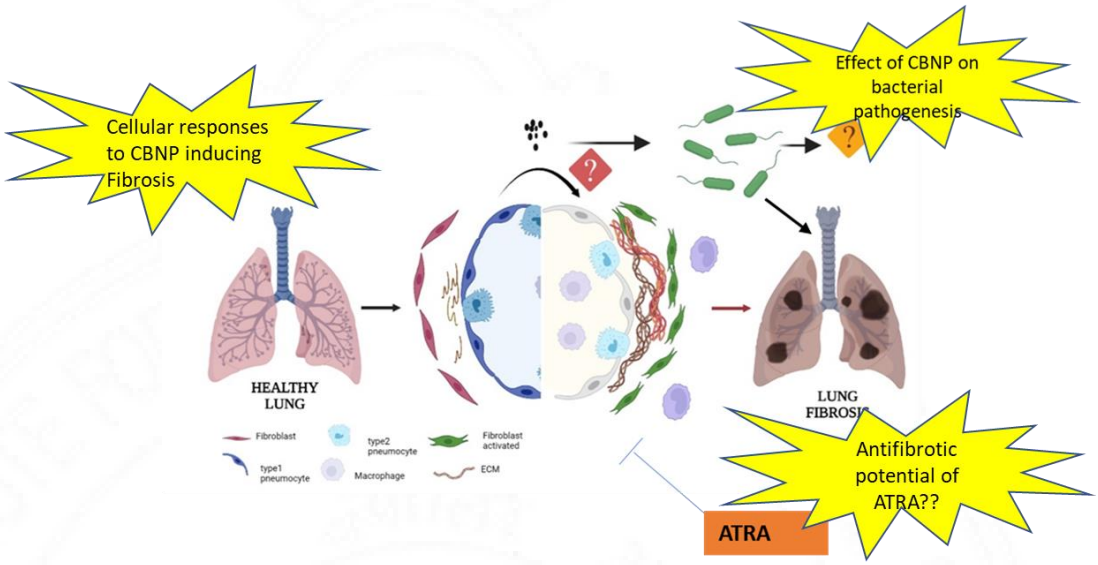

Fig 1.1 Pictorial representation of questions asked in the mechanism of CBNP-induced fibrosis. The study focuses on the mechanisms of cellular responses that drift the normal healing response to aberrant fibrosis on nanoparticle exposure which results in loss of organ function and also on the triagonal interaction of cell-material and microbe to understand the preponderance of a challenged alveolar epithelium to microbial infection. The current study also assesses ATRA (All-trans retinoic acid) as a suitable antifibrotic therapeutic molecule.

2. REVIEW OF LITERATURE

2.1. Carbon Nanoparticles

Carbon is the second most abundant element in the human body being the main component of sugars, fats, proteins, DNA, and so on. Carbon with six electrons composed of 4 external shell electron orbitals can hybridize into sp^1, sp^2, and sp^3, and these configurations present carbon as the most fascinating element in the universe. Carbon can exist in different molecular forms possessing different properties due to different structural arrangements of the same type of atoms. Diamond and graphite are the known natural allotropes of this kind. New allotropic carbons have been discovered recently including carbon nanomaterials. Based on structural organization carbon-based nanostructures can be spherical, horn-shaped, tube-shaped, etc. The family of carbon nanomaterials is growing with the addition of new materials which include carbon black nanoparticles, fullerenes, fibers, and carbon nanotubes . The fascinating properties of these nanomaterials make them suitable candidates for various applications ranging from drug delivery to electronics (Hirsch A, 2010)

Carbon black nanoparticles are nanosized traditional carbonaceous materials with a morphology of aciniform or grape-like aggregates composed of diffused spherical particles. It is a form of pure elemental carbon (Long et al.,2013). C-fullerenes (C60) are closed cage-like symmetrical structures composed of 60 carbon atoms. Carbon nanotubes are fibrous needle-like structures and can exist as single-walled (SWCNT)and multi-walled CNTs (MWCNT). Nano graphite is also a form of carbon nanoparticle which is one atom thick (Yuan et al., 2019).

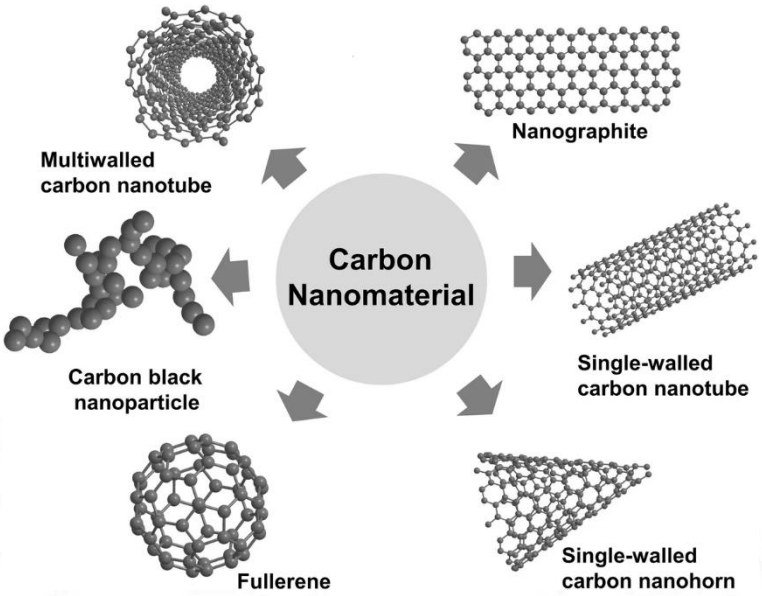

Fig 2.1 Various Carbon-based nanomaterials. Fullerene is a polygonal allotrope of carbon composed of 60-C atoms, Carbon nanotubes (CNT) composed of single graphene sheets (Single-walled CNT) or multiple sheets (Multi-walled CNT). Carbon black nanoparticles are 3-dimensional traditional carbon-based nanoparticles. Nano graphite or graphite nanoplatelets are a one-atom-thick 2-D sheet of carbon atoms. Nanohorns (Single-walled) are horn-shaped single-walled tubules with cone angles of ~ 20^0. (Source – Yuan et al., 2019)

In addition to engineered carbon nanoparticles naturally occurring carbonaceous particulates of size 1-100nm. These materials are released into the atmosphere during combustion, such as methane or propane burning. Fig2. 1 depicts the different types of Carbon nanomaterials (Yuan et al.,2019)

2.1.1. Carbon black Nanoparticles

Carbon black -CB (Chemical Abstracts Service Registry No. 1333-86-4) consisting of pure elemental carbon is the most produced engineered nanoparticle globally (Association ICB 2016, WHO guidelines-2017). CB is one of the top 50 most produced chemicals around the world. They are mainly used in the automotive industry and are also used extensively in rubber products, ink, plastics, paper, dyes, electronics, etc. Carbon black is a product of the thermal decomposition of heavy petroleum raw materials. The global market value of carbon nanoparticles is predicted to rise from 13

billion USD in 2022 to 18 billion USD by 2029. Asia-Pacific dominates the global market of CB. China is the largest producer and consumer. India also tops the list of countries of CB production and consumption (Source-https://www.fortunebusinessinsights.com/industry-reports/carbon-black-market-101718).

Advancements in the application led to the continued rise of carbon black emissions into the atmosphere and estimates of emissions in India and China have already reached 2-3 times higher than predicted (Saputra et al.,2014). Earlier reports imply that the small size of particles in their natural, as well as pelletized state, ensure inhalation, as a major portion falls under the respirable category (Gardiner et al.,1992). This facilitates the entry and deposition of CB into the deep portions of the respiratory tract (Shah et al.,2008). Carbon black has been classified as a group 2B "possible carcinogen" by the International Agency for Research on Cancer (IARC).

Gardiner K (1995) reviewed the respiratory health effect of Carbon black and reported that exposure-response relations of carbon black were evident for forced expiratory volume in one second (FEV1) and forced mid-expiratory flow (FEF25%-75%), opacities in chest radiographs and symptoms of chronic bronchitis. Renwick et al., 2001 reported a dose-dependent effect of CB which concluded that CB can induce pro-inflammatory gene transcription of phagocytosis at low doses and inhibition at high doses. Zhang R et al. 2014, also reported an increased expression of inflammatory biomarkers (IL-1β, IL-6, IL-8, MIP-1βand TNF-α) in the blood of CB-exposed workers. But the possible health effects of Carbon black nanoparticle (CBNP) inhalation remain unknown.

2.1.2. Diesel exhaust nanoparticles

Diesel exhaust nanoparticles (DEP) are carbon-based nanoparticles emitted during the combustion of diesel fuel. The carbon core is adsorbed with polyaromatic hydrocarbons, sulphates, nitrates, and trace amounts of metals and oxides. Diesel engine emissions are the largest source of nanoparticles in urban atmospheres (Harrison et al.,2018). The size and composition of DEP vary. DEP of size less than 30nm diameter contains high molecular weight hydrocarbons derived from unburnt fuel (Shi JP, Harrison RM. 1999). Larger particles contain aggregates of elemental carbon condensed with hydrocarbons which can range from C_{12}> to C_{36}. (Ristimaki J et al.,2007). The number and size distribution of the exhaust particles in an urban environment is also affected by the temperature (Fujitani Yet al., 2012; Gramotnev G, Ristovski Z. 2004)

2. 2. Air pollution and Nanoparticles

Clean air is fundamental to health and well-being. Population explosion, urbanization, and industrial revolutions have significantly compromised air quality around the world. The World Health Organization (WHO) estimates air pollution as the single largest environmental health risk, that leads to the killing of up to 1 in 9 people globally (Source: https://www.environment.nsw.gov.au). The U.S. Environmental Protection Agency defines the Air quality index (AQI) as a key tool to assess the quality of air in the immediate environment and thereby the health effects raised by the air(https://www.airnow.gov). The major pollutants assessed for calculating AQI includes ground-level ozone, particle pollution, carbon monoxide, and sulfur dioxide. WHO reveals that a great majority of the global population (99%) are breathing air

that exceeds limits of unhealthy for everyone i.e 151-200 AQI while 101-150 is unhealthy for the sensitive population and 51-100 is moderate air quality and 0-50 AQI forms good air quality. In this scenario, it is the low- to middle-income countries that suffer the most. It is estimated that household air pollution was responsible for 3.2 million deaths in 2020 which included over 237000 deaths of underage children.

Particle pollution (particulate matter-PM) consists of mixtures of solids, and liquid particles of suspended organic and inorganic substances which can be directly or by secondary emissions, released into the atmosphere. WHO reveals that PM affects more people than any other pollutant. It can be fine or coarse depending on size. The PM deposits in the various regions of the respiratory tract and can even be transferred into the bloodstream. WHO distinguishes dust to be **inhalable** that can reach the upper airways (PM<10µm), **thoracic** that can penetrate the airways of the lung (PM<2.5µm), and the **respirable dust** fraction which can enter the alveoli, the gas exchange region and can even cross the air-blood *barrier (*Krug, HF et al. (2011), Kreyling, WG et al. (2013). Fig 2.2 represents the possible transport pathway of particles in the lung.

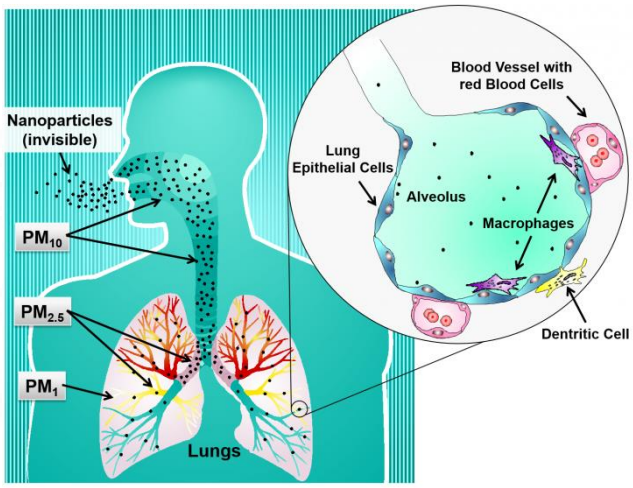

Fig2.2 Illustrates size-dependent particle deposition in the respiratory tract. Particles less than 1µm can reach as far as the gas exchange regions of the lungs- the alveoli and interact with the cellular components of the alveoli. Particles in this size range pose a greater threat of crossing the air-blood barrier (Source: *Krug, HF et al. (2011)*

2.3 Inhalation risk of Nanoparticles

Nanoparticles(NPs) are particles with a size of 1-100nm in diameter and they fall in the category of PM_1. They have the potential to cross the air-blood barrier but in most cases, the applied dose could be recognized by macrophages and thereby elicit clearance from the respiratory tract. Technological advances, high rate of urbanization, industrialization, vehicular emission, and extreme and episodic events (dust storms, volcanic eruption, forest fires, firework activity, and crop residue burning, etc) have contributed to the release of nanoparticles in high concentrations especially in Asian countries (Saxena et al., 2020; Sonwani et al., 2021). Inhalation is a major route of entry NPs and can elicit inflammatory responses and oxidative stress in the lungs, breaching the epithelial cells, the first line of innate defence mechanism (Rothen-Rutishauser et al., 2008; Nemmar et al., 2013). Gurjar et al.,2016 reported that

respiratory diseases in Delhi are 12 times the national average, and 30%of the population was found suffering from 166 different respiratory diseases. Many *invitro* and *invivo* models are being discovered to evaluate the extent and outcome of exposure. To reduce the impact of atmospheric pollutants countries are trying to devise new measurements, Saxena and Sonwani, 2020); however there is a lack of studies on the effects of NPs on human health, especially in Asian countries (Sonwani, 2021).

2.4 Respiratory System and Alveoli

The respiratory system is crucial for life as it allows us to breathe, but breathing is not the only function of the system. To maintain life, cells need a continuous supply of oxygen. The respiratory and circulatory systems provide this continuous supply and remove waste products of metabolism along with regulation of blood pH (Dezube,2021). The human respiratory system starts from Nose and mouth and extends to the deep-seated portions including the alveoli. Lungs, the system's functional units, are the organs with the largest surface area in the body representing a unique interface with the external environment. Lungs are composed of a wide array of cell types that face continuous mechanical, chemical, immunological, and xenobiotic stress over a lifetime (Schneider et al.,2021). The lung has more than 40 different cell types making it unique among organs in the diversity and function of individual cell types, such as mechanical, sensory, transporting, secretory, etc (Stone et al.,1992). These cells, in particular, should be replenished by the progenitor cells. Compromised repair and regenerative capacity contribute to pulmonary diseases (Kotton and Morrisey, 2014)

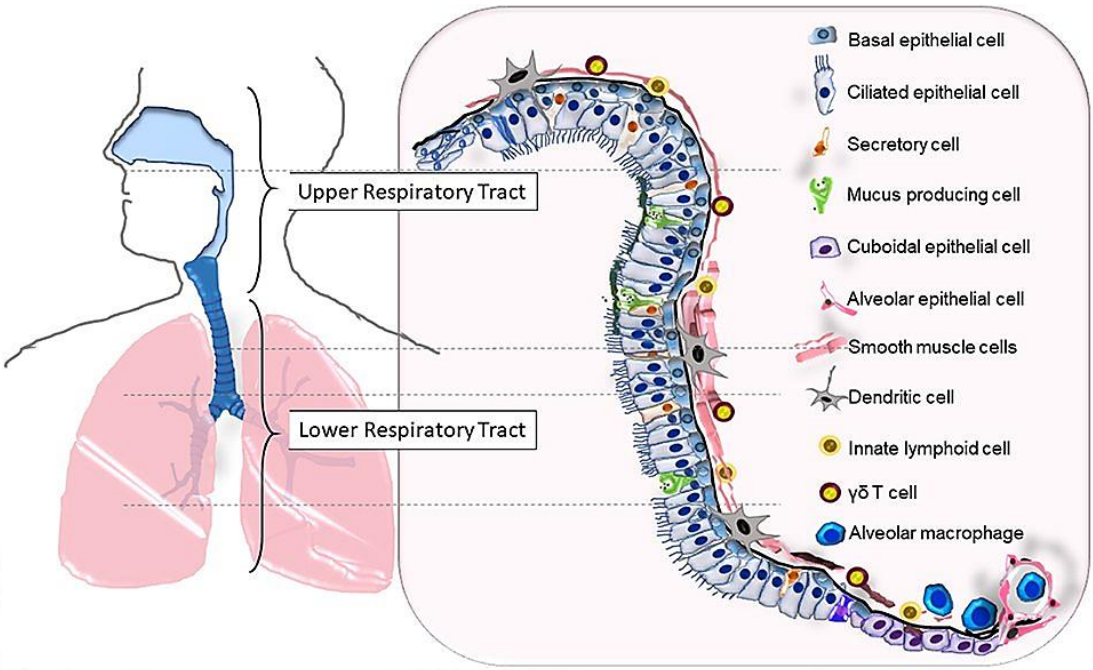

Fig2.3. The Organisation of the respiratory tract. with cellular components. The entire length of the respiratory tract (RT) is spanned with Epithelial cells (ECs) lined with basal cells that are attached to the basement membrane. The beginning and end of the RT are lined by Squamous ECs, the upper RT and the large bronchi are marked up by ciliated and non-ciliated columnar epithelia, while cuboidal epithelia line the small bronchi and bronchioles. Mucus covering the EC is secreted from mucus-producing cells, and airway liquids are secreted from secretory cells, neutralizing immunoglobulins, and antimicrobials. Resident leukocytes such as γδT cells, dendritic cells, and innate lymphoid cells line the mucosa. Alveolar macrophages are found in the lower airways and alveoli. The bronchial smooth muscle cells from the basal end provide structural support and elasticity to the airways. Source: LeMessurier K.S et al,2020

Gas exchange takes place in the alveoli (Parenchyma) which comprise about 90% of the lungs' total volume (Knudsen L, Ochs M,2018). Conducting airways and larger vessels constitute the remaining non-parenchymatous region. Functional units of alveolar clusters are termed acini. Weibel et al.2005 reported that there are around 30,000 acini in the human lung. The inter-alveolar septum separates the alveolar airspace from the blood compartment and hence provides the structural basis for gas exchange (Weibel 1973; Maina and west 2006). Lung alveoli are stabilized by the

pulmonary surfactant system and connective tissue. Within the alveolar septum, the air-blood barrier consists of an alveolar lumen facing **epithelium** capillary lumen facing endothelium, between which there is interstitial space

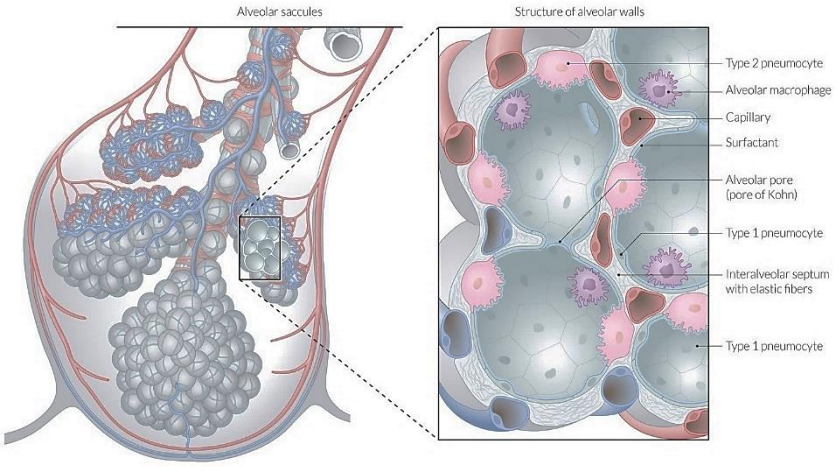

Fig:2.4 Cross-sectional view of alveoli. The cellular components include type 2 pneumocytes, resident macrophages, type 1 pneumocytes, etc. Surfactants synthesize by the epithelial cells reduce the surface tension and prevent alveolar collapse.

Alveolar epithelium is essential for gas exchange and also functions as a barrier to protect our body from hazards. The quick repair and regeneration potential of alveolar epithelial cells in response to injuries restore an intact epithelial barrier. The pulmonary alveolar epithelium is composed mainly of two types of epithelial cells: type I alveolar epithelial cells (AT1) and type II alveolar epithelial cells (AT2).AT1 cells are large squamous cells forming the air-blood barrier's epithelial component ((stone 1992, Hayes 1981). They cover 95% of the alveolar surface area with thin squamous extensions interspersed with type 2 cells. Type 2 cells are small cuboidal cells and have the potential to differentiate into type 1 cells during homeostasis and repair post-injury (CE Barkauskas, et al.,2013, TJ Desai,2014)). They are

characterized by secretory organelles, the lamellar bodies storing surfactant. Crapo et al.1982 reported that the type 1 and 2 cells are distributed at a ratio of 1:2. During the late stages of lung development, there will be an increase in alveolar surface area which is key to proper lung function (Mareena et al.,2021). Electron microscopic studies revealed that there is a thin, continuous lining around alveoli composed of surface film and an aqueous hypo phase (Weibel and Gil 1968) which suggests that alveolar epithelium is covered by a liquid lining and is not directly exposed to air (Bastacky et al.1995). Surfactants present in this hypo phase constitute the thin film at the air-liquid interface (Olmeda et al. 2017).

Human pulmonary surfactants (PS) are endogenous lipoproteins produced in the lungs. PS reduces the surface tension (min of<10 mN/m) at the air-liquid interface on the alveolar surface (Agassandian and Mallampalli, 2013, Sunde et al.2017) which allows the expansion of alveoli and gas exchange (Sadler, B. D., Kaushik, R 2020). Surfactants are complex lipoproteins comprised of 90% lipids and 10% surfactant proteins (by weight) dipalmitoylphosphatidylcholine (DPPC), unsaturated phosphatidyl choline, phosphatidyl glycerol, cholesterol other phospholipids, and neutral lipids constitute the lipid fraction. Plasma proteins (3%) and Surfactant proteins-SP-A(5%), SP-B (0.7%), SP-C (0.8%), and SP-D (0.5%) constitute the total surfactant proteins (Wang et al.2021). SP-A and SP-D are large,collagen-like, and hydrophilic, glycoproteins that belong to the collectin family which are part of the innate immune response. They protect the lungs by stimulating phagocytic clearance of inhaled particles or pathogens. Being an abundant surfactant it accounts for 2-3% w/w of SPs. It enhances phospholipid absorption at the Air-liquid interface (ALI)

regulates the Type2 PS secretion, binds specific moieties, and prevents the plasma protein-mediated inhibition of surfactant function (Echaide et al., 2017). SP-A and SP-D bind to neutralize viruses (Watson et al.,2019) and help preserve lung homeostasis by acting as immune scavenge receptors (Nayak et al., 2012). SP-Band SP-C,(14 and 6 kDa) the hydrophobic, apolipoproteins constituting 1-2%w/w of total SPs (Echaide et al., 2017 reduce the surface tension by spreading the surfactant layer at the ALI (Weaver, T. E., and Conkright, J. J. (2001).

The alveolar interstitium, the bounded space between the epithelial and endothelial basal lamina contains cells and a network of collagen and elastic fibers (Knudsen and Ochs, 2018). Most abundant among the cells are “fibroblasts”.The importance of alveolar mesenchyme in directing epithelial proliferation and differentiation became a focus by the mid-1990s. Functions of alveolar fibroblasts include

- Provide an ECM (Extra cellular matrix) scaffold for the expansion of epithelial cells and modulate the process.
- Provide tensile forces to extend and thinning of septal walls during secondary septation
- Provide paracrine cues to epithelium and endothelium to proliferate and differentiate (Mareena et al.,2021)

The cytoskeletal apparatus of fibroblasts contain actin, myosin which is linked to focal adhesions which connect cell actin to the Extracellular matrix(ECM) which allows the cells to contract the ECM, Hinz B. 2006, Gabbiani 1971)

2.5 Pulmonary fibrosis

Interstitial lung diseases refer to a group of about 100 chronic diseases. Pulmonary fibrosis is one among these characterized by remodelling of the interstitium, destruction of tissue architecture, scarring, and compromised lung function Even though pathogenesis is unclear, chronic epithelial injury and activation of fibroblasts are linked to the disease (Meltzer EB, Noble PW,2008). Idiopathic pulmonary fibrosis (IPF), the most common type of interstitial pneumonia is a chronic and progressive disease of unknown aetiology with a median survival age of 3 years from diagnosis. Raghu et al.,2016 reported an increase in the incidence of IPF at an unprecedented rate, especially in the aged population. Kaul B et al., 2021 reported that IPF and sarcoidosis were the most prevalent ILDs in India and Pakistan. Fig 2.5 represents the relative frequency of ILD subtypes by geography. A single-center study in India that recruited 803 patients between 2015-2017 reported that sarcoidosis (42.2%) and IPF (21.2%) were the most common ILD subtype (Dhooria S et al., 2018). Singh et al., 2017 in the epidemiological evaluation of ILD frequencies in India which involved a multi-centre cohort study between 2012-2015 that recruited 1084 patients from 27 centres also reported the prevalence of IPF as a common ILD subtype in India.

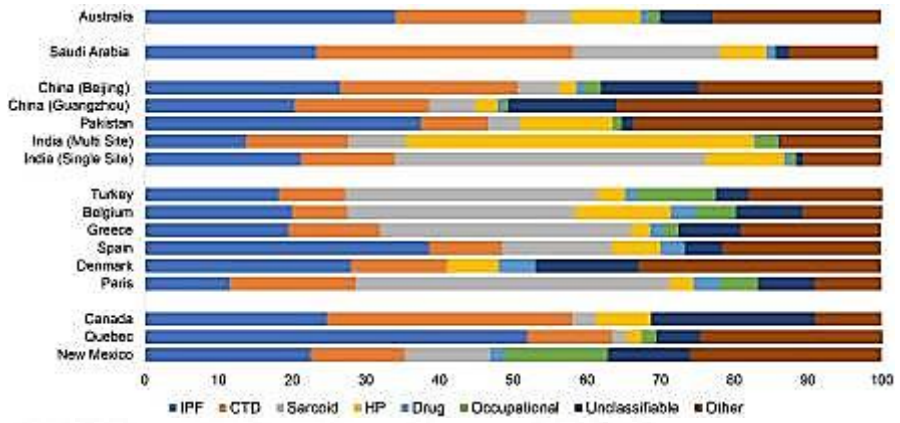

Fig 2.5. Relative frequency of ILD subtypes geographically. IPF, idiopathic pulmonary fibrosis; CTD, connective tissue disease; HP, hypersensitivity pneumonitis. Source: Kaul B et al., 2021

Lung fibrosis is characterized by extracellular matrix deposition, remodelling, and the formation of fibrotic scars. Even though the pathogenesis of IPF remains unclear, IPF is thought to be a consequence of repetitive injury to the respiratory epithelium and dysregulated repair leading to activation and proliferation of myofibroblasts and resultant ECM deposition (Lederer and Martinez, 2018). Various risk factors identified as triggers of IPF are mentioned **in Fig 2.6**

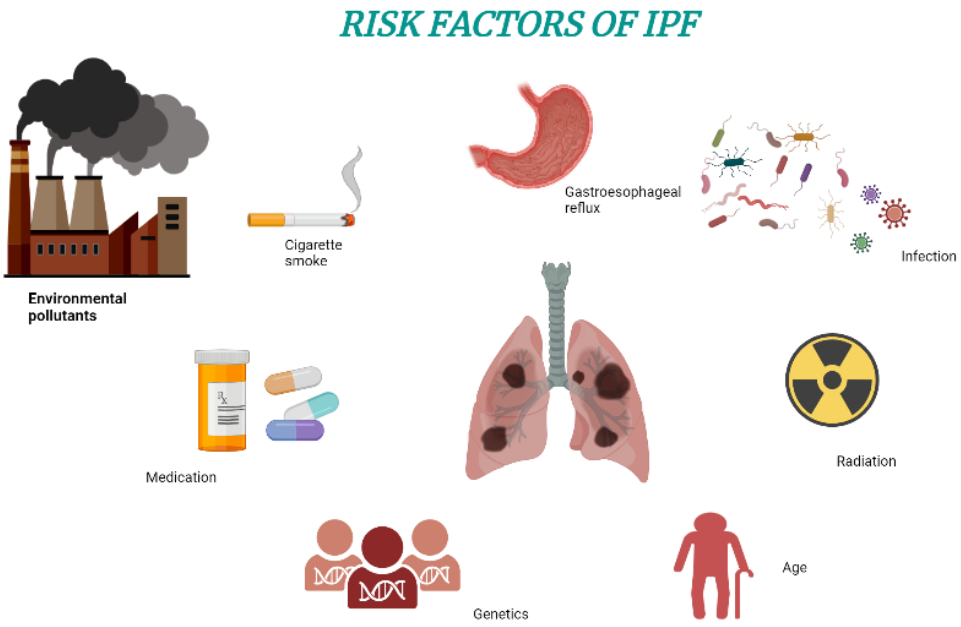

Fig 2.6 represents the risk factors of IPF. intrinsic risk factors include genetics, aging, sex, lung microbiome, etc., co-morbidities include gastroesophageal reflux, diabetes mellitus, herpes virus infection, etc. and extrinsic risk factors include cigarette smoking, environmental exposures

The anti-fibrogenic agents nintedanib and pirfenidone approved by FDA and currently used in therapies showed an effective reduction in morbidity but not mortality (King TE Jr 2014, Hagmeyer L 2016). Research is still progressing to understand the role and origin of fibroblasts as they will be promising targets of antifibrotic therapy.

Evidence-based guidelines recommend that in any adult with chronic exertional dyspnea chances of IPF should be considered. Since, the official ATS/ERS/JRS/ALAT statement on diagnosis and management of IPF suggested it to be a rare incident in ages below 50 and, more common in men than women (Raghu G,2011) the diagnosis of IPF was typically established only in those aged above 50 (Gribbin et al.,2006 and Nathan et al., 2011). The prevalence of IPF in young patients hence was not studied

earlier. Nadrous HF et al., 2005 in their study reported IPF in younger patients <50 yrs which made a change in the diagnostic approach, medical treatment options, and guidelines for IPF (Neurohr C, Behr J (2015), Leuschner G et al., 2018). More than 50,000 new cases of IPF are reported each year. Gender-based studies reported it to be more prevalent in men and women and the basis of this difference is unknown (Tanzira saman et al.,2020). Sesé L et al.,2021 reported that during diagnosis Women appear to have less advanced disease, which they attribute to less exposure history compared to men. They conclude that regardless of gender, the progression of the disease and overall survival remains comparable, but women have less access to lung transplantation.

Several cohort studies conducted in various countries reported an association between IPF and occupational and environmental exposure factors. The Korean National Health and Nutrition Survey revealed that IPF was diagnosed at a younger age and had a longer period of symptoms at the time of diagnosis in people exposed to occupational and environmental dust. The report also states an increase in the mortality of IPF patients in the exposed group (Lee et al.,2015). Park, Y., Ahn, C. & Kim, TH, 2021 concluded their meta-analysis of patient-control studies by stating that environmental and occupational exposure increase the risk of IPF.

IPF at the tissue level can be described as a fibroblast focus underneath the epithelial layer with an immature hyaluronic acid-rich matrix, with increased *αSMA+* myofibroblasts and loss of type1 cell differentiation (Selman and Pardo 2002). The origin of the myofibroblast population in IPF is still an unanswered question. A variety of cells including interstitial fibroblasts, pericytes, and mesothelial cells are known to

differentiate into myofibroblasts in the bleomycin injury model. Epithelial-mesenchymal transition, a mechanism by which epithelial cells lose their phenotypic hallmarks and gain mesenchymal characteristics is now a subject of study (Tanjore H 2009, Chen LJ,2015,)

2.5.1. Epithelial-Mesenchymal transition (EMT)

Epithelial cells are characterized by the apical-basal polarity and formation of tight junctions. EMT is a process by which these cells lose the epithelial characteristics including expression of E-cadherin and gain mesenchymal phenotype characterized by the presence of N-cadherin, Vimentin, Fibronectin, etc. The process was first described by Elizabeth Hay in the 1970s (Hay 1968). Wound healing and fibrosis in disease conditions are considered as the relaunched program of embryonic development (Lovisa S, 2021). This transition includes cytoskeletal and morphological remodelling, acquisition of gene expression profile of fibroblasts, increased migratory capacity, and production of extracellular matrix (ECM)(Kalluri, 2009: Zeisberg and Neilson, 2009). Different types of EMTs have been reported. TypeI EMT is associated with embryonic development, type II EMT is involved in tissue fibrosis, and type III EMT in cancer metastasis. New genetic-engineered models and lineage tracer studies indicate that EMT does not directly transit to myofibroblasts or activated fibroblasts or confer the increased migratory capacity but an intermediate state is formed after initiation termed as partial EMT (p EMT) (Lovisa et al., 2015: Grande et al.,2015). These transitions anyhow will end up in full transition and generation of myofibroblasts, with a direct impact on fibrosis generation (Koopmans and Rinkevich, 2018). Transforming growth factorβ is considered a critical growth factor involved in the process

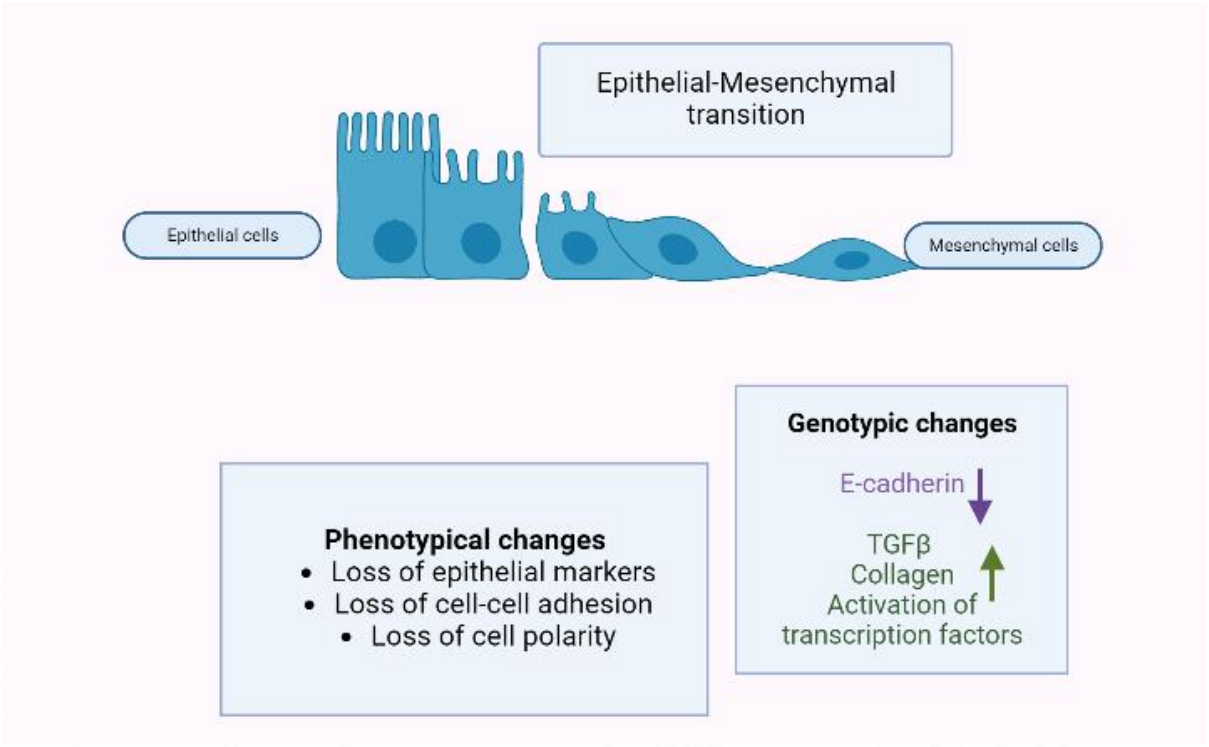

Fig 2.7. Schematic diagram showing the basic mechanism of the Epithelial-to-Mesenchymal Transition. On stimulation of epithelial cells by EMT activators like TGF β the epithelial cells can undergo EMT resulting in the fibroblast phenotype and ultimately in fibrosis.

2.5.2. Signalling pathways in IPF

The development of anti-fibrotic therapies relies on the molecular understanding of the disease. Different mechanisms and their interplay are involved in the differentiation of fibroblasts. Under mechanical strain and tissue stiffness fibroblasts get activated with increased β- and γ-actin and αSMA (Smooth muscle actin) along with expression of ED-A (splice variant of fibronectin) (Henz et al . 2001, Tomasek JJ et al.2002). Integrins also play a role as they connect ECM to actin fibres, allowing the conversion of mechanical cues to biochemical ones that are nuclear-dependent.

Differentiation of myofibroblasts is driven by the signalling of biochemical growth factors. In the context of fibrosis, many growth factor families are extensively assessed. Among them transforming growth factor (TGF)-β and Wingless/Int (WNT) signalling pathways are emphasized as key mediators (Leask A, Abraham DJ, 2004:Clevers H, Nusse R.2012)

2.5.2.1. Canonical TGF-β Signalling

The TGF-β superfamily consists of multiple proteins that govern several physiological processes, including pluripotency, cell fate determination, proliferation, and differentiation. Over 30 members of the family are described so far in humans which include TGF-βs, inhibins, nodal, growth/differentiation factors GDFs, activins, and Bone morphogenetic proteins (BMPs). TGF-β1 among this superfamily is considered to be a key molecule in fibrosis evidenced by research (Leask A, Abraham DJ, 2004). Hence canonical signalling through TGF-β1 needs to be focussed.

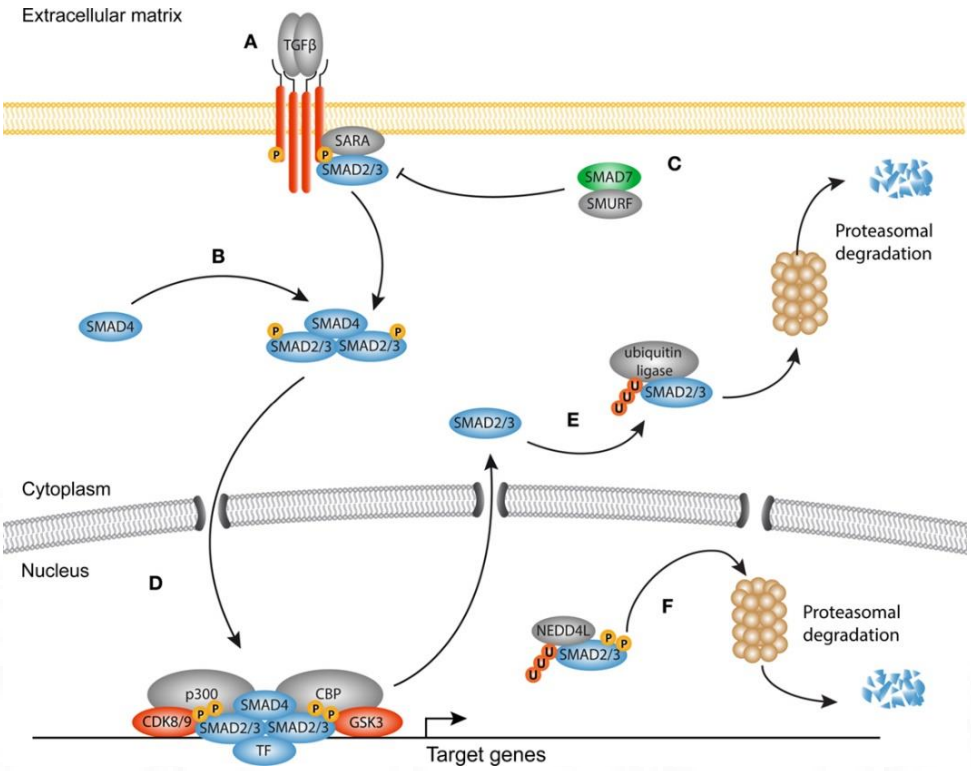

Fig 2.8 Cartoon describes, in a nutshell, the canonical TGFβ signalling in Fibrosis. The ligand binding to the receptors induces phosphorylation of the receptors and this will eventually activate type I receptors which then phosphorylate selected Smads. The activated Smads (R-Smads) then form a complex with a common Smad4 and these smad complexes translocate into the nucleus, where they regulate the transcription of target genes. Activation of R-Smads by type I receptor kinases is inhibited by Smad6 or Smad7. R-Smads and Smad4 shuttle between the nucleus and cytoplasm.

TGF-β in an inactive state is associated with Latency -associated peptides (LAPs) and latent TGF-β-binding proteins (LTBPs) forming a large latent complex (LLC). The active TGF- β is released from this complex upon injury, binding of integrins together with increased mechanical forces or by proteolytic cleavage. This facilitates the active TGF- β homodimer to interact with its receptors (type I and II). The binding of ligands initiates the phosphorylation of the SGSGSG domain on the receptors. This will activate the receptor I which in turn bind and phosphorylate Smad proteins which are the key modulators of the pathway. Three classes of Smads- Receptor regulated smads

(R-Smads-:Smad2 &3)), Common partner Smads (Co-Smads-Smad4), and inhibitory smads (I -Smads:6&7). Ligand binding to type 1 receptor phosphorylate R-Smads and form heteromeric complexes with Co-Smad. R-Smad and Co-Smad consist of a C-terminal MH2 domain connected by a linker region and N-terminal MH1. Phosphorylation of the MH2 domain initiates the nuclear shuttle of Smad complexes together with Smad -binding elements to regulate the transcription of target genes (Massagué J,2012, Shi Y and Massagué J,2003.Alarcon et al.2011).

Numerous scientific studies (Pulichino et al.2008, Takizawa H et al.2001, Wang et al.2007, Kaimori et al.2007) have demonstrated the role of TGF beta signalling as a key regulator in heart, lung, and Kidneys myofibroblast biology. Fig depicts the TGF-β signalling in fibrosis. Fibrotic tissues show elevated TGF-β levels and accumulation of Smads in the nucleus together with upregulated expression of TGF-β target genes and decreased I-Smad expression. Despite being the key regulator reports also suggest that TGF-β is not the only signalling pathway regulating the fibrotic cascade. Piersma B, Bank RA, and Boersema M (2015) stated that the inhibition of Smad signalling does not completely attenuate fibrotic response suggesting the involvement of several other signalling cascades.

2.5.2.2. Canonical WNT-β catenin signalling

Wingless related-integration site (Wnt)/β-catenin signalling is evolutionarily conserved and plays a crucial role in stem cell self-renewal across several tissue epithelia. The term Wnt is a portmanteau from Drosophila as wingless and Int1 in the mouse. Their role in foetal development critically in the formation and polarity of the primary body axis is well described (Niehrs C 2012, Petersen CP, Reddien PW.2009).

Recent shreds of evidence reveal the fact that they are versatile growth factors in homeostasis and disease (Piersma B, Bank RA 2015).

WNT ligands bind to Frizzled (Fz) receptors- a family of seven transmembrane receptors. In dampened or WNT off state WNT antagonists outnumber the ligands. Phosphorylation of cytoplasmic β-catenin by Glycogen synthase kinase 3(GSK3) and Casein kinase (CK)1, subunits from β-catenin destruction complex triggers Ubiquitination and proteasomal degradation of β-catenin by the E3 ubiquitin ligase β-transducin repeat-containing protein (Aros, C.J., Pantoja, C.J. & Gomperts, B.N.2021). Upon WNT transcription and translation, the ligand encounters Porcupine, an endoplasmic reticulum protein that palmitoylates N-terminal residues of Wnt leading to ligand secretion (Barott et al.,2011). Ligand binding to the Fz receptors functions with low-density lipoprotein receptor-related proteins (LRP) 5&6 Co-receptors. The binding of ligands phosphorylates LRP in the cytoplasmic tail by CK1 and GSK3. At the same time, β-catenin ubiquitination and degradation will be limited. The interaction of activated Fz/LRP complex with Disheveled(DVL), GSK3, and Axin will prevent catenin degradation. Axin directly interacts with β-catenin, CK1, GSK3, adenomatous polyposis coli (APC), and the ubiquitin ligase β-TrCP (Zeng et al.2005). Sequestration of Axin and GSK 3 hence is critical for the inactivation of β-catenin degradation. Alternatively, internalization of LRP5,6 aggregates together with destruction complex in multivesicular bodies make them unavailable to interact with β-catenin also helps β-catenin escape from ubiquitination (Taelman VF et al.,2010). Stabilized β-catenin accumulates in the nucleus and associates with T-cell

factor/lymphoid enhancer-binding factor-1 (TCF/Lef-1) and activates downstream targets like c-MYC, AXIN2, CYCLIN D1 Fig depicts the WNT signalling.

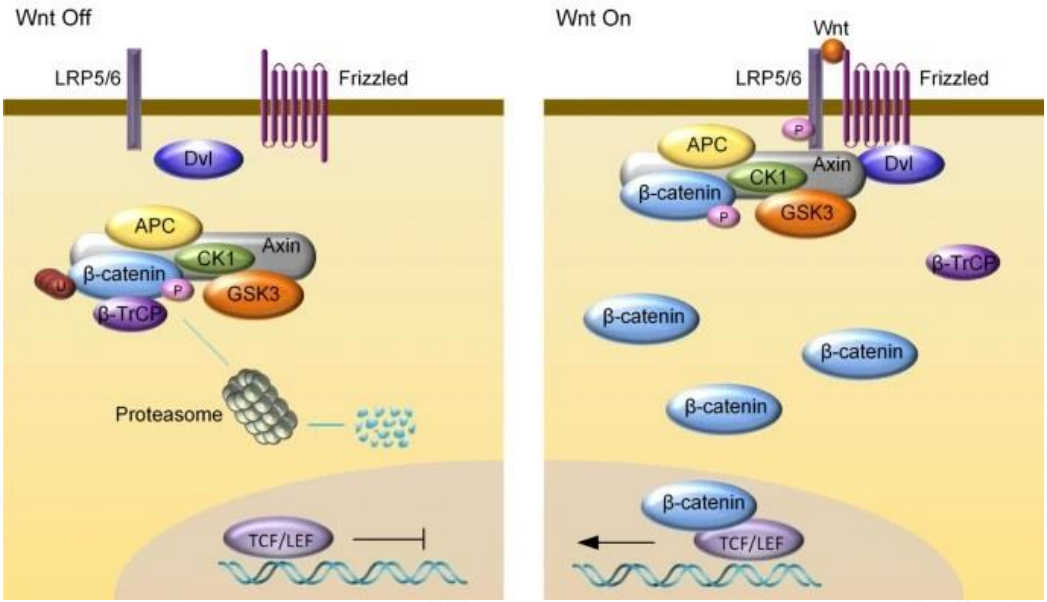

Fig 2.9 Schematic representation of Wnt/β-catenin pathway. In the absence of the Wnt ligand, the βcatenin is phosphorylated and ubiquitinated by Ubiquitin E3 ligase β-TrCP and marked for proteasome degradation. On activation of Wnt signalling by binding of Wnt ligand to Fz receptor and LRP5/6 coreceptors, the destruction complex is inactivated and β-catenin is stabilized and this eventually results in activation of target genes. (Source- Gao, C., Xiao, G. & Hu, J, 2014)

Several research works emphasized the key role of WNT signalling in the fibrogenesis of various organs like the heart, lung, skin, etc (Duan J et al.2012, Henderson et al, 2010, Sato M 2006). Increased expression of WNT agonists or silencing of endogenous WNT antagonists like Dickopff (DKK) and sec FRP (sFRP) leads to aberrant WNT signalling (Beyer et al 2012, Dees et al.2014). Several reports suggest

that sustained nuclear accumulation of β-catenin is a trigger of fibrogenesis (Hamburg et al.2012, Dees et al.2014).

TGF -β signalling can also proceed through several other non-canonical signalling pathways like mitogen-activated protein (MAP) kinases (ERK, p38, and JNK), phosphatidylinositol-3-kinase (PI3K), and Rho-like GTPases, YAP/TAZ(Yes-associated protein (YAP) and its ortholog transcriptional coactivator with a PDZ-binding domain (TAZ)

2.6 In-vivo and *In-vitro* models of Lung fibrosis

Pulmonary fibrosis is one of the most challenging diseases to manage. Even though a single model is unable to recapitulate the nature of fibrosis, it still can provide valuable insights into fibrotic mechanisms thereby in the development of therapeutic moieties. Animal models have been used widely in understanding the complex fibrotic cascade as well as in testing new drug efficiency. Among the *in vivo* models, Bleomycin-induced pulmonary fibrotic models are the best characterized (Jenkins RG et al.2017). But they failed to represent the exact pathophysiological process in IPF. Fluorescein isothiocyanate (FITC) has also been used to induce lung fibrosis and resulted in alveolar injury and acute reactions. Intratracheal delivery of fibrotic cytokines by viral vectors is also used which recreates early mild inflammation and rapid fibrosis onset in mouse models. Fibrosis in Occupational exposure to Silica and Asbestos has been assessed in rat models (Shoeb M et al. 2019). Radiation-induced fibrosis is mostly studied by whole thorax irradiation in mice (JinH.2020). Genetically modified animal models are also studied for the influence of genetic factors on disease progression.

Despite all the possible flaws, animal models are still valuable for a better understanding of fibrosis.

Most of our current understanding of lung fibrosis is provided by *in vitro* models. Submerged 2D cultures were initially used for assessing cellular fibrotic responses. As science progressed new and complex *in vitro* systems were designed. These cell culture models lack diversity of cell types and fail to reproduce dynamic cellular interplay.

Air-liquid interface (ALI) *in-vitro* inhalation models are now used in research as they are more realistic and mimic the pulmonary region than classic *in vitro* models (Ghislaine Lacroix,2018). Lung organoids from stem cells, lung-on-chip, and organoid cultures are also gaining popularity as they overcome the failures of traditional submerged culture systems even though long-term mechanistic studies are still unchaperoned (Leonard-Duke J et al.2020).

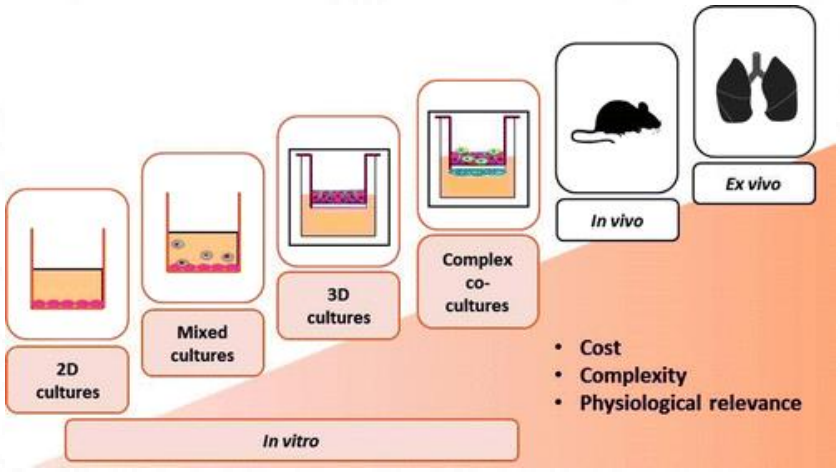

Fig 2.10. Respiratory models. The cost of development and maintenance increases with complexity in line with the physiological relevance of the models. Source: Ghislaine Lacroix,2018

2.6.1. Electric cell-substrate impedance sensing as an in-vitro system to study cell-material interactions

Electric cell-substrate impedance sensing (ECIS) is a real-time, label-free, non-invasive impedance-based method to study cellular responses to stimuli. Impedance measurement of the cells are facilitated by growing them in special culture chambers which contain gold electrodes. A small alternating current (AC) is applied across the gold electrodes and potential difference formed across is measured. The insulating property of the cell membrane offers resistance to the free flow of current which in turn result in increased electric potential. Measuring the cellular impedance gives information regarding cell attachment, morphology, function, and motility (https://www.biophysics.com). In advanced ECIS equipment, impedance is often converted into resistance and capacitance, which helps in obtaining more accurate data on cell behaviour.

Impedance measurement by varying the frequency of AC reveals time course changes in cell behaviour like barrier integrity and membrane capacitance. Models like ECIS Z-theta use AC frequencies ranging from 100-64,000 Hz. This equipment detects subtle morphological variations which will be left unexplored in endpoint analyses.

Multiple AC frequencies help in understanding cellular responses to external stimuli. At low AC frequencies(<2000 Hz) the current flow through intercellular junctions and reveals changes in the spaces under or between cells thereby helping in understanding barrier function. At high AC frequencies (>32,000 Hz) current capacitively flows through the insulating membrane. The impedance measurement at these frequencies is

affected by cell coverage and is useful for measuring cell growth rate and cytotoxicity. Giaever and Keese provided the first evidence of impedance-based cellular responses (Giaever and Keese, 1991)

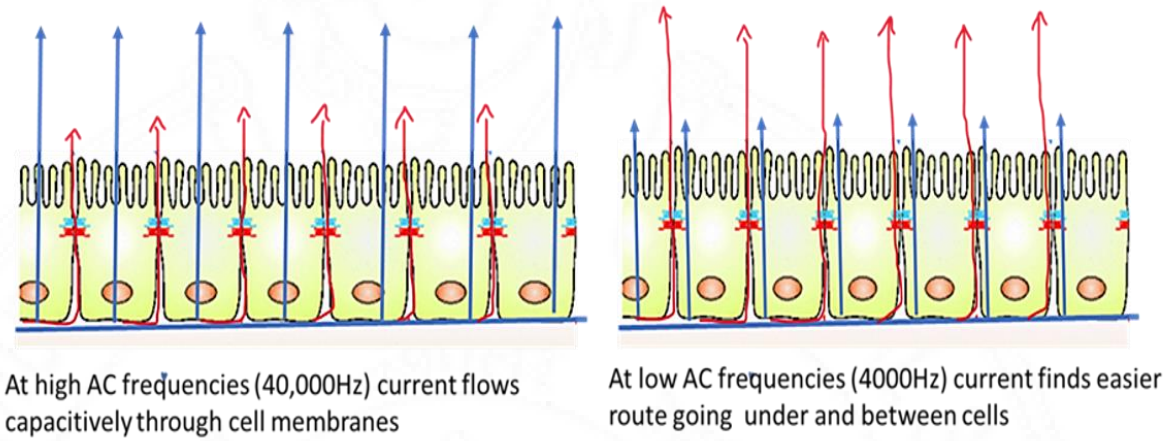

Fig2.11 Illustrates the cross-section of the ECIS well array covered by confluent cell monolayer inside and the path of current flow is indicated by the arrows. (Source-Navas and Nandkumar A, 2022)

Each cell type has a characteristic growth and adhesion curve in ECIS controlled by seeding densities. As the cell attaches to the electrode and spread inside wells there will be a gradual increase in resistance and a decrease in capacitance. As the cells cover the electrodes completely i.e., after the formation of an intact monolayer the resistance value will be in a plateau. Further differences in resistance patterns on external stimuli reveal cellular response to that stimuli or injury.

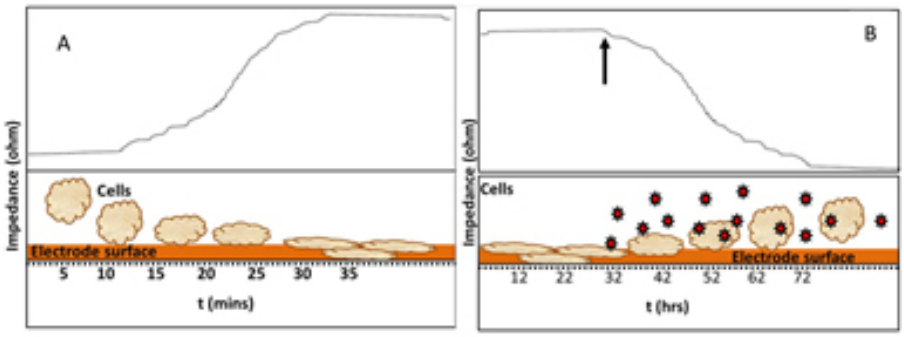

Fig 2.12. The pattern of impedance measurement in the ECIS. As the cell attaches and spreads an increase in impedance is observed. Once the electrodes are fully covered by the confluent monolayer the impedance attains a plateau. The effect of an external injury on cellular integrity is revealed by the variations in impedance (Source- https:/www.biophysics.com)

ECIS can be used to study multiple aspects of cell behaviour and thereby could be used in studies including toxicology, cancer biology, and other related fields. Recent reports suggest the effective application of ECIS in understanding the effect of pollutants (Navas and Nandkumar A, 2022) and also in microbial pathogenesis (Keerthi and Nandkumar, 2022)

2.7. Air pollution and respiratory bacterial infections

Airborne microbes can significantly influence human health. Bacterial components like lipopolysaccharides are ubiquitous in the environment. They form a component of airborne particulate matter and induce a strong host response and amplify the immune response triggered by other PM components like transition metals (Rylander 2006). Increasing evidence suggests a positive correlation between air pollution and chronic respiratory diseases like cystic fibrosis (Jassal et al, 2013; Brugha et al., 2018). In analyzing the cystic fibrosis foundation registry in 2000 Goss et al., observed that increase in PM 2.5 was associated with increased case reports of fibrosis (Goss et al.,

2004). Experimental studies have reported that the host defense system can be compromised by environmental pollutants (Yang et al., 2018; Glencross et al., 2020) and can predispose humans to upper respiratory infections (Liu et al., 2019). The possible mechanisms remain unclear.

Ambient air pollutants may not only affect human health through direct interaction but also can affect bacterial behaviour. Mushtaq et al., 2011 reported increased bacterial invasion and adhesion by *Streptococcus pneumonia* to human primary bronchial epithelial cells upon PM exposure which suggest that particulate matter or components of particulate matter can modulate the virulence factors of respiratory pathogens. Accordingly, exposure to pollutants may enhance adherence to airway epithelium and further invasion and also in bacterial virulence traits like the formation of biofilm which are aggregates of microorganisms held together by self-produced polymer matrix that facilitate prolong survival in diverse environmental conditions(Kostakioti M.et al., 2013: Arianna Pompilio & Giovanni Di Bonaventura 2020)

3. MATERIALS AND METHODS

The study consists of four phases. Phase1 deals with the development of *in-vitro* systems suitable to study fibrosis. Phase II deals with understanding cell-material interactions where the cellular responses of alveolar cells to industrially important carbon nanoparticle -the Carbon black nanoparticle was assessed. Phase III deals with the assessment of the anti-fibrotic potential of All-trans retinoic acid, and finally, Phase IV deals with the assessment of Cell-material-microbial interactions. The summary of the present work is depicted in Fig 3.1

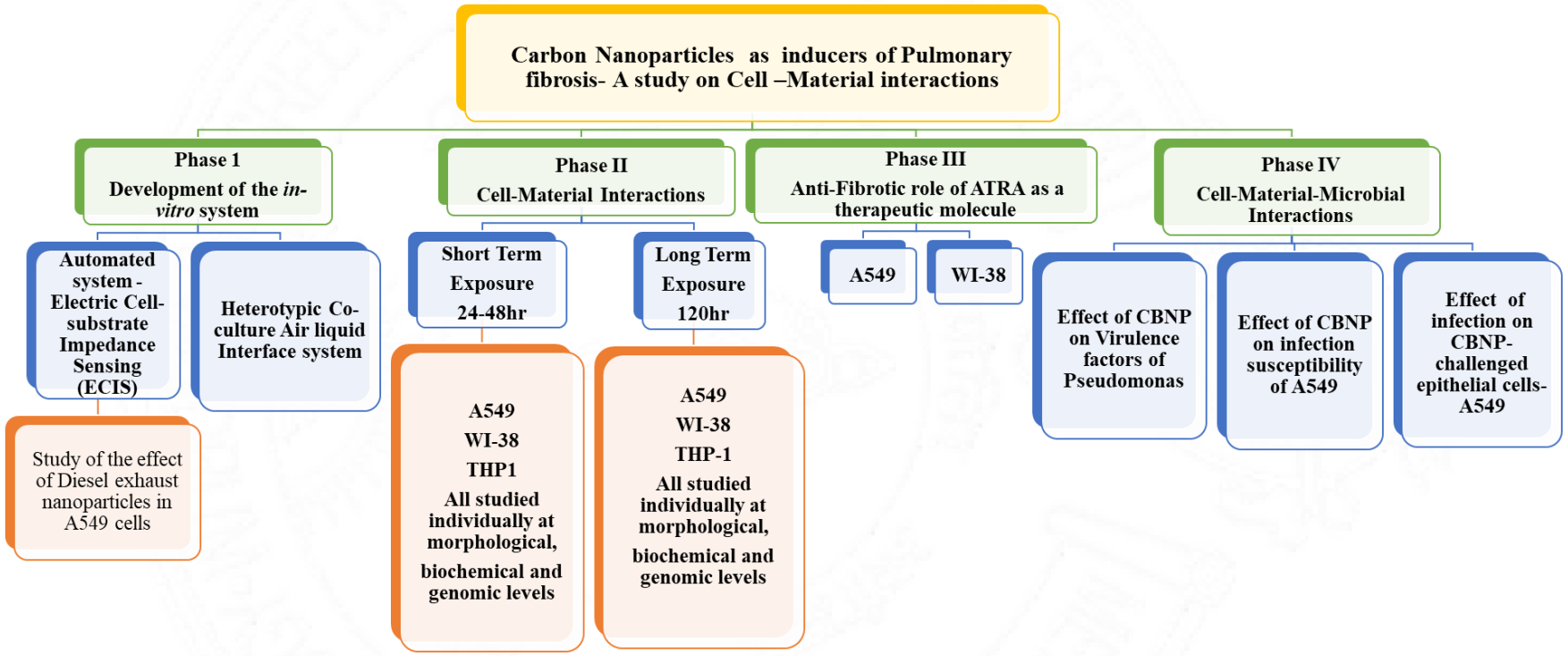

Fig 3.1. Flow chart depicting a summary of the present work

3.a. Materials used in the study

3. a.1. Carbon nanoparticles used in the study

3.a.1.1. Carbon black nanoparticles: Carbon black nanoparticle (Nouryon, Amsterdam, Netherlands) was a noble gift by Dr. Ramesh. P, Scientist G, Division of Polymeric Medical Devices, SCTIMST.

3.a.1.2. Diesel Exhaust Nanoparticle - The diesel exhaust particle was collected from a diesel car engine exhaust. The exhaust particles were collected into a cellulose ester filter as total suspended particulates. Particles were collected by sonicating the filter for 45 min in 5 mL of ultrapure water using a bath sonicator. The suspension was then centrifuged at 10,000 rpm for 15 min and lyophilized (Lyolab). A stock solution of diesel exhaust particles was prepared in complete cell culture media (F12K supplemented with 10%FBS) and sonicated before exposure to cells.

3.a.2. Cell types

3.a.2.1. A549 – a lung adenocarcinoma cell line used as a representative of type II alveolar epithelial cells (AEC) as it possesses properties like surfactant protein C synthesis, an important function of type II pneumocytes. In the lung, the type II pneumocytes are considered the progenitor cells for type I pneumocytes and the initiator cells of the fibrotic cascade. A549 cells were initiated in 1972 by D.J. Giard, et al. through an explant culture of lung carcinomatous tissue from a 58-year-old Caucasian male. A549 cells were purchased from American Type Culture Collection (ATCC-Manassas, USA (CCL-185™) and were used at passage numbers 22-29. The cells were maintained in Nutrient Mixture F-12 Ham, Kaighn's Modification

(Himedia) with L-Glutamine supplemented with 10% fetal bovine serum (FBS), Gentamicin (10 µg/mL) and Amphotericin B (2.5 µg/mL) and incubated at 37^0C with 5% CO2. Upon 90% confluence, the cells were trypsinized and subcultured at a 1:6 ratio.

3.a.2.2. WI-38 - Lung fibroblast cell line, representative of fibroblasts, the effectors of the fibrotic cascade. WI-38 cells were initiated from the lung tissue of a 3-month-old, female, embryo. WI-38 cells were purchased from ATCC (CCL-75) and maintained in DMEM medium supplemented with 10% fetal bovine serum (FBS), Gentamicin (10 µg/mL), and Amphotericin B (2.5 µg/mL) and incubated at 37^0C with 5% CO2. Passage numbers 14- 20 were used in the study. Upon 90% confluence, the cells were trypsinized and subcultured at a 1:4 ratio.

3.a.2.3. THP1- the monocyte cell line, representative of immune cells, the mediators of the fibrotic cascade. This cell line was initiated from the peripheral blood of an acute monocytic leukemia patient. THP1- Acute monocytic leukemia cell lines purchased from National Centre for Cell Sciences (NCCS), Pune were maintained in suspension culture in RPMI-1640 medium supplemented with 10% FBS in 37^0C, 5% CO2 incubator. Upon 90% confluence, the cells were trypsinized and subcultured at a 1:6 ratio.

Ham's F12 (Kaighn's) Medium, Dulbecco's Modified Eagle medium (DMEM), Rosewell Park Memorial Institute (RPMI) 1640, Amphotericin B(250 µg/mL), and gentamicin(50 mg/mL) solutions were purchased from Himedia Pvt Ltd (Mumbai, India). Fetal bovine serum (FBS) was purchased from Cellclone (Genetix Pvt Ltd, India) Dimethyl sulphoxide was purchased from ATCC (Virginia, USA).

All the cells used in the study were cryopreserved in freezing media containing 50% FBS, 45% respective cell culture medium, and 5% DMSO and stored at -80 ^{0}C or liquid nitrogen.

3.1 Phase I – Development of the *In-Vitro* System

Fibrosis is the result of cellular interactions to injury /stimuli. To delineate the molecular mechanisms of fibrosis, cell-cell interactions, both unicellular and multicellular, were studied. For this purpose, two different types of in-vitro systems were developed suitable to understand monotypic and heterotypic cell responses.

A study of the effects of nanoparticles in the alveolar region is of utmost importance as they constitute the functional units of the respiratory system. The alveolar epithelium is composed of alveolar epithelial type1 cells and type 2 cells. 95% of the alveolar surface is covered by type 1 cells, and together with endothelial cells and basal membrane, they enable optimal gas exchange between the red blood cells in the blood and the air in the alveoli of the lung (Crapo et al.,1982).

Type 2 cells are the stem cells of the alveolar region producing different surfactant proteins, serve as progenitor cells and provide essential components of innate immunity (R J Mason, 2006). In addition, alveolar fibroblast cells are mainly responsible for ECM production and serve as effector cells during repair following an injury.

3.1.1. Electric Cell-Substrate Impedance Sensing (ECIS)

Electric cell-substrate impedance sensing (ECIS) is an automated submerged monotypic *in-vitro* 2D system- for the analysis of cellular effects of pollutants like

carbon nanoparticles. ECIS is a non-invasive biophysical approach employing AC signals to monitor living cells *in vitro*. Changes in the resistance offered by the adherent cells to current flow provide information about barrier integrity, cell morphology, etc. in terms of resistance, impedance, and capacitance.

We validated the system using Diesel exhaust particles, a form of carbon nanoparticle. The cell-material interactions were assessed by exposing the A549 cells to varying concentrations of DEP. The results were compared with endpoint analyses like 3-(4,5-Dimethylthiazol-2-yl)- 2,5-diphenyltetrazolium bromide (MTT), Lactate dehydrogenase (LDH), and Neutral red uptake (NRU) assays.

3.1.1.1. Diesel exhaust particle characterization

The morphology of DEP was characterized by Transmission electron microscopy. (JOEL JEM USA).

3.1.1.2. Impedance measurement with ECIS

ECIS (Applied Biophysics) was used to study the effect of diesel exhaust particles on A549 cells. Here array type- 8W10E+ (Applied Biophysics, NY, USA) consisting of eight wells was used. Each well has two sets of 20 circular active electrodes with 250 µm diameter located on inter-digitated fingers to provide measurements of 40 electrodes. The experiment was performed following the method described by Szuleck et al., 2014)

Before the experiment, the array holder was warmed to 37^0C in the incubator. 400µL of complete cell culture medium was added to each of the 8 wells. The arrays were placed on the station - the array holder. The connectivity and impedance of each well were checked. Electrodes were stabilized, and cell-free impedance was measured at 4000Hz.

After 1 h, the impedance measurement was paused and arrays were removed. The media in the wells were replaced with fresh F12K medium. A549 cells were seeded at a density of 10^4 cells per well. Impedance measurement was carried out till confluence. At confluence, impedance measurement was paused and the medium in the wells was replaced by DEP in F12k medium and incubated for another 24 h. The data was analyzed using Zθ ECIS analysis software. After normalization, the data were plotted against time.

3.1.1.3 Assessment of Cell viability

The MTT assay assesses the metabolic reduction of 3-(4,5-dimethylthiazol-2-yl)-2,5-diphenyl-tetrazolium bromide reagent to formazan crystals. Briefly, A549 cells (1×10^4) were seeded into each well of a 96-well plate and incubated overnight at 37^0C, 5% CO 2. Cells were treated with different concentrations of DEP (1, 10, 20, 40, 80, 160, 320 µg/mL) for 24 h. Following exposure, the medium was removed and cells were washed with PBS. 50 µg/well MTT solution in PBS was added to each well and incubated for 4h. Precipitated purple formazan crystals were dissolved with 100µl DMSO (ATCC, USA). Absorbance was read at 540 m (Synergy H1 Multimode reader, Bio-Tek Instruments Inc). Percentage viability was calculated by

$$\text{Viability\%} = A_{expt} - A_{blk} / A_{cnt} - A_{blk} * 100$$

A_{expt} = absorbance of the experimental group,

$A_{blk'}$ = absorbance of the blank group

A_{cont} = absorbance of the control group.

3.1.1.4 Assessment of Plasma membrane integrity

Lactate dehydrogenase (LDH) is a stable cytosolic enzyme released from cells only during the loss of plasma membrane integrity. LDH assay provides information about the intactness of the plasma membrane upon exposure to external stimuli.

A549 (1 × 10^4 cells) were seeded into each well of a 96-well plate and incubated overnight at 37^0C, 5% CO2. Cells were treated with different concentrations of DEP (1, 10 20, 40, 80,160,320 µgm/mL) for 24 h. LDH assay was done by using CytoTox96® non-radioactive cytotoxicity assay kit from Promega (Madison, USA). Cell control for maximum LDH release was provided by one set of cells treated with complete lysis solution for 45 min. 50 µL of the culture supernatant from all wells was transferred to a new 96-well plate to which 50 µL of the enzyme-substrate solution was added and incubated for 30 min. Stop Solution was added, and the absorbance signals were measured at 490 nm (Synergy H1Multimode reader).

3.1.1.5. Assessment of Lysosomal integrity.

Borenfreund and Puerner originally developed the Neutral red uptake assay, a simple and accurate method. The neutral red assay measures the lysosome integrity based on the uptake of vital dye neutral red by live cells. Briefly, A549 cells were seeded in a 96-well plate at a density of 1×10^4 cells/well and incubated at 37^0C overnight. 1% neutral red reagent was also prepared and incubated separately at 37^0C overnight. After incubation, A549 cells were treated with different concentrations of DEP 1, 10, 20, 40,80,160,320 µg/mL for 24h. After treatment, 10 µL of 1% neutral red was added to each well and incubated for 3h at 37^0C with 5% CO2. At the end of the incubation period, the dye was removed and the wells were washed with PBS. The dye entrapped inside the cell was solubilized using an acid-alcohol desorbing agent (1% glacial acetic

acid and 90% ethanol mixed V/V) and the plates were incubated in the dark for 30 min. Absorbance was read at 540 nm in the Synergy multimode reader.

3.1.2. Heterotypic Co-Culture Air-Liquid Interface System

Alveolar epithelial cells are the initiators of fibrotic response and fibroblasts are the effectors of fibrosis. An in-vitro system suitable to study fibrosis should contain the initiator as well as the effector. Hence a co-culture system capable of simulating the alveolar region was developed. Fibrosis is a chronic response, and as such an invitro system developed to study fibrosis should maintain the structural and functional integrity in culture for a longer period. Therefore, the developed co-culture system was assessed for integrity in long-term culture.

3.1.2.1 Development of heterotypic co-culture Air-liquid Interface system

For better simulation of in-vivo conditions, an air-liquid interface co-culture system was developed. A549 cells and WI38 cells maintained in complete F12K medium and DMEM supplemented with FBS and antibiotics were used in this study.

The heterotypic co-culture system was designed with human epithelial type II cells (A549 cell line) on the apical part and human lung fibroblasts (WI-38) on the bottom part of a transwell insert. Co-cultures were formed by adapting protocols previously published (Lehman et al.,2010; G. Hilton et al.,2018) with some modifications. Briefly, WI-38 cells cultured in DMEM complete media supplemented with 10%FBS, Gentamycin, and Amphotericin B at 37^0C 5%CO2 were seeded on the basal side of the BD Falcon inserts (6 well and 24 well-pore sizes 0.4 µm) in the inverted position

at a density of 10^4 cells/cm^2 (Final volume/support = 400µL). Then, the inserts with the cells were incubated for 3h at 37^0C, 5% CO2 in another plate using the bottom as the lid to allow cell adherence to the membrane. After incubation, transwell TM supports were washed in PBS and kept upright in a new plate. Subsequently A549 cells (cultured in F12K supplemented with 10% FBS, Gentamycin (50 mg/mL), and Amphotericin B (250 µg/ mL) and incubated at 37^0C, 5% CO2, were seeded to the apical side ($2.9x10^5$ cells/cm2). This co-culture model was under submerged culture for 4days covered with F12K in the upper and DMEM in the lower chamber of the insert (volume changes according to insert size). After 4 days, the culture was uplifted to the air-liquid interface by removing the medium from the upper chamber. The co-cultures were cultured for up to 15 days and the medium in the basolateral chamber was changed every 3 days. Cell numbers were fixed as per the observations made by Stone et al., 1992). This model system was compared with

(i) Air-Liquid interface cultures of A549 cells alone without WI-38 cells on the basal side of inserts

(ii) Submerged monocultures (covered with complete medium F12K) of A549 alone

(iii) Submerged co-culture (A549 and WI-38) grown in transwell inserts

3.1.2.2. Assessment of barrier integrity of the *invitro* system

Transepithelial electrical resistance (TEER) is an excellent indicator of barrier integrity. TEER of the developed *in-vitro* system was measured using an Evom2 Voltohmmeter equipped with 4 mm chopstick electrodes (World Precision Instruments

Inc., FL, USA). To measure TEER at the ALI, 1 mL of the corresponding medium was added onto the apical side of a 6-well insert. All TEER values were corrected for the resistance of a cell-free insert (≈130 Ω) and the surface area of a 6-well insert (4.67 cm2). Briefly, the transwell insert was placed in the volt ohmmeter chamber and the electrical resistance/potential difference was measured. This was repeated using a blank insert without cells, and the measurements were corrected by subtracting this value. The TEER was calculated by multiplying the measured resistance with the surface area of the inserts

3.1.2.3. Assessment of Permeability of the *invitro* system

Permeability studies of co-cultures were carried out by the method described by Ren H, Birch N, and Suresh V. (2016). Paracellular transport of sodium fluorescein (MW = 367 Da) was used to assess barrier integrity.

The co-culture system was developed as described in section 3.1.2.1 in a 24-well transwell plate. After uplifting to the air-liquid interface, the culture medium was removed from the basolateral compartment, and the monolayer was washed twice with warm HBSS (37^0C). 1.5 mL of HBSS was added to the basolateral compartment and plates were then returned to the incubator at 37^0C for 30 minutes to equilibrate. Sodium fluorescein (0.5 mL of 10 µM in HBSS) was added to the apical chamber. 100 µL samples from each well were taken from the basolateral compartment at every 30 min interval up to 120 min. An equal amount of fresh and warm HBSS was added. After confirming the linear diffusion of sodium fluorescein, samples were taken at 0, 30, and 60 minutes to measure the permeability. The fluorescence of the samples was

measured in black, 96-well plates using the Synergi multimode system with excitation and emission wavelengths of 460 nm and 515 nm, respectively. The concentration of fluorescein in the basolateral compartment was calculated and plotted as a function of time. Permeability coefficients P app were calculated using the equation

$$\boldsymbol{P\ app} = \left(\frac{\mathbf{dC}}{\mathbf{dt}}\right) * \frac{\mathbf{V}}{\boldsymbol{A*C0}}$$

dC/dt = slope of a linear fit to concentration vs. time plot,

V = volume of HBSS in the receiver chamber,

A = surface area of the membrane (1.12 cm2), and

C0 = concentration of fluorescein added to the donor (apical) compartment (10 μM).

3.1.2.4. Assessment of structural and functional integrity of the *invitro* system

The structural and functional integrity of the above-detailed in-vitro system was assessed by actin and Surfactant Protein C (SPC) immunostaining. The transwell membranes were fixed in 4%PFA (paraformaldehyde) at room temperature for 15min. Washed in PBS for 3 min. The cells were permeabilized with 0.2%Triton-x 100 for 20min at room temperature and blocked in 5% serum in PBS at room temperature for 60 min. One set of membranes (5^{th}, 7^{th}, and 14^{th} day) was stained with rhodamine-phalloidin to assess cytoskeletal integrity. Another set of the membrane (14th day) was incubated with primary antibodies against SPC in PBS (1:500) at 4^0C overnight. Following washing with PBS for 3-10 min the membranes were incubated with FITC labeled anti-rabbit IgG antibodies(1:500) at room temperature. The membranes were

then incubated with Hoechst 33342, washed in PBS again, and covered with a coverslip. Images were acquired by Carl Zeiss Microscope and processed on Axiovision software.

3.2. PHASE II - CELL-MATERIAL INTERACTIONS

Carbon black nanoparticle (CBNP) was used in this part of the study. CBNP was selected owing to its economic importance and widespread occurrence.

The interactions of these nanomaterials on the major cell types of the alveolar compartment of the lungs were studied to understand the molecular cues leading to alveolar fibrosis and delineate the preponderance of the alveoli to an infectious challenge.

3.2.1. Characterization of the Nanoparticle

3.2.1.1. High-Resolution Transmission Electron microscopy (HRTEM)

The size and morphology of the CBNP were analyzed using HRTEM: JOEL/JEM2100 equipped with a LaB6 electron gun with a point resolution of 0.23nm and lattice resolution of 0.14nm operating at 200kV. The dispersed CBNP was deposited on a 300-mesh carbon-coated copper grid. After solvent evaporation, samples were observed under image mode. Selected Area Electron Diffraction (SAED) was used to qualitatively assess the nature of carbon black.

3.2.1.2. Hydrodynamic size determination of CBNP by Dynamic light scattering

Dynamic light scattering measures the intensity of the laser light that is scattered from dissolved macromolecules or suspended particles. Hydrodynamic sizes of particles can vary from their primary size. Hydrodynamic size and surface charge have a significant role in the biological responses elicited by the particle. The

hydrodynamic size was assessed by dispersing the CBNP in F12K medium supplemented with 10% FBS (CCM). 1 mg/ mL of CBNP was dispersed in CCM and transferred into a cuvette. Hydrodynamic diameter and dispersity of CBNP in solution (polydispersity index (PDI) were measured by DLS. This was carried out using Malvern Zetasizer 64 Nano ZS (UK).

3.2.1.3. Surface charge determination of CBNP by Zeta potential

Electrophoretic light scattering is used to assess the Zeta potential or surface charge of CBNPs. 1 mg/ mL of CBNP was dissolved in CCM and transferred into a cuvette and surface charge was assessed using a Zetasizer Nano ZS (Malvern, 52 USA) instrument

3.2.2 Short-term exposure of alveolar cells to CBNP

Cellular response to short-term exposure to CBNP was studied at the morphological, biochemical, and molecular levels in cell lines A549, WI-38, and THP1. The summary of this phase is depicted in Fig: 3.2

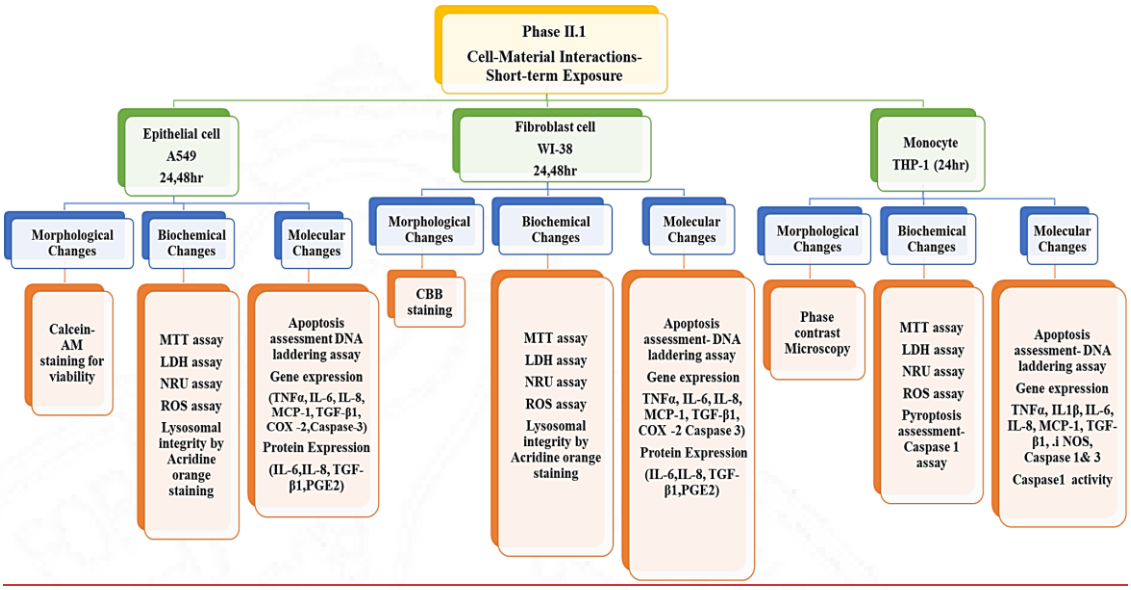

Fig:3.2 Flow chart representing the summary of the first sub-phase of Phase II. Cell-Material-interactions on Short- term exposure to CBNP

3.2.2.1. Common protocols used throughout the study

Some protocols were followed repeatedly throughout the study. Exposure conditions may differ but the method of assay followed is the same for all the cell lines (A549, WI-38, THP1) which will be described in this section.

3.2.2.1.1. MTT assay

MTT colorimetrically measures the activity of mitochondrial enzyme succinate dehydrogenase. 1X10^4 cells were seeded to each well of a 96-well plate and grown overnight in a complete cell culture medium (F12K with 10% FBS and antibiotics). Cells were then treated with different concentrations of Carbon black nanoparticles (1,5,10,20,40,80,160 µg/mL) for 24 h and 48h (24h for THP-1). At the end of the treatment period, the medium was removed and 100 µl of 5 mg/mL MTT reagent in 1X PBS was added in the dark, and the cells were incubated in a 37^0C incubator for 3-

4 h till violet color precipitates were visible. The cells were then solubilized by removing MTT and adding 50µl of DMSO. The absorbance was read at 540 nm using Synergy H1 multimode reader. Normal dividing cells processed similarly but without adding CBNP was the control.

$$Percentage\ viability = \left(\frac{A\ expt - A\ blk}{A\ cnt - A\ blk}\right) * 100$$

A_{expt} = absorbance of the experimental group,

$A_{blk'}$ = absorbance of the blank group

A_{cont} = absorbance of the control group.

3.2.2.1.2. Lactate dehydrogenase assay

Lactate dehydrogenase (LDH) assay helps in the assessment of plasma membrane integrity by evaluating released Lactate dehydrogenase. LDH is a stable cytosolic enzyme released upon cell lysis. LDH assay was done using CytoTox 96® Non-Radioactive Cytotoxicity Assay kit (Promega). Release of LDH from damaged cells is measured by supplying lactate, NAD+(oxidized Nicotinamide adenine dinucleotide), and INT (iodonitrotetrazolium or 2-(4-iodophenyl)-3-(4-nitrophenyl)-5-phenyl-2H-tetrazolium) as substrates in the presence of diaphorase enzyme. The amount of red formazan color formed is proportional to the number of lysed cells.

In brief, 1 × 10 ^4 cells were seeded into each well of a 96-well plate. Cells were treated with different concentrations of CBNP (1,5, 10, 20, 40, 80,160 µg/mL) for 24h and 48 h (24 h for THP-1). One set of cells treated with complete lysis solution for 45 min served as cell control for maximum LDH release. 50 µL of culture supernatant from all wells was transferred to a new 96-well plate. 50 µL of enzyme substrate solution was added to each well and incubated for 30 min. LDH was assessed

using Promega cytotox96 ®non-radioactive kit. Stop Solution was added, and the absorbance signals were measured at 490nm using Synergy H1 multimode reader. Percentage cytotoxicity was calculated by equation,

$$\text{Percentage cytotoxicity} = 100 * \frac{\text{Experimental LDH release}}{Maximum\ LDH\ release\ (OD\ 490)}$$

3.2.2.1.3. Neutral Red Uptake assay (NRU assay)

The neutral red assay measures the lysosome integrity based on the uptake of vital dye neutral red by live cells. A modified protocol of Borenfreund and Puerner (1985) was followed. Briefly, cells were seeded in a 96-well plate at a density of 1x10^4cells/well and incubated at 37^0C overnight. Meanwhile, the neutral red reagent was also prepared and incubated at 37^0C overnight. The next day, cells were treated with different concentrations of CBNP 1, 10, 20 40,80,160 µg/mL for 24-48 h (24 h for THP-1). After treatment, 10 µL of 1% neutral red reagent was added to each well and incubated for 3 h at 37^0C with 5% CO2. At the end of the incubation period, the dye was solubilized and the wells were washed with PBS. The dye entrapped inside the cells was solubilized using acid alcohol desorbing agent (1% glacial acetic acid and 90% ethanol, 50% ethanol: V/V) and the plate was kept in the dark for 30 min. Absorbance was read spectrophotometrically at 540 nm (Synergy H1). The absorbance was normalized to control

3.2.2.1.4. Intracellular ROS by DCFHDA assay

The production of intracellular ROS (Reactive oxygen species) was determined by a fluorimetric probe, DCFH-DA (Dichloro dihydro fluorescein diacetate), which passively enters the cell. The resultant compound dichlorofluorescein (DCF) formed

from the reaction with intracellular ROS is highly fluorescent. Briefly, for the assay, cells were seeded at a density of 1×10^{4} cells/well and cultured for 24 h. Cells were exposed to different concentrations of CBNP (1, 5, 10, 20, 40, 80,160 µgm/mL) and ROS was assessed after 6h and 24 h. 0.09% hydrogen peroxide (H2O2) treated cells were used as the positive control. Untreated cells served as the negative control. After treatment, cells were washed with PBS and incubated with DCFH-DA (1µM) for 45 min in the dark, and excess DCFH-DA was removed and replaced with 200µL PBS. Fluorescence was measured using a microplate reader (Synergy Biotek) with excitation and emission at wavelength 485 and 535 nm, respectively.

Fold increase in ROS production was calculated by the following equation (Ling, LU., Tan, KB., Lin, H. et al., 2011).

$$Fold\ increase = \frac{F\ test - F\ blank}{F\ control - F\ blank}$$

F test = fluorescence readings from the particle-exposed wells

F blank = fluorescence readings from the F control represent the untreated cells

F control = fluorescence readings from the cells treated with H2O2 positive control

3.2.2.1.5. Acridine orange staining for lysosomal integrity

Acridine orange (AO) is a weak base capable of crossing plasma membranes and staining nucleic acids and lysosomes. This metachromatic dye can differentiate lysosomes (reddish-orange granules) from other cellular components (diffuse green) at low concentrations. Under acidic conditions, AO becomes protonated and gets trapped within lysosomes. AO accumulation in lysosomes leads to a shift in excitation from green to red (530nm to 620nm). AO becomes deprotonated on lysosomal membrane damage or with a rise in the pH of lysosomes and crosses back into the

cytoplasm which shifts the emission from red to green (Syed K. Sohaebuddin and Liping Tang, Volkmar Weissig, et al. (eds.)2013). Here we have used AO staining to assess the integrity of the lysosomal membrane of cells exposed to various concentrations of CBNP. Briefly, cells (1x10^6 cells in 500µL CCM/coverslip) were seeded onto coverslips placed in a 6-well plate. 3 mL complete medium was added to each well after 20 min of incubation. Then plates were incubated overnight, the medium was changed and exposed to various concentrations of CBNP (10, 20, 40, 80,160 µg/mL) for 24 and 48h. Meanwhile, acridine orange stock solution was prepared (1mg/mL) and stored at 4^0C. On the day of staining, a 5 µg/mL working solution was prepared in a cell culture medium. The culture medium was removed and cells were rinsed three times with 1 mL of 1X PBS. 2 mL of AO solution was added to each well and incubated for 15 min. Excess dye was washed with PBS and coverslips were imaged under the fluorescence microscope (Carl Zeiss Axiovision inverted trinocular research microscope).

3.2.2.1.6. DNA laddering Assay

DNA laddering is a sensitive assay to evaluate cytogenetic damage. DNA fragmentation is one of the hallmarks of apoptosis and is caused by activated nucleases.

The laddering assay was performed as per the protocol described by Rahbar Saadat Y et al., 2015. Briefly, $3x10^6$ cells were cultured in F12K medium in 60mm dia dishes at 37^0C overnight. The cells were exposed to CBNP (20, 40, 80, 160 µg/mL) for 48 h. Staurosporine (Sigma, USA) treated cells served as the positive control. The concentration and time point of exposure for the assay were fixed based on previous analyses. The cell culture medium was collected and centrifuged at 5000 rpm for

5 min., the supernatant was discarded and 500µL of lysis buffer was added (recipe described in appendix). Meanwhile, the plates were washed with PBS, and cells were harvested with 500 µL of lysis buffer after incubation at room temperature for 10 min. The harvested cells and pellet of centrifuged cells were pooled together, transferred to a new eppendorf, and incubated in a water bath set at 65 ^{0}C for 5 min. After cooling, 700 µL of chloroform-isoamyl alcohol (24:1) was added and centrifuged at 12000 rpm for 5 min. The aqueous phase was transferred to a new tube, and an equal volume of ice-cold isopropanol was added. After mixing by gentle inversion, the tubes were centrifuged again at 12000 rpm for 5 min. The supernatant was discarded, and the pellet was air-dried for 10-15 min. The dried pellet which was DNA was dissolved in 50 µL of autoclaved distilled water. The DNA was quantified spectrophotometrically using Nanovue (GE-healthcare, Chicago, Illinois, United States). Equal amounts of DNA from these samples were electrophoresed on a 1.5% agarose gel containing 0.5 µg/mL ethidium bromide in 1X TBE (Tris/Borate/EDTA). The gel was run at 5 V/cm for 1-2 h and the DNA bands were visualized using UV-transilluminator (Bio-Imaging system, Syngene, UK)

3.2.2.1.7. mRNA expression

3.2.2.1.7.a. RNA extraction

Total RNA was extracted from experimental groups using Trizol™ (Invitrogen). 0.3-0.4 mL trizol was added/10^{7} cells and mixed thoroughly to ensure complete cell lysis. After 5 min incubation at room temperature, 100 µL of chloroform was added to the lysate and incubated for 2-3 min. It was then centrifuged at 12000xg for 15 min at 40 ^{0}C. The upper aqueous phase was transferred to a new tube. RNA was then precipitated using 250 µL of isopropanol and centrifuged at 12000xg for 10 min at

40^0C. A gel-like pellet was obtained at the bottom of the tube. The pellet was resuspended in 5µL of 75%ethanol. The sample was vortexed and centrifuged at 4 ^{0}C at 500xg for 5 min. After discarding the supernatant, the pellet was air-dried. This pellet was resuspended in 10-50µL of RNase-free water. Purity was assessed using Nanovue (GE health care, Chicago, USA) by obtaining the ratio of absorbance at 260nm/280nm. A ratio of 1.5 -2 was considered pure and was further used for DNA synthesis, the first step in mRNA analysis. Less pure samples were re-extracted using trizol.

3.2.2.1.7.b. cDNA synthesis

Reverse transcription was carried out using a reverse transcription core kit (Origin diagnostics, India).

The reaction setup was as follows:

Reagents	**Volume**
#RNA+Primer (0.5µL)	1-2µL
5x RT reaction buffer (includes 10mM dNTPs)	2µL
8 mM DTT	0.5µL
Reverse Transcriptase	0.5µL
RNase inhibitor	10 µL
RNase free water	Made up to 20µL

Table: 1. Reagents used in cDNA synthesis and volumes used in each reaction. # Volume of RNA depends on the concentration of RNA.

The reaction conditions were set with initial incubation at 50 ^{0}C for 60 min in which reverse transcriptase is activated and c DNA synthesis is initiated and the final inactivation of reverse transcriptase with incubation at 95 ^{0}C for 5 min. (Thermal cycler-Bio-Rad Laboratories, Hercules, CA, USA)

3.2.2.1.7.c. Real-time polymerase chain reaction

Takyon™ was used for Sybr green qRT-PCR. The kit components and reaction volumes are mentioned in Table 2.

Reagent	**Volume used**	**Final concentration**
Takyon master mix	10 µL	1X
Forward primer	2 µL	50-300 nM
Reverse Primer	2 µL	50-300 nM
CDNA template	2 µL	-
Water	Made up to 20 µL	

Table: 2 Reagents used for RT-PCR. Equal volumes of cDNA templates were used for the study.

qTower^{3}G Real-time PCR (Analytik Jena, Japan) was used for qRT-PCR assays. Reaction setups are detailed in Table :3

Step	Temperature	Time
Takyon activation	95^0C	3min
Denaturation	95^0C	3 s
Annealing/ Extension	$50\text{-}60^0$C***	20-30 s
Go to step2 loop-39		
Melt curve analysis from $50\text{-}95^0$C		

Table: 3 RT PCR reaction conditions. *** annealing temperature was set according to the melting temperature - TM of primers.

m RNA expression was quantified by ΔΔCt method, with GAPDH as the internal control using the following formula: Ct is the cycle threshold

Δ Ct = Ct target-Ct reference gene

ΔΔ Ct was calculated as :

ΔΔ Ct= (Ct target–Ct reference) sample – (Ct target-Ct reference) control

Relative fold of target mRNA levels of treated with respect to control = 2 ^- ΔΔCt

3.2.2.1.8. Cytokine expression using Enzyme-linked immune sorbent assay (ELISA)

The cytokine expression was quantified from the supernatant of cells exposed to CBNP. The expression of inflammatory and pro-fibrotic cytokines was quantitatively

assessed using Enzyme-Linked Immuno Sorbent Assay kits (G biosciences-St. Louis, MO, USA). Cell culture supernatant was collected. Centrifuged at 2500 rpm for 20 min. Protein concentration was estimated by the Bradford method (Bradford, MM. 1976). An equal concentration of protein calculated from the standard graph was used for ELISA. ELISA kits were purchased from G Biosciences and the assay was performed as per the manufacturer's instruction.

Briefly, the samples (blank, standard, and test samples) were diluted as per the manufacturer's instruction and incubated in specific antibody pre-coated wells. After washing, wells were incubated with biotinylated antibodies. Streptavidin-HRP was added which binds to the biotinylated antibody. Unbound streptavidin-HRP was washed after incubation. The substrate solution was added and incubated for color development. The reaction was terminated by the addition of an acidic stop solution and the absorbance was read at 450 nm. The unknown concentrations were calculated from the standard curve.

3.2.2.2 Alveolar epithelial cell response in the short-term exposure (up to 48 h)

3.2.2.2.1. Morphological changes

Morphological change and Viability of cells after particle exposure was assessed by Mammalian Live/Dead ™ viability/ cytotoxicity test kit (Molecular probes) as per instructions provided by the manufacturer. The assay discriminates live cells from dead cells by simultaneously staining with green-fluorescent calcein-AM to indicate intracellular esterase activity and red-fluorescent ethidium homodimer-1 to indicate loss of plasma membrane integrity. Hence live cells will appear green and dead cells red.

Briefly, A549 cells after CBNP (10, 20, 40, 80, 160 µg/mL) exposure for 24 and 48 h were washed gently with PBS (x3 times). Depending on the surface area 50-100µL of staining solution (0.5 µL of Calcein AM +2 µL of Ethidium bromide homodimer 1 in 1mL PBS) was added and incubated for 30 min and imaged using Carl Zeiss Axiovision inverted trinocular research microscope.

3.2.2.2.2. Biochemical changes in A549 on short-term CBNP exposure

The biochemical changes in A549 were assessed by MTT assay, LDH assay, Neutral red uptake (NRU) assay, ROS assay, and Acridine orange staining following the protocols described in earlier sections (3.2.2.1.1 to 3.2.2.1.5)

3.2.2.2.3. Molecular changes in A549 on short-term CBNP exposure

Molecular changes assessed in A549 cells exposed to CBNP for short-term duration include

- **Assessment of Apoptosis by DNA laddering assay**
- **mRNA expression (**TNFα, IL-6, IL-8, MCP-1, TGF-β1, COX -2 and Caspase 3) by q RT-PCR
- Cytokine expression (IL-6, IL-8, TGFβ, PGE2) by ELISA

The molecular changes were assessed following the protocol described earlier (Sections 3.2.2.1.6- 3.2.2.1.8).

3.2.2.3 Fibroblast cell response to short-term exposure to CBNP

3.2.2.3.1 Morphological changes

Coomassie brilliant blue (CBB) staining developed by Pena (1980) was done to assess the morphological changes in fibroblast cultures with some modifications. For staining, WI-38 cultures / grown on glass coverslips (1x10^6 cells/coverslip) were

exposed to CBNP. After CBNP exposure (10, 20, 80, 160 µg/mL) for 24 and 48 h cells were fixed in 3% glutaraldehyde for 15 minutes in PBS. The coverslips were then immersed in the CBB staining solution for 1 hour, rinsed several times in water, air dried, and imaged using a light microscope (Olympus BX43, Japan).

3.2.2.3.2. Biochemical changes

The biochemical changes in WI-38 cells were assessed by MTT assay, LDH assay, Neutral red uptake (NRU) assay, ROS assay, and Acridine orange staining following the protocols described earlier (3.2.2.1.1 to 3.2.2.1.5)

3.2.2.3.3. Molecular changes

Molecular changes assessed in WI-38 cells exposed to CBNP for short-term duration include

- **Assessment of Apoptosis by DNA laddering assay**
- **mRNA expression (**TNFα, IL-6, IL-8, MCP-1, TGF-β1, COX -2 and Caspase 3) by q RT-PCR
- Cytokine expression (IL-6, IL-8, TGFβ, PGE2) by ELISA

The protocol followed for each analysis is described in Sections 3.2.2.1.6 to 3.2.2.1.8

3.2.2.4. Monocyte cell-THP1 response to Short- term CBNP exposure

3.2.2.4.1. Morphological changes

Morphological changes in THP1 cells were assessed by Phase contrast Microscopy THP-1 cells (1X10^6 cells) were seeded into each well of 6 well plates in Complete RPM1-1640 media supplemented with FBS. After overnight incubation, cells were exposed to CBNP (20, 40, 80, 160 µg/mL) for 24 h. Then the plates were centrifuged (Remi)at 1000rpm for 3 min and the pellet was washed in complete media and dropped into coverslips for Phase contrast imaging (Zeiss Axiovision)

3.2.2.4.2. Biochemical changes

3.2.2.4.2.1. The biochemical changes in THP-1 cells on short-term CBNP exposure were assessed by MTT assay, LDH assay, Neutral red uptake (NRU) assay, and ROS assay following the protocols described earlier (3.2.2.1.1 to 3.2.2.1.4)

3.2.2.4.2.2. Expression of Caspase 1 activity

Caspase 1 assay of THP1 cells exposed to CBNP was done by using a Caspase -1 Glo® 1 -Inflammasome assay kit (Promega, WI, USA). First, the reagents were equilibrated to room temperature and then reconstituted the reagents. The assay was performed as per the kit protocol. Cell culture media without cells served as blank and unexposed cells served as the negative control in the assay.

Briefly, the cells were seeded in 96 well plates and exposed to CBNP for 24hrs. The treated groups were split into two. To one-half of the wells 100µL Caspase -1 Glo® reagent was added. To the other half of Caspase, -1 Glo®YVAD-CHO (inhibitor of caspase 1) was added. After sealing the plate, the plate was shaken at 400 rpm for 30s. Then the plate was incubated at room temperature for 1h for the stabilization of luminescence. The luminescence was read at 60, 90 and 120 min respectively. The background was subtracted from the experimental and control groups and luminescence intensities were plotted.

3.2.2.4.3 Molecular changes

Molecular changes in THP-1 assessed include:

- **Assessment of Apoptosis by DNA laddering assay**
- **mRNA expression (**TNFα, IL-6, IL-8, i NOS, MCP-1, TGF-β1, COX -2, IL-1β, Caspase1, and Caspase 3) by q RT-PCR

The protocol followed for each analysis is described in Sections 3.2.2.1.6 and 3.2.2.1.7

3.2.3 Long-term exposure of alveolar cells to CBNP up to 120 h

Cellular response to short-term exposure to CBNP was studied at the morphological, biochemical, and molecular levels in cell lines A549, WI-38, and THP1. The summary of this phase is represented in Fig: 3.3

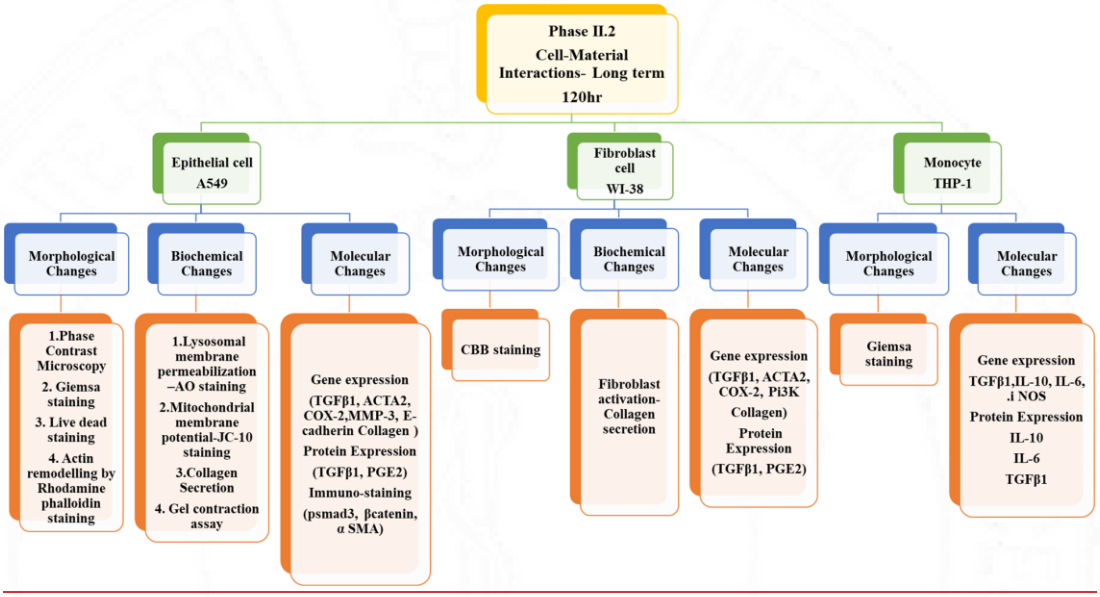

Fig: 3.3 Flow chart illustrating a summary of Phase II.2. Cell-Material - Interactions on Long -term exposure to CBNP.

3.2.3.1 Exposure conditions

A549, WI-38, and THP1 cells were seeded at a concentration of 1x10^5 cells/well in a 24-well plate in complete cell culture media. After overnight incubation at 37^0C, 5% CO2, media were changed and cells were exposed to low concentrations(1-20µg/mL) of CBNP, which was marked as day 1. Media was changed to cell culture media with reduced serum concentration (2.5%). Secretion of TGFβ1 cytokines will be stimulated

in reduced serum conditions or under serum starvation. Here we have used reduced serum-containing media for further experiments. On day 2 again, the medium was changed and exposure conditions were repeated. After 120 h of exposure or on day 5 we observed a change in morphology.

For all the cell types, the experimental conditions were the same for prolonged exposure. The schematic representation of the exposure conditions is depicted in Fig:3.4

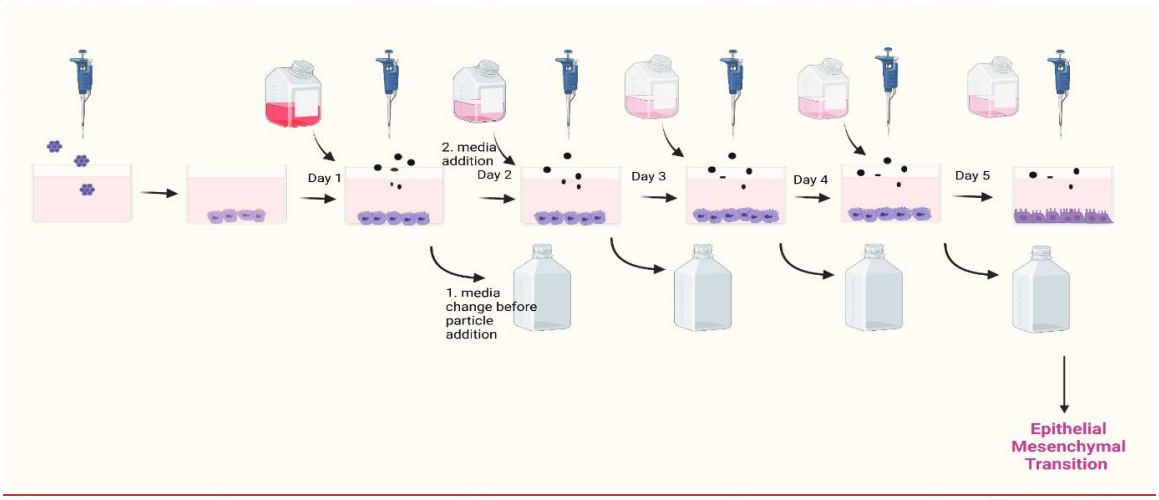

Fig 3.4 Schematic representation of prolonged exposure of CBNP to alveolar epithelial cells.

3.2.3.2 Alveolar epithelial cell response to long-term exposure to CBNP

3.2.3.2.1 Morphological changes

3.2.3.2.1.1. Phase contrast microscopy

A549 cells were seeded into a 24-well plate. The exposure conditions were as described in section 3.2.3.1. The change in morphology was assessed under a phase contrast microscope (Zeiss Axiovision)

3.2.3.2.1.2. Giemsa staining

The cellular morphology of A549 cells was studied using Giemsa staining. The cells were seeded on a cover glass placed in a six-well plate at an initial density of 1×10^6 cells per we l. After prolonged exposure to CBNP, Cells were washed with ice-cold PBS and fixed using 4 % formaldehyde for 15 min. The cells were then stained with 10 % Giemsa solution for 5 min. After washing with PBS, slides were observed under a light microscope (Olympus).

3.2.3.2.1.3. Live dead staining by calcein AM-EthD1

The viability of A549 cells after long-term CBNP exposure was assessed by Calcein AM-EthD1 Mammalian live-dead assay kit. The methodology followed is described in section 3.2.2.2.1.

3.2.3.2.1.4. Actin remodelling by Rhodamine Phalloidin staining

F-actin staining was done using rhodamine phalloidin. Briefly, cells both control (CBNP Unexposed) and test (CBNP exposed) cells (1x10^4 cells/Coverslips) were washed in PBS and fixed with 3.7% formaldehyde solution in PBS for 10 min at room temperature. Triton X-100 in PBS was added and incubated for 3-5 min. Cells were incubated with 5µL methanolic stock solution of the fluorescent phallotoxin in 200µL PBS was added and incubated for 20 min at room temperature. Excess stain was washed with PBS and counterstained with Hoechst 334352. After washing off the excess counterstain with PBS, images were acquired using a fluorescence microscope (Carl Zeiss- Axio vision).

3.2.3.2.2 Biochemical changes in A549

3.2.3.2.2.1 Lysosomal membrane permeabilization in A549 cells

Lysosomal integrity of A549 cells after prolonged exposure to CBNP was assessed by Acridine orange staining. The methodology followed is described in section 3.2.2.1.5.

3.2.3.2.2.2 Mitochondrial membrane potential of A549 cells

Mitochondrial membrane potential (MMP-($\Delta\psi$M) is one of the key parameters of mitochondrial health and function. Change in MMP was analyzed by JC10 probe (5, 5′, 6, 6′tetrachloro-1, 1′, 3, 3′- tetraethyl benzimidazolyl carbocyanine iodide). JC-10 is a cationic, lipophilic dye that accumulates in the mitochondria in a potential-dependent manner. The dye forms reversible red-fluorescent JC-10 aggregates inside energized healthy mitochondria with high membrane potential (540/590nm). When the membrane potential collapses, the cells fail to retain the dye and the dye returns to its monomeric green form in the cytoplasm (490/525nm). In brief, the cells were seeded at an initial seeding density of 5x10^5 cells/ coverslip per well in a 6-well plate and exposed to CBNP for a prolonged time at varying concentrations. After exposure to the CBNP, the cells were washed twice in PBS and were incubated for 30 min at 37^0C with 1 µM JC-10 dye. The cells after washing with PBS were observed under a fluorescence microscope (Axio Scope.A1, Carl Zeiss, Germany) using green and red filters.

3.2.3.2.2.3 Collagen quantification by Sirius red

Collagen estimation from EMT cells was done by the protocol described by Keira SM et al.,2004. The essay is divided into two sub-methods (1) the extraction of collagen from the cellular layer and the culture medium; and (2) The precipitation of chromogenic reaction between collagen and the dye Sirius Red. For the assay, A549

cells were seeded at a density of 1x10^6 cells /dish in a 60mm cell culture dish and exposed to CBNP for a prolonged time as described in the previous section.

3.2.3.2.2.3.1. Collagen extraction

Total protein and collagen from the cellular layer were extracted by the addition of a protein extraction solution after rinsing the culture with PBS. The extraction solution preparation is described in the appendix. The cellular layer was scraped at 4^0C. Total protein was extracted from the layer by sonication of the layer (3x15s, 30-sec interval, 20Hz at 4^0C). The sonicated extract was used for collagen precipitation with 25% ammonium sulfate for 24 h at 4^0C under constant agitation. Then collagen was isolated by centrifugation at 40000g for 30 min at 4^0C. The supernatant was discarded and the pellet was solubilized in 2 mL acetic acid (0.5M). The collagen in the culture medium was precipitated as in the cellular layer with 25% (NH4)2SO4 for 24 hours at 4^0C, under constant agitation. The solution was then centrifuged at 40000xg,30min at 4^0C. The pellet was collected and solubilized in acetic acid (2 mL,0.5M) collagen extract quantified.

3.2.3.2.2.3.2 Collagen chromogenic precipitation with Sirius Red

500 µL of collagen extract aliquots were transferred to Eppendorf tubes and collagen was precipitated with 1mL 0f 50 µM Sirius Red in acetic acid (0.5M). After giving a short spin, eppendorfs were kept in a resting position for 30 min at room temperature. The eppendorfs were then centrifuged at 30000xg for 30 min. The pellets were eluted in 1mL 0.1N potassium hydroxide (KOH). The absorbance was determined spectrophotometrically at 540nm. Rat tail collagen type1 in acetic acid was used for plotting the standard curve

3.2.3.2.2.4. Collagen gel contraction assay

Contractility is a characteristic function of fibroblasts. During EMT, the epithelial cells acquire mesenchymal characteristics. Here we have assessed the contractility of CBNP-exposed epithelial cells that underwent EMT by a collagen-based contraction assay. The procedure assesses the contraction of cells embedded in type I collagen gel three-dimensionally. It is considered an ideal tool for the evaluation of contractility. A modified protocol of Mikami. Y et al.,2016 was followed for the assay. Instead of direct CBNP treatment, here we have used a conditioned medium of CBNP-exposed A549 cells for the assay.

Briefly, Cell culture medium from days 1-5 of CBNP-exposed A549 cells was collected and stored at -800 C. Meanwhile, A549 cells at a density of 1x10^6 cells/dish were seeded on 6 well culture plates with 3 mL cell culture medium. Once the wells were confluent, the culture medium was aspirated and cells were trypsinized with 0.05% Trypsin/EDTA. The cells were collected by centrifugation at 150xg for 4 min at room temperature. Simultaneously, Collagen type 1 gel was mixed with 4x concentrated culture medium and kept in ice. The cell density was checked and the gel medium was added to the cells to achieve a density of 3x10^5 cells/well (6.0 × 10^5 cells/mL) gently and quickly. 500 µL of the mixture was dispensed into each well of a 24-well non-treated plate without air bubbles and incubated the plate for 15 min at 37^0C. Once the gel was set, it was transferred to a 60mm tissue culture dish containing conditioned medium of CBNP-exposed A549 cells collected previously along with reduced serum-containing medium in the ratio 2:1. The dishes were returned to incubator and medium (conditioned medium+reduced serum-containing medium) was

changed every day. The collagen gel size was measured from day1-day5 using a gel documentation system (Syngene).

3.2.3.2.3 Molecular changes in A549 cells after prolonged CBNP exposure

Molecular changes assessed in A549 cells exposed to CBNP for long-term duration include

- mRNA expression of cytokines TGFβ, ACTA2 (α-smooth muscle actin), COX-2 (Cycloxygenase-2), MMP (Matrix metalloprotease), TIMP (Tissue inhibitors of metalloprotease), E-cad (E-Cadherin), Collagen1 were assessed by q RT-PCR. The methodology is described earlier (3.2.2.1.7)
- Cytokine expression (PGE2, TGFβ) was assessed by ELISA (3.2.2.1.8)

3.2.3.2.4 Unravelling the Signalling cascades by Immunostaining

Phosphorylation of smad3, nuclear translocation of β- catenin, and expression of α-smooth muscle actin are hallmarks of epithelial-mesenchymal transition. Here we have assessed the canonical TGFβ-smad3-signalling by immunostaining of psmad3, β-catenin, and α-smooth muscle actin. Briefly, A549 cells after prolonged exposure to CBNP (1x10^4 cells/ coverslip in each well of 6 well plates) were fixed in 4%PFA at room temperature for 15 min. Washed in PBS for 3 min. The cells were permeabilized with 0.2%Triton-x 100 for 20 min at room temperature and blocked in 5% serum in PBS at room temperature for 60 min. The membrane was then incubated with Primary antibodies against psmad3, β catenin, and α smooth muscle actin in PBS (1:500) at 4^0C overnight. Following washing with PBS for 3-10 min the membranes were incubated with FITC labeled anti-rabbit IgG antibodies(1:500) at room temperature. The

membranes were then incubated with Hoechst 33342 (1:2000 dilution in PBS), Was ed in PBS again, Inverted, and placed in a glass slide. Images were acquired by Carl Zeiss Microscope and processed on Axiovision software

3.2.3.3 Fibroblast response on long-term (120 h) exposure to CBNP

3.2.3.3.1 Morphological changes

Coomassie brilliant blue staining was done to assess the morphological changes in fibroblasts after prolonged CBNP exposure (3.2.2.3.1)

3.2.3.3.2 Biochemical changes

Extracellular matrix synthesis and secretion is the prime role of Fibroblast cells. The activation of fibroblasts is marked by this character. Fibrosis is characterized by uncontrolled proliferation and activation of fibroblasts. Collagen secretion from fibroblast cells after prolonged CBNP exposure was assessed as a marker of fibroblast activation (3.2.3.2.2.3)

3.2.3.3.3 Molecular changes

Molecular changes were assessed by

- m RNA expression (TGFβ, ACTA2, COX2, Collagen 1,PI3K) was assessed by q RT-PCR
- Cytokine expression was quantified by ELISA. The methodology is described earlier (3.2.2.1.7.- 3.2.2.1.8)

3.2.3.4 Monocyte response on long-term exposure (120 h) to CBNP

3.2.3.4.1. Morphological changes

Morphology change in THP1 after prolonged exposure to CBNP was assessed by Giemsa staining (3.2.3.2.1.2)

3.2.3.4.2. Molecular changes

m RNA expression (TGFβ, IL-6, IL-10, i NOS) was assessed by q RT-PCR. Cytokine expression (IL-10, TGF-β) was assessed by ELISA.

3.3 Phase III: Study the effect of All-Trans Retinoic Acid (ATRA) as a therapeutic molecule

All trans-retinoic acid is an active metabolite of vitamin A, which can regulate the proliferation and differentiation of various cell types. Previous reports suggest ATRA can upregulate surfactant synthesize in alveoli epithelial cells on cellular insult (George UM, Ashna U, Kumar SS, Nandkumar AM 2013) Here we have assessed the antifibrotic potential of ATRA on the initiator and its effector cells of fibrosis precisely the epithelial and fibroblast cells.

3.3.1. The effect of All trans-retinoic acid on cellular viability

A549 cells (F12k) and WI-38 (DMEM) cells were cultured in separate 96-well plates (1x10^4 cells/well). After overnight incubation in the complete cell culture media supplemented with FBS (10%), the media in cell culture was replaced with reduced serum (1% FBS). After 3 h cells were treated with 0.1, 1, and 10µM concentrations of ATRA in reduced serum media (F12K for A549 and DMEM for WI-38). The cell viability was assessed by MTT assay

3.3.2 Plasma membrane integrity

A549 cells and WI-38 cells were exposed to ATRA. The culture supernatant after ATRA exposure was collected and LDH assay was carried out.

3.3.3 Effect of ATRA on the Functionality of A549 cells

0.1 and 1µM ATRA-treated A549 cells were exposed to CBNP. Two sets of cells at a seeding density of 1x10^6 cells/well were maintained in 6well plates. One set plate was pre-treated with ATRA and then exposed to CBNP (120 h) at concentrations that elicited a significant EMT in A549 cells. Cells in the second set of plates were first exposed to CBNP for a prolonged time (120 h) and then exposed to CBNP. m RNA expression of SPC and inflammatory cytokines were assessed by qRT-PCR. Cytokine expression of TGFβ1 and PGE2 were quantified by ELISA.

3.3.4 Effect of ATRA on fibroblast activation

Collagen gel contraction was done to assess the contractility of ATRA pre-treated WI-38 cells exposed to CBNP. mRNA expression of TGFβ1, α SMA, Collagen, PI3K were assessed by qRT-PCR. Protein expression of TGFβ1 and PGE2 were assessed by ELISA

3.4 Phase IV. Cell-material-Microbial interactions.

In this section, the effect of CBNP on the pathogenicity of *Pseudomonas* a common respiratory pathogen was analyzed in the **first part**. In the **second part**, the effect of CBNP on the susceptibility of A549 cell monolayers to infection by *Pseudomonas* was analyzed. The **final part** attempted to understand the paracrine signalling mechanism on cell-cell-microbial interaction subsequent to CBNP exposure when challenged with a bacterial pathogen. This was achieved by treating the CBNP-exposed alveolar cells with conditioned media of *Pseudomonas* lysate-treated immune cells (THP1). The summary of phase III is depicted in **Fig:3.5**.

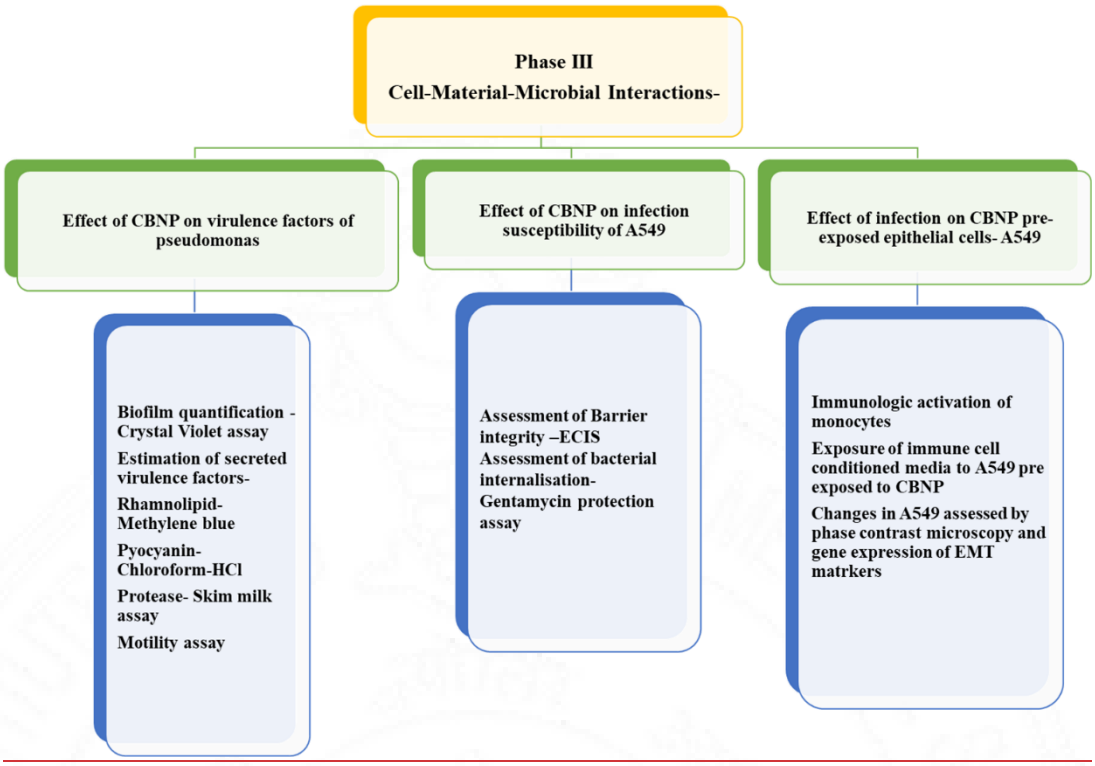

Fig:3.5 Flow chart representing summary of phase III. Cell-material-microbial interactions.

3.4.1 Effect of CBNP on virulence factors of Pseudomonas aeruginosa

3.4.1.1 Bacterial Strains and culture conditions

P. aeruginosa ATCC 27853 was obtained from the American-type culture collection. The cultures were cryopreserved in Soyabean casein digest medium (TSB) containing 15% glycerol as cryoprotectant. The cultures were revived in TSB and maintained in soybean casein digest agar (TSA) slants and stored at 4^0C for a month. Once revived, the isolates were used up to 5 passages by subculture. For CBNP exposure studies, 100µL of overnight cultures in TSB adjusted to an OD of 1 at 600nm were transferred to 96 well plates. CBNP diluted in bacterial culture media was added at different concentrations (1,5,10,20,40,80,160 µg/mL). The plates were incubated

for varying time points. All microbial culture reagents used for the study were purchased from Himedia, India.

3.4.1.2 Biofilm quantification by Crystal Violet assay.

The ability of *Pseudomonas* strains to form biofilms in the presence of CBNP was assessed by Crystal Violet (CV) assay as described by O.Toole, with slight modifications (O'Toole,2011). After CBNP exposure to *Pseudomonas* (3.4.1.1), the medium from each well was removed, washed with PBS thrice, and stained with 0.1%Crystal violet. After 15 min incubation, the unbound stain was washed off with PBS thrice. The bound CV was eluted with 95% ethanol. An uninoculated culture medium was used as a negative control. Absorbance at 600nm was measured using Synergy H1multimode reader (BioTek USA).

3.4.1.3 Estimation of secreted virulence factors

3.4.1.3.1 Estimation of Rhamnolipid by methylene blue

Rhamnolipids were quantified by the method described by Rasamiravaka et al.,2016. After the exposure of *Pseudomonas* to varying concentrations of CBNP and incubation for 48 h, the pH of the *P. aeruginosa* culture supernatant was adjusted to 2.3 using 1 N HCl. Rhamnolipid extraction from 500 µL supernatant was done using 500 µL of ethyl acetate. The extraction was repeated thrice, supernatants were pooled, and centrifuged at 10,000 rpm for 10 min, and the pellet was air dried to remove ethyl acetate. The air-dried samples were mixed with 1 mL of chloroform containing 100 µL of methylene blue and incubated at 25°C to 28°C for 15 min. 0.2 M HCl was added to the mixture, vortexed, and centrifuged at 10,000 rpm for 10 min. Rhamnolipid collected by the same method from nanoparticle unexposed bacterial culture served as

control. The absorbance of the aqueous phase was measured at 630 nm using the multimode reader.

3.4.1.3.2 Estimation of Pyocyanin by Chloroform-HCl method

Pyocyanin was estimated from an acidified solution of culture supernatant following the method of Essar et al.,1990. After the exposure of *Pseudomonas* to varying concentrations of CBNP and incubation for 48 h, culture supernatant was collected. 450 µL of chloroform, and 150 µL 0.2 M HCl was added per mL of the culture supernatant, vortexed, and centrifuged at 10,000g (2 min at 4^0C). The absorbance of the pink-colored upper aqueous layer was measured at 520 nm using the multimode reader. An aqueous layer of *P. aeruginosa* culture unexposed to CBNP was used as a control.

3.4.1.3.3. Estimation of Protease by Skim-milk assay

Protease secretion was estimated from culture supernatants of biofilms by the method described by El-Mowafy et al.,2014. Briefly, 500 µL of cell-free supernatant of the *Pseudomonas* culture after CBNP exposure was added to 1 mL of 1.25% w/v skimmed milk solution and incubated at 37^0C for 30 min. The turbidity formed by protease activity was measured at 600 nm using the multimode reader (BioTek USA). Protease secretion from unexposed bacterial culture served as control.

3.4.1.3.4 Effect of CBNP on the motility of *P. aeruginosa*

Swimming motility is a unicellular behaviour that requires a functional polar flagellum. The plate-based swimming motility assay measures the degree of this flagellar-dependent motility of the bacterium. Motility was assessed in 0.3%agar plates. Plate preparation for Motility assay is described in the appendix. A small volume of CBNP-exposed *P. aeruginosa* cultures after 48 h incubation was stabbed

into the agar layer of the plate. Care was taken not to reach the base of the Petri plate. The plates were incubated upright at 37^0C for 24 h. Bacterial culture unexposed to CBNP served as control.

3.4.2 Effect of CBNP on infection susceptibility of A549.

This phase of the study focuses on understanding the effect of carbon blank on the infection susceptibility of alveolar epithelial cells. Suitable tools in assessing this triagonal interaction of cell-material-microbe are a major problem. Hence we studied this interaction using a real-time non-invasive method, ECIS-Electric cell-substrate impedance sensing. ECIS is an impedance-based method to study cell response to external stimuli

Tight junctions of AECs (alveolar epithelial cells) provide cellular sealing which is integral to the maintenance of the AEC barrier integrity. Bacterial pathogens breach the epithelial lining integrity to feed on nutrients and disseminate deeper into tissues. In defense against these pathogens, the epithelium has multiple layers of microbial sensing and innate defense systems built in that act as countermeasures against microbial invasion.

3.4.2.1 Assessment of Barrier integrity of CBNP pre-exposed A549 cells upon bacterial infection using ECIS

The changes in barrier integrity of CBNP-exposed cells on *Pseudomonas* infection were assessed using ECIS. Before starting the experiment the array holder was warmed to 37^0C. 400µL of complete cell culture medium was added to the 8Well. The connectivity and impedance of each well were checked. The electrodes were stabilized, and cell-free measurements were taken at multiple frequencies (MFT). After the measurements were paused, Cells were seeded to each well at a density of

10^4 cells/well. Measurements were re-started and once the impedance plateaued the cells were exposed to varying concentrations of CBNP for 24 h. After exposure, the measurement was paused again and the medium was changed to F12K without antibiotics, and cells were infected with *Pseudomonas* at a Multiplicity of infection 50:1(Bacteria: cell ratio) and impedance measurement was resumed. Following 24 h infection, the experiment was stopped and results were assessed using Z theta software.

3.4.2.2 Assessment of bacterial internalization by Gentamicin protection assay

Internalization of bacteria was assessed by gentamicin protection assay. Gentamicin cannot penetrate the eukaryotic cell and kill internalized bacteria. This helps in differentiating bacteria that succeed in penetrating eukaryotic cells and those that could not. On losing cell membrane integrity more bacteria will be internalized. Cells after CBNP exposure was infected with *Pseudomonas*. The cells were washed with PBS thrice and treated with 100 µg/mL concentration of Gentamicin for 20min at 37^0C. The cells were lysed using 0.1%triton X-100. Cell lysates after serial dilution were plated on soybean casein digest agar and incubated overnight at 37^0C. Colony-forming units were counted and plotted.

3.4.3 Effect of infection on CBNP-exposed A549 cell

On bacterial invasion, immune cells are recruited to the site of infection. The immune cells secrete a plethora of mediators like cytokines and growth factors. The effect of this secretome in a pro-fibrotic milieu needs to be studied. Repeated injury and persistent inflammation together with defective repair mechanisms favor excessive fibroproliferation. This part of the study focused on understanding those multicellular interactions and the influence of paracrine signaling in the onset of fibrosis. The immune cell

3.4.3.1. Establishing optimal immunologic activation of immune cell

To initiate a signaling cascade optimal immunologic activation of immune cells should be established. Optimal activation of immune cells (THP1) is considered to be achieved in the treatment of the cells with a particular amount of bacterial lysate which should retain the viability of the cells and at the same time secrete cytokines at a concentration enough to activate downstream signaling cascades.

3.4.3.2. *P. aeruginosa* lysate preparation

A modified protocol of Borthwick et al., 2010 was followed . ATCC 27853 Strains were grown overnight on TSB, harvested into PBS, and OD was adjusted to 0.2 (600 nm). Before incubation with deoxyribonuclease II (200 mg/mL) at 37^0C for 1 h, the suspension was sonicated at an amplitude of 10% for 3 min on ice) and Lysates were then treated with proteinase K (2 mg/mL) at 60 ^{0}C for 2 h, and boiled for 20 min (inactivating proteinase K) and stored at -80 ^{0} C before exposing to cells.

3.4.3.3. Immunologic activation of immune cells

THP-1 cells (1×10^6 cells/mL) were activated with *P. aeruginosa* lysate by treating the cells with various concentrations of lysate (12.5, 25, 50,100,200, 400 µL/mL) for 6h (Borthwick et al.,2010). Viability was assessed using the MTT assay. Immunologic activation was assessed by quantifying the Cytokine expression (IL-8, IL1β, and TNF α) in supernatants by ELISA.

3.4.3.4. Understand the influence of Paracrine signalling

THP-1 cells (1×10^6 cells/mL) after *P. aeruginosa* lysate (12.5 µL·mL−1) activation for 6h were pelleted, the supernatant was collected and this conditioned medium from THP-1 cells was added to A549 cells exposed to CBNP (120 h) for 24 hrs. The effect

of activated immune cell secretome-mediated paracrine signalling in alveolar cells was assessed by

3.4.3.4.1 Change in morphology

Change in the morphology of CBNP-exposed A549 cells after treatment with activated THP1 cells conditioned media was assessed by Phase contrast microscopy (Zeiss)

3.4.3.4.2 m RNA expression of cytokines

The effect of paracrine signalling in alveolar epithelial cells was assessed by mRNA expression of cytokines (TGFβ, α SMA, E-Cad, PGE2, MMP, Collagen) in the epithelial cells by q RT-PCR.

3.5. Statistical Analysis

All experiments were done thrice in triplicates. Mean±SD was plotted. Two-way ANOVA and student's *t*-test were used for statistical analysis with the help of GraphPad Prism 6 software.

4. RESULTS

The results consist of four phases

Phase 1 deals with the development of ***in-vitro*** systems suitable for studying fibrosis. **Phase II** deals with understanding **cell-material interaction**s. Here the effect of carbon black nanoparticles (CBNP) on alveolar cells on short-term and long-term exposure was assessed to understand the molecular cues leading to alveolar fibrosis. **Phase III** deals with the assessment of All-trans retinoic acid as an **antifibrotic therapeutic molecule.**

Phase IV deals with understanding **cell-material-microbial interactions**, particularly with the epithelium, to delineate the preponderance of challenged alveolar epithelium to an infection.

4.1. Phase1: Development of the *in-vitro* systems

Pulmonary fibrosis is a progressive disease characterized by excessive matrix deposition leading to the destruction of lung architecture and ultimately, in loss of organ function. Noxious stimuli can trigger aberrant repair processes and disrupt normal tissue homeostasis. The unicellular, as well as multicellular responses to these stimuli, need to be assessed. Hence two different *in-vitro* systems were developed. **Electric cell-substrate impedance sensing**- The first is an automated real-time, label-free method for assessing monotypic cell behaviour. The interaction between the epithelial and fibroblasts are considered to be central to the pathogenesis of lung fibrosis.

A second system was developed and evaluated for long-term stability which is a heterotypic air-liquid interface co-culture system specifically made of alveolar

epithelial cells and lung fibroblasts. This system could be utilized in the future for prolonged exposure studies.

4.1.1 Electric cell-substrate impedance sensing- ECIS

ECIS is a real-time label-free method to analyze cellular behaviour to an external injury or stimuli. The system measures changes in impedance or resistance in adherent monolayers grown in arrays with gold electrodes at the bottom. The readings are taken in real-time and provide information faster vis-à-vis endpoint or labeled assays. By varying the Alternate current (AC) frequencies, information like the barrier integrity, morphological changes, etc of the adhered cells can be studied. In the advanced Zθ equipment used in the current study, the impedance is broken down to resistance and capacitance providing more reliable data and making the system an advanced form of cellular impedance-based assays.

Diesel exhaust particles (DEP) formed from incomplete combustion of diesel fuel are components of particulate matter in air pollution. In the first part of Phase1 of the current study, A549 cells' (representative of alveolar epithelium) response to DEP exposure was assessed using ECIS and compared to regular endpoint analyses like MTT, LDH, and NRU.

4.1.1.1 Characterization of DEP

Suspended DEP after 25 min of sonication was analyzed by Transmission electron microscope**.** TEM analysis showed the morphology of collected DEP to be diffused spheres having nanoparticle size of 30±4 nm (Fig 4.1).

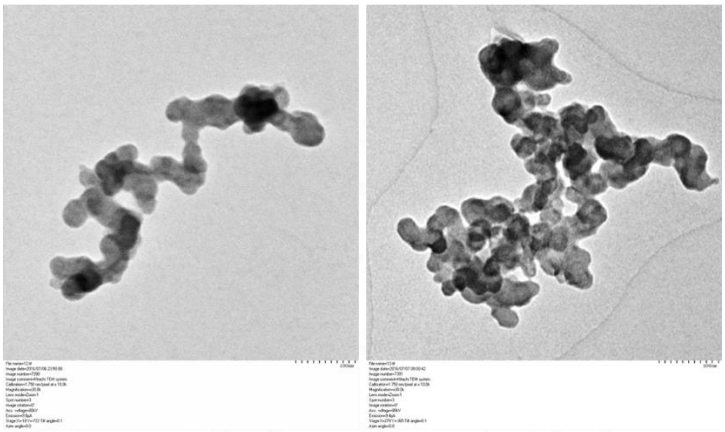

.

Fig 4.1. Transmission electron micrographs of DEP.TEM analysis of DEP collected from vehicle exhaust showed the morphology of the particle to be diffused spheres.

4.1.1.2 Diesel exhaust particle exposure reduces alveolar epithelial cells' barrier integrity.

ECIS was used to assess the change in epithelial morphology on a challenge with DEP. ECIS sensed the change in morphology in terms of variations in impedance or resistance offered by the A549 cell monolayer to an AC frequency of 4kHz. The non-invasive biophysical approach showed a dose-dependent drop in impedance on exposure to DEP. The fluctuations in electrical properties of cell-covered electrodes reflected dynamic morphology changes resulting from monolayer disruption following DEP exposure. The resistance value for the highest dose of DEP (320 µg/mL) exposed cells reached ~ 950Ω after 24 h of exposure whereas the untreated control wells reached more than 1.2kΩ. Decreased resistance to current flow implies loss of cell-cell adhesion via cell junctional proteins and disruption of the monolayer with loss of barrier integrity (Fig 4.2). The impedance was broken down to its component's resistance and capacitance. The capacitance increased with decreased resistance in a dose-dependent manner (Fig 4.3).

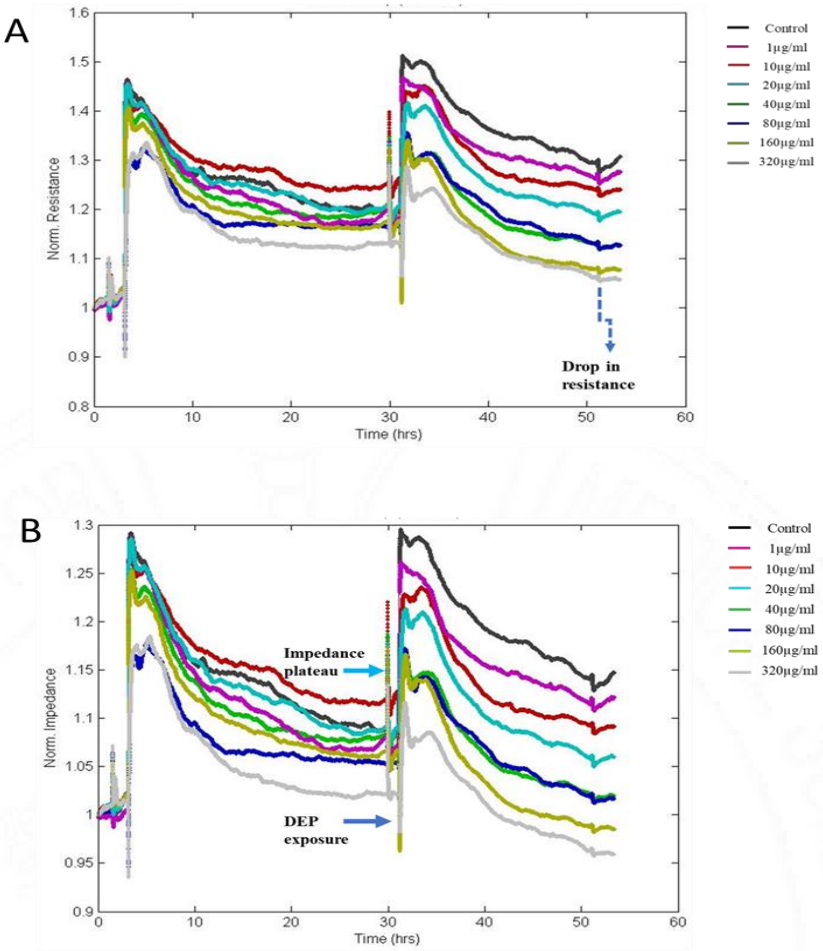

Fig 4.2: Change in resistance of DEP-exposed A549 cells. A) Normalized resistance v/s time and B) Normalised impedance v/s time graphs. Resistance decreases in a dose and time-dependent manner after the exposure to DEP, indicating a reduction in resistance to current flow through the junctions. After 24 h of DEP exposure resistance in wells exposed to high doses (320 µg/mL) showed values nearly equivalent to initial seeding indicating loss of cell-cell interaction and loss of barrier integrity. Colour palettes represent the dose of exposure.

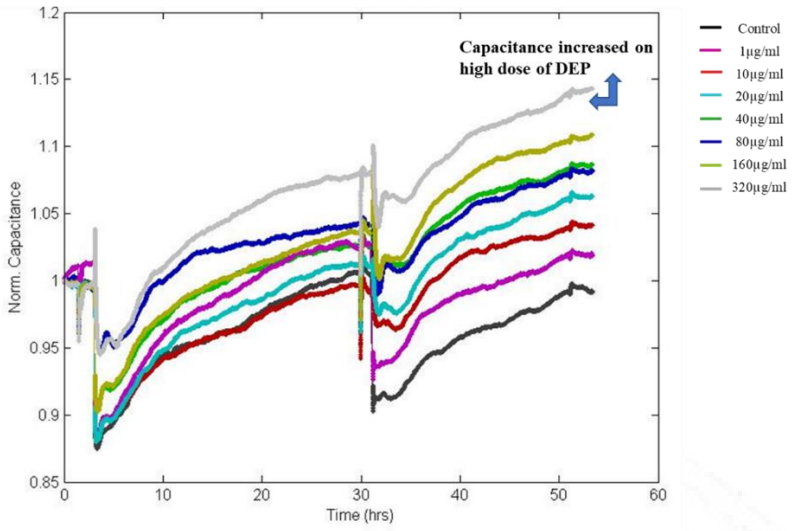

Fig4.3: Change in capacitance of A549 on DEP exposure. Normalized Capacitance V/s time graph to DEP exposed A549 cells. Capacitance is increasing in a dose and time-dependent manner after exposure to DEP.

4.1.1.3 Classic endpoint cytotoxicity analyses

4.1.1.3.1 Exposure to DEP induced a dose-dependent reduction in the viability of alveolar epithelial cells

After exposure to different concentrations of DEP for 24 h, the viability of A549 was measured by MTT assay (Fig 4.4.a). After exposure, a dose-dependent reduction in the viability of alveolar epithelial cells was observed. The lowest concentration of 1µg/mL was found to be non-cytotoxic. 40 µg/mL DEP decreased the viability by more than 50%. The highest dose (320 µg/mL) exposure reduced the viability to 23.05%.

4.1.1.3.2 The plasma membrane integrity of A549 was reduced by higher concentrations of DEP

A significant increase in LDH release at doses of 40 ug/mL and above DEP. The amount of LDH released is proportional to the number of lysed cells. Loss of plasma membrane integrity is indicative of cell death. 40% cytotoxicity was observed at 20

µg/mL concentration and more than 50% cytotoxicity was observed above 40 ug/mL doses indicating that higher concentrations were cytotoxic (Fig 4.4. b).

4.1.1.3.3 DEP-induced lysosomal disruption in alveolar epithelial cells

Viable cells maintain Intact lysosomes. The neutral red uptake assay uses the absorption of weak cationic dye neutral red (3-amino-7-dimethylamino-2-methylphenazine hydrochloride), into lysosomes to assess the toxicity of a test substance. The retention of the dye was found to be dose-dependent (Fig 4.4. c). At higher concentrations, cells failed to retain the dye, implying that DEP is cytotoxic and causes lysosomal destabilization.

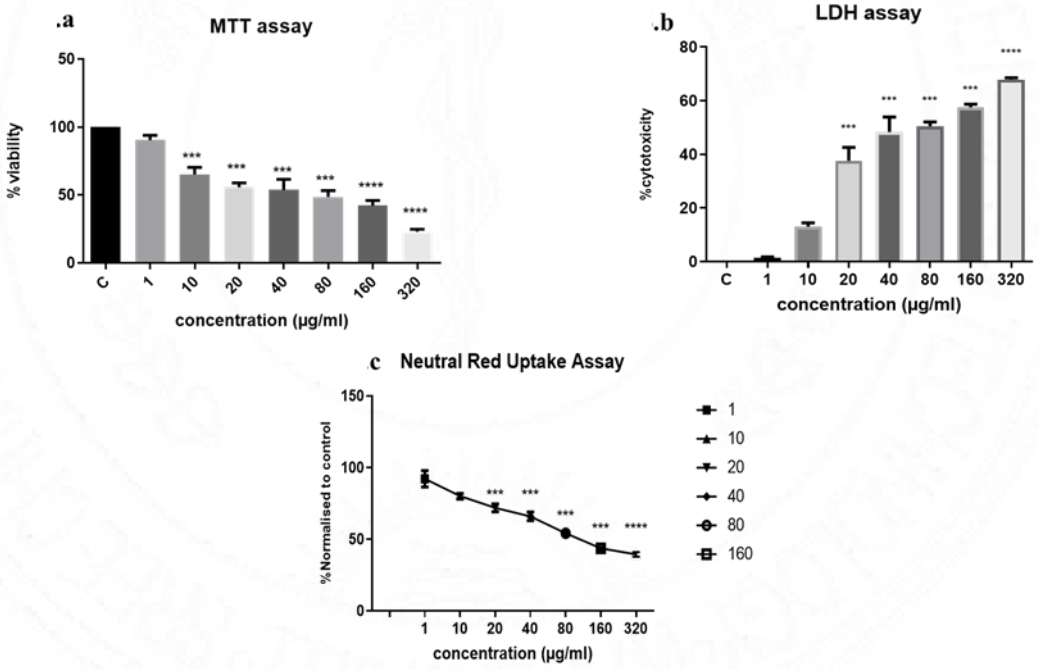

Fig 4.4. Classic endpoint cytotoxicity analyses. (a) MTT assay of A549 cells exposed to DEP implied a dose-dependent increase in cytotoxicity. (b) LDH cytotoxicity assay on DEP exposure. (.c) Neutral Red retention in DEP-exposed cells. At higher concentrations, lysosome intactness was affected and less than 30% of cells were retaining the dye. The results are expressed as mean±SD of 3 independent experiments. ***p<0.001and ****p<0.0001 found to be significant. Control wells were not treated with DEP.

4.1.2 Heterotypic Co-Culture Air-Liquid Interface System

4.1.2.1 Development of heterotypic co-culture Air-liquid Interface (ALI) system

To improve the physiologic relevance of *in-vitro* models of alveoli an Air liquid interface co-culture system was developed. The *in-vitro* system developed was superior to submerged cell culture systems, which are technologically simple but non-physiologic. In the developed system type 2 alveolar epithelial cells (represented by A549 cells) were seeded on the apical (air) side of a porous/perforated transwell insert membrane and fibroblast cells (represented by WI38 cells) were seeded on the basolateral side of the membrane (Fig 4.5).

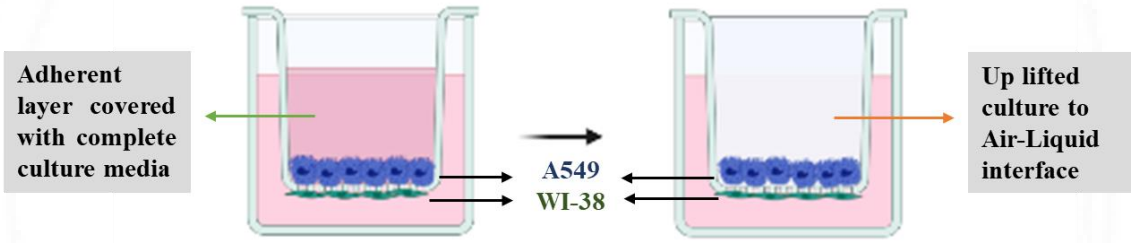

Fig 4.5 Pictorial representation of the establishment of heterotypic Air-liquid interface culture system. A549 cells were seeded at the apical side and WI-38 were seeded at the basolateral side of transwell inserts. The adhered cultures were uplifted to ALI by removing the complete culture media from the apical compartment.

4.1.2.2 Co-culture and Upliftment to ALI enhances barrier integrity of the *in-vitro* system

Trans epithelial electrical resistance, TEER, is widely used as a measure of cell monolayer integrity via tight junction formation. TEER of the monocultures (submerged and ALI) and co-cultures (submerged and ALI) were determined (at 37^0C)

at regular intervals. The TEER measurements of the ALI co-cultures showed an increase in resistance to the flow of current over time due to decreased gaps in the monolayer. The increased resistance is an indication of the formation of tight junctions by the cells. The upliftment to the Air liquid interface of the co-culture system showed a significant increase in TEER values from 26.46 ±1.47 Ohm*cm^2 to 172.39±3.8 Ohm*cm^2 within 15 days of culture. In contrast, the ALI culture of A549 alone showed fluctuating TEER values which initially increased to 108 Ohm*cm^2 from 28.3 Ohm*cm^2 after 8 days of upliftment and then a reduction to 64.3 Ohm*cm^2 by the 15th day. Both the submerged mono and co-culture systems had given TEER values below 40 Ohm*cm^2 throughout the culture period (Fig 4.6).

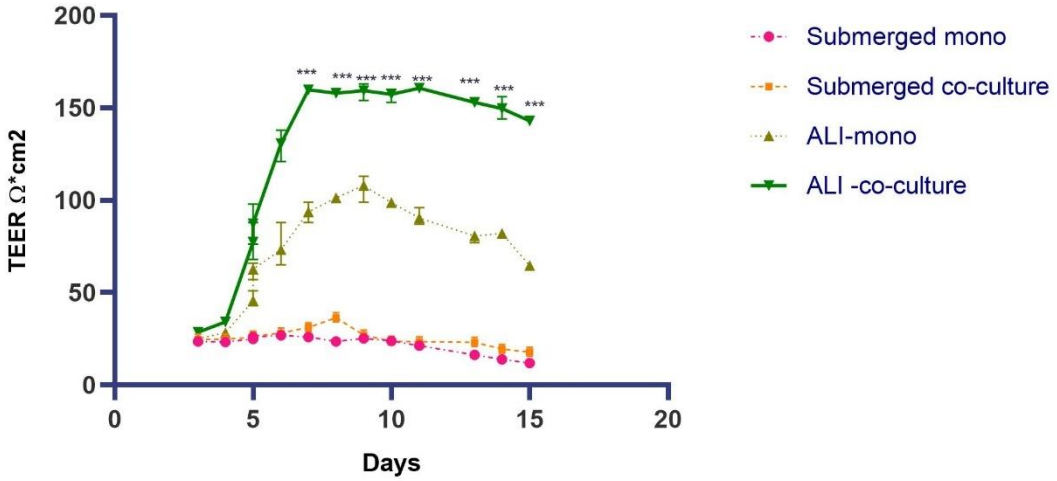

Fig 4.6 Change in transepithelial electrical resistance of A549 adherent layer with respect to time. Four culture conditions were studied: ALI-Mono and co-cultures exposed to atmospheric air and submerged cultures- mono and co-cultures in culture media. Each data point represents the mean ± SD (n = 5). Statistical analysis done by ANOVA ***p<0.001 indicate significance.

4.1.2.3 ALI co-cultures show reduced trans-membrane permeability

The uptake of the anionic fluorescent sodium fluorescein by the cell layers was characterized for ALI monoculture and co-culture on different days. The ALI co-

culture showed reduced paracellular permeability (353±13.44 cm/s) whereas ALI monoculture showed an increased permeability (676.6 ±35.3 cm/s) (Fig 4.7). The permeability constants for ALI co-cultures in the transwell presented the largest reduction, indicating intact cell morphology and monolayer integrity. The results imply the enhanced formation and maintenance of alveolar cell tight junctions in an air-exposed environment.

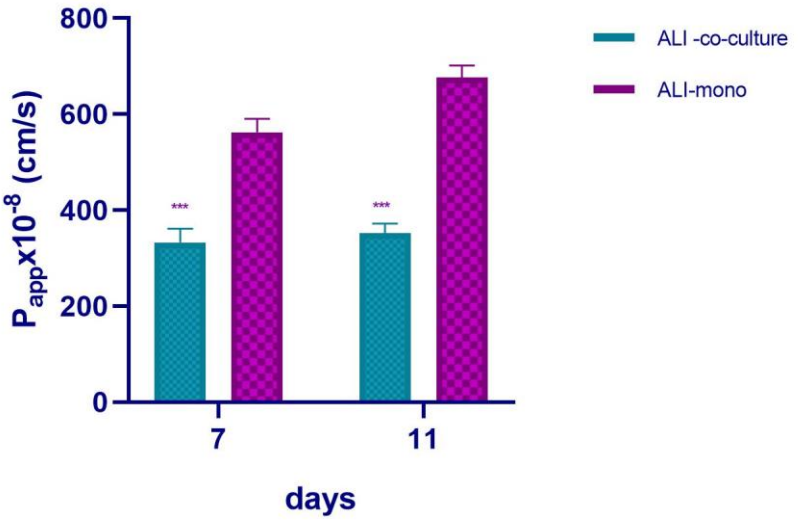

Fig 4.7 Apparent permeability of ALI cultures(n=4) Papp measured in the apical-to-basolateral direction on days 7 and 11. Reduced permeability was evident in ALI co-cultures. Data are shown as mean ± SD; ***, P < 0.001

4.1.2.4 ALI co-cultures maintain cytoskeletal and functional integrity

Actin staining by rhodamine-phalloidin and surfactant protein C staining for junctional integrity proved that ALI co-cultures maintained integrity for 15 days. The cytoskeletal integrity of cultures was maintained till day 15. Actin filaments provide the structural framework and mechanical support to cells. They determine cell shape and enable cell migration. The dynamic actin cytoskeleton helps in maintaining cell polarity, cell-cell

interactions, etc. Actin cytoskeletal staining by rhodamine-phalloidin showed an intact cytoskeleton till the 15th day of culture. The type 2 alveolar cells play a critical role in maintaining the homeostasis of the lung by secreting Surfactant proteins that maintain the surface tension and prevent alveolar collapse. Among the four surfactants, A, B, C, and D, Surfactant protein C (SP-C) is the unique marker of alveolar type 2 cells. The functionality of ALI co-cultures was assessed by expression of SP-C. Immunostaining of the co-culture inserts showed that SP-C expression was maintained till day 15 of ALI culture (Fig 4.8).

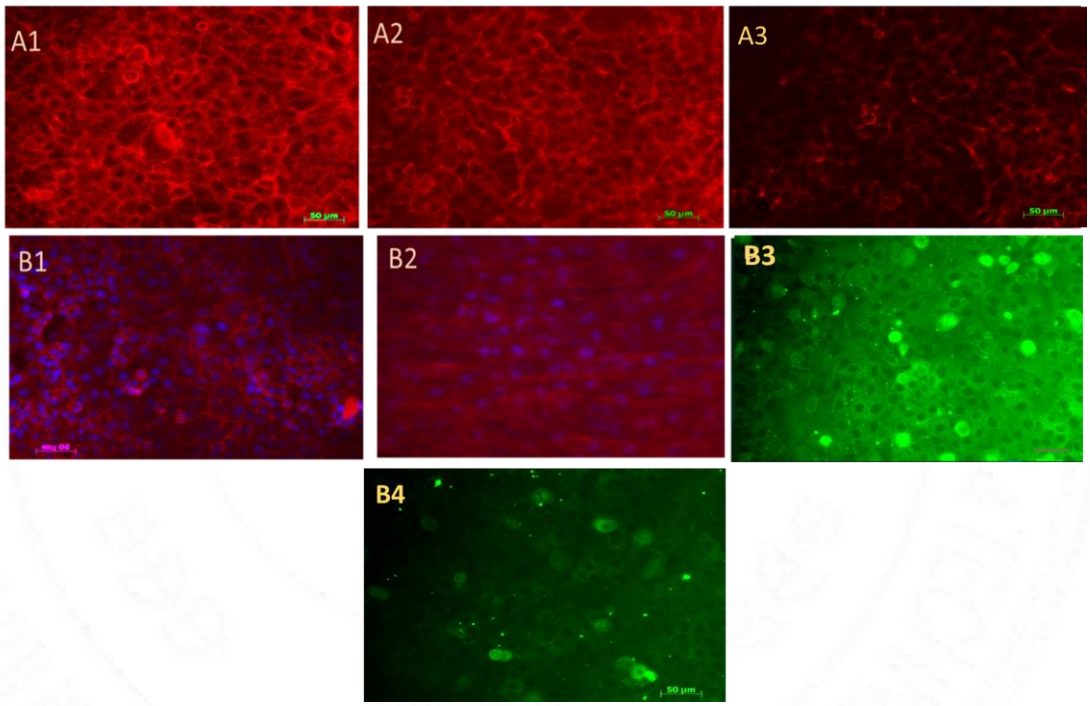

Fig 4.8 Immunofluorescent staining of ALI co-culture inserts. The actin staining showed the cytoskeleton to be intact on day 7 (A1), day 11 (A2), and day 15 (A3). B1 and B2 represent the slices of Z-stacked image of actin staining of A549 and WI-38 cells seeded on both sides of the transwell membrane (day 11). B3 (day 11) and B4 (day 15) show SP-C expression in the ALI co-culture system, pointing to the functional integrity of the *in-vitro* system. Magnification bars -50 µm**.**

4.2 Phase II. Cell-Material interactions.

4.2.1 Characterisation of Carbon black Nanoparticle (CBNP)

4.2.1.1 High-resolution Transmission electron microscopy

The size and morphology of the CBNP were assessed by High-resolution Transmission electron microscopy. The HR-TEM micrograph of the particle is represented in **Fig 4.9.** The size of **CBNP** nanoparticles was found to be 53 ±8nm using image J. Morphology was found to be spherical. The qualitative assessment of SAED (Selected area electron diffraction) demonstrated the amorphous nature of CBNP marked by the presence of halo rings.

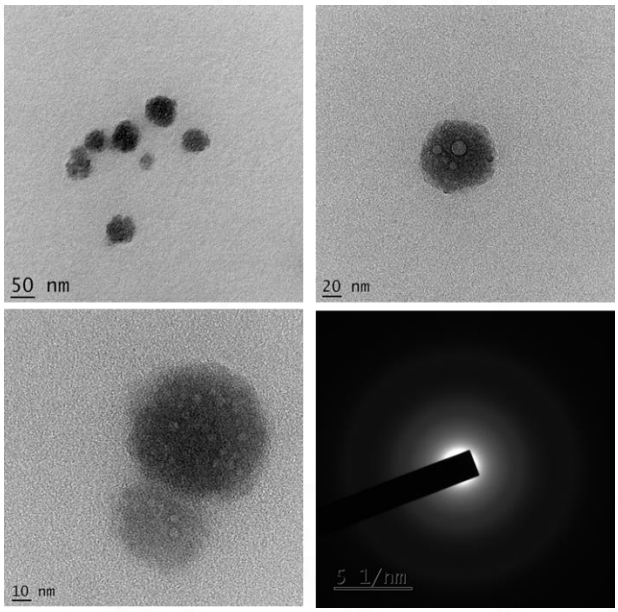

Fig 4.9 HRTEM images of CBNP nanoparticles show the particle morphology to be spherical. SAED shows the presence of halo rings.

4.2.1.2 Hydrodynamic size by Dynamic light scattering (DLS)

Hydrodynamic size is an important parameter for understanding the behaviour of nanoparticles in a biological system. The hydrodynamic size (Z-average) of CBNP in the cell culture medium was found to be 383.3±38.7nm with a polydispersity index of 0.22. (Fig 4.10).

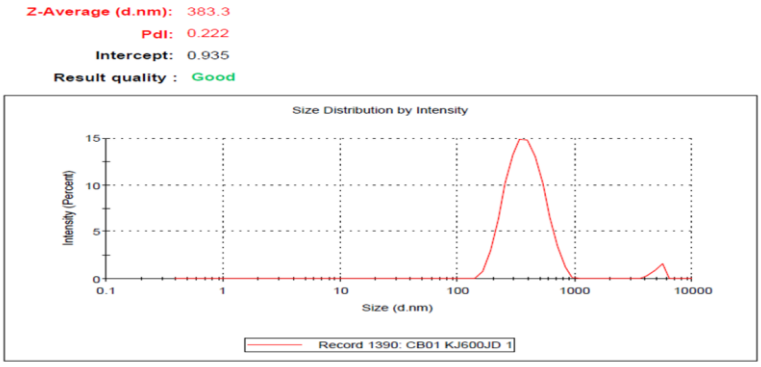

Fig 4.10: DLS graph of CBNP shows the hydrodynamic diameter of the particle to be 383±38.7 nm

4.2.1.3 Surface charge of CBNP was determined by Zeta potential

Surface charge was analyzed as it is a major determinant of particle dispersibility. The surface charge of the Carbon black nanoparticle was measured by zeta potential and found to be 7.82±3.74 mV.

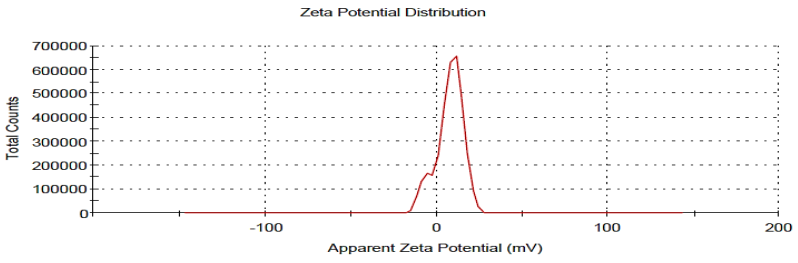

Fig 4.11: Zeta potential analysis of CBNP

4.2.2 Effect of CBNP on Short-term Exposure to alveolar cells

These effects were analysed at the morphological, biochemical and molecular-genomic level to the three major alveolar cells representing the alveolar epithelial cells, fibroblast cells and immune cells.

4.2.2.1 Alveolar epithelial cell response

4.2.2.1.1 Morphological Changes and Viability of A549

CBNP induces a concentration-time-dependent reduction in cell viability. Live cells distinguished by the presence of ubiquitous intracellular esterase take up the non-fluorescent cell permeable calcein AM and convert it to green fluorescent calcein. EthD1 (Ethidium homo dimer1) enters cells with damaged membranes and fluoresces red. Live-dead staining of CBNP-exposed A549 cells for 24-48 h indicated that, at 24 hours upto 80 µg/mL cell viability was maintained while 160 µg/mL proved cytotoxic, while exposure for 48 h induced cytotoxicity from 40 µg/mL and with 160 µg/mL exposure inducing a significant uptake of EthD1 and the fluorescence peaked at 48h (Fig 4.12).

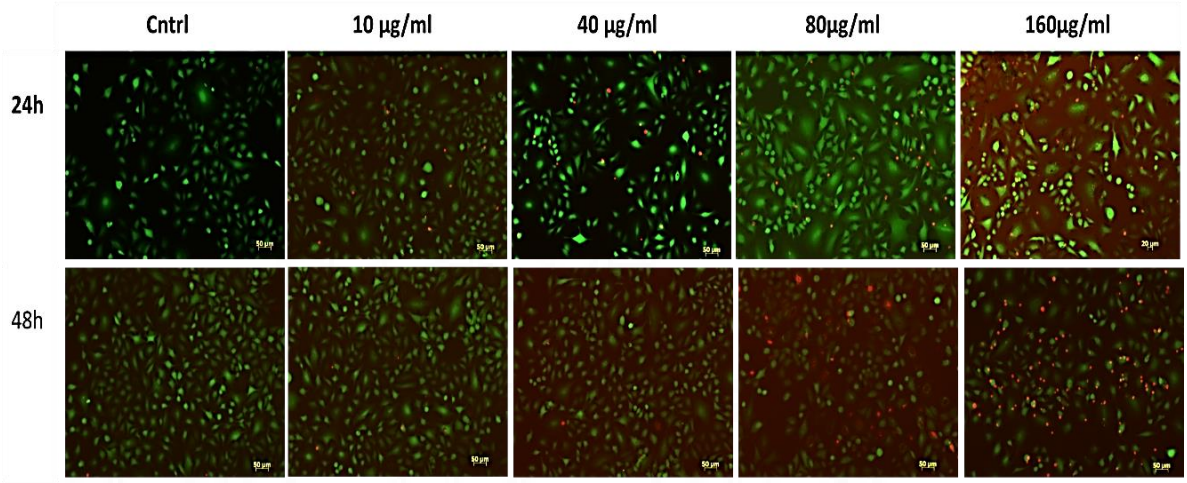

Fig 4.12 Live-dead staining of A549 cells exposed to CBNP for 24h and 48h. Unexposed cells served as control (Ctrl). Increased red fluorescence indicated the loss of cell viability at 160 µg/mL CBNP exposure at both time points - scale bar 50µm.

4.2.2.1.2 Biochemical changes in A549 on short-term exposure to CBNP

4.2.2.1.2.1 High concentrations of CBNP induced loss of cell viability in alveolar epithelial cells

A concentration and time-dependent cytotoxicity were evident from the MTT assay. After 24h exposure, the viability was 97.2%, 91.6%, 93.25%, 84.25%, 75.2%, 71.4%, and 63.4% on 1,5,10,20, 40, 80, 160 µg/mL respectively (Fig 4.13). It was evident that by 24h of exposure the mitochondrial activity was found to be less than 75% for high concentrations. Exposure to low concentrations (1,5,10, 20µgm/mL) was found to be non-cytotoxic. Whereas, 48h exposure to 40,80,160 µg/mL reduced the viability to 66.2%, 59.8%, and 51% respectively which implied that high concentrations of CBNP by 48h exposure induced a significant reduction in cell viability.

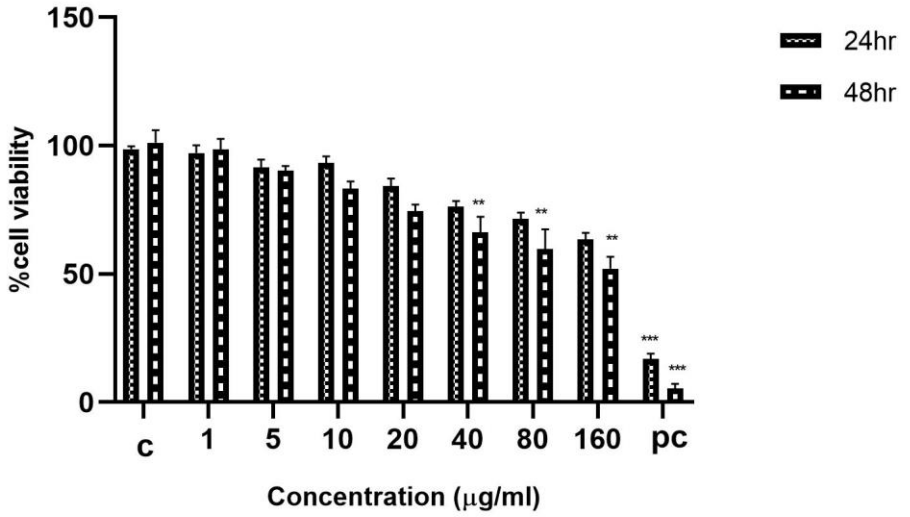

Fig 4.13 MTT assay of A549 cells exposed to CBNP for 24 and 48h. The values are expressed as percentage viability concerning control. Phenol-treated cells were used as a positive control (pc). Negative control wells (c) were not exposed to CBNP The data represent the mean ± SD of three independent experiments. Statistical significance is indicated by **p< 0.01and ***p<0.001.

4.2.2.1.2.2 CBNP induces concentration and time-dependent reduction in plasma membrane integrity

The loss of plasma membrane integrity of cells is indicated by the release of lactate dehydrogenase (LDH) into the culture supernatant. We observed a concentration and time-dependent increase in LDH release from CBNP-exposed alveolar epithelial cells (A549). After 48h exposure, high concentrations, ie, 40-160 µg/mL induced significant release of the stable cytosolic enzyme into the culture medium indicating the loss of plasma membrane integrity of the cells exposed to those concentrations. Low concentration (1,5,10,20 µg/mL) exposure did not show significant LDH release at both time points (Fig 4.14).

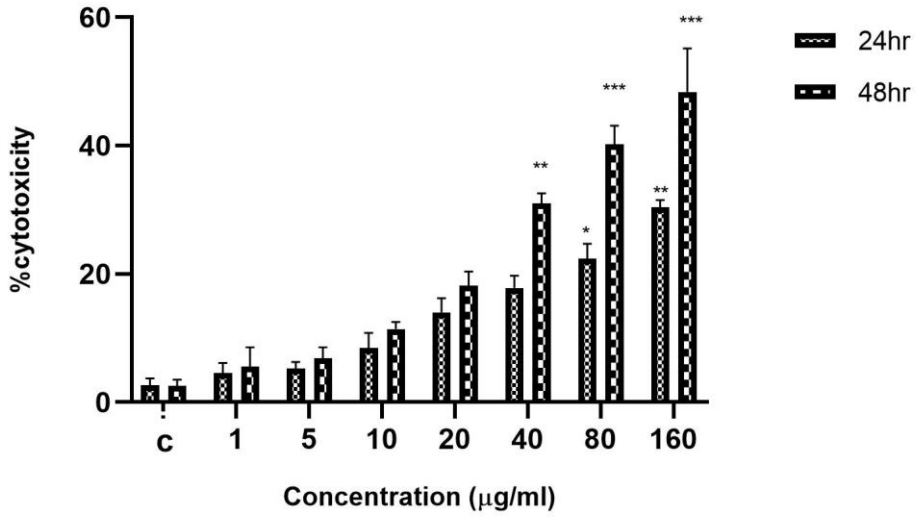

Fig 4.14 LDH assay of A549 cells exposed to CBNP for 24 and 48h. Complete lysis of A549 cells with lysis solution provided max. LDH release to the supernatant. Percentage cytotoxicity was calculated as a ratio of experimental absorbance/ Max. LDH release x 100. Control wells were not exposed to CBNP. The data represent the mean ± SD of three independent experiments. Statistical significance is indicated by *p< 0.05, **p< 0.01and ***p<0.001.

4.2.2.1.2.3 High concentrations of CBNP induce loss of lysosomal membrane integrity

Reduction in lysosomal integrity was evidenced by loss of the cell's ability to retain the neutral red. Agreeing with the previous biochemical analyses we observed a reduction in the lysosomal integrity of A549 cells exposed to high concentrations of CBNP after 48h of exposure (Fig 4.15).

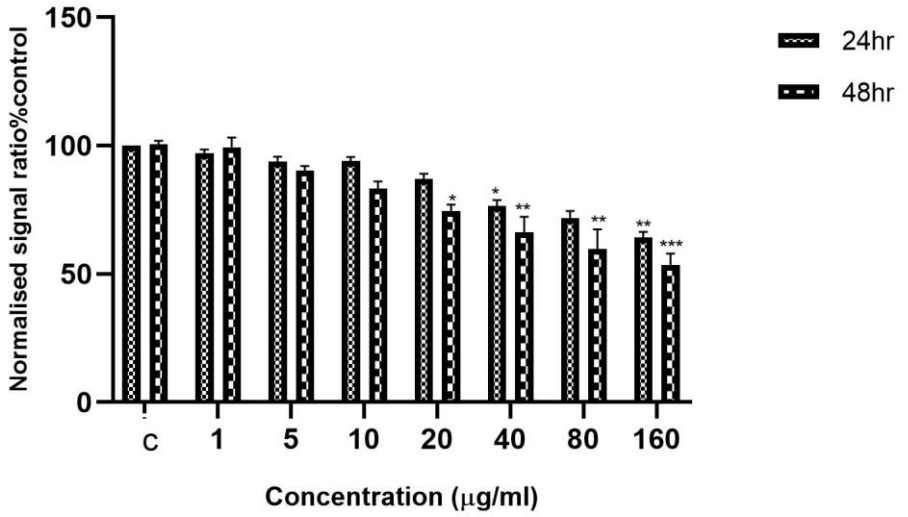

Fig 4.15 Neutral red uptake of A549 cells exposed to CBNP for 24 and 48h. The values are expressed as percentages with respect to control. The data represent the mean± SD of 3 independent experiments. Statistical significance is denoted by *p< 0.05, **p< 0.01and ***p<0.001.

4.2.2.1.2.4 High concentrations of CBNP on short-term exposure induces reactive oxygen species production

Intracellular ROS production is one of the initial cellular responses to a stimulus or injury. Hence, the ROS production at early time points after CBNP exposure was assessed. ROS production was found to be increasing at initial time points and peaked at 6 h post-exposure to high concentrations of CBNP (24 fold at 40 µg/mL:30 fold at 80 µg/mL: and 36 fold at 160 µg/mL exposure respectively) (Fig 4.16). A reduction in fold change across the groups was observed at 24 h exposure wells which could be attributed to the dose-dependent reduction of cell viability.

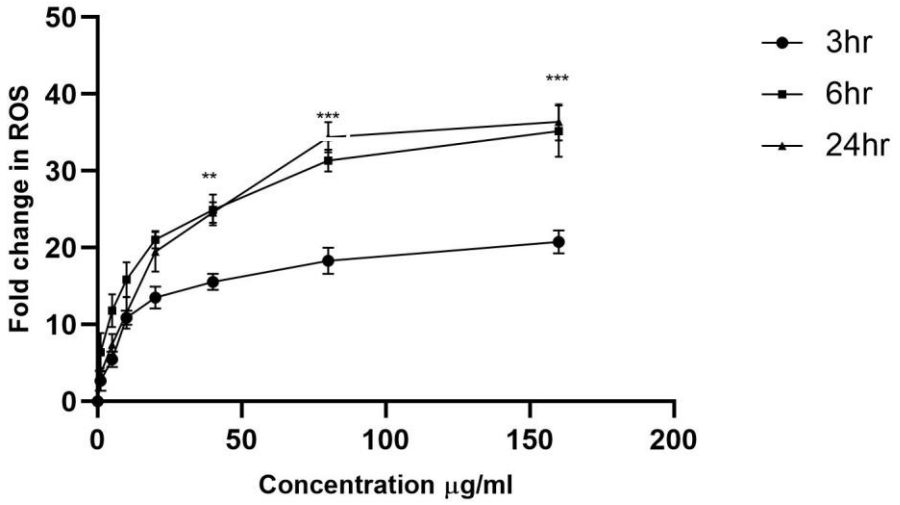

Fig 4.16 ROS production in A549 cells exposed to CBNP for 3h,6h, and 24h using DCFH-DA. The values are expressed in fold change in ROS with respect to control. The data represent the mean ± SD of 3 independent experiments. Statistical significance is denoted by *p< 0.05, **p< 0.01and ***p<0.001.

4.2.2.1.2.5 High concentrations of CBNP induce loss of lysosomal integrity

CBNP-induced lysosomal damage was assessed by AO staining after 48h exposure. Cellular blebbing, loss of lysosomal membrane integrity, etc. were observed in high concentration (80, 160 µg/mL) CBNP- exposed cells. The rise in pH and AO deprotonation were indicated by the shift in fluorescence from red to green at this concentration (Fig 4.17). Cellular blebbing (white arrow) at 80 µg/mL pointed towards loss of lysosomal integrity (D- white arrow) at 80 µg/mL, rounding off, and shift in fluorescence (E- orange arrows) at 160 µg/mL imply concentration-dependent cytotoxicity of CBNP in alveolar epithelial cell

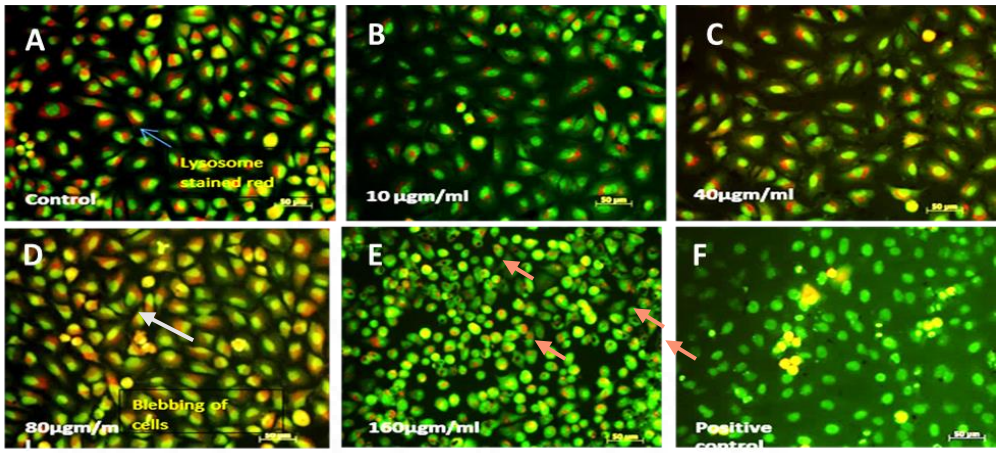

Fig 4.17 Lysosomal integrity of CBNP- exposed A549 cells after 48h of exposure. The intact lysosomes in healthy cells stained red (A,B). Loss of lysosomal integrity evidenced by cellular blebbing (D- white arrow) at 80 µg/mL, rounding off, and shift in fluorescence (E- orange arrows) at 160 µg/mL imply concentration-dependent cytotoxicity of CBNP in alveolar epithelial cells. Scale bar -50 µm.

4.2.2.1.3 Molecular changes in A549

4.2.2.1.3.1 High concentrations of CBNP-induced DNA laddering in A549 cells

In Fig 4.18 DNA laddering was evident in CBNP-exposed alveolar epithelial cells. Ladders of low molecular weight between 100-200bp were observed in wells loaded from 160 µg/mL CBNP exposed cells (lanes 5&6) CBNP exposed cells, higher molecular weight DNA bands were seen clearly attesting to the fact the cytotoxic effect of CBNP cause DNA fragmentation.

.

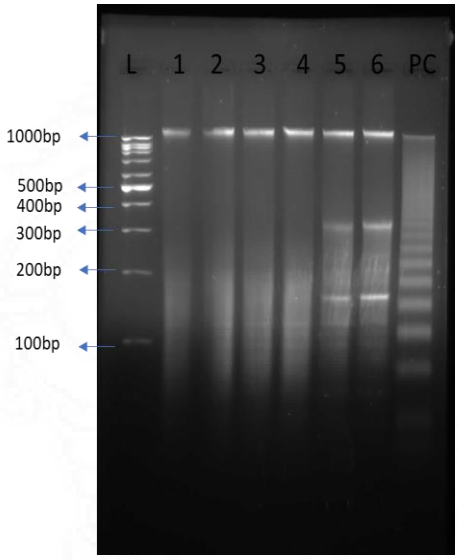

Fig 4.18 DNA ladder assay of CBNP- exposed A549 cells. Lane L: Marker DNA, 1 Control, 2: 20 µg/mL CBNP, 3: 40µg/mL CBNP, 4: 80 µg/mL CBNP, Lane 5 and 6:160 µg/mL CBNP, PC is a positive control. Base pairs (bp) of DNA markers are indicated on the left side of the figure.

4.2.2.1.3.2 Analysis of mRNA modulation in Gene expression by q RT- PCR

4.2.2.1.3.2.1. Q RT-PCR assessed gene expression of inflammatory cytokines.

Tumor Necrosis Factor-α (TNF-α)-the inflammatory cytokine secreted, by alveolar epithelial cells, functions as an alert signal in host defence to induce the production of other inflammatory mediators. Here we observed an upregulation of TNF-α (up to 4 fold) in A549 cells after 24h CBNP exposure (Fig4.19 A) and up to 5.2 fold after 48 h exposure of 160 µg/mL CBNP (Fig 4.19 B).

Interleukin-6 is a pleiotropic cytokine and its role in lung inflammation is well studied. CBNP exposure to A549 cells significantly upregulated IL-6 expression after 24h (up to 3 fold) (Fig 4.19). Further, upregulation in IL-6 expression was observed after 48h of high-concentration CBNP exposure (160 µg/mL) (Fig 4.19 B).

Interleukin 8 (IL-8), is a potent neutrophil attractant and activator, and also plays a significant role in acute lung injury. Exposure to CBNP induced significant

upregulation of IL-8 expression after 24h (up to 3.3 fold) in a dose-dependent manner. the fold change was increased to 3.8 fold by 48h exposure to high concentrations of CBNP (Fig 4.19 A& B).

Monocyte chemoattractant protein-1 (MCP-1) is a key chemokine that regulates the migration and infiltration of monocytes/macrophages. Migration of monocytes from the bloodstream across the vascular endothelium is needed for the innate defence mechanism activation and in response to inflammation. A significant upregulation in MCP-1 expression was observed in A549 cells on CBNP exposure (up to 6 fold) (Fig 4.19 A, B).

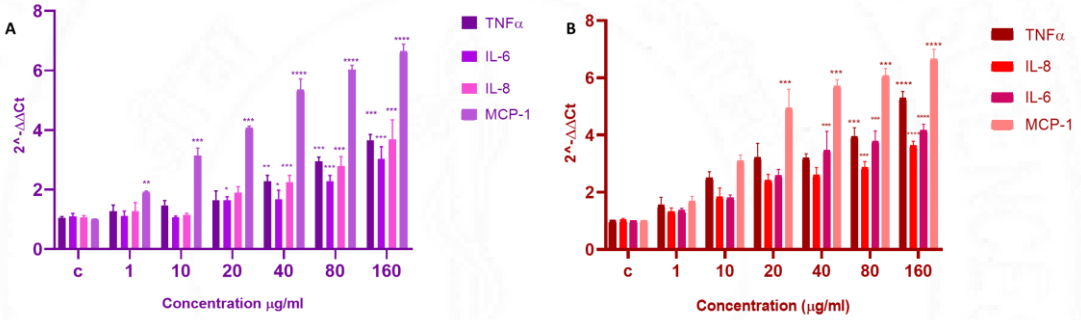

Fig 4.19 Pro- inflammatory cytokine expression in A549 cells exposed to CBNP for 24(A) and 48h (B). Fold change in gene expression (2^-ΔΔCt) has been plotted. Cytokines TNFα, IL-6, IL-8, MCP-1 were assessed. N=3, statistical analysis carried out by ANOVA **p<0.01,***p<0.001,****p<0.0001were considered significant.

4.2.2.1.3.2.2 Short-term exposure to CBNP could not initiate fibrotic responses

Prostaglandin E2 (PGE2) is a potent proinflammatory mediator and is an important factor in regulating fibroblast proliferation. PGE2 is the main product of two cyclooxygenases COX1 and COX2.COX1 is constitutively expressed and COX2 is induced in presence of injury or infection. mRNA expression analysis of COX2 showed that the 24h CBNP exposure induced COX2 production in A549 cells up to 6

fold in a dose and time-dependent manner. This indicates that short-term CBNP exposure is inducing an inflammatory response in alveolar epithelial cells.

Transforming growth factor β1 is a highly pleiotropic cytokine actively involved in lung organogenesis and homeostasis, and also in many respiratory diseases. It is considered a key fibrotic cytokine activating many downstream signalling cascades. High concentrations of CBNP didn't elicit TGF β activity. An interesting observation was obtained on gene expression analysis of TGF β1 cytokine. Low concentrations of CBNP (1-10 µg/mL) induced upregulation of TGF β1 (up to 3 fold) by 48h of exposure (Fig 4.20).

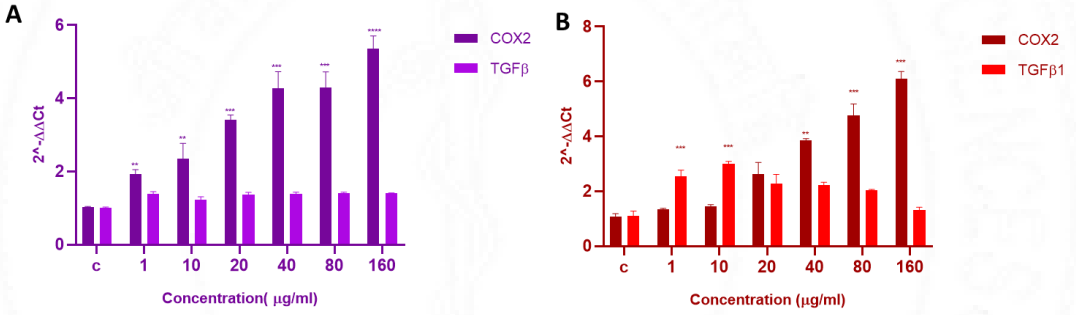

Fig 4.20 Pro fibrotic cytokine expression in A549 cells on short-term CBNP exposure. A549 cells were exposed to CBNP for 24(4.20 A) and 48h (4.20 B). Fold change in gene expression (2^-ΔΔCt) has been plotted. Cytokines COX 2 and TGFβ1 were assessed. N=3, statistical analysis carried out by ANOVA. **p<0.01, ***p<0.001,****p<0.0001were considered significant.

4.2.2.1.3.2.3 Short-term exposure to CBNP induces apoptotic cell death in alveolar epithelial cells

Caspase 3 the lysosomal enzyme is involved in the apoptotic pathway and is more specific in the detection of apoptotic cells compared to other methods like TUNEL. Upregulation in Caspase3 gene expression (up to 4 fold) was observed in short term exposure of high concentrations (80-160 µg/mL) of CBNP to A549 cells. The result

indicated apoptotic cell death of A549 cells on short-term exposure to higher concentrations of CBNP (Fig 4.21).

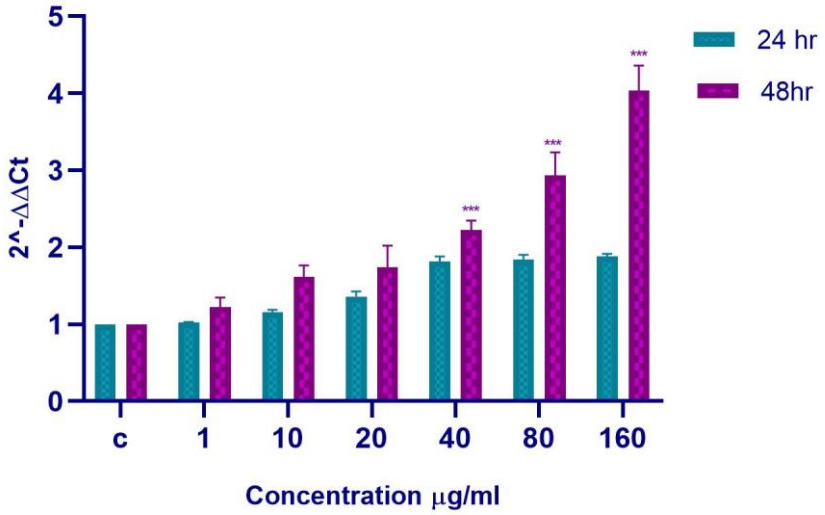

Fig 4.21 Gene expression analysis of Caspase 3 in A549 cells exposed to CBNP for 24 and 48h.Caspase 3 expression was upregulated in a time and dose-dependent manner. N=3 statistical analysis carried out by ANOVA**p<0.01,***p<0.001were considered significant.

4.2.2.1.3.3. Cytokine Protein quantification by Enzyme-linked immunosorbent assay -ELISA

Protein quantification by ELISA of IL-6, IL-8, TGF β -1 and PGE2 indicated that high concentrations of CBNP induce an inflammatory response in alveolar epithelial cells on short-term exposure.IL-6 and IL-8 and PGE2 concentrations were higher in CBNP-exposed cell supernatant. Increased TGF-β1 secretion from low-concentration CBNP-exposed cells indicated the activation of a fibrotic cascade (Fig 4.22). At the same time, the pro-inflammatory cytokines IL-6, and IL-8 were secreted under the influence of higher concentrations of CBNP for 48 hours.

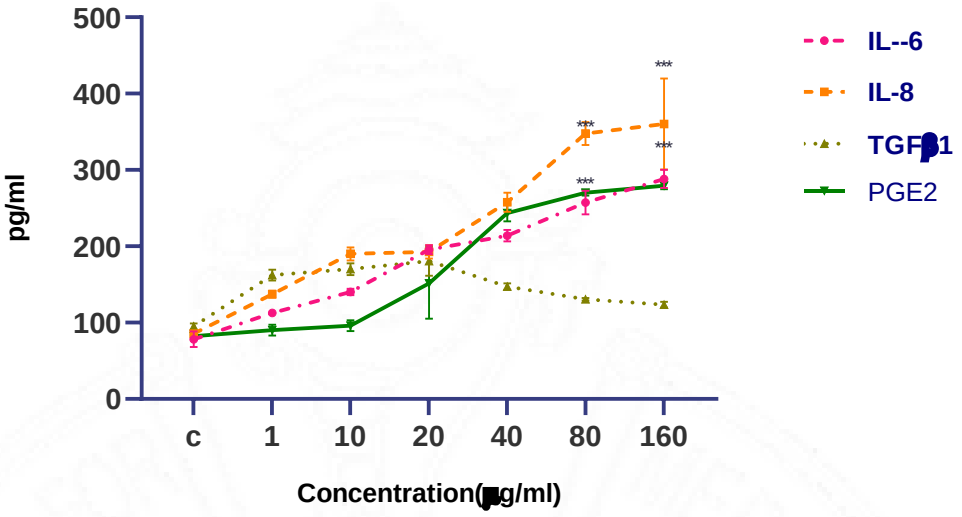

Fig 4.22 Protein quantification of A549 cells on short-term CBNP exposure. IL-6, IL-8, and TGFβ1 released into the culture medium at 48h CBNP exposure was quantified by ELISA. Increased TGFβ release was observed in low-concentration exposed cells. Whereas high concentrations elicited pro-inflammatory cytokine release. N=3 statistical analysis carried out by ANOVA**p<0.01,***p<0.001were considered significant.

4.2.2.2 Fibroblast cell- Response to short-term exposure to CBNP

4.2.2.2.1 Morphological changes in WI-38 on short-term CBNP exposure by Coomassie brilliant blue (CBB) staining

Coomassie Brilliant Blue staining was done to assess the morphological changes in WI-38 cells on CBNP exposure. Cell rounding-up and loss of viability were evident in CBB-stained cells exposed to higher concentrations of 80 and 160 µg/mL. The viability of WI-38 cells was decreasing in proportion to concentration and time of particle exposure (Fig 4.23 at 48 hours in condition 160 µg/mL black arrows indicates loss of cell morphology).

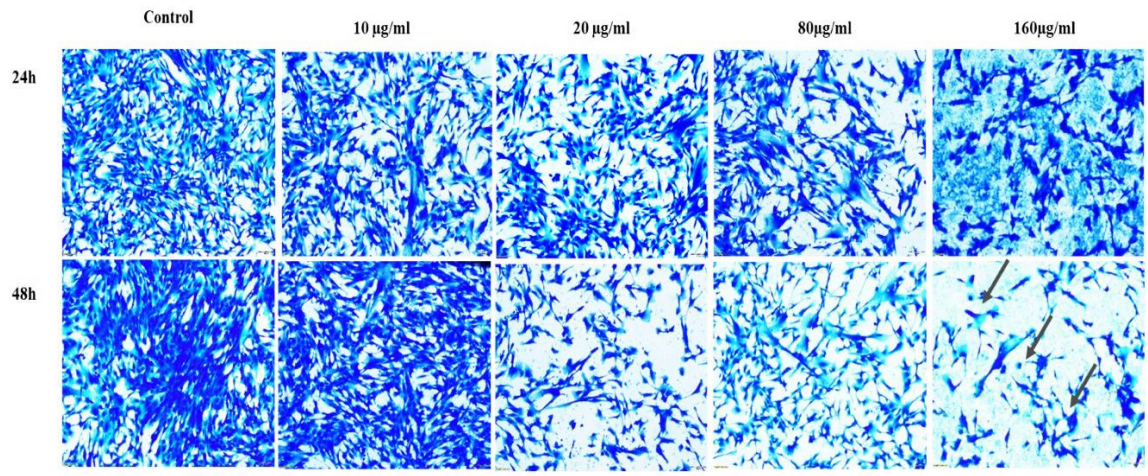

Fig 4.23: CBB staining of WI-38 cells exposed to CBNP for 24 and 48h. Dose-time-dependent changes in viability were evident from CBB staining images of WI-38. Black arrows indicate loss of cell morphology. Scale bar 100µm Magnification 20x.

4.2.2.2.2 Biochemical changes in WI-38

4.2.2.2.2.1 CBNP induced dose-dependent cytotoxicity in Fibroblasts

High doses of CBNP (80,160 µg/mL) induced loss of viability in fibroblast cells as observed in the MTT assay results. The viability of WI-38 cells was found to be 98.3%,97%, 92%, 87%, 77%, and 73% for 1, 5, 10, 20, 40, 80, and 160 µg/ml treatments respectively. Low concentrations did not show any significant change in viability. A significant decrease in mitochondrial activity was observed in 40 µg/mL (66%), 80 µg/mL (58%), and 160 µg/mL (52%) after 48 h CBNP exposure (Fig 4.24). An increase in absorbance was observed in low concentrations (1,10,20 µg/mL) after 48 h exposure which was not significant.

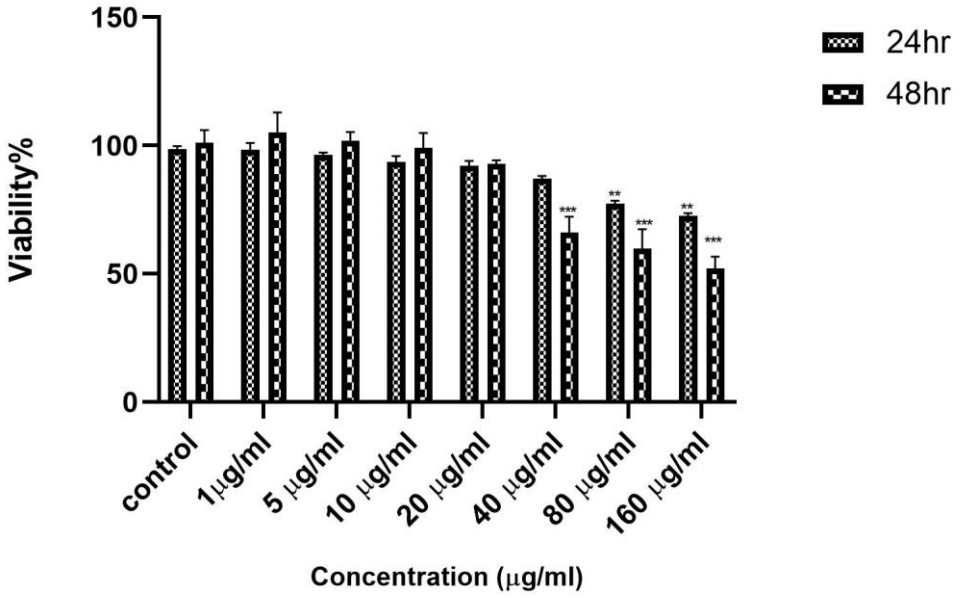

Fig 4.24 MTT assay of WI38 cells exposed to CBNP for 24 and 48h. The values are expressed as percentage viability concerning control. Control wells (c) were not exposed to CBNP The data represent the mean ± SD of three independent experiments. Statistical significance is indicated by **p< 0.01and ***p<0.001.

4.2.2.2.2.2 High doses of CBNP induced loss of plasma membrane integrity on short-term exposure.

The release of Lactate dehydrogenase increased with an increase in CBNP concentration and exposure time. The percentage of cytotoxicity increased up to 52% by 160 µg/mL of CBNP exposure by 48 h. Low concentrations of CBNP did not show any significant change in LDH release. 80 µg/mL of CBNP also induced a reduction in viability (38%) by 48 h exposure (Fig 4.25).

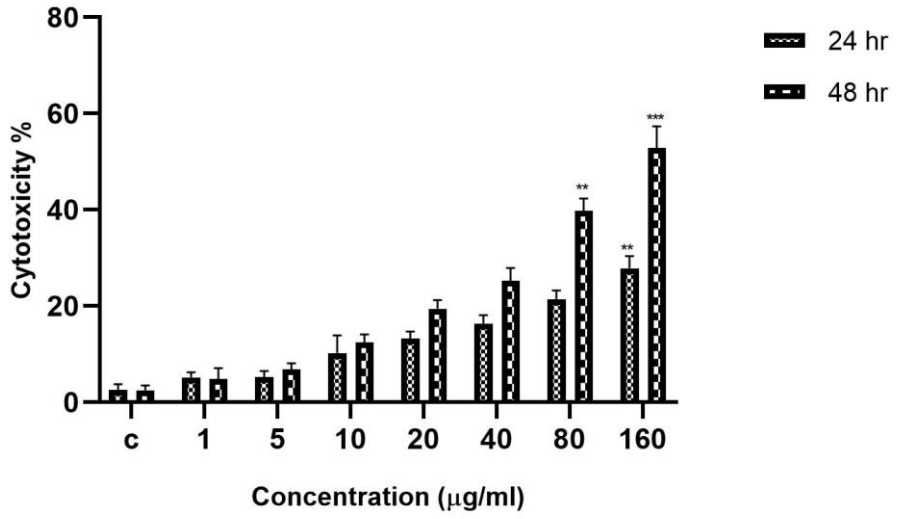

Fig 4.25 LDH assay of WI-38 cells exposed to CBNP for 24 and 48h. Complete lysis of WI-38 cells with lysis solution provided max. LDH is released to the supernatant. Control wells were not exposed to CBNP. The data represent the mean ± SD of three independent experiments. Statistical significance is indicated by *p< 0.05, **p< 0.01and ***p<0.001.

4.2.2.2.2.3 High concentrations of CBNP induced loss of lysosomal integrity in fibroblast cells.

The cell's inability to retain the vital dye neutral red indicated that high doses of CBNP alter lysosomal integrity. The loss of membrane integrity was proportional to the concentration of CBNP. Significant reduction in lysosomal membrane integrity was observed in 40 μg/mL (64%), 80 μg/mL (60%), and 160 μg/mL (55%) by 48 h exposure (Fig 4.26).

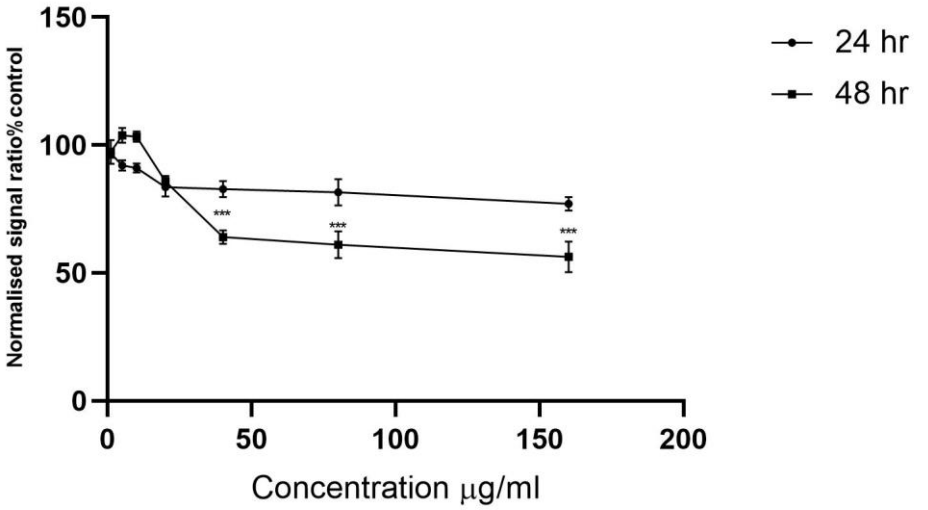

Fig 4.26: Neutral red uptake of WI-38 cells exposed to CBNP after 24 h and 48 h. The values are expressed in percentage with respect to control. The data represent the mean ± SD of three independent experiments. Statistically, a significant difference is denoted by ***p<0.001

4.2.2.2.2.4 CBNP exposure induced oxidative stress in fibroblast cells in a dose-time-dependent manner.

Reactive oxygen species production is an innate defence mechanism by the cells on exposure to an injury or stimuli. ROS production is also an initial response of the cells. Short-term CBNP exposure induced the ROS production at initial time points. On comparison along the time of exposure, a reduction in fold change in ROS production was visible between 6 h and 24 h which also points towards the fact that ROS is an immediate response to injury or stimuli. The fold change increased to more than 35 fold in 160 µg/mL exposure by 6 h (Fig 4.27).

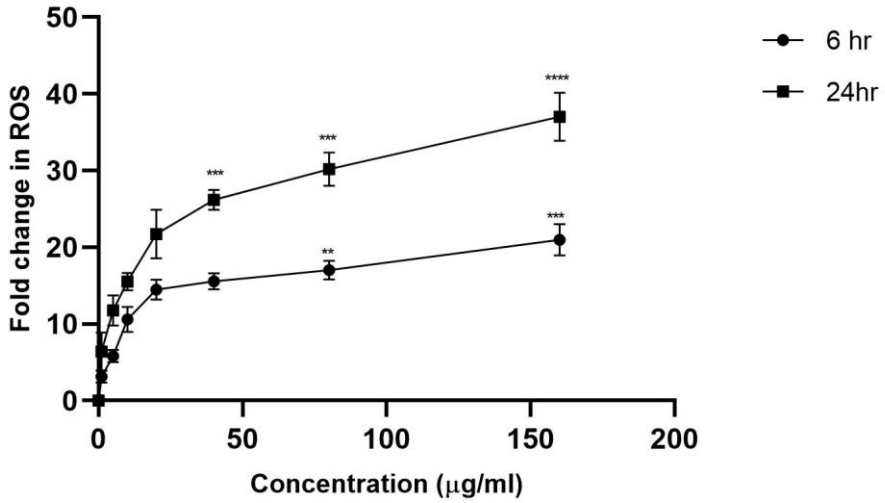

Fig 4.27: ROS assay of short-term CBNP exposed WI 38 cells. An increase in fold change was observed across the concentrations which implies a dose-dependent increase in ROS production in WI-38. Independent experiments, **p<0.1 and ***p<0.001 was considered significant.

4.2.2.2.2.5 High concentrations of CBNP-induced lysosomal destabilization in fibroblast cells on short-term exposure

Lysosomal destabilization in fibroblast cells on CBNP exposure was assessed by Acridine orange staining. The fluorescence micrographs showed that 48h exposure to CBNP (80,160 µg/mL) shifted the emission from red to green, indicating the lysosomal de-stability within fibroblast cells on high concentration CBNP exposure (orange arrows in Fig:4.28 at 48 h when exposed to 160 µg/mL).

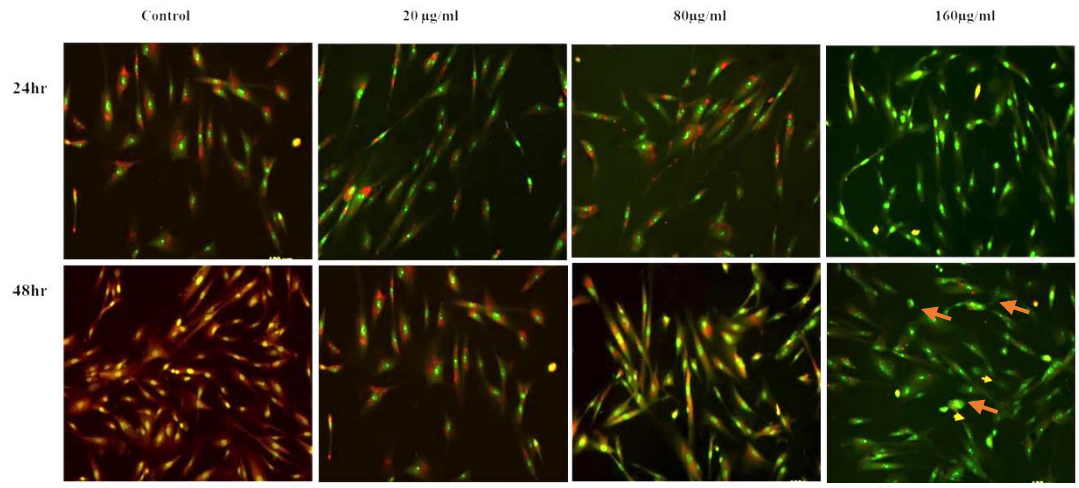

Fig 4.28: AO staining of WI-38 cells exposed to CBNP for 24 and 48h. Arrows indicate the shift in red to green fluorescence due to AO deprotonation in high-dose (160 µg/mL) CBNP-exposed cells. Scale bar 50µm

4.2.2.2.3 Molecular changes in WI-38 to short term CBNP exposure

4.2.2.2.3.1 CBNP induced DNA laddering in fibroblast cells

DNA laddering is a hallmark of apoptosis. Here characteristic DNA ladders in high-concentration CBNP-exposed fibroblast cells were observed. Low molecular weight DNA ladders were visible on agarose gel in 160 µg/mL CBNP treated cells (Fig 4.29-Lane6). Low-concentration CBNP-exposed cells were excluded as they did not show any significant change in viability in previous assays.

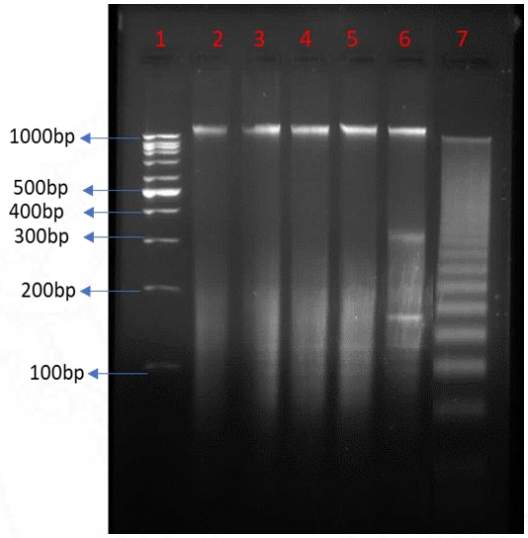

Fig 4.29 DNA ladder assay. Lane 1: Marker DNA, lane 2: Control, Lane 3: 20 µg/mL CBNP Lane 4: 40µg/mL CBNP, Lane 5: 80 µg/mL CBNP, Lane 6: 100 µg/mL, lane 7 positive control CBNP. Base pairs (bp) of DNA markers are indicated on the left side of the figure

4.2.2.2.3.2 Cytokines Gene expression studies

4.2.2.2.3.2.1 Short-term exposure to CBNP induced a pro-inflammatory response in WI38

Gene expression analysis of TNF α, IL-6, IL-8, and MCP1 cytokines showed that the CBNP exposure significantly upregulated all the cytokine expression. A dose and time-dependent increase in the mRNA levels of the evaluated proinflammatory cytokines by 24 hours (Fig4.30A) and this effect was continued upto 48 hours (Fig4.30B).

Tumor Necrosis Factor α expression increased to 2.6- fold on 160 µg/mL exposure by 24 h. More than 3 fold change in gene expression was observed on 48 h exposure to high doses of CBNP (Fig 4.30).

Interleukin 6 and interleukin 8 expression was also upregulated by CBNP exposure. Up to a 2.5-fold change was observed in fibroblasts when challenged with high concentration of CBNP. The fold change further increased to 3 fold on 48 h exposure (Fig 4.30).

Monocyte chemoattractant protein1 is the major stimulator of the innate immune mechanism. Here we observed an increase in gene expression of MCP1 in fibroblast cells in a dose-dependent manner. A very significant increase in fold change of gene expression: 4.1 fold (40 µg/mL-), 5.3 fold (80 µg/mL), and 5 fold (160 µg/mL) was noted at high concentration CBNP exposed cells. A reduction in fold change was observed in 160 µg/mL treatments when compared to 80 µg/mL after 48 h exposure which is considered insignificant (Fig 4.30).

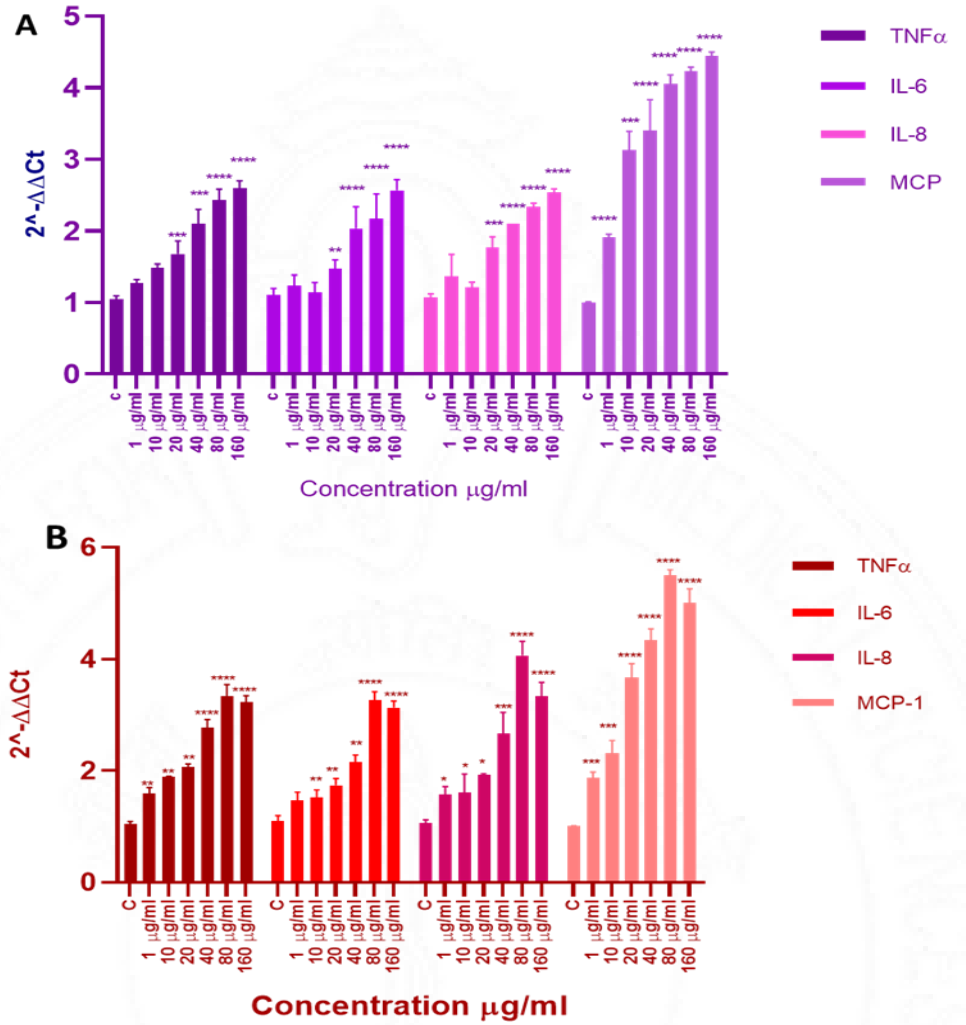

Fig 4.30 Proinflammatory cytokine expression of WI38 cells exposed to CBNP A) 24h and B)48h. Fold change in the expression of TNF α, IL-6, IL-8, and MCP-1 was assessed. Fibroblast cells unexposed to CBNP served as control. The fold change in gene expression was assessed by ANOVA. Significance is indicated by *p<0.5,**p<0.01,*** p<0.001 and ****p<0.0001

4.2.2.2.3.2.2 Short-term exposure to high concentrations of CBNP could not induce a fibrotic response in fibroblast cells.

Prostaglandin E2 (PGE2) is a major eicosanoid product of fibroblast. COX2 is involved in PGE2 synthesis. Upregulation in gene expression of COX 2 was observed

in WI-38 cells exposed to CBNP 24 and 48 h. COX 2 expression increased up to 3 fold in cells exposed to high concentration of CBNP (160 µg/mL) by 24 h. The expression of COX2 showed a 4 fold increase on exposure to high concentrations of CBNP by 48 h (Fig 4.31).

Transforming growth factor β1 is a critical growth factor in the onset of fibrosis. A significant change in TGF β1 was not observed in 24h CBNP-exposed WI38 cells. An upregulation in the gene expression of up to 2-fold was observed when CBNP was exposed at a low concentration of 10 µg/mL to WI 38 cells by 48h. No significant variation was observed in TGF β1 expression at high concentrations (>40 µg/mL) in treated cells by 48 h of exposure (Fig 4.31B).

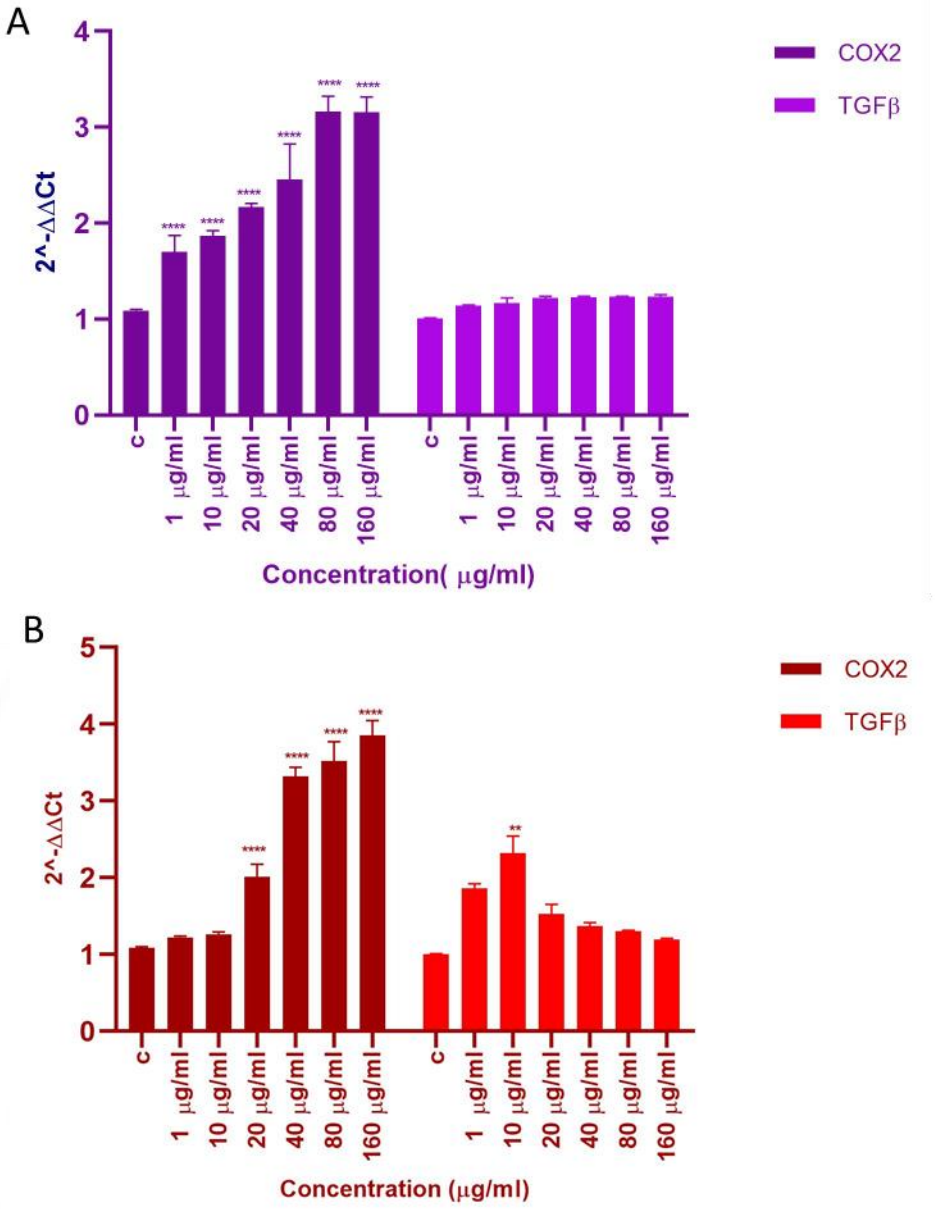

Fig 4.31 Pro fibrotic cytokine expression of WI38 cells exposed to CBNP a) 24 h and b)48 h. Fold change in the expression of TGF β1 and COX-2 was assessed. Fibroblast cells unexposed to CBNP served as control. The fold change in gene expression was assessed by two-way ANOVA. Significance is indicated by **p<0.01,*** p<0.001 and ****p<0.0001

4.2.2.2.3.2.3 High concentrations of CBNP-induced upregulation of Caspase3 gene expression

Caspase 3 is a critical protease involved in the apoptotic pathway, which catalyses the specific cleavage of key cellular proteins. Assessing the Caspase 3 gene expression by q RT-PCR was to understand mechanism of apoptosis in WI-38 cell when challenged with high concentrations of CBNP catalyse the specific cleavage of many key cellular proteins. Caspase 3 gene expression upregulation was observed at high concentrations of CBNP-exposed cells by 48 h. Relative fold change observed was 2 fold, 3 fold, and 3.83 fold in 40 µg/mL,80 µg/mL, and 160 µg/mL respectively. Significant changes were not observed in low concentrations across both periods of exposure 24 and 48 h of exposure (Fig 4.32).

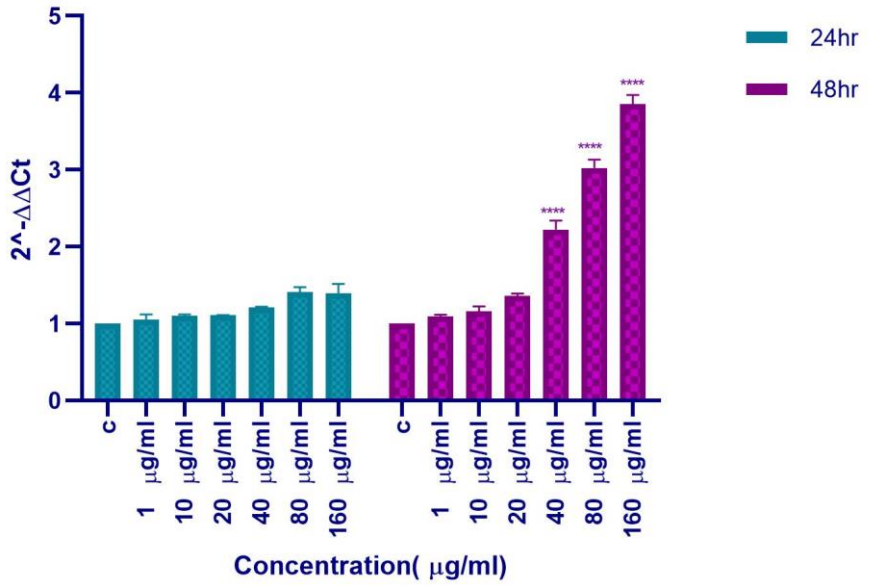

Fig 4.32 Caspase 3 gene expression in WI-38 cells exposed to CBNP for 24h and 48h. Fold change increased up to 3.83 in high concentration CBNP exposed cells on 48h exposure.

Unexposed cells served as controls. ANOVA was used to assess the data. N=3 independent experiments.***p<0.001 indicate the statistical significance.

4.2.2.2.3.2.4 Short-term exposure to CBNP induces secretion of proinflammatory cytokines

ELISA was done to assess the protein expression of proinflammatory and profibrotic cytokines in CBNP-exposed fibroblasts after 48 h exposure. An increase in pro-inflammatory cytokine production was evident in high-concentration CBNP-exposed cells (>40 µg/mL). Low concentrations did not induce a significant change in protein expression. However, the pro-fibrotic proteins TGFβ1, a slight increase in expression was observed in low concentrations (<40 µg/mL) by 48 h exposure (Fig 4.33).

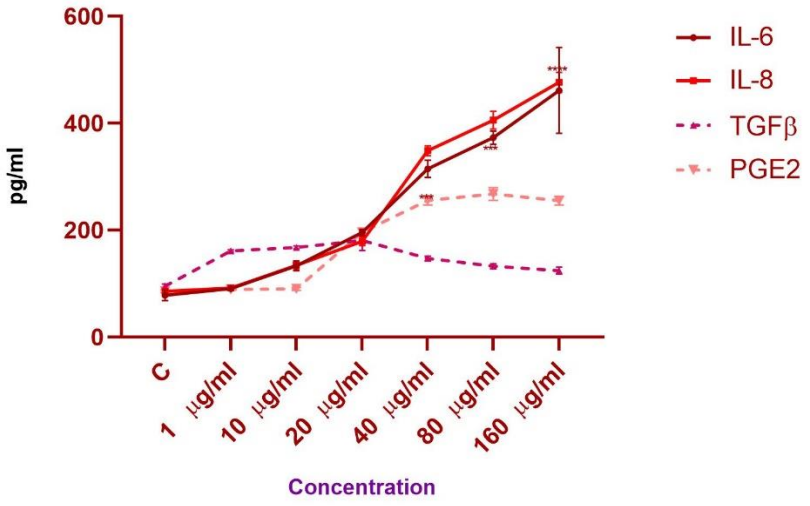

Fig 4.33 Cytokine expression in WI38 cells by ELISA after exposure to CBNP. Inflammatory cytokine expression was increased on CBNP exposure. Unexposed cells served as control. Statistical analysis was performed by ANOVA. Significance indicated by ***p<0.001 and ****p<0.0001.

4.2.2.3 Monocyte response to short-term CBNP exposure

4.2.2.3.1 CBNP-induced change in cell size and morphology of monocytes

The 24 h exposure to high concentrations of CBNP induced cell enlargement and loss of morphology in monocytes (Fig: 4.34.(1) and (2A). Phase contrast microscopy of CBNP-exposed THP1 cells showed that the size of cells was increased (80-160 µg/mL upto 3 fold and a marked reduction in viability was also observed (Fig:4.34 (2B).

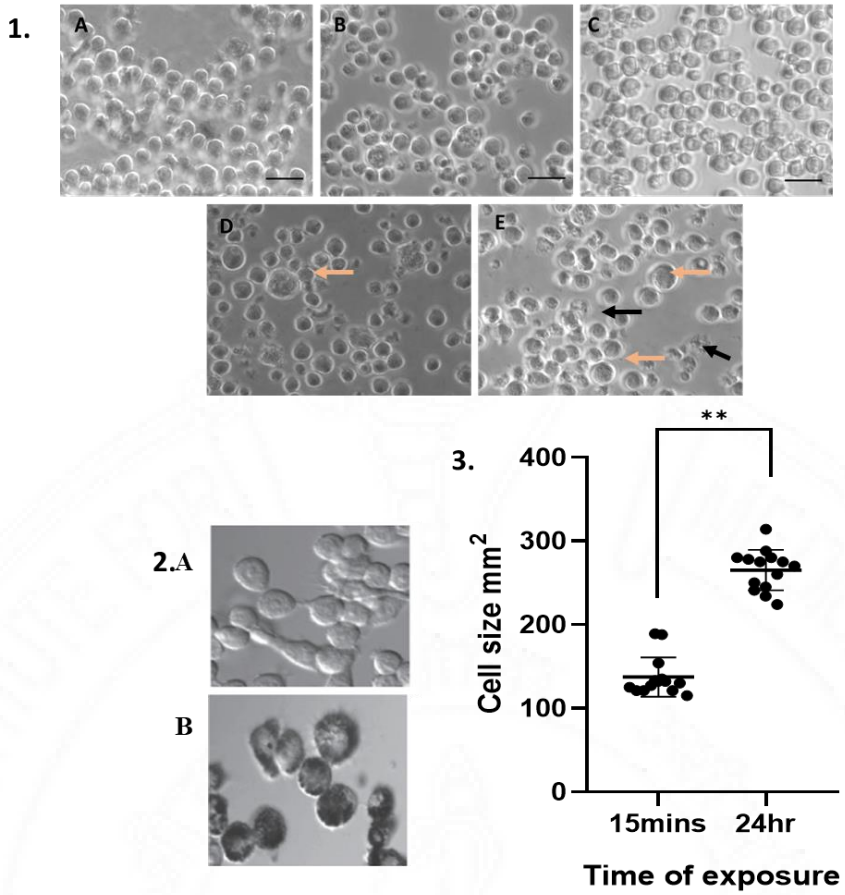

Fig 4.34: Analysis of change in cell morphology and size of THP1 cells after short-term CBNP exposure. (1.) Phase contrast microscopic image of THP1 cells exposed to CBNP. A, control, B. 20 µg/mL, C. 40 µg/mL, D. 80 µg/mL, E.160 µg/mL . An increase in cell size is indicated by yellow arrows cell death is indicated by black arrows. Fig (2) shows the difference in cell size in A. control and B.80 µg/mL. Fig 3 shows a graphical summary of the change in Cell size of 80 µg/mL exposed cells after 15 min and 24 h. The images were assessed with image J. The graph summarises independent triplicate experiments. **p<0.01 was considered significant.

4.2.2.3.2 Biochemical changes in THP 1 on short term-CBNP exposure

4.2.2.3.2.1 Short-term exposure of CBNP induced dose-dependent change in the viability of monocyte THP1. High concentration exposure for 24 h significantly reduced the mitochondrial activity of THP1 cells. The viability reduced to 60% at the highest dose exposure ie,160 µg/mL (Fig 4.35).

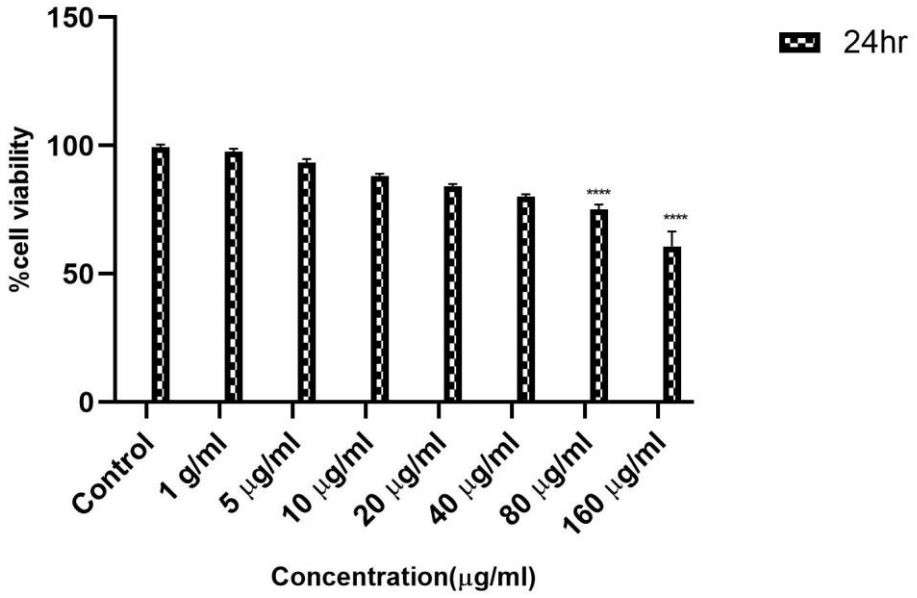

Fig 4.35 MTT assay of THP1 cells exposed to CBNP for 24 h. The values are expressed as percentage viability with respect to control. Control wells I were not exposed to CBNP The data represent the mean ± SD of three independent experiments. Statistical significance is indicated by ***p<0.001.

4.2.2.3.2.2 Short-term exposure to CBNP affected plasma membrane integrity of Monocytes

LDH is a stable cytosolic enzyme released into the culture supernatant from cells with compromised membrane integrity. An increase in LDH in the culture was observed in high-concentration CBNP-exposed cells indicating the cytotoxicity of CBNP. 35% cytotoxicity was observed in 80 µg/mL CBNP-exposed cells and the cytotoxicity increased to 55% in 160 µg/mL CBNP-exposed cells after 24 h exposure (Fig 4.36).

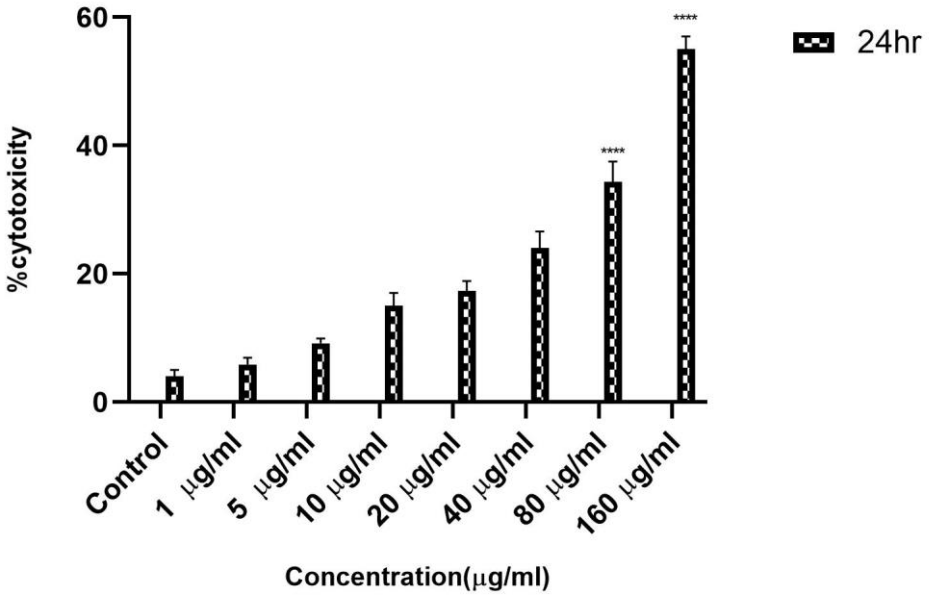

Fig 4.36 LDH assay of THP1 cells exposed to CBNP for 24 h. Complete lysis of THP1 cells with lysis solution provided max. LDH release to the supernatant. Control wells were not exposed to CBNP. The data represent the mean ± SD of three independent experiments. Statistical significance is indicated by ***p<0.001.

4.2.2.3.2.3 CBNP induced lysosomal membrane leakage in monocytes

Short-term exposure to high concentrations of CBNP in monocytes induced loss of lysosomal membrane integrity. From the neutral red uptake assay, it was evident that the high-concentration CBNP (80 µg/mL and 160 µg/mL) exposed cells were unable to retain the dye. The percentage uptake reduced to 51% in 160 µg/mL CBNP-exposed cells which pointed to the lysosomal damage and outflow of the Neutral red dye (**Fig 4.37)**

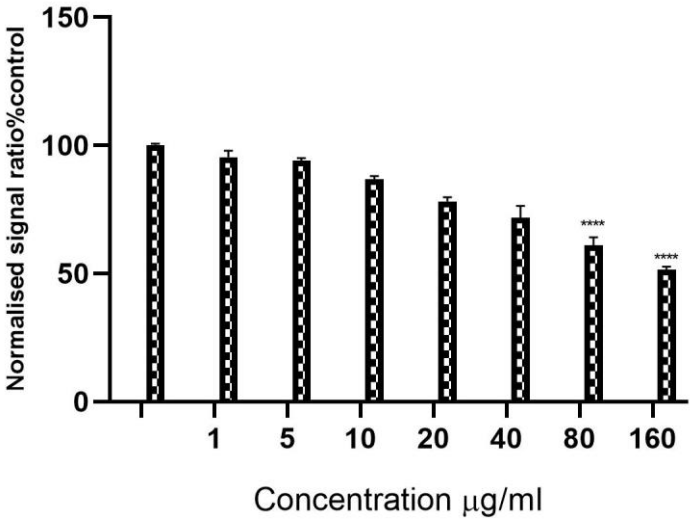

Fig 4.37 Neutral red uptake assay of THP1 cells exposed to CBNP for 24 h. The values are expressed in percentage with respect to control. The data represent the mean ± SD of three independent experiments. Statistically, significant difference is denoted by ***p<0.001

4.2.2.3.2.4 CBNP Induced oxidative stress in monocytes

Reactive oxygen species function as secondary messengers in many critical signalling pathways. However, an elevated intracellular level of ROS can induce oxidative stress in cells which will damage lipids, proteins, and DNA. An increased ROS production was observed in high doses CBNP exposed cells (>40 µg/mL). The fold change peaked by 6 h exposure and a reduction in fold change was observed at further time points in the same treatment (Fig 4.38). ROS is an early response to any stimuli by the cells which will substantiate the observation.

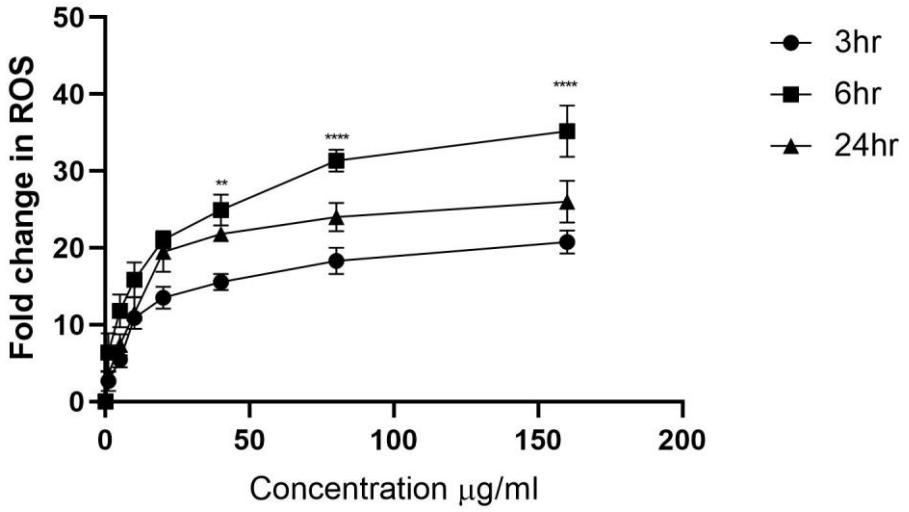

Fig4.38 ROS assay of THP1 cells exposed to CBNP for varying time points. An increase in fold change across time points was observed which implies a dose-dependent increase in ROS production in THP1. Independent experiments, **p<0.1 and ***p<0.001 was considered significant.

4.2.2.3.2.5 CBNP induced caspase 1 activity in THP1 cells.

The caspase1 activity of CBNP cells was quantified using a caspase1 assay kit (Promega). Luminescence from THP1 cells exposed to CBNP significantly increased indicating enhanced Caspase 1 activity. Treatment with the inhibitor of caspase 1 activity YVAD-CHO significantly downregulated the luminescence (Fig 4.39). The assay demonstrates CBNP induces pyroptotic cell death in THP1 cells.

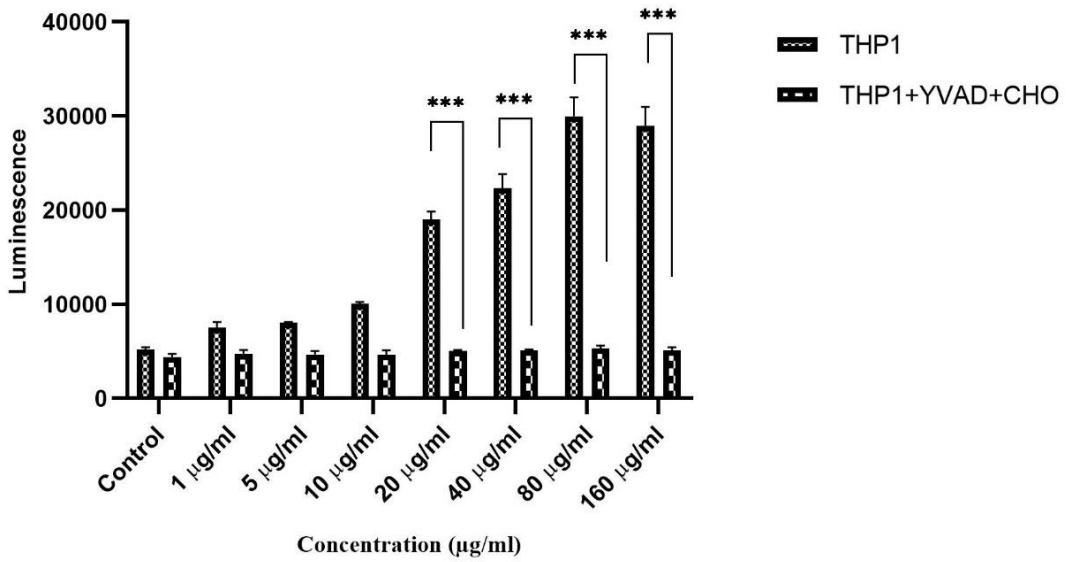

Fig 4.39 Caspase 1 assay of THP1 cells exposed to CBNP. Increased caspase 1 activity was evident from the luminescence. The addition of inhibitor YVAD-CHO reduced the activity. Cells unexposed to CBNP served as control. Data were assessed by two-way ANOVA. Significance is indicated by*** $p<0.001$

4.2.2.3. Molecular changes in THP-1-after short term CBNP exposure

4.2.2.3.1 CBNP did not induce DNA laddering in THP1 cells

DNA laddering is characteristic of apoptotic cell death. DNA ladder assay of CBNP exposed THP1 cells that did not show the presence of DNA ladders. A thick band of unfragmented DNA was observed in all the wells of agarose gel (Fig 4.40).

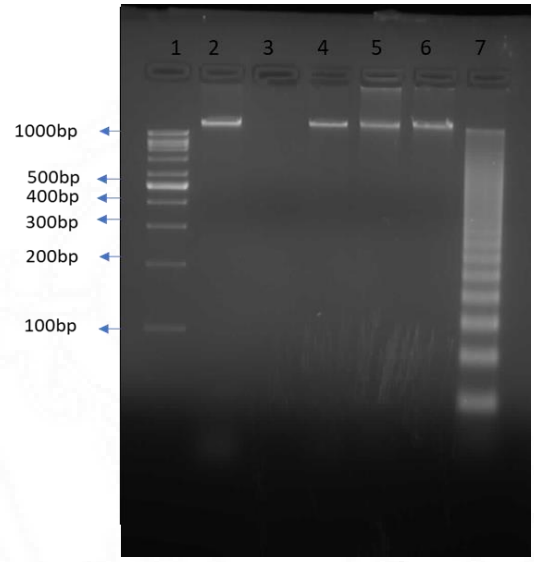

Fig 4.40 DNA laddering assay of THP1 exposed to CBNP. Lane 1 marked is a marker, lane 2 control, lane 4 is 40 µg/mL, lane 5 is 80 µg/mL, lane 6 is 160 µg/mL and lane 7 is positive control (Staurosporine treated cells).

4.2.2.3.2 CBNP induced IL-1β and TNF-α gene expression in monocytes

Inflammatory cytokine gene expression in monocytes exposed to CBNP for 24 h was evaluated by RT-PCR. As seen in Fig 4.41. IL-1β gene expression was upregulated in THP1 cells in a dose-dependent manner. Fold change in gene expression was increased up to 5 fold in high-dose treatment

IL-8 and IL-6 gene expression in THP1 showed a different trend compared to epithelial as well as fibroblasts (Fig 4.41). Here we observed a minor upregulation in IL-6 and IL-8 but the change was insignificant in statistical analysis.

.i NOS (induced Nitic oxide synthase) is secreted by monocytes and macrophages and is involved in Nitric oxide synthesis, a key pro-inflammatory molecule that mediates redox-dependent pathogen clearance by phagocytic cells. Here CBNP exposure failed to upregulate iNOS expression.

TNFα expression was upregulated up to 1.75 fold on CBNP exposure. MCP-1 expression was found to be downregulated on short-term CBNP exposure (Fig 4.41)

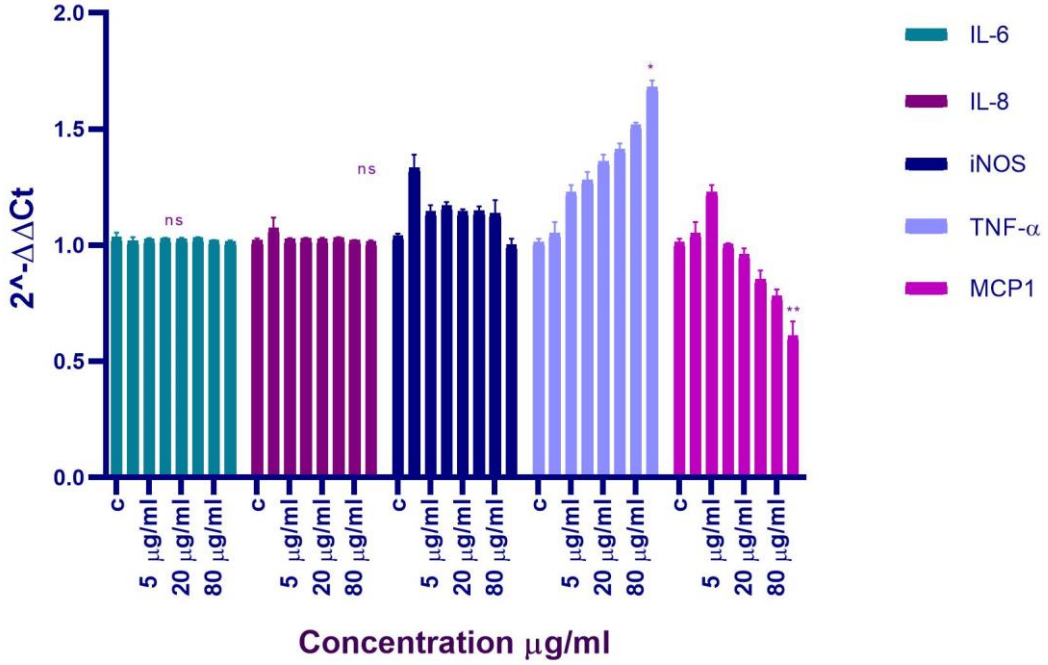

Fig 4.41 Gene expression of cytokines in THP1 cells exposed to CBNP for 24h.Upregulation of TNF α was observed in THP1 cells. Cells unexposed to CBNP served as control. Two-way ANOVA assessed the fold change in gene expression. Significance is indicated by *p<0.5,**p<0.01,*** p<0.001 and ****p<0.0001

4.2.2.3.3 CBNP induced Pyroptotic cell death in monocytes

The absence of a DNA ladder and increased cell membrane leakage evidenced by DNA ladder assay and LDH assays indicated the possibility of cell death mechanism different from apoptosis and necrosis- the possibility of pyroptotic mechanism of cell death was investigated. Hence we assessed caspase and IL-1 β gene expression in CBNP-exposed THP1 cells at varying concentrations of CBNP.

Caspase 1 and IL-1 β are markers of Pyroptosis while caspase 3 is upregulated during apoptosis. A 4.7-fold increase in gene expression of Caspase1 was observed in higher-concentration CBNP-exposed cells (40,80 &160 µg/mL). The IL-1 β expression was upregulated up to 5-fold on CBNP exposure. Caspase 3 did not show upregulation under conditions of experimentation (Fig 4.42).

.

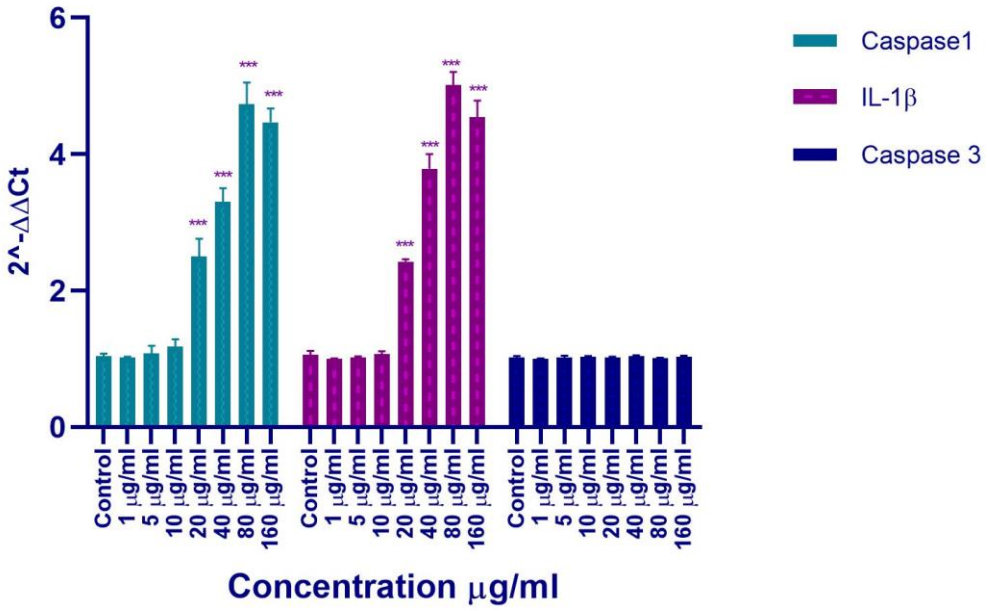

Fig 4.42 Gene expression of Pyroptotic markers in THP1 cells exposed to CBNP for 24h.An upregulation of Caspase1 and IL-1β was observed in THP1 cells. Cells unexposed to CBNP served as control. The fold change in gene expression was assessed by two-way ANOVA. Significance is indicated by*** $p<0.001$.

4.2.3 Long-term exposure of CBNP in alveolar cells

4.2.3.1 Alveolar epithelial cells response

4.2.3.1.1 Morphological changes in A549 cells on prolonged CBNP exposure

4.2.3.1.1.1 Prolonged exposure to low concentrations of CBNP induced morphological changes in A549 cells.

Low concentrations of CBNP (1,5,10,20 &40 µg/mL) induced loss of epithelial morphology. The cuboidal morphology was lost and the cells showed spindle-shaped morphology. The effect was more pronounced in 5-10 µg/mL treatment (Fig 4.43)

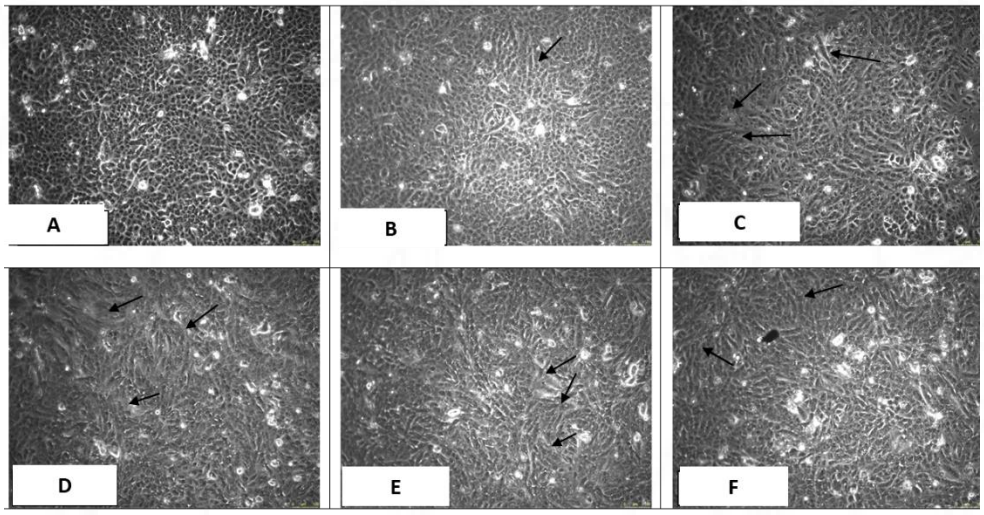

Fig 4.43 Phase contrast microscopy of A549 cells exposed to low concentrations of CBNP. A, control, B- 1 µg/mL, C-5 µg/mL, D-10 µg/mL, E-20 µg/mL and F-40 µg/mL. Black arrows indicate the spindle-shaped morphology of A549 cells. Scale 100µm

4.2.3.1.1.2: Prolonged exposure to CBNP induced Epithelial-Mesenchymal transition (EMT) in alveolar epithelial cells.

Giemsa staining of alveolar epithelial cells clearly showed that the A549 cells lost the cuboidal epithelial morphology and acquire the spindle morphology characteristic of

mesenchymal cells by 120 hours of exposure to low doses of CBNP. This morphology change is denoted as EMT or Epithelial-Mesenchymal Transition (Fig 4.44-B&C).

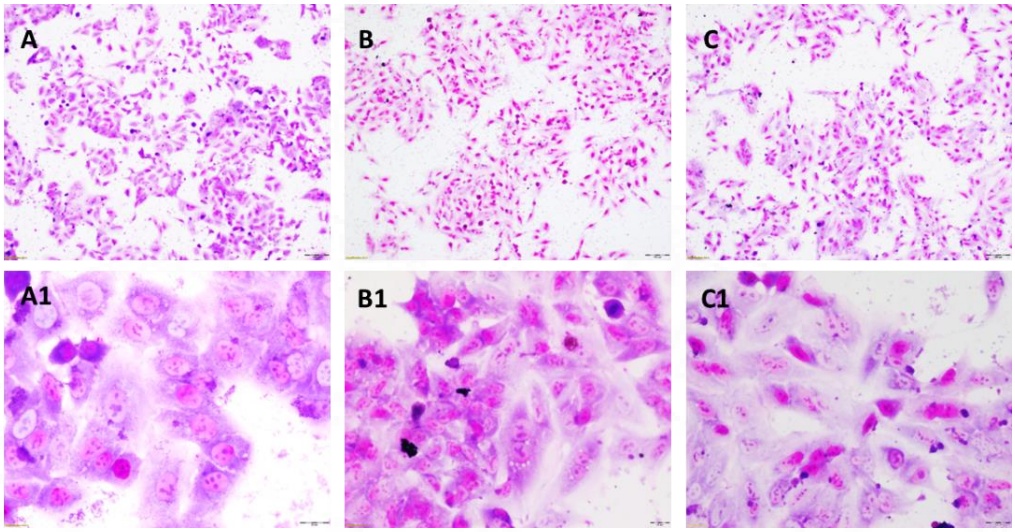

Fig 4.44 Giemsa staining of A549 cells exposed to CBNP for a prolonged time. A-control, B-5 µg/mL, C-10 µg/mL Magnification 20x. A1, B1, and C1 are the images at higher magnification of the same (Mag 40x)

4.2.3.1.1.3 Prolonged exposure to low concentrations did not affect cell viability.

Live dead staining of A549 cells exposed to CBNP showed that prolonged exposure to CBNP did not induce cell death. Cellular uptake of calcein AM was high up to 20 µg/mL exposure (Fig 4.45 B-E) upon 40 µg/mL treatments the cellular uptake of ethidium homodimer increased indicating the loss of cell viability in the same (Fig 4.45 F).

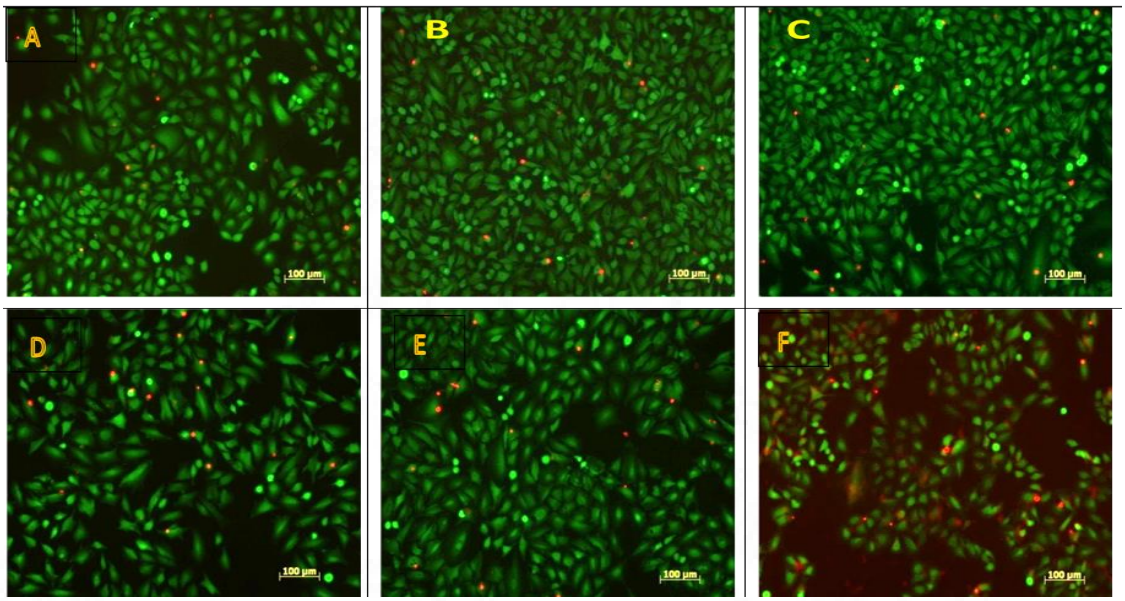

Fig 4.45 Live dead staining of A549 cells exposed to CBNP. A-control, B-1 µg/mL, C-5 µg/mL, D-10 µg/mL, E-20 µg/mL and F-40 µg/mL. Increased uptake of ethidium was observed in 40 µg/mL. Scale 100µm

4.2.3.1.1.4 Prolonged exposure of CBNP-induced actin remodelling in epithelial cells

Actin cytoskeletal remodelling is a hallmark of EMT. The actin remodelling by CBNP was assessed using rhodamine- phalloidin stain. From Fig 4.46 B & C, a change in the cuboidal morphology of typical epithelial cells (Fig 4.46 A) to elongation towards a spindle shape was observed.

The staining implies a clear actin reorganization from cortical thin bundles to thick parallel bundles in a dose-dependent manner (Fig 4.46)

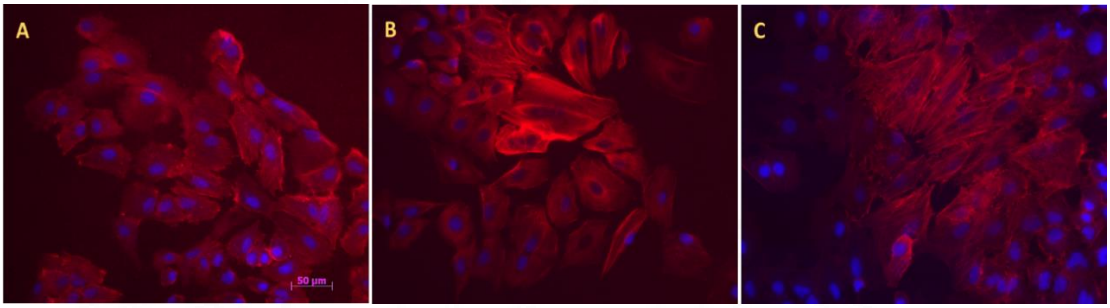

Fig 4.46 Actin staining by rhodamine-phalloidin of A549 cells exposed to CBNP. A-control, B-5 µg/mL, C-10 µg/mL. The change in morphology is evident in C. Scale 50µm. Magnification 20x.

4.2.3.1.2 Biochemical changes in A549 cells on prolonged CBNP exposure

4.2.3.1.2.1 Prolonged exposure to higher concentrations induced lysosomal destabilization in alveolar epithelial cells

AO staining indicates lysosomal integrity in cells. A shift in red to green fluorescence was observed in A549 monolayer on 40 µg/mL of CBNP-after prolong exposure of 120 h. The shift in fluorescence is an indication of lysosomal destabilization. An increase in red fluorescence was observed in low-concentration 1, 5, 10 & 20 µg/mL (Fig 4.47 B, C, D) treated cells although there is seen a gradual shift as concentration increases. During EMT the lysosome number and lysosomal protease activity are increased.

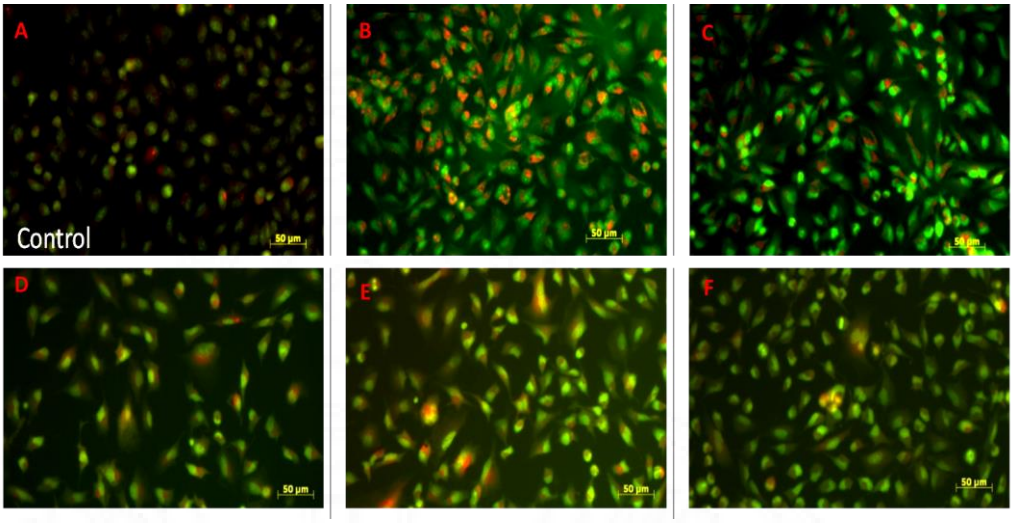

Fig 4.47 AO staining of prolonged CBNP exposed A549. A, control, B- 1 µg/mL, C-5 µg/mL, D-10 µg/mL, E-20 µg/mL and F-40 µg/mL. Increased red fluorescence is evident in B. Shift in fluorescence is visible in F. Mag 20X scale 50µm.

4.2.3.1.2.2 Prolonged CBNP exposure induced a change in Mitochondrial membrane potential.

Here the change in mitochondrial membrane potential (ΔΨm) upon prolonged CBNP exposure to JC10 dye was assessed. Decreased ΔΨm upon CBNP exposure was observed with an increase in green fluorescence in cells in a dose-dependent manner. 1-10 µg/mL treatment did not alter ΔΨm (Fig 4.48).

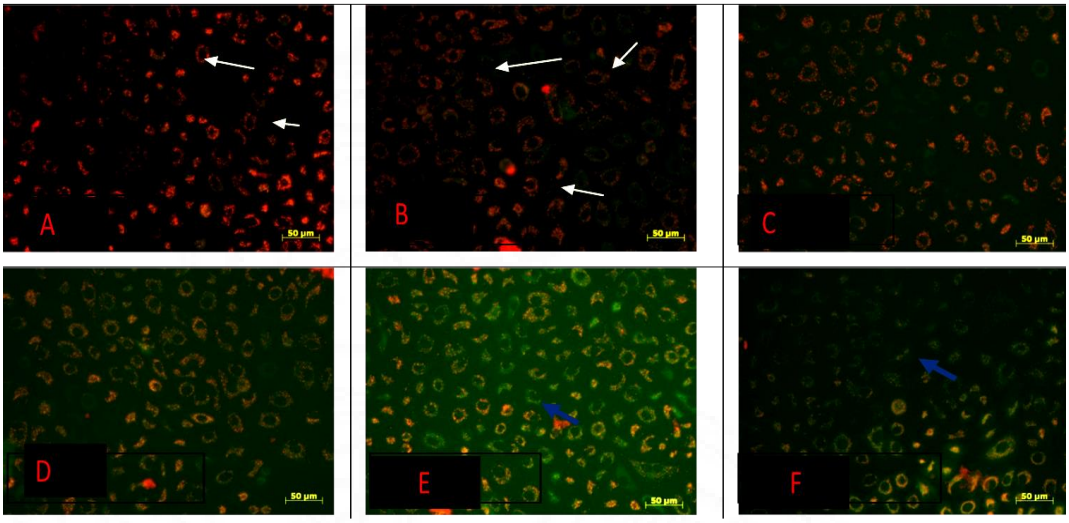

Fig 4.48 JC-10 staining of A549 cells exposed to CBNP. A, control,B- 1 µg/mL, C-5 µg/mL, D-10 µg/mL, E-20 µg/mL and F-40 µg/mL. An increase in green fluorescence was observed. Scale 50µm Mag 20X.

4.2.3.1.2.3 Prolonged CBNP exposure induces collagen synthesize in A549 cells.

Collagen synthesis and secretion are characteristics of mesenchymal cells. The collagen secretion in EMT cells was assessed by the collagen menstruation procedure described in the methodology. Increased collagen production was observed in EMT cells upon prolonged CBNP exposure (Fig 4.49).

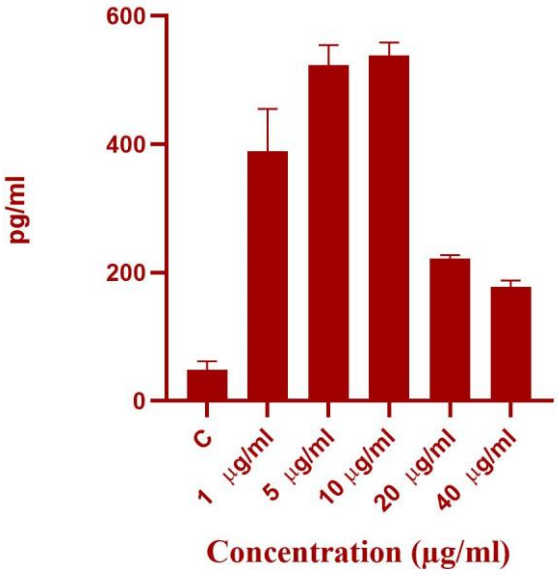

Fig 4.49 Collagen estimation assay of EMT cells after CBNP exposure. Spectrophotometric quantification of collagen showed an increased absorbance in 1-10 µg/mL CBNP-treated cells. Unexposed cells served as control.

4.2.3.1.2.4 Contractility of epithelial cells was increased upon prolonged CBNP exposure.

Contractility is a key function of fibroblast cells. A gel contraction assay was performed to evaluate the contractility of cells undergoing EMT. The gels containing cells treated with conditioned medium from CBNP-exposed cells were smaller than the control gels. A significant reduction in gel size (50% of the initial size) was visible after day 5 (Fig 4.50).

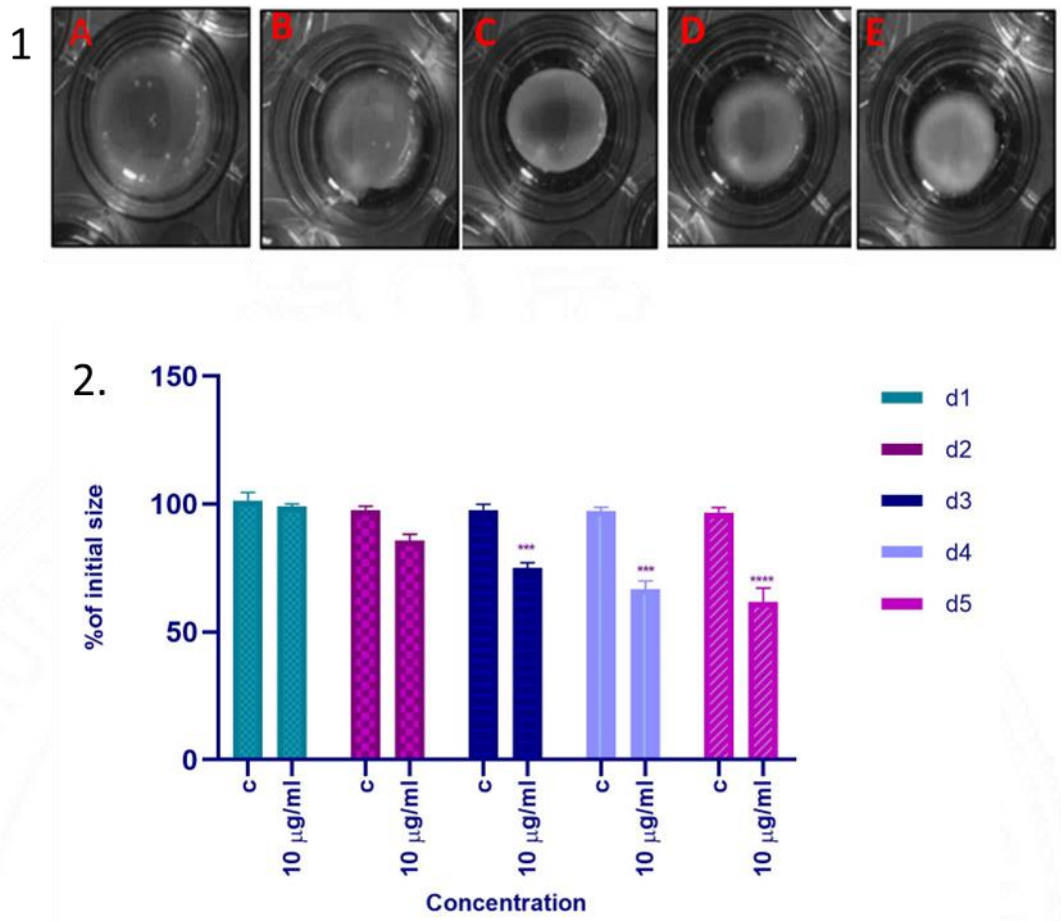

Fig 4.50. Contractility of epithelial cells on CBNP exposure. Fig 1. Image of gel exposed to conditioned media of 10 µg/mL CBNP exposed cells from **day to day5**.Fig 4.42.2 Graph representing the difference in gel size across the 5-days of treatment period with conditioned media vis~a~vis unexposed cells.

4.2.3.1.3 Molecular changes

4.2.3.1.3.1 CBNP-induced upregulation of EMT markers

TGF-beta signalling has been shown to play an important role in EMT. The prolonged CBNP significantly upregulated TGFβ expression up to 6.3fold (Fig 4.51). Reduction in expression was observed in higher concentrations owing to the cytotoxicity of the same.

Fold increase up to 4 fold was observed in the ACTA 2 gene (Fig 4.51) which is involved in the transcription of alpha-smooth muscle actin another marker of EMT. Prostaglandin E2 critically downregulates fibroblast activation and mediates inflammatory responses. Downregulation in PGE2 expression was observed in CBNP expose cells indicating the activation of a pro-fibrotic cascade than inflammatory signalling.

Matrix metalloproteinases MMPs are critical in tissue remodelling. MMP-3 has been directly implicated in epithelial-mesenchymal transformation (EMT). Compared to unexposed control, an upregulation in MMP3 expression up to 4 fold was observed in CBNP-exposed cells (Fig 4.51). At the same time, Tissue inhibitors of metalloproteinases expression were downregulated.

E cadherin is the cell adhesion molecule characteristic of epithelial cells. A downregulation in E-cadherin expression was observed in CBNP-exposed epithelial cells (Fig 4.51). CollagenA1 genes characteristic of fibroblasts were upregulated in CBNP-exposed cells. A fold change of 4.3 was observed in nanoparticle-exposed cells (Fig 4.51).

Protein expression of EMT markers TGFβ and PGE2 was done by ELISA. A significant increase in TGF expression was observed in CBNP-exposed epithelial cells. PGE2 expression remained equivalent to control levels, only high concentration elicited expression of PGE2 and was considered to be significant (Fig 4.52).

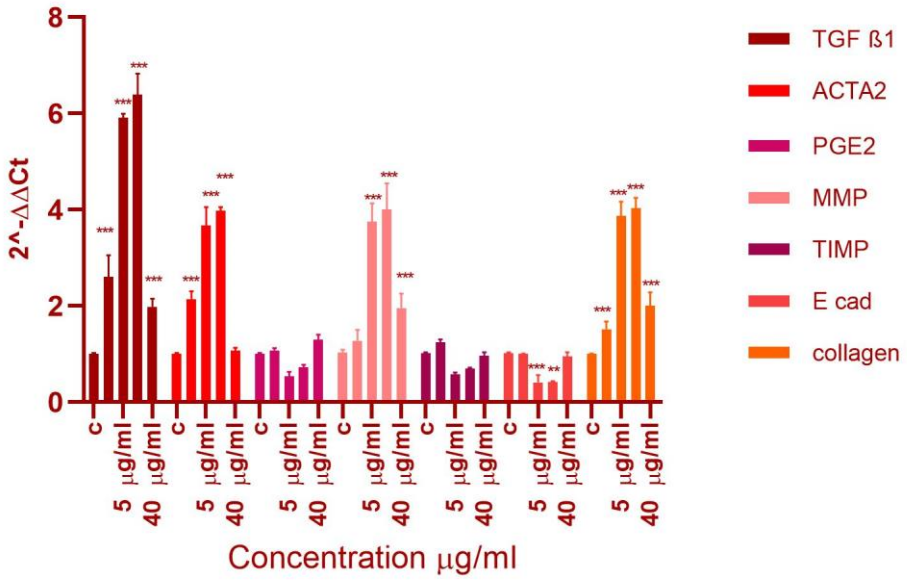

Fig 4.51 Gene expression of EMT markers. A significant upregulation in fibroblast markers was evident in CBNP-exposed cells. The fold change in gene expression was assessed by two-way ANOVA. Significance is indicated by*** p<0.001.

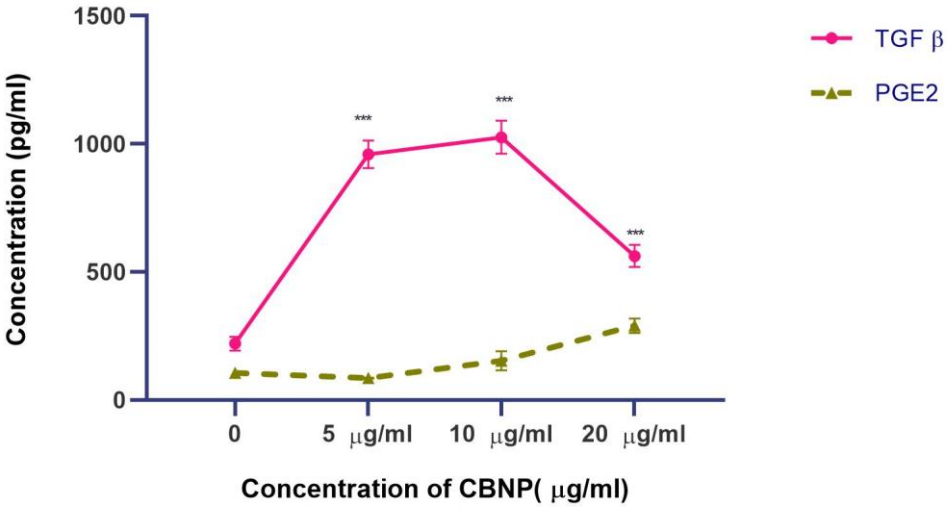

Fig 4.52 Protein quantification of EMT markers by ELISA. TGFβ expression was increased in CBNP exposure whereas PGE2 expression remained unaltered. The data represent the mean ± SD of three independent experiments. Statistically, significant difference is denoted by ***p<0.001

4.2.3.1.3.2 CBNP induced EMT through canonical *Smad-wnt* signalling

Activation of canonical signalling pathways was assessed by immunostaining of modulators in the EMT signalling cascade.

Smad3 is a key intracellular mediator of TGFβ signalling regulated through phosphorylation by the TGFβ receptor complex. Transcription factors like *Snail1* and *Twist*, interact with *Smads* to form EMT-promoting *Smad* complexes that can repress the epithelial genes or activate mesenchymal genes. Phosphorylated *smads* are indicators of the activation of signalling cascade. The presence of phosphorylated smad3 (*psmad3*) in CBNP-exposed cells was assessed by immunostaining. 10 µg/mL treatment induced a significant change in earlier assays. Hence the immunostaining proceeded with that concentration. Control cells stained negative for psad3 (Fig 4.53 A1). The presence of *psmad3* was evident in CBNP-exposed cells (Fig 4.53.A2)

β-catenin is a key component of the canonical Wnt signalling pathway that plays pivotal roles in cell differentiation and embryogenesis. Nuclear translocation of β-catenin is a hallmark of EMT. Here nuclear translocation of β-catenin was assessed in CBNP-exposed cells. β-catenin in control cells was found to be concentrated in adherens junctions (Fig 4.53 B1) whereas in CBNP-exposed cells the presence was observed in the nuclear region (Fig 4.53.B2). This implies the nuclear translocation of β-catenin in CBNP-exposed cells.

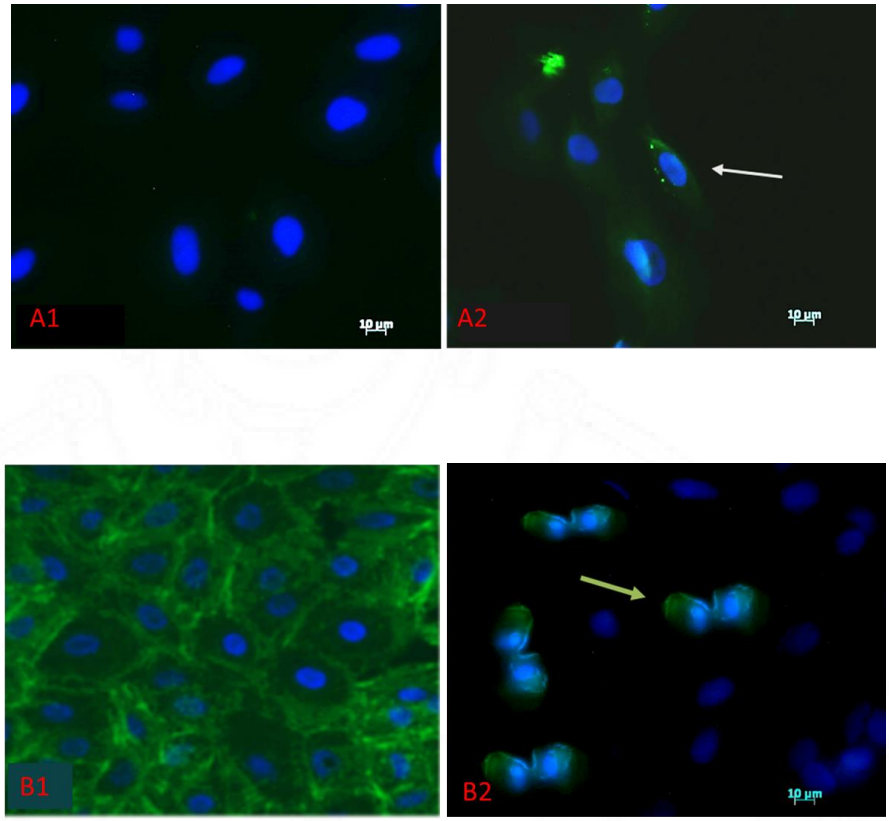

Fig 4.53 Immunostaining of EMT modulators. Palette A- Immunostaining of *psmad3*. A1-control and A2- 10 µg/mL CBNP exposed cells. A2 stained positive for *psmad3*.Palette B - Immunostaining of β-catenin. B1-control and B2 10 µg/mL CBNP exposed cells. Nuclear translocation of β-catenin in CBNP-exposed cells is indicated by yellow arrows. Scale 10µm, Mag 40x

4.2.3.3.1.3 CBNP induced α smooth muscle actin (α SMA) expression in A549 cells

α Smooth muscle actin is a hallmark of active fibroblast cells. The presence of SMA was evident in CBNP-exposed alveolar epithelial cells. The positive staining indicates activation of downstream signalling of the *smad-wnt* cascade(Fig 4.54 A2).

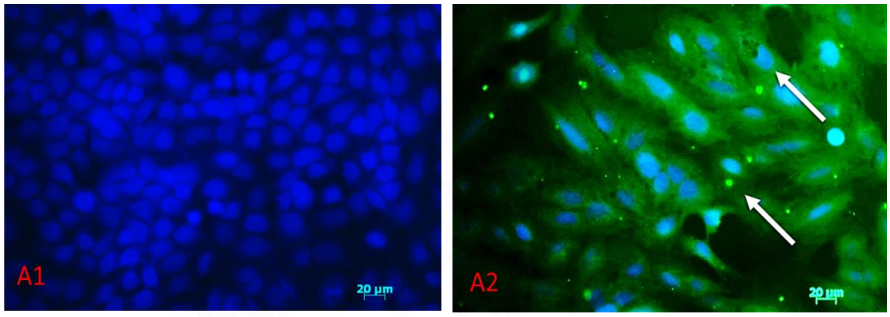

Fig 4.54 Immunostaining of α SMA in CBNP exposed A549 cells. A1-Control and A2 10 µg/mL CBNP exposed cells. The presence of α SMA in CBNP-exposed cells is indicated by white arrows. Scale 20µm, Mag 20x.

4.2.3.2 Fibroblast cells

4.2.3.2.1 Morphology changes in Fibroblast cells

Low concentrations induced fibroblast proliferation in WI-38 cells. Prolonged exposure to low concentrations of CBNP (up to 10 µg/mL) increased fibroblast population evidenced by CBB staining Fig 4.55.A) and Live dead staining of WI-38 cells (Fig 4.55 B).

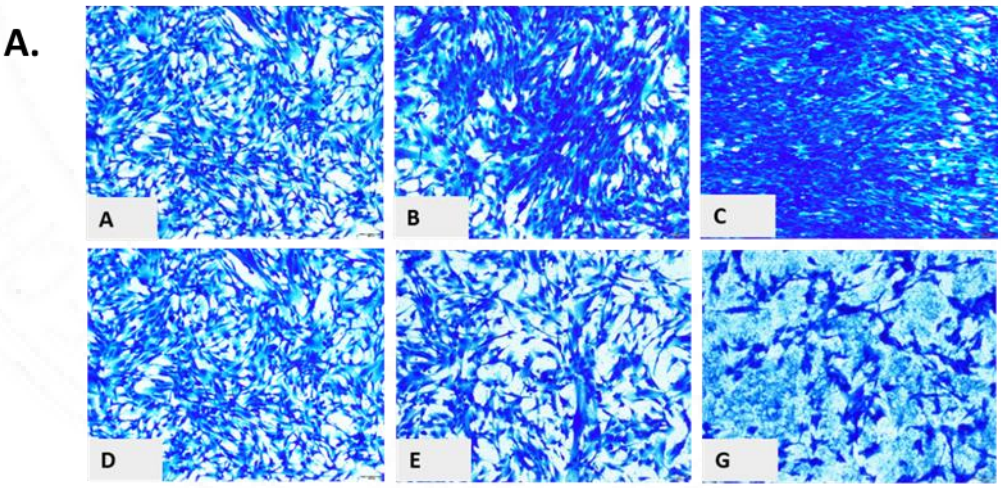

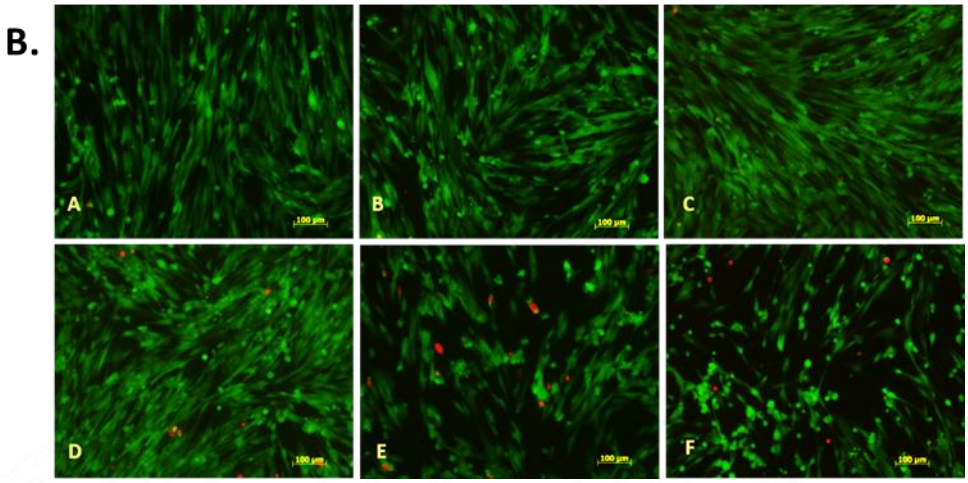

Fig 4.55 Morphological changes in WI-38 cells. **CBB staining** (A) of WI-38 cells exposed to CBNP, **B- Live dead staining** of WI-38 cells exposed to CBNP. A, control, B- 1 µg/mL, C-5 µg/mL, D-10 µg/mL, E-20 µg/mL and F-40 µg/mL. Scale 100µm Mag 20x

4.2.3.2.2 Biochemical changes

4.2.3.2.2.1 Prolonged CBNP exposure induced collagen secretion in fibroblast cells.

CBNP-exposed fibroblast cells were assessed for collagen synthesis by the collagen menstruation procedure described in the methodology. Increased collagen production was observed in fibroblast cells upon prolonged CBNP exposure (Fig 4.56). Increased collagen secretion indicates activation of fibroblasts.

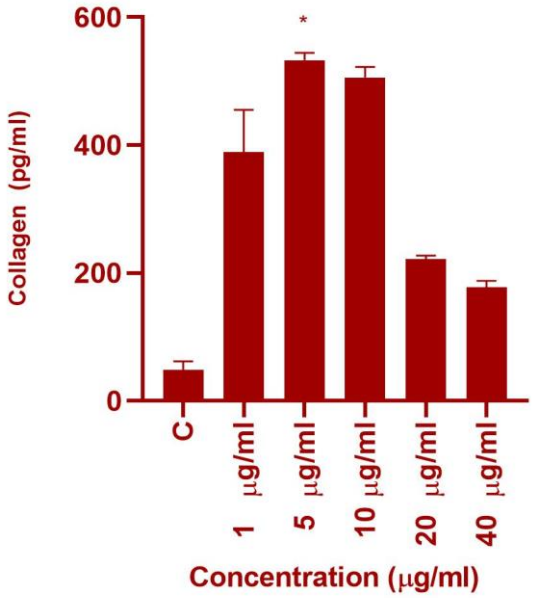

Fig 4.56 Collagen estimation assay of WI38 cells after CBNP exposure. Spectrophotometric quantification of collagen showed an increased absorbance in 1-10 µg/mL CBNP-treated cells. Unexposed cells served as control. The data represent the mean ± SD of three independent experiments. Statistically, significant difference is denoted by ***p<0.001

4.2.3.2.3 Molecular changes

4.2.3.2.3.1 CBNP induced fibroblast activation markers

Gene expression of TGF β1, ACTA2, PGE2, Collagen and PI3K were assessed (Fig4.57 A)

TGF β1 plays a critical role in fibroblast activation. An upregulation of up to 3.8-fold in gene expression of TGF β1 was observed in fibroblast cells exposed to low concentrations of CBNP (1-10 µg/mL).

ACTA 2 expression was upregulated up to 5-fold in CBNP-exposed cells. PGE2 expression was downregulated whereas collagenA1 expression was upregulated up to

4.9-fold. PI3K Phosphoinositide 3 kinase is a critical gene involved in fibroblast proliferation. Upregulation of PI3K up to 5.5 fold was evident from q RT-PCR analysis of gene expression. Prostaglandin E2 expression was found to down-regulated on CBNP exposure whereas TGFβ expression was induced. The protein quantification by ELISA provided results agreeing with the gene expression analyses (Fig 4.57 B).

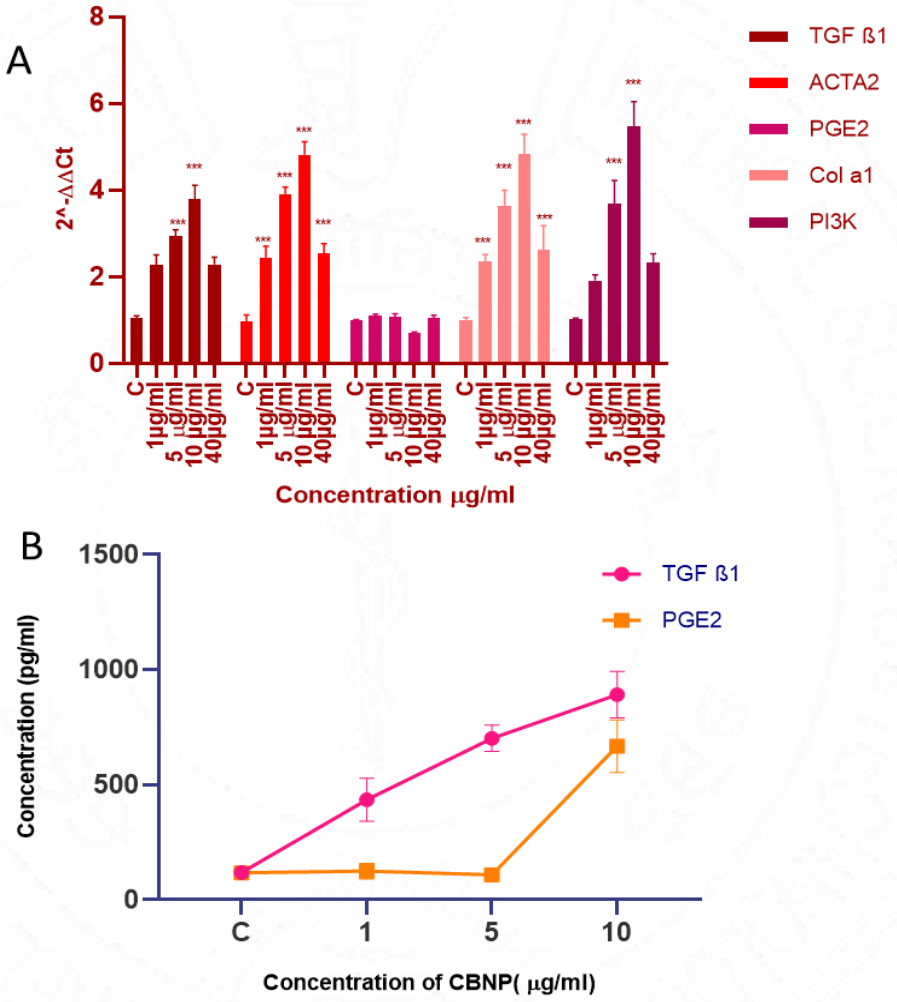

Fig 4.57 Gene expression and Protein expression of Fibroblast activation markers. A significant upregulation in fibroblast markers was evident in CBNP-exposed cells. A) Gene expression of fibrotic markers, B) Protein quantification of fibrotic markers by ELISA. The data represent the mean ± SD of three independent experiments. Statistically, significant difference is denoted by ***p<0.001

4.2.3.3 Monocyte response to prolong CBNP exposure

4.2.3.3.1 Morphological changes

4.2.3.3.1.1 Prolonged CBNP exposure induced morphology change in THP1 cells

Giemsa staining showed a clear change in the morphology of low-concentration CBNP-exposed cells (Fig 4.58). The characteristic round morphology of the suspension cells was changed to that of differentiated macrophages with elongations.

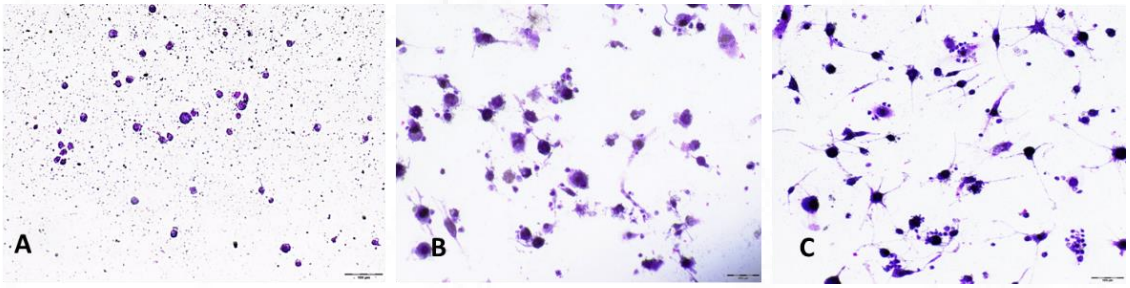

Fig 4.58 Giemsa staining of THP1 cells exposed to CBNP.A control, B-5 µg/mL, C-10 µg/mL. Change in morphology was evident in CBNP exposed cells compared to control. Scale-100µm Mag 10x

4.2.3.3.2 Molecular changes

4.2.3.3.2.1 Prolonged CBNP exposure induced M2 polarisation in monocytes

Monocytes can be differentiated into M1 and M2 phenotypes. M1 is involved in inflammatory responses whereas M2 is in wound healing. responses and fibrosis. Prolonged exposure to CBNP is inducing polarisation to the M2 phenotype characterized by TGFβ1 (up to 3.2-fold) and IL-10 upregulation (3.8-fold) and downregulation of pro-inflammatory cytokines. A nonsignificant upregulation was

observed in iNOS gene expression (Fig 4.59 A). Protein expression data correlated to the gene expression. CBNP induced a significant increase in IL-10 along with TGF β secretion (Fig 4.59B).

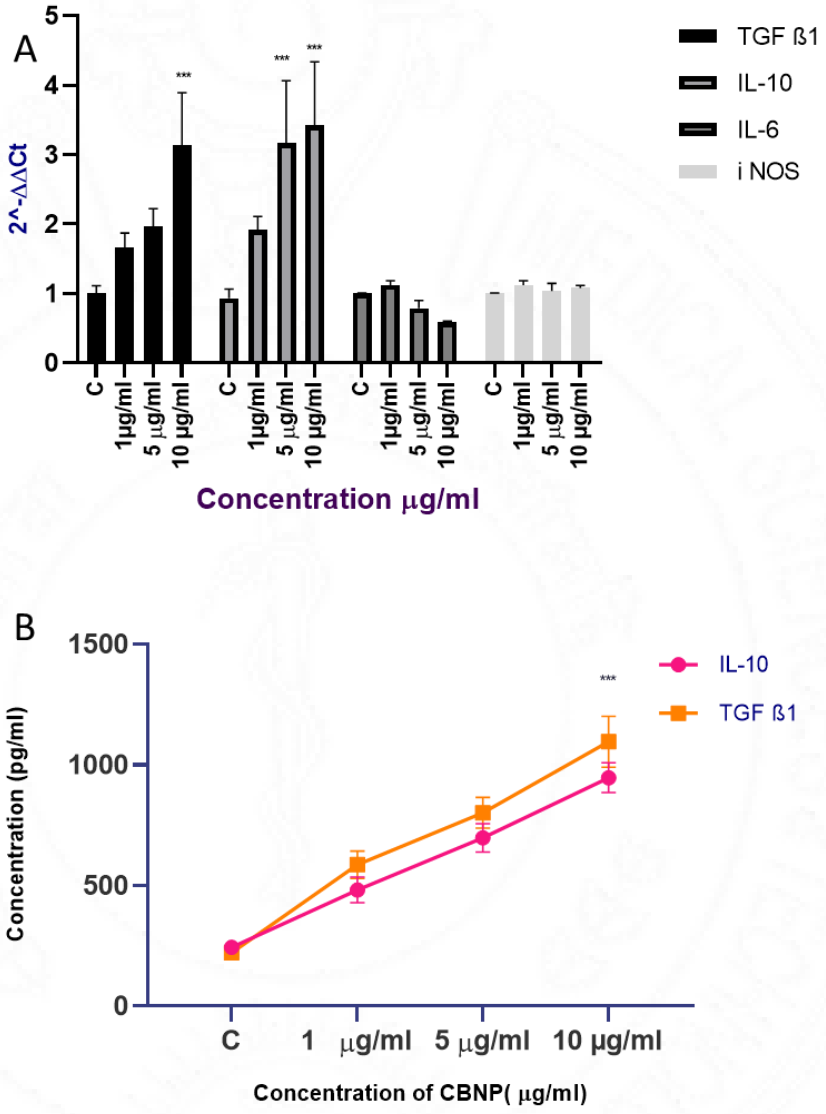

Fig 4.59 Gene expression and protein quantification of cytokines secreted by THP1 cells on prolonged CBNP exposure. A. Gene expression and B. Protein quantification of M2 polarisation markers. The markers were upregulated on CBNP exposure. The data represent the mean ± SD of three independent experiments. Statistically, significant difference is denoted by ***p<0.001

4.3 Phase III. Study the effect of All-Trans Retinoic Acid (ATRA) as an antifibrotic Therapeutic molecule

4.3.1 Effect of ATRA on cell viability

ATRA treatment should not affect the cell viability. In order to select suitable ATRA dose for further assessment of anti-fibrotic potential cell viability of A549 and WI-38 was assessed by MTT (Fig 4.60 A) and LDH assay (Fig 4.60 B).

0.1µM and 1µM concentrations of ATRA did not elicit any change in cell viability. The result was consistent in all the cell types assessed.10µM concentration of ATRA induced significant cytotoxicity evidenced by the reduction in mitochondrial activity as well as increased LDH leakage compared to control. Hence 10µM was evicted from further experiments.

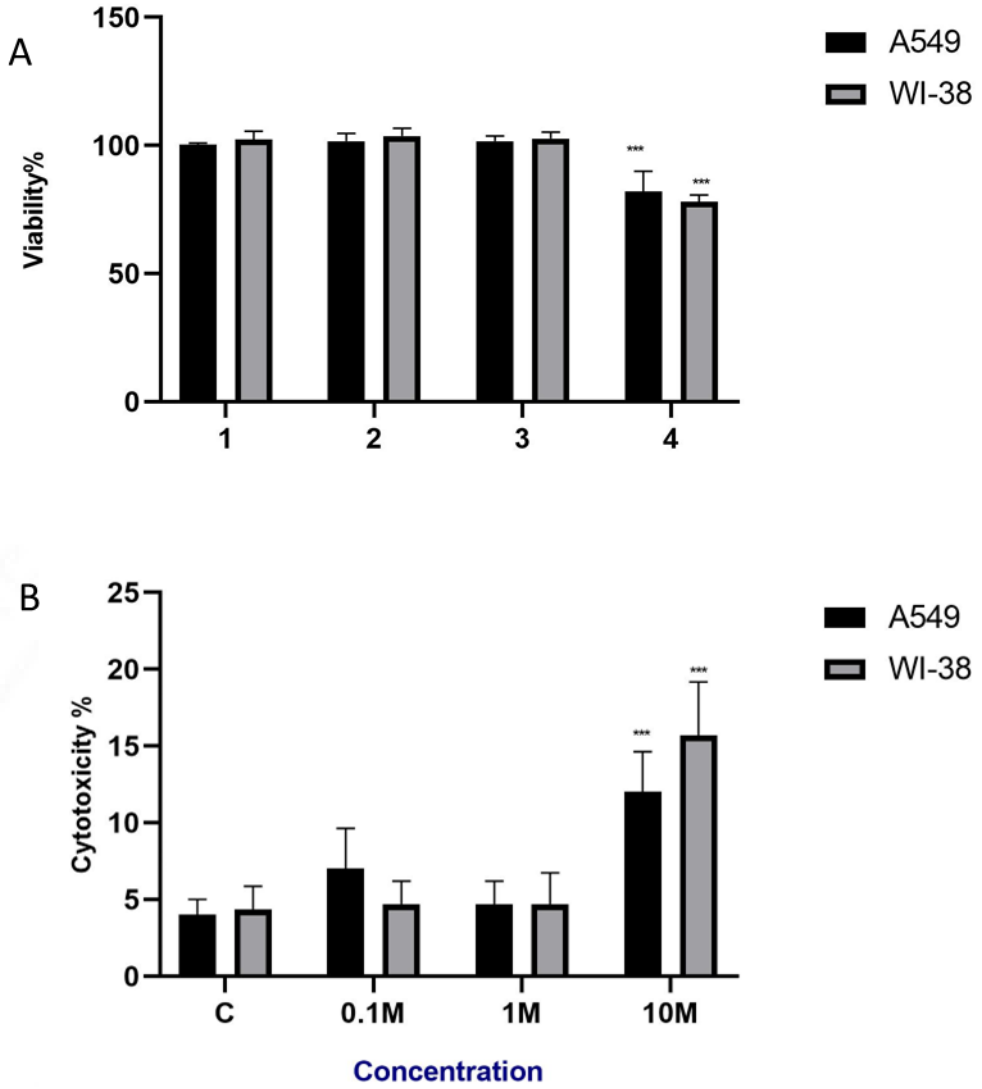

Fig 4.60 Effect of ATRA on cell viability. MTT (A) and LDH assay (B) of ATRA treatment in A549, and, WI-38 cells. The results are expressed as mean±SD of 3 independent experiments. ***p<0.001and ****p<0.0001 found to be significant. Control wells were unexposed to ATRA.

4.3.2 ATRA improves Functionality of A549 cells

The effect of ATRA in down-regulating the EMT markers induced by CBNP was assessed (Fig 4.61). Pre-treatment of ATRA was found to be beneficial in down-regulating EMT induced by CBNP. Gene expression of critical pro-inflammatory genes and surfactant genes was assessed initially in both 0.1 and 1µM concentration

treated groups. 1µM concentration significantly downregulated the inflammatory and fibrotic gene expression and also enhanced Surfactant protein C expression (up to 2 fold).

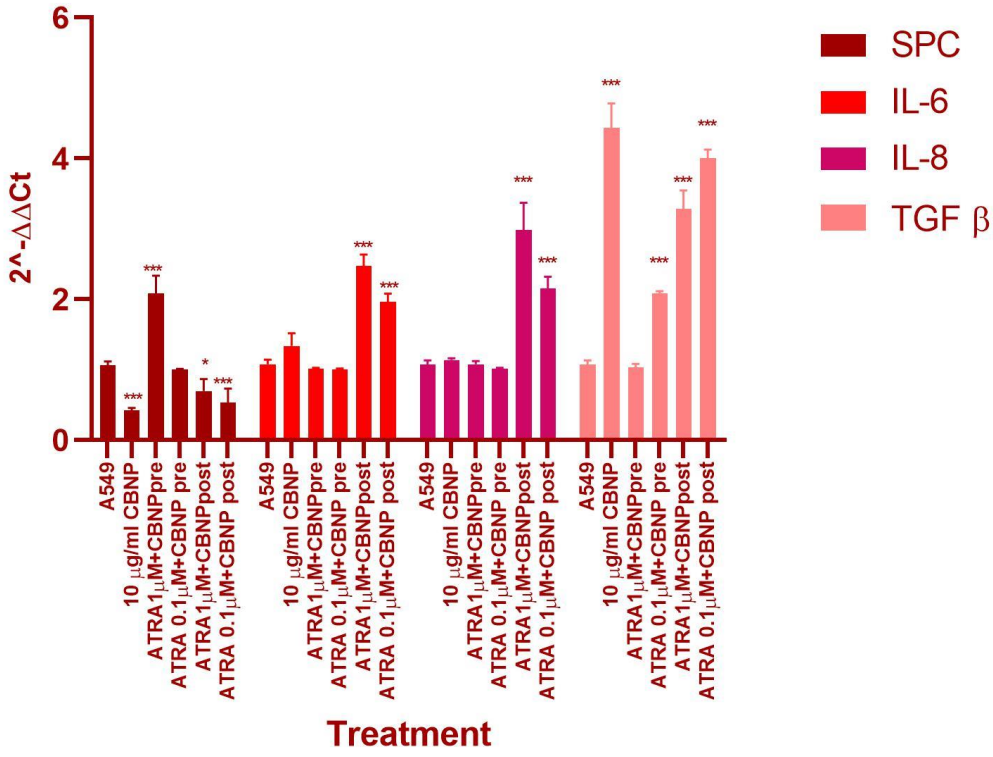

Fig 4.61 Effect of ATRA on cell functionality. Gene expression of SPC, IL;-6.IL-8 and TGF were assessed. The difference in pre-treatment and post-treatment. The values are expressed in percentage with respect to control. Control wells (c) were not exposed to ATRA. The data represent the mean ± SD of three independent experiments. Statistical significance is indicated by **p< 0.01.1µM ATRA restores EMT induced by CBNP

4.3.2 ATRA prevented EMT induction by CBNP exposure in alveolar epithelial cells.

1µM ATRA effectively downregulated the EMT marker genes (Fig 4.62 A). The gene expression was downregulated and was equivalent to untreated control. The

downregulation of EMT implied the anti-fibrotic potential of ATRA. Protein quantification of EMT markers was also assessed in alveolar epithelial cells pre-treated with ATRA (Fig 4.62 B).

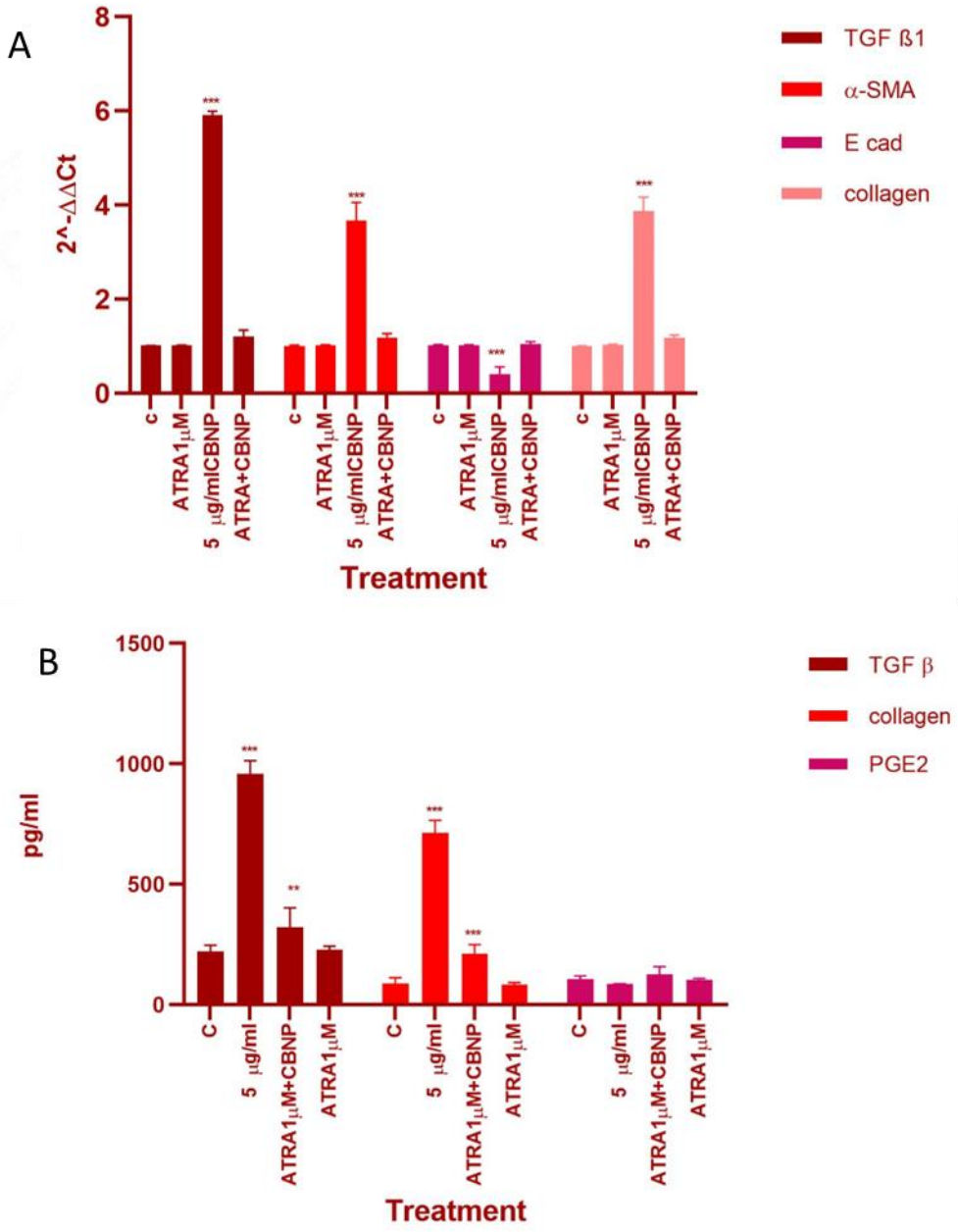

Fig 4.62 Gene expression and protein quantification of EMT markers of A549 cells pre-treated with ATRA on CBNP exposure. Unexposed cells served as control. A. Gene expression

analysis show restoration of upregulated EMT markers by CBNP exposure. B. ELISA analysis agrees with the gene expression data**P<0.01, ***p<0.001 was considered to be significant.

4.3.4 Effect of ATRA on fibroblast cells

4.3.4.1 ATRA reduces the contractility of fibroblast cells activated upon CBNP exposure.

The collagen gel contraction assay was done to evaluate the contractility of fibroblasts.

ATRA pre-treated cells showed reduced contractility (Fig 4.63.1).

The gel size was equivalent to the control. Cells exposed to conditioned medium from CBNP exposed cells showed a remarkable reduction in gel size which was restored in ATRA pr-treated cells (Fig 4.63.2).

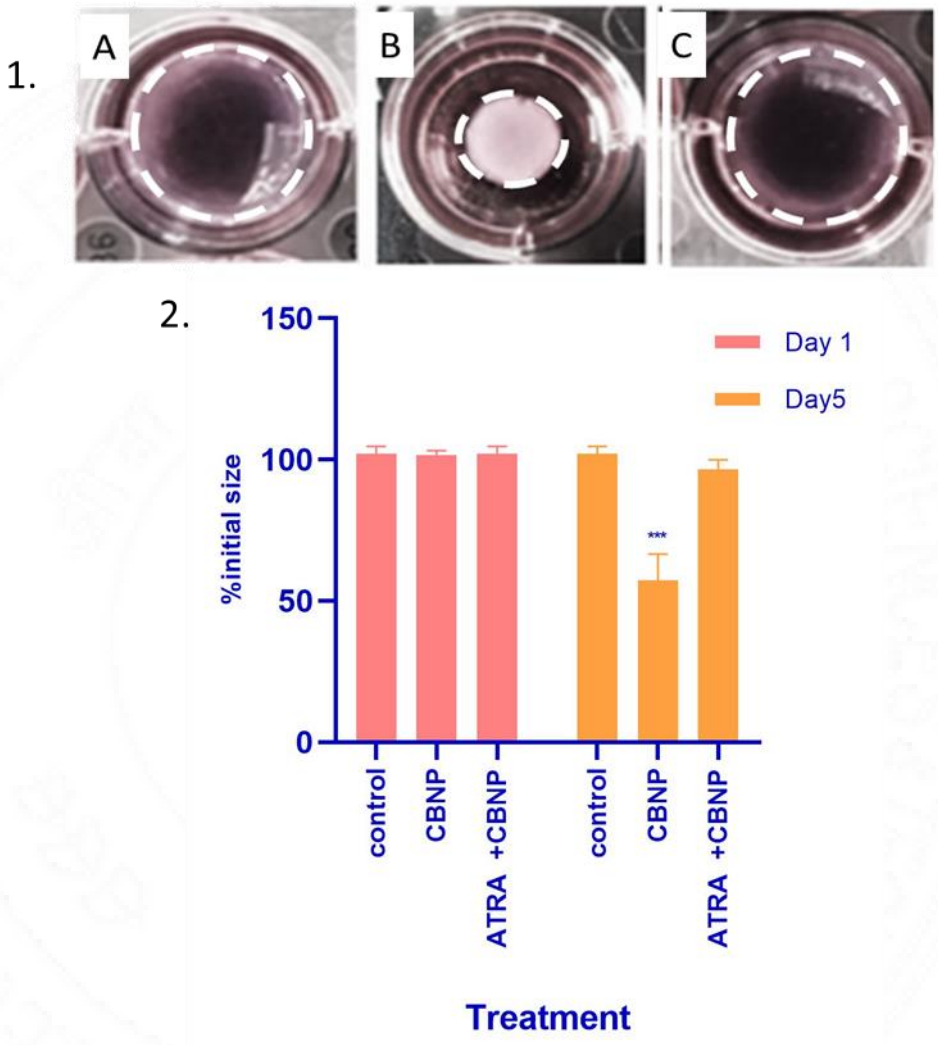

Fig 4.63 Gel contraction assay of fibroblast cells pre-treated with ATRA. Conditioned media of CBNP exposed cells showed a reduction in gel size on day5 (1). The gelsize was restored on ATRA treatment indicating the prevention of fibroproliferation and activation. 1.Images of gel contraction assay.(2) Quantification of gel size. Unexposed cells served as control. ***p<0.001 was considered to be significant.

4.3.4.2 ATRA prevented fibroblast activation in WI-38 cells by CBNP

CBNP exposure induced significant upregulation of activation markers. Pre-treatment of WI-38 cells with ATRA prevented fibroblast activation. The anti-fibrotic role of ATRA was evident from the gene expression and protein quantification data of WI-38 cells (Fig 4.64.A). The pre-treatment of ATRA maintained the gene expression at a basal level equivalent to the control

All the cytokines assessed were significantly down regulated on ATRA treatment. The downregulation in gene expression was evident in protein expression also (Fig 4.64.B). ATRA prevented the fibrotic cascade activation induced by CBNP. It is very clear that ATRA pretreatment is inhibiting the activation of pro-fibrotic cytokines and, is thereby a suitable candidate for anti-fibrotic therapy.

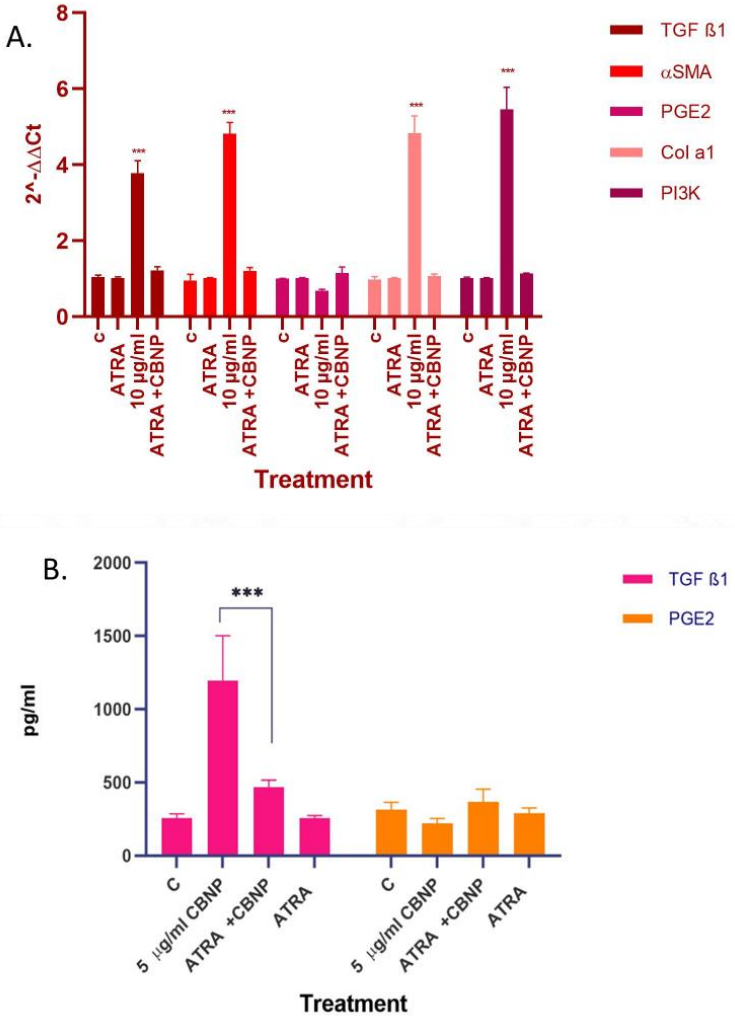

Fig 4.64 Gene expression and protein quantification of fibroblast cells pre-treated to ATRA on CBNP exposure. **A. Gene expression** analysis show down regulation of Fibroblast activation markers on ATRA treatment. **B. Protein expression** analyses indicate reduced release of pro-fibrotic markers on ATRA treatment. Unexposed cells served as control. ***p<0.001 was considered to be significant.

4.4 Phase IV. Cell-material-microbial interactions

Pseudomonas aeruginosa is a Gram-negative and ubiquitous, environmental bacterium. Due to a range of mechanisms for adaptation, survival, and resistance to multiple classes of antibiotics, infections by this opportunistic pathogen *P.*

aeruginosa strains can be life-threatening and it is emerging worldwide as a public health threat. The effect of CBNP on *P. aeruginosa* pathogenesis was studied in three levels

4.4.1 Effect of CBNP on virulence factors of *Pseudomonas aeruginosa*

4.4.1.1 Biofilm quantification

Biofilms are a cluster of bacteria formed when they grow attached to a surface. Biofilms are composed of cells, exopolysaccharides, eDNA, etc which form an aggregate protecting the bacteria from the host immune mechanism as well as antibiotic therapy. *Pseudomonas* is a known biofilm producer.

Biofilm production of *Pseudomonas* ATCC 27853 was assessed on CBNP exposure. The biofilm formation was found to be increased in CBNP-exposed bacteria (Fig 4.65). Low concentrations of CBNP (1-10 µg/mL) for 48 h showed increased biofilm production. Biofilm production was not evident in high-concentration (>20 µg/mL) CBNP-exposed groups.

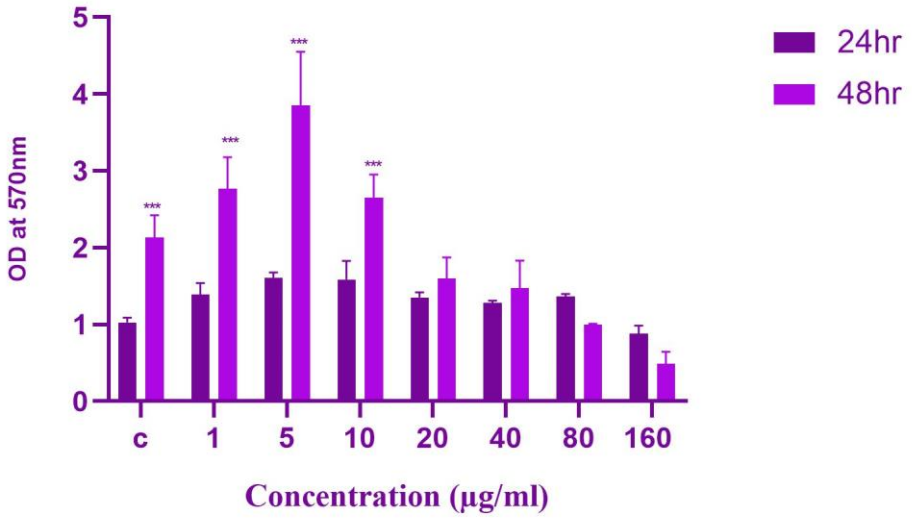

Fig 4.65 Crystal violet assay for biofilm quantification of CBNP exposed P. *aeruginosa* for 24 h and 48 h. *Pseudomonas* ATCC 27853 showed a significant increase in biofilm production.***p<0.001 was considered to be significant.

4.4.1.2 Low concentrations of CBNP induced Virulence factors expression in *Pseudomonas*

Pyocyanin is one of the major virulence factors produced by *Pseudomonas*. Pyocyanin induces disruption of mitochondrial membrane potential and inhibition of protein synthesis in host cells, eliciting cytotoxic activity. It is also known to induce biofilm production. Pyocyanin production in CBNP-exposed cells was assessed by acidified chloroform method. Low concentrations of CBNP induced pyocyanin expression in *Pseudomonas*. High concentrations did not induce a significant change in pyocyanin expression (Fig 4.66 A)

Rhamnolipids of *Pseudomonas* play a significant role in the invasion of the epithelial cell layer. Rhamnolipids help in surface attachment, and colony formation as well as play a key role in maintaining the architecture of biofilms. Low concentrations of CBNP were found to induce rhamnolipid expression whereas in high-concentration CBNP-exposed cells the rhamnolipid expression was equivalent to unexposed controls (Fig 4.66A).

Proteases are key factors involved in biofilm dispersion and exopolysaccharide production. The expression was assessed by skim milk assay. Agreeing with the expression of other virulence factors an upregulation in protease expression was observed in Low concentration CBNP exposed cells (Fig 4.66 B).

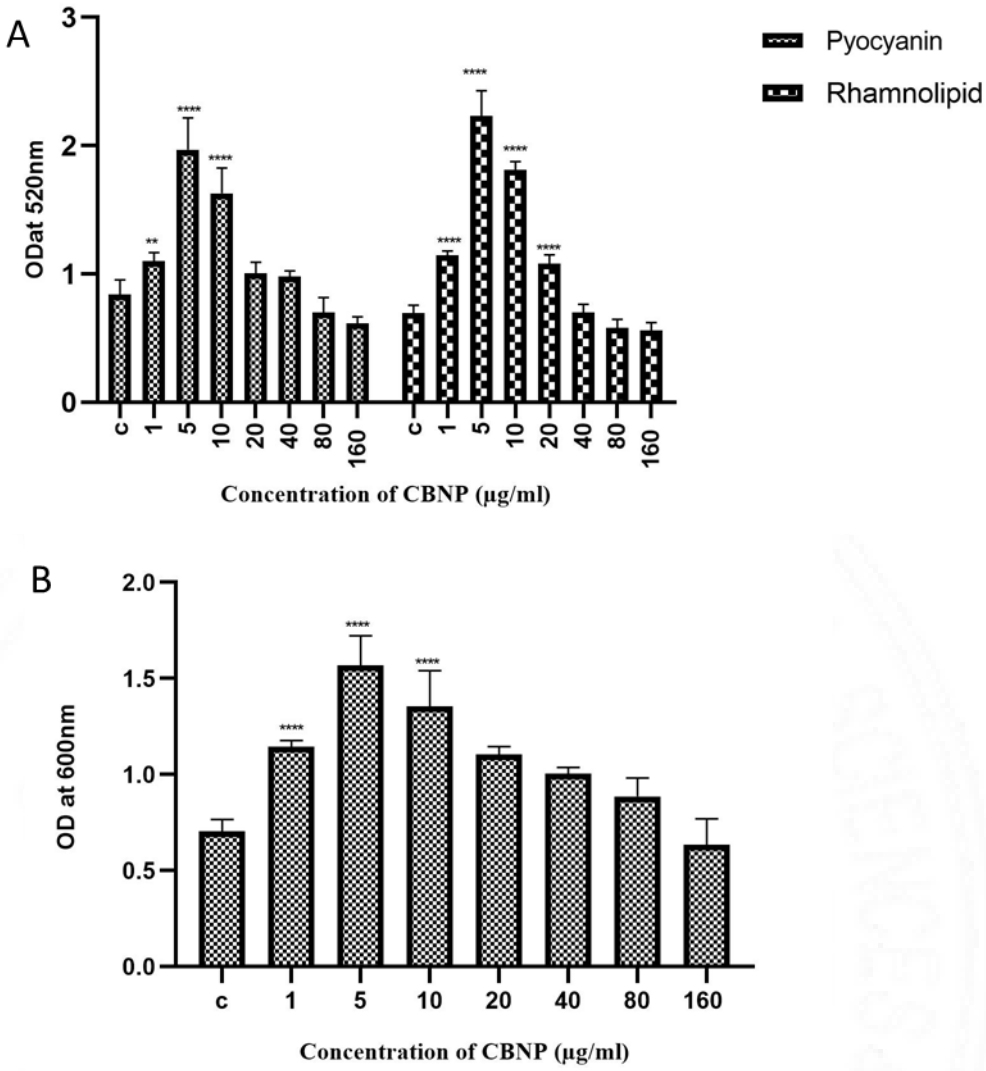

Fig 4.66 Assessment of virulence factors in *Pseudomonas* exposed to CBNP. Expression of all the virulence factors were increased in low dose CBNP exposed cultures. Unexposed cells served as control. Two-way ANOVA was used for statistical analysis .***p<0.001 was significant.

4.4.1.3 CBNP exposure affected motility of *Pseudomonas* ATCC

Biofilms are bacterial aggregates enveloped in extracellular polymeric substances. Bacteria can switch from their motile nature to sessile. Induction of stress responses usually results in the transition from single cells to biofilm and loss of motility. Here

reduction in motility of *Pseudomonas* ATCC 27853 was observed on exposure to CBNP (Fig 4.67). The reduction in motility was dependent on concentrations of CBNP. Concentrations that showed increased virulence factor expression showed reduced motility. The result confirmed that these concentrations induced biofilm formation.

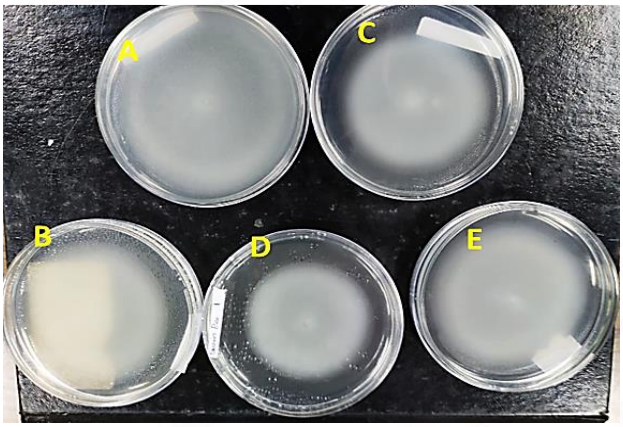

Fig 4.67 Motility assay of P. *aeruginosa* A.control, B- 1 µg/mL, C-5 µg/mL, D-10 µg/mL, E-20 µg/mL CBNP exposed bacterial cells. Reduced motility is visible for 5 and 10 µg/mL CBNP exposure. Reduction in motility is observed in the same concentrations of CBNP which increased biofilm production.

4.4.2 Effect of CBNP on infection susceptibility of A549

4.4.2.1 Challenged alveolar cells are susceptible to infection.

Tight junctions of AECs (alveolar epithelial cells) provide intercellular sealing and are integral to the maintenance of the epithelial barrier integrity. Bacterial pathogens breach this epithelial lining to feed on nutrients and disseminate deeper into tissues. In defence against these pathogens, the epithelium has multiple layers of microbial sensing and intrinsic defence systems built in that act as countermeasures against

microbial intruders. We assessed whether CBNP exposure can affect the infection susceptibility of alveolar epithelial cells.

ECIS- was used for the analysis. ECIS is a Real-time, label-free, non-invasive method superior to end-point analyses. Exposure to CBNP affected the barrier integrity of the monolayer (Fig 4.68). The decrease in resistance depending on concentration implied the same. Infection by *Pseudomonas* ATCC 27853 after CBNP exposure reduced the impedance significantly and this reached till the -cell-free measurements. Time taken for the resistance to reach the cell-free measurements were in proportion to the concentration of CBNP exposed .ie, higher concentration CBNP exposed wells reached cell-free measurement within 6-8 h post post-infection. Change in cell morphology was followed by change in barrier integrity and was evident from the 3-dimensional graphs of Frequency v/s Time v/s Resistance (Fig 4.69). The reduction in resistance was dependent on concentration of CBNP used in pre-exposure of A549. A drastic and immediate reduction was observed in high dose CBNP challenged cells on infection. The capacitance on the other hand was increasing as the resistance to current flow decreased at these infection points (Fig 4.70) Change in resistance at higher frequency (>16000 Hz) reached cell-free on later time points. This indicated that on infection barrier integrity was initially affected and the pathogen gained access to the cells and this resulted in loss of cell morphology in later time points (Fig 4.68). The 3D graphs in Fig 4.71 clearly indicate the difference in rate of resistance change depending on CBNP concentration after infect which pointed the increased susceptibility of challenged epithelial monolayer to infection.

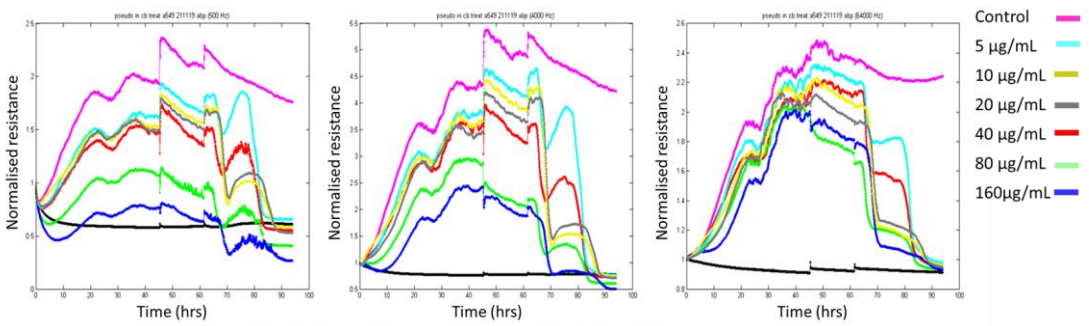

Fig 4.68 Normalised Resistance v/s time graph of A549 cells pre-exposed to CBNP and infected with *Pseudomonas* in varying frequencies(500Hz, 4000Hz, and 64 kHz). After infection drastic reduction in impedance was observed for high dose CBNP treated wells and it reached cell-free nearly 6-8 h post-infection (blue line).

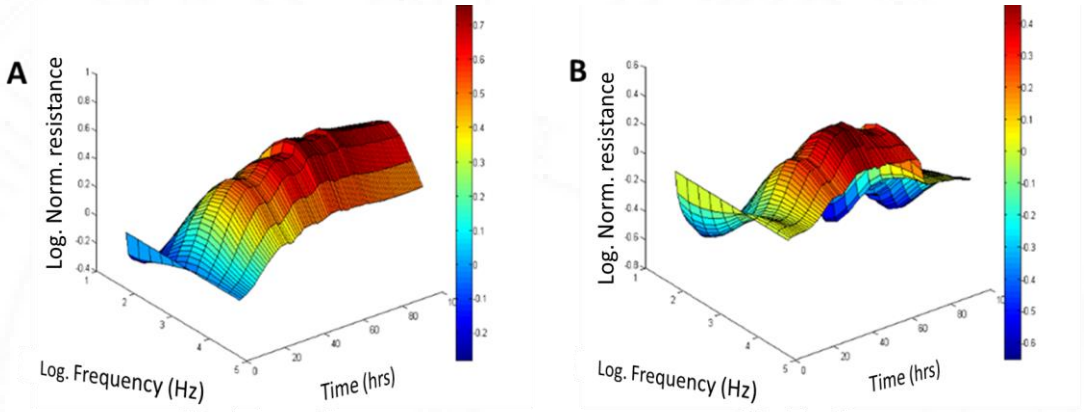

Fig .4.69 3D graph of frequency v/s time v/s resistance of control and highest dose of CBNP treated well. The graph indicates the reduction in resistance upon time and frequency.

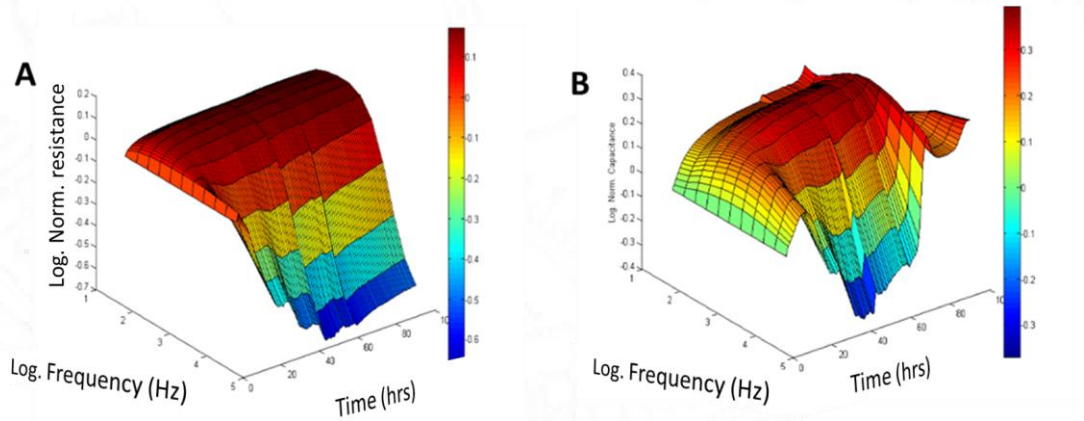

Fig 4.70 The capacitance v/s time v/s frequency graph of control and highest CBNP exposed wells. The capacitance was decreasing for control wells whereas it was increased in

the highest CBNP-exposed wells after infection. Capacitance results are in inverse relation to the resistance measurements.

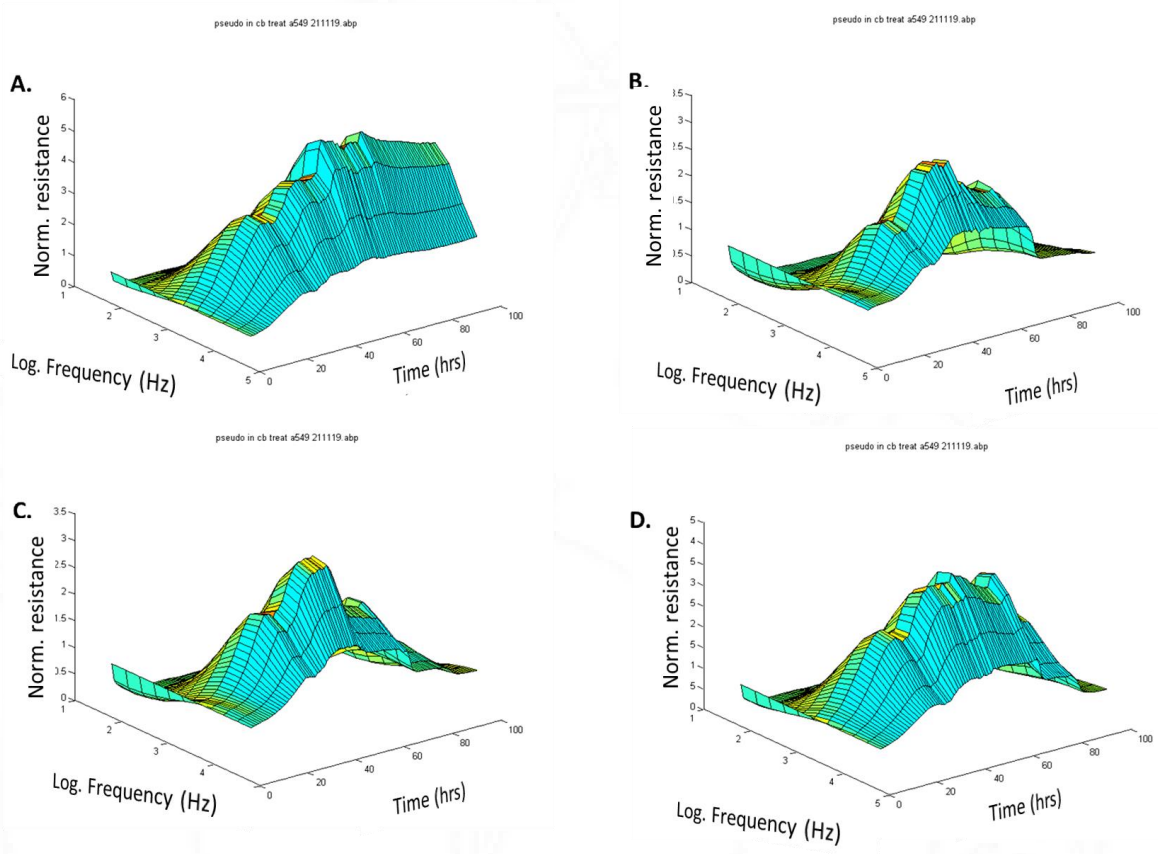

Fig 4.71 3D Normalised resistance v/s Log frequency v/s Time graph of A.control B.160 µg/mL C. 80 µg/mL D. 20 µg/mL CBNP exposed *Pseudomonas* infected wells. The drop in resistance is indicated in B at early time points compared to other wells indicating that challenged cells are more susceptible to bacterial infection.

4.4.2.2 CBNP pre-exposure increases bacterial internalization A549 cells

The immune system eliminates bacteria using phagocytosis. Internalization of bacteria is an indication of cell barrier integrity. Breached barriers promote the internalization of bacteria. An increased internalization of *Pseudomonas* was observed by CBNP-pre-

exposed A549 cells. The data indicate that CBNP pre-exposure affects the barrier integrity of the adherent layer and paves way for bacterial internalization (Fig 4.72)

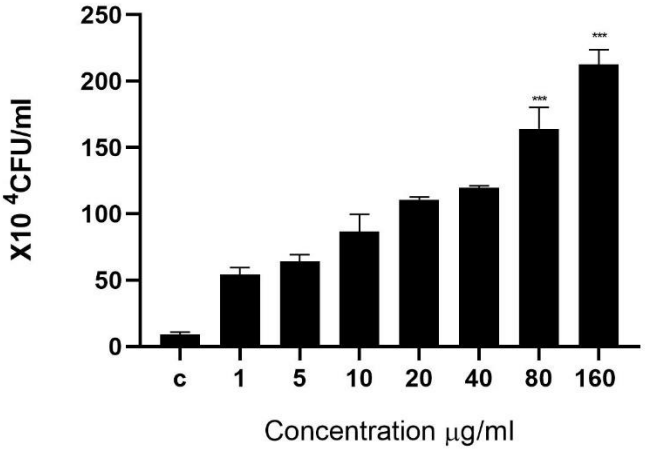

Fig 4.72 Gentamicin protection assay: Internalisation of bacteria was assessed by gentamicin protection assay. Viable counts of internalized bacteria were obtained by gentamicin protection assay. An increase in internalization was observed after 3 h bacterial infection. N=3, statistical analysis done by t-test.***p<0.001 indicate significance.

4.4.3 Effect of infection on CBNP pre-exposed epithelial cells- A549

4.4.3.1Establishing optimal immunologic activation of immune cell- THP1 cells by *P. aeruginosa* lysate

Cell-cell interaction could also be mediated by Paracrine signalling. The effect of activated immune cells in a fibrotic milieu should be understood -Immune cell activation is the initial host response to an infection. We assessed the Effect of *P. aeruginosa* on EMT via the activation of immune cells

Treatment of the THP-1 with 12.5 μL/mL to 400 μL/mL was assessed for viability and cytokine production. *P. aeruginosa* lysate induced a significant increase, therefore, the release of IL-8, IL-1β, and TNF-α (Fig 4.73 B&C), while maintaining cell viability >80%. Concentrations >12.5 μL/ mL *P. aeruginosa* lysate induced enhanced cytokine

release and compromised cell viability (Fig 4.73 A). We, therefore, used *P. aeruginosa* lysate concentration of 12.5 µL·mL−1 in subsequent experiments

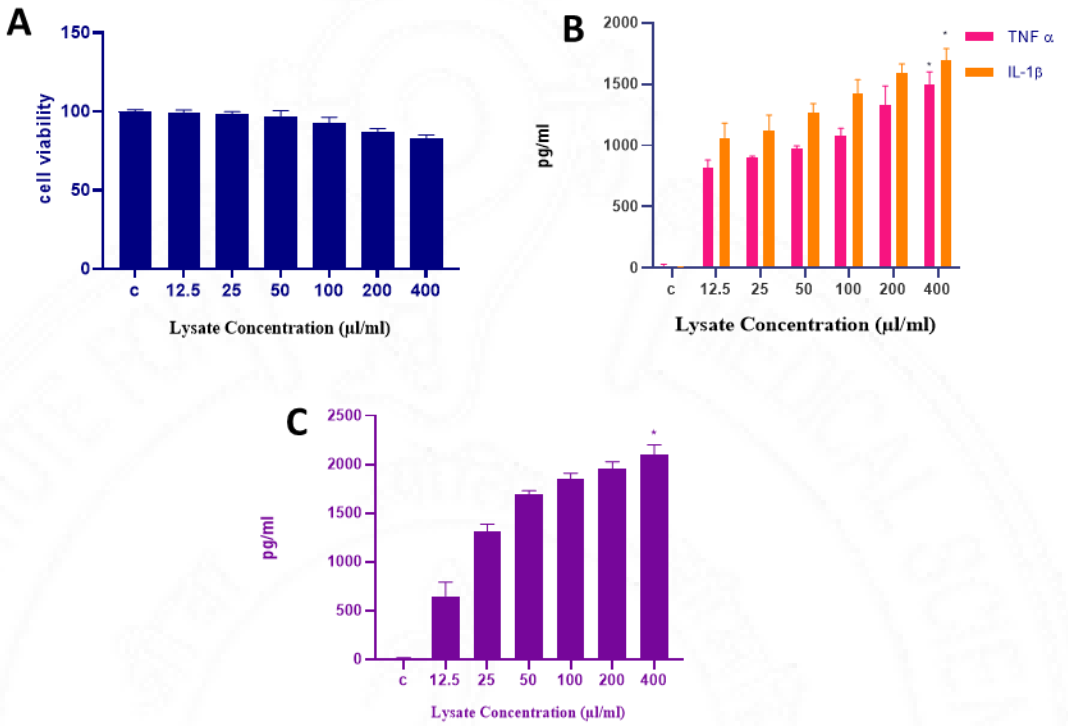

Fig 4.73: Cytokine release by THP-1 cells stimulated with *Pseudomonas aeruginosa*. THP-1 cells (1×10^6 cells/mL) were stimulated with PA lysate (at 0, 12.5, 25, 50, 100, 200 or 400 µL·mL−1) for 24 h. **A. Cell viability** was assessed by MTT assay**, B**, **ELISA of tumor necrosis factor (TNF)-α, IL-1β,** and **C. ELISA of interleukin (IL)-8.** Results showed a dose-dependent decrease in cell viability from 96% in control to 72% at a concentration of 400 µL·mL−1 PA lysate. (b) PA lysate induced a dose-dependent increase in IL-1β and TNF-α release up to a concentration, c) PA lysate induced a dose-dependent increase in IL-8. Data are presented as mean±sem. *: p<0.05.

4.4.3.2 Conditioned media from monocytes activated with *Pseudomonas* lysate treatment accentuated EMT induced by CBNP.

Phase contrast microscopy showed enhanced elongation of A549 cells after immune cell secretome treatment (Fig 4.74). Morphology changes and gene expression of CBNP-exposed cells (4.74) treated with immunologically activated THP1 cell media

(Pseudo+CBNP) indicated that secretory components from immunologically activated immune cells accentuated EMT. Further upregulation of all the EMT marker genes was observed in conditioned media-exposed A549 cells compared to CBNP exposure alone. This indicates that P.*aeruginosa* lysate accentuates fibrotic responses previously triggered in alveolar epithelial cells. The results imply that bacterial infection on a challenged alveoli can increase the risk of fibrosis.

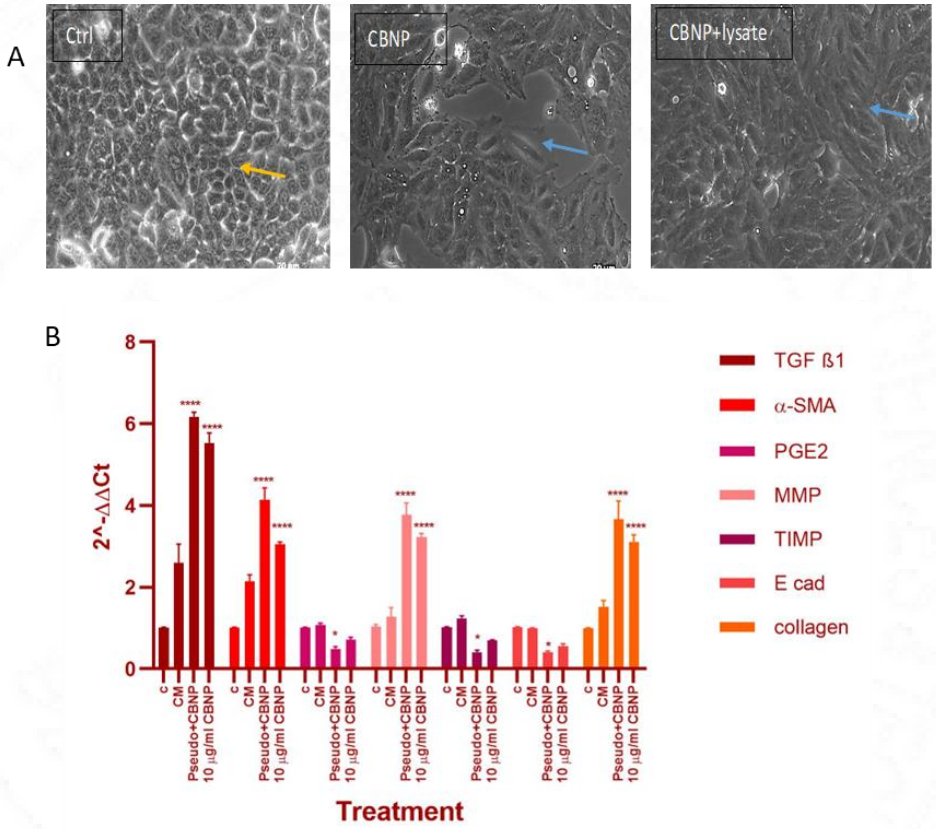

4.74 Morphology changes and Gene expression analysis of CBNP exposed A549 cells treated with immune cell secretome. Conditioned media from THP-1 cells activated with *Pseudomonas aeruginosa* (PA) lysates showed accentuated epithelial-to-mesenchymal transition. Untreated alveolar epithelial cells maintained the classic "cobblestone" morphology characteristic of epithelial cells, CBNP treated cells showed spindle morphology. EMT marker's gene expression was further upregulated on conditioned media treatment. Statistical analysis was done by ANOVA. *p<0.05 ***: p<0.001,****p<0.0001 were considered significant.

5. DISCUSSION

Nanotechnology is a wide and growing field of applied science, with applications ranging from the manufacture of beauty products, and electronics to biomedical uses. Advancement of nanotechnology leads to increased manufacture of different types of nanoparticles which eventually get released into the air, water, and soil intentionally and unintentionally. Sources of nanoparticles are not limited to anthropogenic activities. Natural processes like forest fires, volcanic eruptions, etc, also release nanoparticles into the environment. Because of the small size (less than 100nm) and relatively high surface area, nanoparticles display elevated reactivity. Most of the engineered nanoparticles are made up of carbon, silicon, metals, and oxides. Directly or indirectly, they can adversely affect the environment and human health (Powell and Kanarek, 2006).

Within a short time of discovery carbon-based nanoparticles gained significant interest. The commercial use of carbon-based nanomaterials extends to technical, medical, agricultural, and environmental fields. Regardless of the field of application the increasing worldwide production and use leads to the intentional and unintentional release of carbon nanoparticles into the environment and prediction of the effect on living organisms is still difficult (Zaytseva, Neumann, 2016)

Fullerenes, carbon nanotubes (single-walled, multi-walled), graphene, and carbon black are major types of carbon-based nanomaterials. The unfiltered exhaust gases from the incomplete combustion of diesel fuel also contain nanoparticles of a central carbon core and adsorbed chemical moieties like polyaromatic hydrocarbons.

Carbon black nanoparticles are industrially important particles produced by the thermal decomposition of hydrocarbons (Chen et al., 2014). Carbon black

nanoparticles are composed of elemental carbon and are one of the top 50 most produced chemicals worldwide. its application includes fields like rubber manufacture, printing, tire pigmentation, catalyst, etc (Okano et al., 2018, Song et al., 2018). The predominance in industrial applications and worldwide manufacture leads to the release of CBNP into the atmosphere, forming a part of ultra-fine particulate matter. Inhalation is the main route of entry of CBNP into the human body Although some studies used CBNP as a carbonaceous analog of particulate matter (Long C.M, 2013; Harber et al.,2003;) a conclusive study on the effect of CBNP in the lower tract comprising the functional unit of the lung is still lacking. The lack of suitable in-vitro systems to understand cell-material interactions hamper the deep understanding of the responses triggered by these nanoparticles which are addressed in the study.

In the current work, an effort has been made to understand the interactions of alveolar cells with carbon black nanoparticles and delineate the molecular mechanisms of cell-material interactions. The effect of CBNP on alveolar epithelial cells, fibroblasts, and monocytes on short and long-term exposure was studied. Environmental effects are not limited to direct exposure effects, the present study also attempted to understand the triagonal interaction of cell-material-microbe thereby in the preponderance of human to infection. An attempt was also made to understand the material-microbial interactions that the scientific world left unexplored but in reality warrants immediate attention.

5.1 Phase 1. Development of *in-vitro* system.

5.1.1 Electric cell-substrate impedance sensing for assessment of monotypic cell behaviour

The initial stage of the phase1 utilized Electric cell-substrate impedance sensing (ECIS), the non-destructive label-free method to assess the unicellular behaviour of adherent cells to external injury or stimuli. The barrier integrity of alveolar epithelial cells represented by A549 on Diesel exhaust particle exposure was assessed. Epithelial cells form the first line of innate immune defense. They form monolayers with tight junctions and prevent external agents from penetrating deep into tissues. Our results indicate a dose-dependent reduction in epithelial barrier integrity evidenced by a reduction in cellular resistance (Fig 4.2 & 4.3). The result was compared with other end-point cytotoxicity analyses like MTT, LDH, and NRU (Fig 4.4). The ECIS system outranks the traditional endpoint analyses because of the ability to generate continuous real-time measurements. The study demonstrates that the method can be effectively utilized for evaluating the effect of environmental pollutants like DEP on cells' barrier integrity, making ECIS an effective system for high throughput toxicity assays. The effect of a stimulus inducing a rapid change in cells followed by recovery will be missed in endpoint cellular analyses but projected in ECIS. Despite the active use of Superparamagnetic iron oxide nanoparticles in the biomedical field ECIS demonstrated a change in the cellular impedance of endothelial cells (Astanina et al., 2014), a fact useful in defining safe strategies or protocols for the clinical application of nanoparticles. Lehman et al., (Lehmann et al., 2009) observed disruption of occludin in epithelial; cells when exposed to high DEP concentrations but they used standard

reference materials. In contrast, the current study used DEP collected freshly from engine exhaust (Fig 4.1) simulating *in-vivo* conditions more precisely. We observed a reduction in cell viability and increased LDH release in MTT and LDH assay. A dose-dependent reduction in the retention of neutral red dye was also evident. Cudazzo et al. reported NRU reduction as an implication of the lysosomotropic potential of E-cigarettes. Our observation also implies a reduction in the retention which could be due to changes in the acidic compartment. Our study demonstrates that ECIS could be effectively used as a valuable tool in understanding cellular responses to external stimuli or injury compared to endpoint analyses.

5.1.2 Heterotypic co-culture system

In the next stage of Phase 1, an *in-vitro* co-culture system was developed to understand multicellular responses. The lack of suitable in-vitro systems hampers the study of fibrosis, especially in the identification of antifibrotic agents. Since lung fibrosis is a chronic response a system suitable for long-term studies should be developed. Also, it should consist of the initiator and effector cells. Epithelial cells are the initiator cells in fibrosis and fibroblasts are the main effector cells. An *in-vitro* system combining both the cells and simulating invivo conditions was developed. The heterotypic Air liquid interface co-culture system is the result. The developed system showed superiority in terms of barrier integrity as well as function. The improved TEER values in the ALI co-culture system (Fig 4.6) along with reduced fluorescein permeability (Fig 4.7) showed the same. Ren et al.,2016 reported A549 have a reduced barrier integrity. Our data suggest that co-culture with fibroblasts and uplifting to ALI have significantly improved the barrier property of A549 cells. Air-liquid interface culture

systems were developed previously for understanding lung diseases such as chronic obstructive pulmonary fibrosis but they fail to represent cellular interactions of pulmonary fibrosis as they lack the presence of fibroblast cells, the effector of fibrosis (Jiang et al.,2018; Schruf et al.,2020).

The intactness of the cells' cytoskeleton as well as stable surfactant protein C expression in alveolar epithelial cells following Air-liquid interface upliftment (Fig 4.8) suggests the structural and functional integrity of the developed co-culture system. Surfactant protein C is a biomarker of type II alveolar epithelial cells. SP-C enhances the spreading of phospholipids at ALI and lowers the surface tension thereby playing a pivotal role in alveolar epithelial homeostasis (Mulugeta S, Beers MF, 2006).

5.2 Phase II. Cell-material interactions

5.2.1 Characterisation of CBNP

The biological effects of engineered nanoparticles are dictated by their physicochemical characteristics like size, chemical composition, charge, shape, and surface chemistry (Braakhuis HM et al., 2014; Luyts K et al., 2013). These characteristics indeed determine the capacity of nanoparticles to react with their immediate environment (Monopoli MP et al.,2011). The size of the Carbon black nanoparticle used in the study was 53±8nm and was spherical in shape (Fig.4.9). The size of nanoparticles largely affects the distribution kinetics of particles and their accumulation (Nel et al.,2006). Reports suggest that spherical nanoparticles are prone to more cellular uptake compared to fibers or nanotubes (Champion JA et al., 2006). Sheet-like and needle-like nanoparticles have shown increased cytotoxicity (Zhao et al.,2013). An increase in size was observed on analysis of the hydrodynamic size of

particles in complete cell culture medium containing serum (Fig.4.10). Bihari P et al., 2008 reported improved stability of nanoparticles on sonication and dispersion in serum-containing media. Surface charge is another important characteristic of particles controlling their cellular response. The zeta potential of CBNP was found to be~ 7.82mV (Fig.4.11). Invitro and certain invivo studies conducted on different nanoparticles suggested that a positive zeta potential is associated with greater cytotoxicity (Nagy A et al., 2012; Li RB et al., 2013; Kim J et al., 2016). This behaviour could be attributed to the greater chances of electrostatic interaction between the positively charged particle and negatively charged phospholipids of the cell membrane enabling a higher particle uptake. Contrary to the current observation some studies also reported reduced cellular uptake of cationic nanoparticles by the formation of larger agglomerates that could not be internalized (Usman et al., 2020)

5.2.2 Effects of CBNP exposure on alveolar cells

The alveolar region comprises alveolar epithelial cells, fibroblasts, and immune cells. The responses of each cellular component to CBNP exposure on short-term (24-48 h) and long-term (120 h) were assessed.

5.2.2.1 Short-term exposure to CBNP induces proinflammatory responses and cell death

The exposure of CBNP to alveolar epithelial cells, fibroblasts, and monocytes showed that short-term exposure to CBNP (24-48 h) elicited a pro-inflammatory response in the cells. Dose and time-dependent cytotoxicity was also observed in all the cell types.

In alveolar epithelial cells and fibroblasts, high doses of CBNP induced loss of cell viability evidenced by MTT, LDH, and NRU assays (Fig.4.12 - 4.15 and 4.23 - 4.26). The current study also reports an increase in ROS production and loss of lysosomal integrity in CBNP-exposed A549 cells by 48 h exposure (Fig.4.16-4.17 and 4.27-4.28). The increase in ROS and loss of lysosomal integrity can activate an inflammatory cascade and further cell death. It has been reported previously that nanoparticle exposure affects numerous intracellular organelles (Yu K.-N et al.,2015, Guo C et al.2018). ROS had gained attention as a central mediator in growth, differentiation, progression, and cell death (Zhang et al., 2013). Previous reports suggest that an increase in ROS can modify cell-signalling pathways and successively mediate many processes including inflammation and aging (Jixiang 2016).

Short-term CBNP exposure also induced significant upregulation in the expression of cytokines like IL-6, IL-8, and TNF α after 48 h exposure (Fig 4.19 and 4.31). The result implies that high doses of CBNP are activating a pro-inflammatory response which forms a part of the innate defense mechanism. The caspase 3 gene – a regulator of apoptotic pathway expression was significantly upregulated in high doses of CBNP-exposed alveolar cells implying the activation of apoptotic cell death (Fig 4.21 and Fig 4.32). Bader Almutairi et al., 2021 reported that stainless steel nanoparticles induce apoptotic cell death in human liver cells via Reactive oxygen species production and activating the caspase-3 activity. Elemental carbon is considered chemically inert but reports suggest that inert substances can elicit inflammatory responses when exposed at nanoscale compared to the bulk equivalent (Oberdörster G.1994, Stone v et al., 1998, Beck-Speier I et al., 2005). The increased surface area and the elemental nature of the particle can be the contributing factors to the dose-dependent cellular effect.

Low concentrations of CBNP proved to be non-cytotoxic at the same time an upregulation in pro-fibrotic cytokines like TGFβ1 (Fig 4.20 and Fig 4.31) was observed which implicated a dose-dependent difference in cellular response. Previous reports suggests that repeated injury leads to chronic inflammatory responses and fibrosis in tissues undergoing chronic injury or repair ((Barbe et al., 2021),(Barr and Barbe, 2002) ,(Kjaer, 2004). These observations suggest the importance of prolonged repetitive injury or stimuli which guided the work to proceed with prolonged exposure studies.

5.2.2.2 Short-term exposure to CBNP-induced pyroptotic cell death in monocytes

The present study report that CBNP induced cytotoxicity in monocytes in a dose-dependent manner (Fig. 4.35-4.37). 24 h exposure itself brought a significant reduction in cellular viability and increased lactate dehydrogenase release from cells. After CBNP treatment the cell size increased which is the opposite of cellular condensation occurring during apoptosis (Fig. 4.34). Increased LDH release together with the absence of DNA laddering (Fig. 4.40) was observed in CBNP-exposed monocytes. Monocyte exposure to CBNP led to inflammasome activation characterized by caspase 1 activation and IL-1β upregulation (Fig 4.39-4.42). These observations suggested that CBNP is inducing another form of cell death in monocytes- Pyroptosis which was further confirmed with a pyroptosis inhibitor (Fig 4.39).

Pyroptosis is another form of cell death that proceeds through the activation of inflammasome, leading to the cleavage of caspase 1 to its active form. Activation of caspase1 cleaves the cytokine IL-1β. Previous studies report the association of the release of active IL-1β with pyroptosis on stimulation by microbial antigens (Miao

et al., 2010, Suzuki et al., 2007., Sauer et al., 2010). Here we observed the pyroptosis activation in absence of a microbial stimulus. Monack et al., 2001 and Fink et al., 2006 reported that caspase 1-induced cell death can proceed independently of other cytokines like IL-18 in absence of the microbial stimulus.

Loss of membrane integrity is a hallmark of Pyroptosis (Fink et al.,2005, Fink S. L., Cookson B. T. (2006)). Although the exact mechanism is unknown, membrane pore formation leading to cell swelling and lysis has been demonstrated in line with the observation. The current study supports pyroptosis after CBNP exposure with evident cell swelling, caspase1 activation, and cell death. Increased ROS generation was observed in monocytes after short-term CBNP exposure depending on dose of treatment (Fig. 4.38). Enhanced ROS generation are often associated with macrophage pyroptosis (Wang et al., 2019).

5.2.2.3 Long-term exposure to CBNP-induced fibrotic responses in alveolar cells

A recent WHO annual report declared that sustained exposure to sub-chronic PM2.5 is a threat to human health (World health statistics 2021). Studies are focussing on acute lung injury and less is known about nanoparticle-induced chronic injuries.

5.2.2.3.1 Low concentrations of CBNP induced Epithelial-mesenchymal transition in alveolar epithelial cells.

Prolonged exposure (5 days) to low concentrations (1-10 µg/mL) of CBNP induced an evident morphological change in alveolar epithelial cells (Fig.4.43-4.46). The CBNP-exposed cells changed their characteristic cobblestone morphology of epithelial cells to spindle-shaped cells which are characteristic of mesenchymal cells. This change in

morphology is called Epithelial-mesenchymal transition (EMT). During EMT the cells lose their apicobasal polarity and acquire mesenchymal phenotypes like cytoskeletal rearrangements, acquisition of gene expression profile of fibroblasts, and ability to produce extracellular matrix (Kalluri 2009). Idiopathic pulmonary fibrosis is characterized by uncontrolled deposition of ECM which leads to scar formation and loss of organ function (Leask 2004). Fibroblasts and their activated forms are responsible for this ECM deposition (Gabbiani 2003). During normal wound healing response, these fibroblasts undergo apoptosis after epithelialization. Whereas in response to fibrotic stimuli the fibroblasts persist and continue to lay down the ECM.

Researchers suggest that sources of these fibroblasts are not limited to tissue-resident ones and bone marrow-derived ones but also non-mesenchymal origin like epithelial cells. The process of EMT involves a series of biochemical changes leading to phenotypic changes in epithelial cells (Inoue et al.,2015). Growth factors secreted by these activated cells like TGFβ further initiate the vicious cycle of ECM deposition by activating fibroblasts (Gabbiani 2003).

Increased cell proliferation was observed in biochemical analyses of CBNP-exposed epithelial cells . The Acridine orange staining of prolonged CBNP exposed cells implied an increase in lysosomal number and further turnover (Fig.4.47). Increased lysosomal activity during EMT has been reported before(Kern U et al.,2015). Mitochondrial dysfunction has been linked to many diseases(Kang et al.,2005). A previous study reported that EMT-promoted mitochondrial dysfunction was accompanied by increased ROS generation and decreased $\Delta\Psi m$ (Yuan et al.,2012). In line with those observations mitochondrial membrane potential of Prolong CBNP

exposed alveolar epithelial cells was also analyzed. The CBNP exposure decreased ΔΨm and was evidenced by JC10 staining results (Fig. 4.48).

Actin remodelling in CBNP-exposed epithelial cells by rhodamine-phalloidin staining demonstrated a clear actin reorganization from cortical thin bundles to thick parallel bundles in a dose-dependent manner (Fig.4.46). A previous study on EMT reported that dynamic actin remodelling takes place during mesenchymal transition(Haynes et al., 2011). The contractile function of epithelial cells that underwent Epithelial-Mesenchymal Transition was assessed by Gel contraction assay, which is an ideal in vitro model for the evaluation of contractility, which is one of the characteristic functions of fibroblasts (Fig.4.50). Fibroblast attachment to collagen type1 produces mechanical tension that leads to a reduction of gel size when they are embedded. A significant reduction in gel size was observed in CBNP-conditioned media-treated cells. The conditioned media of prolonged CBNP-exposed alveolar epithelial cells are a reservoir of cytokines including TGFβ1 which were later quantified in the study. The presence of these factors contributed to the EMT of epithelial cells embedded in the gel. The gel contraction assay is comparable to assays like cell migration and offers higher reproducibility. Muir AB, et al 2015 reported the use of a Gel contraction assay for assessing EMT.

Collagen synthesis and secretion are characteristics of fibroblast cells. The Prolong CBNP exposed epithelial cells that underwent EMT were assessed for collagen secretion ability. A significant dose-dependent increase in collagen content was observed in CBNP-exposed epithelial cells (Fig.4.49).

Agreeing with all the biochemical analyses the molecular analyses of prolonged CBNP-exposed epithelial cells showed significant changes in EMT markers' gene expression and protein expression (Fig 4.51 - 4.52). EMT is characterized by the downregulation of epithelial markers and the upregulation of mesenchymal markers. A significant upregulation in mesenchymal markers (more than twofold) like TGFβ1, Collagen1, ACTA2(smooth muscle actin), and MMP along with downregulation of epithelial markers like E-cadherin was evident from q RT-PCR analyses. Prostaglandin E2 limits fibroblast proliferation and activates an inflammatory cascade leading to a healing response. A downregulation in PGE2 as well as Tissue inhibitors of metalloproteases (TIMP) was observed. Yue et al., described TGFβ like cytokine as Titan of lung fibrogenesis(Yue et al., 2010). Role of TGFβ in epithelial injury, activation of fibrotic cascades and in matrix remodelling were described earlier (Khalil and Greenberg, 1991). Collagen, metalloproteases and smooth muscle actin are downstream effectors of TGFβ mediated signalling cascade.

5.2.2.3.1.1 Prolonged CBNP activates TGFβ -smad- β catenin signalling.

TGFβ **is the** critical growth factor involved in fibrosis which is rapidly induced in the onset of an injury and attracts immune cells, and fibroblasts which release more TGFβ and thereby remain in the autocrine loop. Detachment of latency-associated peptide (LAP) activates TGFβ and activates downstream signalling. *Smads* are a family of transcriptional activators of the pathway. Phosphorylation of receptor-smads(2&3) and binding to common smad (co-smad-4) allows the translocation of the *smad* signal to the nucleus (Leask and Abraham, 2004). *Sand 3* is required for TGFβ induced gene expression. The nuclear translocation of phosphorylated *smad3* is an indication of

EMT gene expression. The current study highlights the presence of phosphor *smad3* in the nuclear region pointing to the activation of smad signalling in epithelial cells (Fig.4.53). TGFβ signalling can cross-talk with canonical Wnt/β (Miao et al.,2013). The Wnt signalling regulates the effect of *smad* signals and prolonged activation of β catenin has been shown to be involved in scarring (Liu et al., 2011). In normal cells inactive β catenin remains complexed with E cadherin. With the activation of Wnt signalling, the complex is disrupted and β catenin is free to translocate to the nucleus. On long-term exposure, nuclear translocation of β catenin was evident in CBNP-exposed epithelial cells (Fig. 4.53). Henderson et al.,2010 in their study on alveolar cells showed that β catenin is necessary for the transcription of α smooth muscle actin. The expression of α-smooth muscle actin is a clear indication of fibroblast phenotype. Prominent α-smooth muscle actin expression was observed in epithelial cells on prolong CBNP exposure (Fig. 4.54)

5.2.2.3.2 Prolonged exposure to low doses of CBNP activates fibroblasts.

Uncontrolled proliferation and activation of fibroblasts result in tissue fibrosis. Prolonged exposure of CBNP-induced fibroblast proliferation in WI38 cells (Fig. 4.55). Fibroblasts are stimulated by an array of cytokines such as TGFβ1, IL-13, leukotrienes, etc. (Eap et al .,2012; Fehgali and Wright,1997) and they secrete growth factors like TGFβ, chemokine, etc which activate fibroblasts again and at the same time recruit immune cells which further activate chronic inflammation and the cycle continue to result in uncontrolled deposition of ECM and thereby fibrosis (Flavell et al., 2008). Prolonged exposure to low doses of CBNP induced upregulation of cytokine and growth factor gene expression that activate fibroblasts (Fig. 4.57). PI3K gene

expression was upregulated implying the possible activation of the PI3K pathway. The Phosphatidylinositol 3-kinase (PI3K) signalling pathway is an important pathway regulating cell proliferation, motility, and survival (Yang J et al.,2019). Previous reports (Conte E et al., 2011; Sun Y., Zhang Y., Chi P. 2019) suggest that the overexpression of alpha-smooth muscle actin (α SMA) was related to the PI3K/AKT pathway activation and interaction of TGFβ and PI3K promoted fibrosis. The activated PI3K pathway can function downstream and regulate collagen secretion from activated fibroblasts. Collagen secretion was also enhanced by CBNP exposure which implies fibroblast activation (Fig. 4.56). Lu Y et al., 2010 reported that ROS can initiate fibroblast proliferation through PI3K activation and in turn result in excessive collagen production.

5.2.2.3.3 Prolong exposure to CBNP induced Monocyte polarisation

Monocytes are phagocytic cells that are recruited to the site of injury through a chemokine gradient. At the site of injury or infection, during phagocytosis, they secrete chemokines that lead to the further recruitment of other immune cells. In the lung, they differentiate into pulmonary macrophages and dendritic cells. Macrophage activation can be of two types. Classical “M1” polarization that leads to initiation of pro-inflammatory response characterized by significant upregulation of inducible nitric oxide synthase and “M2” polarization that down-regulates inflammatory response and promotes resolution of inflammation and initiation of fibrosis (Wynn TA, Chawla A, Pollard JW.2013).

Changes in cell morphology during polarization are less understood. We observed a change in the morphology of monocytes from spherical to elongated on prolonged

CBNP exposure (Fig. 4.58). McWhorter FY, et al., 2013 observed that macrophages exhibit variations in morphology when stimulated with cytokines in-vitro. They found that the elongation of cells induced polarization toward an M2 phenotype and diminished pro-inflammatory cytokine production. The mechanism of transduction of these physical changes to biochemical cues that regulate polarization remains unknown. Elongation of cells has been shown to influence nuclear changes including chromatin condensation and histone modification in other cell types (Versaevel M et al., 2012; Li Y et al., 2011) which could be the driving factor of morphology changes in monocyte as well. A significant upregulation in the anti-inflammatory cytokine, IL-10, and profibrotic growth factor, TGF β1 was observed during prolonged exposure of CBNP to Monocytes (Fig. 4.59). The upregulation of iNOS expression was not statistically significant and IL-4 expression was on basal levels. These implied that CBNP exposure was initiating an M2 polarization in monocytes.

Altogether the prolonged exposure data suggest that low concentrations of CBNP are inducing a pro-fibrotic response in all types of alveolar cells studied.

5.3 Phase III. All trans-retinoic acid has anti-fibrotic potential.

All trans-retinoic acid (ATRA) is a vitamin A derivative. The anti-inflammatory, anti-migratory effects of ATRA have been described earlier. Lab-generated data suggested that ATRA can enhance surfactant C synthesis in response to tobacco smoke extract (George U,2013). There are conflicting reports on the anti-fibrogenic role of ATRA. Several studies reported the anti-fibrotic role of ATRA in mice (Chiharu T et al.,2006; Dong Z X et al.,2012) whereas Segel et al.,2001 reported ATRA to be non-beneficial in bleomycin-induced fibrosis in rats. Song et al., 2013 suggested that the difference

in ATRA doses used in the study could be a reason for the contradicting results. The current study proposes that exposure time is also critical. Post-fibrosis treatment could not elicit any downregulation of fibrosis response in epithelial cells whereas pre-treatment of cells with ATRA showed beneficial results (Fig. 4.60- 4.63). The data suggests that once the cells enter the fibrotic cascade ATRA would not be a treatment regime whereas pre-treatment with ATRA can protect the alveolar epithelium from fibrotic injury. The study of the anti-fibrotic role of ATRA in fibroblasts also implied that ATRA can significantly control the proliferation and contractility of the fibroblasts activated by CBNP (Fig 4.64).

5.4 Effect of CBNP on respiratory bacterial pathogenesis

5.4.1 CBNP exposure induced biofilm formation of *Pseudomonas aeruginosa*

The increased use of CBNP and worldwide manufacture mark their prominent environmental occurrence as a component of particulate matter. This impacts not only human health but also the microbial community. The current study assessed the impact of CBNP on bacterial virulence. *Pseudomonas aeruginosa* ATCC 27853 was chosen. *P. aeruginosa* is a ubiquitous, opportunistic pathogen. It is one of the most frequently isolated multi-drug-resistant organisms from infections (Pachori P et al., 2019). The ability of *Pseudomonas* to colonize human tissues and medical devices by the formation of biofilms is a global health concern as it leads to chronic infections resistant to antibiotic therapy. An increased biofilm formation by *Pseudomonas* was observed on CBNP exposure after 48 h (Fig.4.65). Biofilms are a structural consortium of bacteria at interfaces that remain embedded in a matrix of exopolysaccharides, proteins, and DNA (Karygianni et al., 2020). The biofilm architecture helps the

organism to overcome the host immune response as well as provide increased antibiotic resistance. Mann R et al., 2021 also reported that repeated exposure to nanosilver induced biofilm formation in *Pseudomonas* even though nanosilver is used in antimicrobial therapy. Biofilm formation is a survival advantage of bacteria in response to environmental stress. The bacteria remain embedded in a self-produced exopolysacharide matrix and eDNA. Nguyen et al.,2019 reported a 13-fold increase in cell attachment density of *Pseudomonas* ATCC 9721 on surfaces modified with amorphous carbon. Kylie et al., 2021 suggested that the electrical conductivity of carbon materials can serve as a conductive element in electron transfer. All the virulence factors, Rhamnolipids, pyocyanin, and protease assessed also suggested a significant upregulation after CBNP exposure (Fig. 4.66). High doses on the other hand failed to show any growth response. These virulence factors play pivotal roles in bacterial pathogenesis (Gellatly, S.L. and Hancock, R.E, 2013). Acquiring biofilm mode motility of bacteria will be limited as the bacteria shift into sessile mode (Guttenplan and Kearns, 2013). Here a reduction in bacterial motility was observed in CBNP exposed for 48 h in motility assay (Fig. 4.67). This result agrees with the CV assay and suggests that low concentrations of CBNP exposure promote biofilm formation in *Pseudomonas aeruginosa*

5.4.2 CBNP exposure predisposes alveolar epithelium to bacterial infection.

Epidemiological studies have shown that exposure to air pollution is associated with respiratory exacerbations (Arbex et al., 2009), otitis media (MacIntyre et al.,2011), and eye infections (Saxena et al., 2003). The SARS-Cov-2 epidemic demographic data also suggest that long-term exposure to air pollution is associated with increased mortality

among COVID-19 patients (Wu X et al., 2020; Federica Nobile et al.,2022). The individual effect of pollution and pathogenic organisms in the respiratory system is studied extensively. In real-life situations, exposure to these agents is frequently simultaneous. The effect of particulate matter on infection susceptibility is least understood. In the current study, the objective was formulated to address the lacunae. ECIS was used for this purpose. The microbial-cell interaction studies are often halted by a lack of suitable tools to understand the pathogenic dynamics. The present study suggests ECIS as a unique platform for understanding cell-material-microbial interactions. A marked difference in resistance was observed during CBNP exposure and further infection along the multiple frequencies (Fig 4.68- 4.71). The data suggest that CBNP induce a dose-dependent change in cellular resistance after 20-24 h exposure but was not cytotoxic as the resistance was not equivalent to cell-free. The *Pseudomonas* infection at a multiplicity of infection, MOI 50:1 in all the wells showed a drastic reduction in resistance depending on the concentration of CBNP used in the well. More precisely high dose CBNP exposed wells showed immediate reduction in resistance within 6-8 h post-infection. Lower concentrations reached cell-free measurements at later time points. Assessing the resistance measurements at multiple frequencies (4k-64 kHz) suggested that bacterial infection initially disrupted the barrier integrity of epithelial cells and gained cellular access after which morphology change resulted. Keerthi, S., and Nandkumar, A.M. 2022 reported that a reduction in barrier integrity precedes loss of cell morphology in *Pseudomonas* infection of alveolar cells using the ECIS platform. The Gentamycin protection assay also proves that CBNP exposure induces barrier integrity loss in alveolar epithelial cells as the high dose CBNP exposed cells showed higher bacterial internalisation (Fig 4.72).

5.4.3 *Pseudomonas* lysate accentuates EMT in alveolar epithelial cells.

The onset of fibrosis is marked by epithelial injury. The cause of insult can be multifactorial including ROS production, Gastroesophageal reflux, and bacterial or viral infections (Hirsch J et al.,1999; Blondeau K et al., 2008; Botha et al., 2008). In this phase of the study, we explored the potential of *Pseudomonas* infection in driving an aberrant epithelial repair in the airway. Our data demonstrate that P. *aeruginosa* lysate can accentuate EMT in epithelial cells through the action of secretory products from activated immune cells' secretome. Evident morphological changes were observed in CBNP challenged A549 cells on treatment with immunologically activated immune cell secretome (Fig 4.74). Optimal immunologic activation of THP1 cells were assessed by secreted pro-inflammatory cytokines from the cells treated with bacterial lysate (Fig 4.73). Recent studies suggest that bacterial lysate has immune modulatory properties (Kaczynska A ET AL.,2022). P. *aeruginosa*-activated immune cell secretome is a reservoir of growth factors and cytokines which can be the driving factors of the effect.

Previous studies suggested that repeated sub-clinical injury along with persistent inflammation in airway epithelium during the onset of defective tissue regeneration favour excessive fibroproliferation (Al-Githmi et al., 2006). Earlier phases of the current study proved that cytokines like TNF-α and IL-1β activate fibrotic response through TGF-β1-driven EMT, which demonstrates a possible link between acute inflammation and epithelial remodelling. Results of this phase suggest that an elevated level of growth factors like TGF-β1(Fig 4.74) mediate the accentuation of EMT by *P. aeruginosa* through paracrine signalling.

6. SUMMARY & CONCLUSION

Nanotechnology beyond any doubt contributes significantly to scientific advancements in many sectors like materials and manufacturing, consumer products, energy, medicine, etc. Research, development, and utilization are at the heart of technology. Rising demand and economic value owes to the novelty and physicochemical properties of the newly developed materials which differ from the bulk materials. The boon can turn into a curse if not properly managed. Despite increasing the worldwide production of nanomaterial to satisfy increased demand, corresponding research on the environmental effects of these materials should be promoted. Environmental effects should not be limited to human health effects. Dose and time-dependent studies should also be supported to better understand these effects.

1. The lack of a suitable *in-vitro* system hinders nanotoxicology studies, particularly in understanding a particle-mediated disease prognosis. Phase I of the study was designed to address this gap.
    - Two types of *invitro* systems were developed.
        a. The electric cell-substrate impedance sensing to assess monotypic cellular behaviour to external injury like nanoscale environmental pollutants. The label-free, 2D system offers a non-invasive real-time understanding of cellular responses. The ECIS model of the alveolar epithelial layer was validated by exposing Diesel exhaust nanoparticles (representing the unintentional source of carbon nanoparticles) to A549 cells (representing type II alveolar epithelial cells). Cytotoxicity of high concentrations of DEP by loss of barrier integrity was evidenced by a drastic reduction of impedance measured at 4000Hz.

b. Heterotypic Air-Liquid interface co-culture system to assess multicellular responses in nanoparticle-induced pulmonary fibrosis. The system comprised alveolar epithelial cells and fibroblast cells representing the initiator and effector cells. The developed system was suitable for prolonged particle exposure studies as it maintained structural and functional integrity for 15 days. High TEER value and low permeability point to the intact barrier integrity of the air-liquid interface co-culture system.

2. Phase II of the work focussed on cell-material interactions, particularly to understand alveolar cell responses to Carbon black nanoparticles- the commercially important carbon nanoparticle.

   - Cellular responses of Alveolar epithelial cells (type II), fibroblasts, and monocytes to short-term and long-term CBNP exposure were studied. Significant understandings of this phase include:

     a. CBNP induced a time and concentration-dependent cytotoxicity

     b. High concentrations induced different modes of cell death in alveolar cells. Apoptosis was observed in alveolar epithelial as well as fibroblast cells, whereas Pyroptosis was the cell death observed in monocytes.

     c. Short-term exposure to high doses of CBNP induced pro-inflammatory responses in alveolar cells. The observation supported the fact that inflammation is an important trigger for tissue regeneration as well as fibrosis.

     d. Prolonged exposure to low doses of CBNP induced profibrotic responses in alveolar cells.

e. CBNP induced Epithelial-mesenchymal transition in alveolar epithelial cells through *smad* wnt-dependent pathway. CBNP exposure at low doses induces upregulation of mesenchymal markers like α SMA, TGFβ1, and Collagen genes and down-regulation of epithelial Cadherin (E-cadherin). Enhanced contractility and collagen synthesis were also observed in epithelial cells.

f. CBNP induced fibroblast activation on prolonged exposure to low concentrations. Pro-fibrotic cytokines gene expression was upregulated by CBNP. The upregulation of PI3K along with increased collagen synthesis implied fibroblast activation.

g. Prolonged exposure to CBNP induces M2 polarisation of monocytes. Enhanced M2 polarization to down-regulates inflammatory reactions and activates the fibrotic cascade. Change in morphology together with upregulation in gene expression of IL-10, and profibrotic growth factor, TGF β1suggested M2 polarisation .

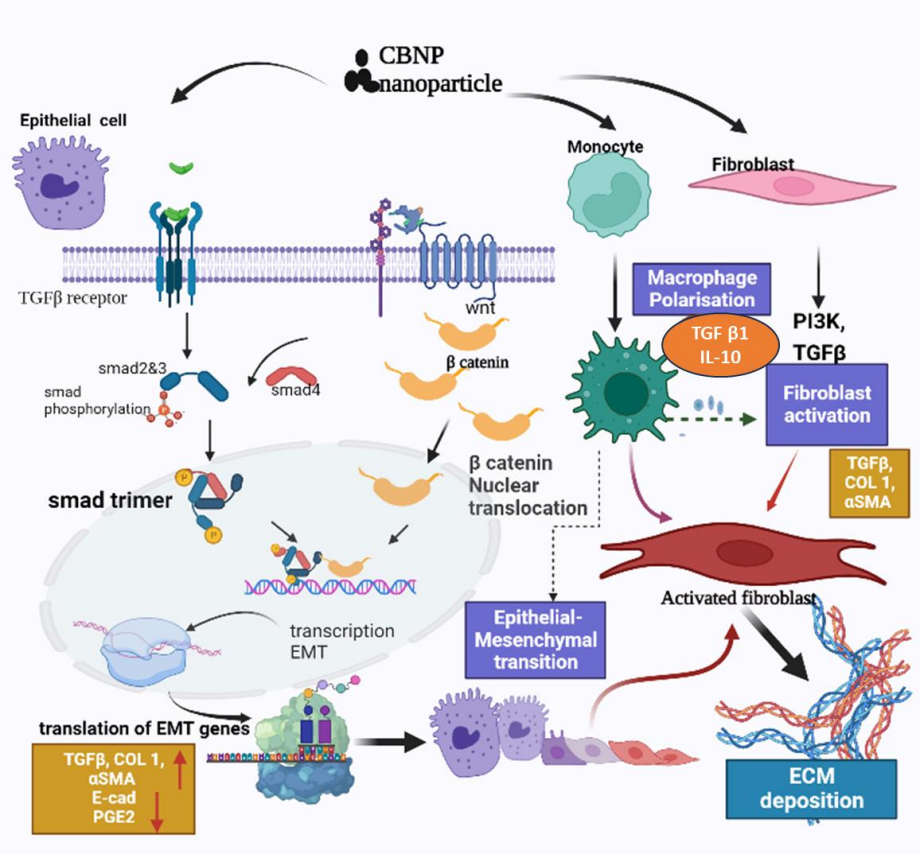

Fig 6.1 Effect of prolonged exposure of CBNP to alveolar cells. CBNP induces pro-fibrotic responses in alveolar epithelial cells, fibroblasts, and monocytes on prolonged exposure. CBNP induced Epithelial mesenchymal transition in epithelial cells, Fibroblast activation and M2 polaristaion in monocytes. The initiation of pro-fibrotic responses can lead to uncontrolled ECM deposition and organ fibrosis will be the result.

3. Phase III dealt with understanding All-Trans Retinoic acid as an anti-fibrotic molecule.

   All trans-retinoic acid is the vitamin A derivative under the retinoid family. It acts as a signalling molecule in the early embryonic development of chordates. ATRA has an important role in lung morphogenesis initiation and also activates genes involved in lung development. Known for its anti-inflammatory role but the antifibrotic potential of ATRA is unexplored. In an attempt to explore the anti-fibrotic potential of ATRA on the CBNP-induced

pro-fibrotic responses of initiator and effector cells of fibrosis, we observed that:

a. 1µM ATRA dose is beneficial. Higher doses are cytotoxic to alveolar cells.
b. Pre-treatment of ATRA can prevent the cells from entering into a fibrotic cascade
c. ATRA downregulated EMT markers expression in epithelial cells
d. The functionality of epithelial cells lost by CBNP exposure was restored by ATRA
e. Fibroblast proliferation, activation, and migration were effectively controlled by ATRA pre-treatment.

4. Phase IV. Dealt with understanding the effect of CBNP on respiratory bacterial pathogenesis.

   Pseudomonas aeruginosa is a gram-negative, ubiquitous, opportunistic pathogen. Due to a range of mechanisms adopted by them for survival and resistance acquired against multiple antibiotic classes, they are emerging as a global health threat. Limited studies are available on the effect of environmental pollutants on bacterial pathogenesis.

   a. Direct exposure of CBNP to *Pseudomonas aeruginosa* induced biofilm formation.
   b. Expression of virulence factors like rhamnolipid, Pyocyanin and Protease, were upregulated on CBNP exposure.
   c. Our ECIS data suggest that CBNP exposure induces a reduction in barrier integrity of the alveolar epithelium in a dose-dependent manner and this enhances infection susceptibility of the epithelial cells to *Pseudomonas*

infection. The drastic and immediate reduction in resistance of high dose CBNP exposed cells on *Pseudomonas* infection as well as increased bacterial internalization, implies the same.

d. The immune cells are the first set of cells recruited to the site of injury or infection. In that case how a bacterial infection modulates these pollutant-induced effects in alveolar cells needs to be understood. For that understanding activated monocyte-conditioned media after *P. aeruginosa* lysate exposure was used to treat CBNP pre-exposed alveolar epithelial cells. This revealed that bacterial infection can accentuate the Epithelial-mesenchymal transition of alveolar epithelial cells

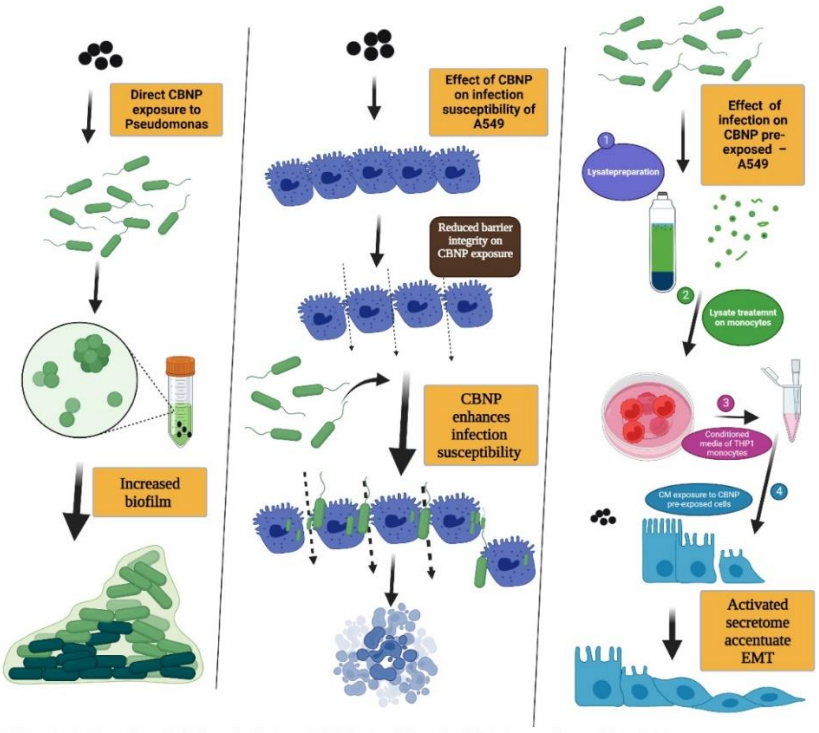

Fig 6.2 Effect of CBNP on P. *aeruginosa* pathogenesis assessed at different levels. Direct exposure of CBNP to *Pseudomonas* induces biofilm formation and upregulation of virulence factors. Infection of CBNP pre-exposed alveolar cells shows enhanced infection susceptibility. P. *aeruginosa* lysate-activated immune cell secretome accentuates particle-induced EMT in alveolar epithelial cells

CONCLUSION

. The work could be concluded as:

1. Two types of *invitro* systems were developed- ECIS model of the alveolar epithelial layer and a heterotypic co-culture model suitable for cell-material interaction studies.
2. Effect of CBNP-

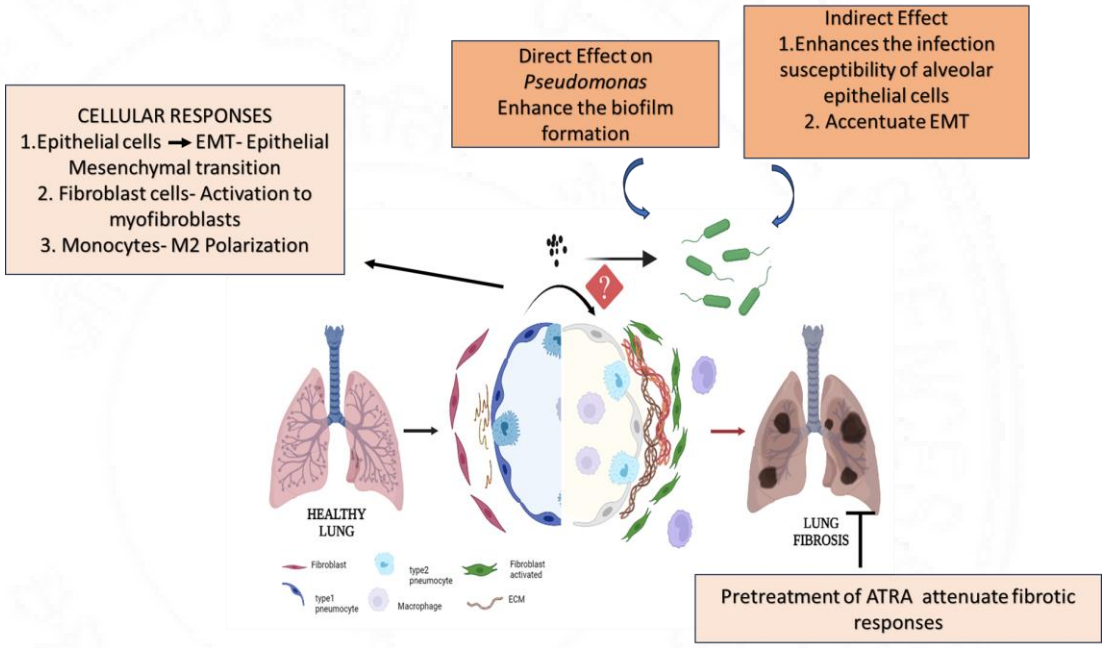

7. REFERENCES

Al-Githmi I, Batawil N, Shigemura N, et al. (2006) Bronchiolitis obliterans following lung transplantation. European Journal of Cardio-Thoracic Surgery 30(6): 846–851. DOI: 10.1016/j.ejcts.2006.09.027.

Allen KylieD, Wegener G, Matthew Sublett D, et al. (2021) Biogenic formation of amorphous carbon by anaerobic methanotrophs and select methanogens. Science Advances 7(44): eabg9739. DOI: 10.1126/sciadv.abg9739.

Almutairi B, Ali D, Yaseen KN, et al. (2021) Mechanisms of Apoptotic Cell Death by Stainless Steel Nanoparticle Through Reactive Oxygen Species and Caspase-3 Activities on Human Liver Cells. Frontiers in Molecular Biosciences 8: 729590. DOI: 10.3389/fmolb.2021.729590.

Arbex MA, de Souza Conceição GM, Cendon SP, et al. (2009) Urban air pollution and chronic obstructive pulmonary disease-related emergency department visits. Journal of Epidemiology and Community Health 63(10): 777–783. DOI: 10.1136/jech.2008.078360.

Archer, S.D.J., Pointing, S.B. Anthropogenic impact on the atmospheric microbiome. Nat Microbiol 5, 229–231 (2020). https://doi.org/10.1038/s41564-019-0650-z

Astanina K, Simon Y, Cavelius C, et al. (2014) Superparamagnetic iron oxide nanoparticles impair endothelial integrity and inhibit nitric oxide production. Acta Biomaterialia 10(11): 4896–4911. DOI: 10.1016/j.actbio.2014.07.027.

Barbe MF, Panibatla ST, Harris MY, et al. (2021) Manual Therapy With Rest as a Treatment for Established Inflammation and Fibrosis in a Rat Model of Repetitive Strain Injury. Frontiers in Physiology 12. Available at: https://www.frontiersin.org/articles/10.3389/fphys.2021.755923 (accessed 9 November 2022).

Barr AE and Barbe MF (2002) Pathophysiological tissue changes associated with repetitive movement: a review of the evidence. Physical Therapy 82(2): 173–187. DOI: 10.1093/ptj/82.2.173.

Beck-Speier I, Dayal N, Karg E, et al. (2005) Oxidative stress and lipid mediators induced in alveolar macrophages by ultrafine particles. Free Radical Biology and Medicine 38(8): 1080–1092. DOI: 10.1016/j.freeradbiomed.2005.01.004.

Bihari P, Vippola M, Schultes S, et al. (2008) Optimized dispersion of nanoparticles for biological in vitro and in vivo studies. Particle and Fibre Toxicology 5(1): 14. DOI: 10.1186/1743-8977-5-14.

Blondeau K, Mertens V, Vanaudenaerde BA, et al. (2008) Gastro-oesophageal reflux and gastric aspiration in lung transplant patients with or without chronic rejection. The European Respiratory Journal 31(4): 707–713. DOI: 10.1183/09031936.00064807.

Borenfreund E and Puerner JA (1985) Toxicity determined in vitro by morphological alterations and neutral red absorption. Toxicology Letters 24(2): 119–124. DOI: 10.1016/0378-4274(85)90046-3.

Borthwick LA, McIlroy EI, Gorowiec MR, et al. (2010) Inflammation and Epithelial to Mesenchymal Transition in Lung Transplant Recipients: Role in Dysregulated Epithelial Wound Repair. American Journal of Transplantation 10(3): 498–509. DOI: 10.1111/j.1600-6143.2009.02953.x.

Borthwick LA, Sunny SS, Oliphant V, et al. (2011) *Pseudomonas aeruginosa* accentuates epithelial-to-mesenchymal transition in the airway. European Respiratory Journal 37(5): 1237–1247. DOI: 10.1183/09031936.00088410.

Botha P, Archer L, Anderson RL, et al. (2008) *Pseudomonas aeruginosa* colonization of the allograft after lung transplantation and the risk of bronchiolitis obliterans syndrome. Transplantation 85(5): 771–774. DOI: 10.1097/TP.0b013e31816651de.

Braakhuis HM, Park MV, Gosens I, et al. (2014) Physicochemical characteristics of nanomaterials that affect pulmonary inflammation. Particle and Fibre Toxicology 11(1): 18. DOI: 10.1186/1743-8977-11-18.

Bradford MM (1976) A rapid and sensitive method for the quantitation of microgram quantities of protein utilizing the principle of protein-dye binding. Analytical Biochemistry 72: 248–254. DOI: 10.1006/abio.1976.9999.

Chamber Rc C and Pf M (2015) Mechanisms of alveolar epithelial injury, repair, and fibrosis. Annals of the American Thoracic Society 12 Suppl 1(Suppl 1). Ann Am Thorac Soc. DOI: 10.1513/AnnalsATS.201410-448MG.

Champion JA and Mitragotri S (2006) Role of target geometry in phagocytosis. Proceedings of the National Academy of Sciences 103(13): 4930–4934. DOI: 10.1073/pnas.0600997103

Chen TT, Chuang KJ, Chiang LL, et al. (2014) Characterization of the interactions between protein and carbon black. Journal of Hazardous Materials 264: 127–135. DOI: 10.1016/j.jhazmat.2013.10.055.

Conte E, Fruciano M, Fagone E, et al. (2011) Inhibition of PI3K Prevents the Proliferation and Differentiation of Human Lung Fibroblasts into Myofibroblasts: The Role of Class I P110 Isoforms. PLoS ONE Chu HW (ed.) 6(10): e24663. DOI: 10.1371/journal.pone.0024663.

Crapo JD, Barry BE, Gehr P, et al. (1982) Cell number and cell characteristics of the normal human lung. The American Review of Respiratory Disease 126(2): 332–337. DOI: 10.1164/arrd.1982.126.2.332.

Cudazzo G, Smart DJ, McHugh D, et al. (2019) Lysosomotropic-related limitations of the BALB/c 3T3 cell-based neutral red uptake assay and an alternative testing approach for assessing e-liquid cytotoxicity. Toxicology in vitro: an international journal published in association with BIBRA 61: 104647. DOI: 10.1016/j.tiv.2019.104647.

Dong Z, Tai W, Yang Y, et al. (2012) The role of all-trans retinoic acid in bleomycin-induced pulmonary fibrosis in mice. Experimental Lung Research 38(2): 82–89. DOI: 10.3109/01902148.2011.646052.

Eap R, Jacques E, Semlali A, et al. (2012) Cysteinyl leukotrienes regulate TGF-β1 and collagen production by bronchial fibroblasts obtained from asthmatic subjects. Prostaglandins, Leukotrienes and Essential Fatty Acids 86(3): 127–133. DOI: 10.1016/j.plefa.2011.11.001.

El-Mowafy SA, Shaaban MI, Abd El Galil KH. 2014Sodium ascorbate as a quorum sensing inhibitor of *Pseudomonas aeruginosa*. Journal of Applied Microbiology. Nov;117(5):1388-99. doi: 10.1111/jam.12631. Epub 2014 Oct 3. PMID: 25175797.

Essar DW, Eberly L, Hadero A & Crawford IP. (1990) Identification and characterization of genes for a second anthranilate synthase in *Pseudomonas aeruginosa*: Interchangeability of the two anthranilate synthases and evolutionary implications. Journal of Bacteriology 172 .884–900

Feghali CA and Wright TM (1997) Cytokines in acute and chronic inflammation. Frontiers in Bioscience: A Journal and Virtual Library 2: d12-26. DOI: 10.2741/a171.

Fink SL and Cookson BT (2005) Apoptosis, pyroptosis, and necrosis: mechanistic description of dead and dying eukaryotic cells. Infection and Immunity 73(4): 1907–1916. DOI: 10.1128/IAI.73.4.1907-1916.2005.

Fink SL and Cookson BT (2006) Caspase-1-dependent pore formation during pyroptosis leads to osmotic lysis of infected host macrophages. Cellular Microbiology 8(11): 1812–1825. DOI: 10.1111/j.1462-5822.2006.00751.x.

Flavell SJ, Hou TZ, Lax S, et al. (2008) Fibroblasts as novel therapeutic targets in chronic inflammation: Fibroblasts in inflammation. British Journal of Pharmacology 153(S1): S241–S246. DOI: 10.1038/sj.bjp.0707487.

Gabbiani G (2003) The myofibroblast in wound healing and fibrocontractive diseases: The myofibroblast. The Journal of Pathology 200(4): 500–503. DOI: 10.1002/path.1427.

Gardiner K, Trethowan WN, Harrington JM, Calvert IA, Glass DC. (1992) Occupational exposure to carbon monoxide and sulphur dioxide during the manufacture of carbon black. The Annals of Occupational Hygiene. Aug;36(4):363-72. doi: 10.1093/annhyg/36.4.363.

Garshick E, Grady ST, Hart JE, et al. (2018) Indoor black carbon and biomarkers of systemic inflammation and endothelial activation in COPD patients. Environmental Research 165: 358–364. DOI: 10.1016/j.envres.2018.05.010.

Gawaziuk JP, Ma X, Sheikh F, et al. (2007) Transforming growth factor- as a differentiating factor for cultured smooth muscle cells. European Respiratory Journal 30(4): 643–652. DOI: 10.1183/09031936.00141805

Gellatly SL and Hancock REW (2013) *Pseudomonas aeruginosa* : new insights into pathogenesis and host defenses. Pathogens and Disease 67(3): 159–173. DOI: 10.1111/2049-632X.12033.

George UM, Ashna U, Kumar SSP, et al. (2013) Effect of tobacco extract on surfactant synthesis and its reversal by retinoic acid-role of cell-cell interactions in vitro. In Vitro Cellular & Developmental Biology. Animal 49(4): 260–269. DOI: 10.1007/s11626-013-9595-3.

Grewal, D.S., 2019. Funding Nanotechnology—A Comparative Study of Global and National Funding. J. Nanom. Nanos. Tech, 105, pp.1-10.

Guo C, Wang J, Jing L, et al. (2018) Mitochondrial dysfunction, perturbations of mitochondrial dynamics and biogenesis involved in endothelial injury induced by silica nanoparticles. Environmental Pollution 236: 926–936. DOI: 10.1016/j.envpol.2017.10.060.

Guttenplan SB and Kearns DB (2013) Regulation of flagellar motility during biofilm formation. FEMS microbiology reviews 37(6): 849–871. DOI: 10.1111/1574-6976.12018.

Hailemariam, Y., Amiri, H.M. and Nugent, K., 2012. Acute respiratory symptoms following massive carbon black exposure. Occupational medicine, 62(7), pp.578-580. https://doi.org/10.1093/occmed/kqs149

Hansen U and Thünemann AF (2015) Characterization of Silver Nanoparticles in Cell Culture Medium Containing Fetal Bovine Serum. Langmuir 31(24). American Chemical Society: 6842–6852. DOI: 10.1021/acs.langmuir.5b00687.

Harrison RM, Rob MacKenzie A, Xu H, et al. (2018) Diesel exhaust nanoparticles and their behaviour in the atmosphere. Proceedings of the Royal Society A: Mathematical, Physical and Engineering Sciences 474(2220): 20180492. DOI: 10.1098/rspa.2018.0492.

Haynes J, Srivastava J, Madson N, et al. (2011) Dynamic actin remodeling during epithelial–mesenchymal transition depends on increased moesin expression. Molecular Biology of the Cell 22(24): 4750–4764. DOI: 10.1091/mbc.E11-02-0119.

He R-W, Braakhuis HM, Vandebriel RJ, et al. (2021) Optimization of an air-liquid interface in vitro cell co-culture model to estimate the hazard of aerosol exposures. Journal of Aerosol Science 153: 105703. DOI: 10.1016/j.jaerosci.2020.105703.

Henderson WR, Chi EY, Ye X, et al. (2010) Inhibition of Wnt/beta-catenin/CREB binding protein (CBP) signaling reverses pulmonary fibrosis. Proceedings of the National Academy of Sciences of the United States of America 107(32): 14309–14314. DOI: 10.1073/pnas.1001520107.

Hiemstra PS, Grootaers G, van der Does AM, et al. (2018) Human lung epithelial cell cultures for analysis of inhaled toxicants: Lessons learned and future directions. Toxicology in Vitro 47: 137–146. DOI: 10.1016/j.tiv.2017.11.005.

Hilton G, Barosova H, Petri-Fink A, et al. (2019) Leveraging proteomics to compare submerged versus air-liquid interface carbon nanotube exposure to a 3D lung cell model. Toxicology in Vitro 54: 58–66. DOI: 10.1016/j.tiv.2018.09.010.

Hirsch A and Backes C (2010) Carbon Nanotube Science. Synthesis, Properties and Applications. By Peter J. F. Harris. Angewandte Chemie International Edition 49(10): 1722–1723. DOI: 10.1002/anie.201000314.

Hirsch J, Elssner A, Mazur G, et al. (1999) Bronchiolitis obliterans syndrome after (heart-)lung transplantation. Impaired antiprotease defense and increased oxidant activity. American Journal of Respiratory and Critical Care Medicine 160(5 Pt 1): 1640–1646. DOI: 10.1164/ajrccm.160.5.9902012.

Huiliang Zhang AMG Xianhua Wang, Yuan Yan, Ming ZhengHeping Cheng (n.d.) ROS regulation of microdomain Ca2+ signalling at the dyads | Cardiovascular Research | Oxford Academic. Available at: https://academic.oup.com/cardiovascres/article/98/2/248/280312 (accessed 8 November 2022).

Inoue T, Umezawa A, Takenaka T, et al. (2015) The contribution of epithelial-mesenchymal transition to renal fibrosis differs among kidney disease models. Kidney International 87(1): 233–238. DOI: 10.1038/ki.2014.235.

International Carbon Black Association. (2019). Carbon black user's guide.

IQAir. (2020). India air quality index (AQI) and air pollution information. AirVisual. Retrieved from https://www.iqair.com/india.

Jiang D, Schaefer N and Chu HW (2018) Air–Liquid Interface Culture of Human and Mouse Airway Epithelial Cells. In: Alper S and Janssen WJ (eds) Lung Innate Immunity and Inflammation. Methods in Molecular Biology. New York, NY: Springer New York, pp. 91–109. DOI: 10.1007/978-1-4939-8570-8_8.

Jiang, S., Jin, L., Hou, H. and Zhang, L., 2019. (n.d.) Polymer-based nanocomposites with high dielectric permittivity. In Polymer-Based Multifunctional Nanocomposites and Their Applications (pp. 201-243). Elsevier.

Kaczynska A, Klosinska M, Janeczek K, et al. (2022) Promising Immunomodulatory Effects of Bacterial Lysates in Allergic Diseases. Frontiers in Immunology 13: 907149. DOI: 10.3389/fimmu.2022.907149.

Kalluri R (2009) EMT: When epithelial cells decide to become mesenchymal-like cells. Journal of Clinical Investigation 119(6): 1417–1419. DOI: 10.1172/JCI39675.

Kalluri R and Weinberg RA (2009) The basics of epithelial-mesenchymal transition. Journal of Clinical Investigation 119(6): 1420–1428. DOI: 10.1172/JCI39104.

Kang D and Hamasaki N (2005) Alterations of Mitochondrial DNA in Common Diseases and Disease States: Aging, Neurodegeneration, Heart Failure, Diabetes and Cancer. Current Medicinal Chemistry 12(4): 429–441. DOI: 10.2174/0929867053363081.

Karygianni L, Ren Z, Koo H, et al. (2020) Biofilm Matrixome: Extracellular Components in Structured Microbial Communities. Trends in Microbiology 28(8): 668–681. DOI: 10.1016/j.tim.2020.03.016.

Keerthi S and Nandkumar AM (2022) Electrical cell-substrate impedance sensing (ECIS) as a tool to study microbial-cell interactions. In vitro models. DOI: 10.1007/s44164-022-00029-6.

Keira SM, Ferreira LM, Gragnani A, et al. (2004) Experimental model for collagen estimation in cell culture. Acta Cirúrgica Brasileira 19. Sociedade Brasileira para o Desenvolvimento da Pesquisa em Cirurgia: 17–22. DOI: 10.1590/S0102-86502004000700005.

Kern U, Wischnewski V, Biniossek ML, et al. (2015) Lysosomal protein turnover contributes to the acquisition of TGFβ-1 induced invasive properties of mammary cancer cells. Molecular Cancer 14(1): 39. DOI: 10.1186/s12943-015-0313-5.

Khadka S, Hashmi FK and Usman M (2020) Preventing COVID-19 in low- and middle-income countries. Drugs & Therapy Perspectives: For Rational Drug Selection and Use 36(6): 250–252. DOI: 10.1007/s40267-020-00728-8

Khadka, N. S. (2020). Air pollution linked to raised Covid-19 death risk. BBC News. Retrieved from https://www.bbc.com/news/health-52351290

Khalil N and Greenberg AH (1991) The role of TGF-beta in pulmonary fibrosis. Ciba Foundation Symposium 157: 194–207; discussion 207-211. DOI: 10.1002/9780470514061.ch13.

Kim J, Chankeshwara SV, Thielbeer F, et al. (2015) Surface charge determines the lung inflammogenicity: A study with polystyrene nanoparticles. Nanotoxicology: 1–8. DOI: 10.3109/17435390.2015.1022887.

Kjaer M (2004) Role of extracellular matrix in adaptation of tendon and skeletal muscle to mechanical loading. Physiological Reviews 84(2): 649–698. DOI: 10.1152/physrev.00031.2003.

Klar S, Poether D-C, Reinert J, et al. (2021) Application of impedance measurement to investigate in vitro inhalation toxicity of bacteria. Journal of Occupational Medicine and Toxicology 16(1): 32. DOI: 10.1186/s12995-021-00317-z.

Leask A and Abraham DJ (2004) TGF-β signaling and the fibrotic response. The FASEB Journal 18(7): 816–827. DOI: 10.1096/fj.03-1273rev.

Lehmann AD, Blank F, Baum O, et al. (2009) Diesel exhaust particles modulate the tight junction protein occludin in lung cells in vitro. Particle and Fibre Toxicology 6(1): 26. DOI: 10.1186/1743-8977-6-26.

Lehmann, A., et al. (2010) A 3D model of the human epithelial airway barrier, in Alternatives to animal testing, L.R. Yarmush ML, Editor. 2010, Artech House. p. 239-260

Li R, Wang X, Ji Z, et al. (2013) Surface Charge and Cellular Processing of Covalently Functionalized Multiwall Carbon Nanotubes Determine Pulmonary Toxicity. ACS Nano 7(3): 2352–2368. DOI: 10.1021/nn305567s.

Li Y, Chu JS, Kurpinski K, et al. (2011) Biophysical regulation of histone acetylation in mesenchymal stem cells. Biophysical Journal 100(8): 1902–1909. DOI: 10.1016/j.bpj.2011.03.008.

Ling L-U, Tan K-B, Lin H, et al. (2011) The role of reactive oxygen species and autophagy in safingol-induced cell death. Cell Death & Disease 2(3): e129–e129. DOI: 10.1038/cddis.2011.12.

Liu J, Wang Y, Pan Q, et al. (2012) Wnt/β-catenin pathway forms a negative feedback loop during TGF-β1 induced human normal skin fibroblast-to-myofibroblast transition. Journal of Dermatological Science 65(1): 38–49. DOI: 10.1016/j.jdermsci.2011.09.012.

Long CM, Nascarella MA and Valberg PA (2013) Carbon black vs. black carbon and other airborne materials containing elemental carbon: physical and chemical distinctions. Environmental Pollution (Barking, Essex: 1987) 181: 271–286. DOI: 10.1016/j.envpol.2013.06.009.

Lu Y, Azad N, Wang L, et al. (2010) Phosphatidylinositol-3-Kinase/Akt Regulates Bleomycin-Induced Fibroblast Proliferation and Collagen Production. American Journal of Respiratory Cell and Molecular Biology 42(4): 432–441. DOI: 10.1165/rcmb.2009-0002OC.

Luyts K, Napierska D, Nemery B, et al. (2013) How physico-chemical characteristics of nanoparticles cause their toxicity: complex and unresolved interrelations. Environ. Sci.: Processes Impacts 15(1): 23–38. DOI: 10.1039/C2EM30237C.

MacIntyre EA, Karr CJ, Koehoorn M, et al. (2011) Residential air pollution and otitis media during the first two years of life. Epidemiology (Cambridge, Mass.) 22(1): 81–89. DOI: 10.1097/EDE.0b013e3181fdb60f.

Mann R, Holmes A, McNeilly O, et al. (2021) Evolution of biofilm-forming pathogenic bacteria in the presence of nanoparticles and antibiotic: adaptation phenomena and cross-resistance. Journal of Nanobiotechnology 19(1): 291. DOI: 10.1186/s12951-021-01027-8.

Manoj MG, Satheesh Kumar MK, Valsaraj KT, et al. (2020) Potential link between compromised air quality and transmission of the novel corona virus (SARS-CoV-2) in affected areas. Environmental Research 190: 110001. DOI: 10.1016/j.envres.2020.110001.

Mason RJ (2006) Biology of alveolar type II cells. Respirology 11(s1): S12–S15. DOI: 10.1111/j.1440-1843.2006.00800.x.

McWhorter FY, Wang T, Nguyen P, et al. (2013) Modulation of macrophage phenotype by cell shape. Proceedings of the National Academy of Sciences 110(43): 17253–17258. DOI: 10.1073/pnas.1308887110.

Miao C, Yang Y, He X, et al. (2013) Wnt signaling in liver fibrosis: Progress, challenges and potential directions. Biochimie 95(12): 2326–2335. DOI: 10.1016/j.biochi.2013.09.003.

Miao EA, Leaf IA, Treuting PM, et al. (2010) Caspase-1-induced pyroptosis is an innate immune effector mechanism against intracellular bacteria. Nature Immunology 11(12): 1136–1142. DOI: 10.1038/ni.1960.

Mikami Y, Matsuzaki H, Takeshima H, et al. (2016) Development of an In Vitro Assay to Evaluate Contractile Function of Mesenchymal Cells that Underwent Epithelial-Mesenchymal Transition. Journal of Visualized Experiments: JoVE (112). DOI: 10.3791/53974.

Monack DM, Navarre WW and Falkow S (2001) Salmonella-induced macrophage death: the role of caspase-1 in death and inflammation. Microbes and Infection 3(14): 1201–1212. DOI: 10.1016/S1286-4579(01)01480-0.

Monopoli MP, Walczyk D, Campbell A, et al. (2011) Physical−Chemical Aspects of Protein Corona: Relevance to in Vitro and in Vivo Biological Impacts of Nanoparticles. Journal of the American Chemical Society 133(8): 2525–2534. DOI: 10.1021/ja107583h.

Morgan A, Babu D, Reiz B, et al. (2019) Caution for the routine use of phenol red – It is more than just a pH indicator. Chemico-Biological Interactions 310: 108739. DOI: 10.1016/j.cbi.2019.108739.

Muir AB, Dods K, Noah Y, et al. (2015) Esophageal epithelial cells acquire functional characteristics of activated myofibroblasts after undergoing an epithelial to

mesenchymal transition. Experimental Cell Research 330(1): 102–110. DOI: 10.1016/j.yexcr.2014.08.026.

Mulugeta S and Beers MF (2006) Surfactant protein C: Its unique properties and emerging immunomodulatory role in the lung. Microbes and Infection 8(8): 2317–2323. DOI: 10.1016/j.micinf.2006.04.009.

Nagy A, Steinbrück A, Gao J, et al. (2012) Comprehensive Analysis of the Effects of CdSe Quantum Dot Size, Surface Charge, and Functionalization on Primary Human Lung Cells. ACS Nano 6(6): 4748–4762. DOI: 10.1021/nn204886b.

Nakajima T, Yoon S-C, Ramanathan V, et al. (2007) Overview of the Atmospheric Brown Cloud East Asian Regional Experiment 2005 and a study of the aerosol direct radiative forcing in east Asia. Journal of Geophysical Research 112(D24): D24S91. DOI: 10.1029/2007JD009009.

Nakajima T, Yoon S-C, Ramanathan V, et al. (2007) Overview of the Atmospheric Brown Cloud East Asian Regional Experiment 2005 and a study of the aerosol direct radiative forcing in east Asia. Journal of Geophysical Research 112(D24): D24S91. DOI: 10.1029/2007JD009009.

Navas A and Nandkumar A M (2022) Electric Cell-Substrate Impedance Sensing (ECIS) for Analyzing the Effect of Environmental Pollutants - A Study of Diesel Exhaust Nanoparticles. Journal of Environmental Science and Public Health 06(02). DOI: 10.26502/jesph.96120166.

Nel A, Xia T, Mädler L, et al. (2006) Toxic Potential of Materials at the Nanolevel. Science 311(5761): 622–627. DOI: 10.1126/science.1114397.

Nemmar A, Holme JA, Rosas I, et al. (2013) Recent Advances in Particulate Matter and Nanoparticle Toxicology: A Review of the In Vivo and In Vitro Studies. BioMed Research International 2013: 1–22. DOI: 10.1155/2013/279371

Nguyen DHK, Wang J, Sbarski I, et al. (2019) Influence of Amorphous, Carbon-Derived Wrinkled Surface Topologies on the Colonization of *Pseudomonas aeruginosa*

Bacteria. Advanced Materials Interfaces 6(7): 1801890. DOI: 10.1002/admi.201801890.

Nikota J, Banville A, Goodwin LR, et al. (2017) Stat-6 signaling pathway and not Interleukin-1 mediates multi-walled carbon nanotube-induced lung fibrosis in mice: insights from an adverse outcome pathway framework. Particle and Fibre Toxicology 14(1): 37. DOI: 10.1186/s12989-017-0218-0.

Nobile F, Michelozzi P, Ancona C, et al. (2022) Air pollution, SARS-CoV-2 incidence and COVID-19 mortality in Rome: a longitudinal study. European Respiratory Journal 60(3): 2200589. DOI: 10.1183/13993003.00589-2022.

O'Toole GA (2011) Microtiter Dish Biofilm Formation Assay. Journal of Visualized Experiments : JoVE (47): 2437. DOI: 10.3791/2437.

Oberdörster G, Ferin J and Lehnert BE (1994) Correlation between particle size, in vivo particle persistence, and lung injury. Environmental Health Perspectives 102(suppl 5): 173–179. DOI: 10.1289/ehp.102-1567252.

Okano M and Watanabe S (2018) Inspection of internal filler alignment in visibly opaque carbon-black–rubber composites by terahertz polarization spectroscopy in reflection mode. Polymer Testing 72: 196–201. DOI: 10.1016/j.polymertesting.2018.10.020.

Pachori P, Gothalwal R and Gandhi P (2019) Emergence of antibiotic resistance *Pseudomonas aeruginosa* in intensive care unit; a critical review. Genes & Diseases 6(2): 109–119. DOI: 10.1016/j.gendis.2019.04.001.

Pena S (1980) A new technique for the visualization of the cytoskeleton in cultured fibroblasts with Coomassie blue R250. Cell Biology International Reports 4(2): 149–153. DOI: 10.1016/0309-1651(80)90069-7.

Pierzyńska-Mach A, Janowski PA and Dobrucki JW (2014) Evaluation of acridine orange, LysoTracker Red, and quinacrine as fluorescent probes for long-term tracking of acidic vesicles. Cytometry. Part A: The Journal of the International Society for Analytical Cytology 85(8): 729–737. DOI: 10.1002/cyto.a.22495.

Porto, L., Silva, D., de Oliveira, A., Pereira, A. and Borges, K. (2019) Carbon nanomaterials: synthesis and applications to development of electrochemical sensors in determination of drugs and compounds of clinical interest. Reviews in Analytical Chemistry, Vol. 38 (Issue 3), pp. 20190017. https://doi.org/10.1515/revac-2019-0017

Powell MC and Kanarek MS (2006) Nanomaterial health effects--part 1: background and current knowledge. WMJ: official publication of the State Medical Society of Wisconsin 105(2): 16–20.

Querol, X., Alastuey, A., Pey, J., Viana, M., Moreno, T., Minguillón, M. C., et al. (2004). Nanoparticles in the atmosphere. Seminario Sem. 8, 24–39.

R.J. Mason. (2006) , EPITHELIAL CELLS | Type II Cells Encyclopedia of Respiratory Medicine,

Raghu G, Rochwerg B, Zhang Y, et al. (2015) An Official ATS/ERS/JRS/ALAT Clinical Practice Guideline: Treatment of Idiopathic Pulmonary Fibrosis. An Update of the 2011 Clinical Practice Guideline. American Journal of Respiratory and Critical Care Medicine 192(2): e3–e19. DOI: 10.1164/rccm.201506-1063ST.

Rahbar Saadat Y, Saeidi N, Zununi Vahed S, et al. (2015) An update to DNA ladder assay for apoptosis detection. BioImpacts: BI 5(1): 25–28. DOI: 10.15171/bi.2015.01.

Rajak R and Chattopadhyay A (2020) Short and Long Term Exposure to Ambient Air Pollution and Impact on Health in India: A Systematic Review. International Journal of Environmental Health Research 30(6): 593–617. DOI: 10.1080/09603123.2019.1612042.

Rasamiravaka T, Vandeputte OM & Jaziri ME. (2016) Procedure for Rhamnolipids Quantification Using Methyleneblue. Bio-Protocol 6 e1783–e1783.

Rc C and Pf M (2015) Mechanisms of alveolar epithelial injury, repair, and fibrosis. Annals of the American Thoracic Society 12 Suppl 1(Suppl 1). Ann Am Thorac Soc. DOI: 10.1513/AnnalsATS.201410-448MG.

Rebecca Dezube. overview of the respiratory system MSD MANUAL https://www.msdmanuals.com/en-in/home/lung-and-airway-disorders/biology-of-the-lungs-and-airways/overview-of-the-respiratory-system.

Ren H, Birch NP and Suresh V (2016) An Optimised Human Cell Culture Model for Alveolar Epithelial Transport. PloS One 11(10): e0165225. DOI: 10.1371/journal.pone.0165225.

Renwick LC, Donaldson K and Clouter A (2001) Impairment of alveolar macrophage phagocytosis by ultrafine particles. Toxicology and Applied Pharmacology 172(2): 119–127. DOI: 10.1006/taap.2001.9128.

Sakai N and Tager AM (2013) Fibrosis of two: Epithelial cell-fibroblast interactions in pulmonary fibrosis. Biochimica Et Biophysica Acta 1832(7): 911–921. DOI: 10.1016/j.bbadis.2013.03.001.

Saputra D, Yoon J, Park H, et al. (2014) Inhalation of Carbon Black Nanoparticles Aggravates Pulmonary Inflammation in Mice. Toxicological Research 30(2): 83–90. DOI: 10.5487/TR.2014.30.2.083.

Sauer J-D, Witte CE, Zemansky J, et al. (2010) Listeria monocytogenes triggers AIM2-mediated pyroptosis upon infrequent bacteriolysis in the macrophage cytosol. Cell Host & Microbe 7(5): 412–419. DOI: 10.1016/j.chom.2010.04.004.

Saxena R, Srivastava S, Trivedi D, et al. (2003) Impact of environmental pollution on the eye. Acta Ophthalmologica Scandinavica 81(5): 491–494. DOI: 10.1034/j.1600-0420.2003.00119.x.

Saxena, P., & Sonwani, S. (2020). Remediation of ozone pollution by ornamental plants in indoor environment. Global Journal of Environmental Science and Management, 6(4), 497-508.

Schruf E, Schroeder V, Le HQ, et al. (2020) Recapitulating idiopathic pulmonary fibrosis related alveolar epithelial dysfunction in a human iPSC-derived air-liquid interface model. The FASEB Journal 34(6): 7825–7846. DOI: 10.1096/fj.201902926R.

Segel MJ, Or R, Tzurel A, et al. (2001) All-trans-retinoic acid (ATRA) is of no benefit in bleomycin-induced lung injury. Pulmonary Pharmacology & Therapeutics 14(5): 403–407. DOI: 10.1006/pupt.2001.0300.

Shah, A.P., Pietropaoli, A.P., Frasier, L.M., Speers, D.M., Chalupa, D.C., Delehanty, J.M., Huang, L.S., Utell, M.J., Frampton, M.W. (2008). Effect of inhaled carbon ultrafine particles on reactive hyperemia in healthy human subjects. Environmental Health Perspectives. 116, 375–380. https://doi.org/10.1289/ehp.10323

Sohaebuddin SK and Tang L (2013) A simple method to visualize and assess the integrity of lysosomal membrane in mammalian cells using a fluorescent dye. Methods in Molecular Biology (Clifton, N.J.) 991: 25–31. DOI: 10.1007/978-1-62703-336-7_3.

Song P, Wan C, Xie Y, et al. (2018) Vegetable derived-oil facilitating carbon black migration from waste tire rubbers and its reinforcement effect. Waste Management (New York, N.Y.) 78: 238–248. DOI: 10.1016/j.wasman.2018.05.054.

Song X, Liu W, Xie S, et al. (2013) All-transretinoic acid ameliorates bleomycin-induced lung fibrosis by downregulating the TGF-β1/Smad3 signaling pathway in rats. Laboratory Investigation 93(11): 1219–1231. DOI: 10.1038/labinvest.2013.108.

Stone KC, Mercer RR, Gehr P, et al. (1992) Allometric Relationships of Cell Numbers and Size in the Mammalian Lung. American Journal of Respiratory Cell and Molecular Biology 6(2): 235–243. DOI: 10.1165/ajrcmb/6.2.235.

Stone V, Shaw J, Brown DM, et al. (1998) The role of oxidative stress in the prolonged inhibitory effect of ultrafine carbon black on epithelial cell function. Toxicology in Vitro 12(6): 649–659. DOI: 10.1016/S0887-2333(98)00050-2.

Suzuki T, Franchi L, Toma C, et al. (2007) Differential regulation of caspase-1 activation, pyroptosis, and autophagy via Ipaf and ASC in Shigella-infected macrophages. PLoS pathogens 3(8): e111. DOI: 10.1371/journal.ppat.0030111.

Swafford DS, Nikula KJ, Mitchell CE, et al. (1995) Low frequency of alterations in p53, K-ras, and mdm2 in rat lung neoplasms induced by diesel exhaust or carbon black. Carcinogenesis 16(5): 1215–1221. DOI: 10.1093/carcin/16.5.1215.

Szulcek R, Bogaard HJ and van Nieuw Amerongen GP (2014) Electric cell-substrate impedance sensing for the quantification of endothelial proliferation, barrier function, and motility. Journal of Visualized Experiments: JoVE (85). DOI: 10.3791/51300.

Tabata Chiharu, Kadokawa Y, Tabata R, et al. (2006) All-trans-retinoic acid prevents radiation- or bleomycin-induced pulmonary fibrosis. American Journal of Respiratory and Critical Care Medicine 174(12): 1352–1360. DOI: 10.1164/rccm.200606-862OC.

Thomas G, Tacke R, Hedrick CC, et al. (2015) Nonclassical patrolling monocyte function in the vasculature. Arteriosclerosis, Thrombosis, and Vascular Biology 35(6): 1306–1316. DOI: 10.1161/ATVBAHA.114.304650.

Usman M, Zaheer Y, Younis MR, et al. (2020) The effect of surface charge on cellular uptake and inflammatory behavior of carbon dots. Colloid and Interface Science Communications 35: 100243. DOI: 10.1016/j.colcom.2020.100243.

Vaïtilingom M, Amato P, Sancelme M, et al. (2010) Contribution of Microbial Activity to Carbon Chemistry in Clouds. Applied and Environmental Microbiology 76(1). American Society for Microbiology: 23–29. DOI: 10.1128/AEM.01127-09.

Versaevel M, Grevesse T and Gabriele S (2012) Spatial coordination between cell and nuclear shape within micropatterned endothelial cells. Nature Communications 3: 671. DOI: 10.1038/ncomms1668.

Wang Y, Shi P, Chen Q, et al. (2019) Mitochondrial ROS promote macrophage pyroptosis by inducing GSDMD oxidation. Journal of Molecular Cell Biology 11(12): 1069–1082. DOI: 10.1093/jmcb/mjz020.

Wichmann H-E (2007) Diesel Exhaust Particles. Inhalation Toxicology 19(sup1): 241–244. DOI: 10.1080/08958370701498075.

Willis BC and Borok Z (2007) TGF-beta-induced EMT: mechanisms and implications for fibrotic lung disease. American Journal of Physiology. Lung Cellular and Molecular Physiology 293(3): L525-534. DOI: 10.1152/ajplung.00163.2007

World Health Statistics. Monitoring health for the SDGs, sustainable development goals. Geneva: World Health Organization; 2021. p. 2021.

Wu X, Nethery RC, Sabath MB, et al. (2020) Air pollution and COVID-19 mortality in the United States: Strengths and limitations of an ecological regression analysis. Science Advances 6(45): eabd4049. DOI: 10.1126/sciadv.abd4049.

Wynn TA, Chawla A and Pollard JW (2013) Macrophage biology in development, homeostasis and disease. Nature 496(7446): 445–455. DOI: 10.1038/nature12034.

Yang J, Nie J, Ma X, et al. (2019) Targeting PI3K in cancer: mechanisms and advances in clinical trials. Molecular Cancer 18(1): 26. DOI: 10.1186/s12943-019-0954-x.

Yu K-N, Chang S-H, Park SJ, et al. (2015) Titanium Dioxide Nanoparticles Induce Endoplasmic Reticulum Stress-Mediated Autophagic Cell Death via Mitochondria-Associated Endoplasmic Reticulum Membrane Disruption in Normal Lung Cells. PLOS ONE Ariga H (ed.) 10(6): e0131208. DOI: 10.1371/journal.pone.0131208.

Yuan X, Zhang X, Sun L, Wei Y, Wei X. (2019)Cellular Toxicity and Immunological Effects of Carbon-based Nanomaterials. Part Fibre Toxicol. Apr 11;16(1):18. doi: 10.1186/s12989-019-0299-z.

Yuan Y, Chen Y, Zhang P, et al. (2012) Mitochondrial dysfunction accounts for aldosterone-induced epithelial-to-mesenchymal transition of renal proximal tubular epithelial cells. Free Radical Biology and Medicine 53(1): 30–43. DOI: 10.1016/j.freeradbiomed.2012.03.015.

Yue X, Shan B and Lasky JA (2010) TGF-β: Titan of Lung Fibrogenesis. Current enzyme inhibition 6(2): 10.2174/10067. DOI: 10.2174/10067.

Zavala J, O'Brien B, Lichtveld K, et al. (2016) Assessment of biological responses of EpiAirway 3-D cell constructs versus A549 cells for determining toxicity of ambient air pollution. Inhalation Toxicology 28(6): 251–259. DOI: 10.3109/08958378.2016.1157227.

Zaytseva O and Neumann G (2016) Carbon nanomaterials: production, impact on plant development, agricultural and environmental applications. Chemical and Biological Technologies in Agriculture 3(1): 17. DOI: 10.1186/s40538-016-0070-8.

Zhang H, Gomez AM, Wang X, et al. (2013) ROS regulation of microdomain Ca2+ signalling at the dyads. Cardiovascular Research 98(2): 248–258. DOI: 10.1093/cvr/cvt050.

Zhang J, Wang X, Vikash V, et al. (2016) ROS and ROS-Mediated Cellular Signaling. Oxidative Medicine and Cellular Longevity 2016: 4350965. DOI: 10.1155/2016/4350965.

Zhang R, Dai Y, Zhang X, et al. (2014) Reduced pulmonary function and increased pro-inflammatory cytokines in nanoscale carbon black-exposed workers. Particle and Fibre Toxicology 11(1): 73. DOI: 10.1186/s12989-014-0073-

Zhao X, Ng S, Heng BC, et al. (2013) Cytotoxicity of hydroxyapatite nanoparticles is shape and cell dependent. Archives of Toxicology 87(6): 1037–1052. DOI: 10.1007/s00204-012-0827-1.

8. APPENDIX

1. DETAILS OF RT-PCR PRIMERS USED IN THE STUDY

GENE	FORWARD 5'-3'	REVERSE 5'-3'
Caspase 1	GCCTGTTCCTGTGATGTGGAG-	TGCCCACAGACATTCATACAGTTTC
Caspase 3	GGGCCTGTTGAACTGAAAAA	CCGTCCTTTGAATTTCTCCA
Collagen	ACGTCCTGGTGAAGTTGGTC	ACCAGGGAAGCCTCTCTCTC
COX2	TCCAAATGAGATTGTGGGAAAATTGCT	AGATCATCTCTGCCTGAGTATCTT
E cadherin	TGC-ACC-GGT-GCAATC-TTC-AA	GTCAGTTCAGACTCCAGCCC
GAPDH	TGTGTCCGTGGTGGATCTGA	CCTGCTTCACCACCTTCTGA
IL-1β	ATAAGCCCACTCTACAGCT	ATTGGCCCTGAAAGGAGAAGA
IL-10	ATGCCCCAAGCTGAGAACCAAGAC	TCTCAAGGGGCTGGGTCAGCTATCCA
IL-6	CAGCCCACTCACCTCACCTCTCTTCAGAAC	TGCAGGAAACTGGATCAGGAC
IL-8	GCTTTCTGATGGAAGAGC	GGCACAGTGGAACAGGACT
iNOS	GAGCTTCTACCTCAAGCTATC	CCTGATGTTGCCATTGTTGGT
MMP	CAAGGCATAGAGACAACATAGA	GCACAGCAACAGTAGGAT
SP-C	ACCCTGTGTGGAGAGCTACCA	TTTGCGGAGGGTCTTTCCT
TGFβ	CAACAACGCCATCTATGAGA	TATTCCGTCTCCTTGGTTC

TIMP	GTGGCACTCATTGCTTGTGG	CAAGGTGACGGGACTGGAAG
TNFα	CAGAGGGAAGAGTTCCCCAG	CCTTGGTCTGGTAGGAGCACG
α-Smooth muscle actin (ACTA)	AACTGTGAATGTCCTGTG	CATAGGTAACGAGTCAGAG

9. ANNEXURES

A. CONFERENCE PRESENTATIONS

Navas Amalu, Kumar Pradeep SS, Nandkumar Maya, Pulmonary Fibrosis: Nanoparticles as Inducers In Shift To Aberrant Wound Healing In The Proceeding Of The International Conference On Biomaterials, Bio diagnostics, Tissue Engineering, Drug Delivery And Regenerative Medicine 2016 at, Indian Institute of Technology (IIT) Delhi at New Delhi. April 15-17, 2016

Amalu Navas, Pradeep Kumar SS, Maya Nandkumar. Effect of diesel exhaust particles on airway epithelial model. Presented at The International Conference On Biomaterials, Bioengineering And, Biotheranostics at Vellore Institute Of Technology, Vellore 26-28th July 2018

Amalu Navas and Maya Nandkumar, Pulmonary fibrotic potential of nano-particulate Carbon Black: Monocyte response to the nanoparticle, Presented in The International Conference On Emerging Advancement In Science And Technology (ICEAST-19) New Delhi Sep-5-6 2019

Amalu Navas and Maya Nandkumar of ROS and LMP contribute to carbon black cytotoxicity to alveolar epithelium presented at The International Virtual Conference on Biomedical Innovations-2020 6-9 Dec 2020

Amalu Navas and Maya Nandkumar Exposure of Carbon black induce profibrotic responses in alveolar epithelium presented in 11th India-Japan science and Technology seminar. Dec 2021

Amalu Navas, Maya Nandkumar ECIS-A promising tool to analyse cell-nanoparticle interactions, Oral presentation, ATM&AGM, Material Research Society of India, Trivandrum chapter, April 30, 2022

Ouriginal by Turnitin

Document Information

Analyzed document	Amalu thesis for plagiarism checking.pdf (D149204961)
Submitted	2022-11-10 05:43:00
Submitted by	Maya A Nandkumar
Submitter email	anmaya@sctimst.ac.in
Similarity	0%
Analysis address	mnaaya.sctims@analysis.urkund.com

Sources included in the report

SA

M.Sc R dissertation thesis in TDU format 7 aug 22 .pdf
Document M.Sc R dissertation thesis in TDU format 7 aug 22 .pdf (D143139191)
1

SA

Central University of Punjab, Bathinda / Pooja Synopsis.docx
Document Pooja Synopsis.docx (D39105476)
Submitted by: poojarajput2321@gmail.com
Receiver: jyoti.parkash.cup@analysis.urkund.com
1

SA

University of Helsinki / yhteenveto180217.pdf
Document yhteenveto180217.pdf (D36105674)
Submitted by: ville.vartiainen@helsinki.fi
Receiver: med-dissertation.hy@analyysi.urkund.fi
1

W

URL: https://www.ncbi.nlm.nih.gov/pmc/articles/PMC8166691/
Fetched: 2021-12-16 02:25:45
1

SA

Master'sThesis_AnnikaHettich.pdf
Document Master'sThesis_AnnikaHettich.pdf (D142314171)
2

SA

Jiwaji University, Gwalior / Devshree Sahu full theses.docx
Document Devshree Sahu full theses.docx (D20958751)

J Environ Sci Public Health 2022;6 (2):189-203 *DOI: 10.26502/jesph.96120166*

Research Article

Electric Cell-Substrate Impedance Sensing (ECIS) for Analyzing the Effect of Environmental Pollutants - A Study of Diesel Exhaust Nanoparticles

Amalu Navas[1], Maya Nandkumar A[2*]

[1]PhD Scholar, Division of Microbial Technology, BMT Wing, SCTIMST, Poojappura, Thiruvananthapuram, Kerala, India

[2]Scientist 'G' and Head, Division of Microbial Technology, BMT Wing, Sree Chitra Tirunal Institute for Medical Sciences and Technology, Thiruvananthapuram-12, Kerala, India

[*]**Corresponding Author:** Dr A Maya Nandkumar, Scientist 'G' and Head, Division of Microbial Technology, BMT Wing, SCTIMST, Poojappura, Thiruvananthapuram, Kerala, India

Received: 11 May 2022; **Accepted:** 18 May 2022; **Published:** 26 May 2022

Citation: Amalu Navas, Maya Nandkumar A. Electric Cell-Substrate Impedance Sensing (ECIS) for Analyzing the Effect of Environmental Pollutants - A Study of Diesel Exhaust Nanoparticles. Journal of Environmental Science and Public Health 6 (2022): 189-203.

Abstract

ECIS is a morphological biosensor that records the electrical properties of cell-covered microelectrodes in an AC circuit, including impedance (ohm), resistance (ohm), and capacitance (µFarad). The objective of the current study was to analyze the suitability of ECIS as a label-free *in vitro* assay system to understand the effect of external stimuli on cells in real-time, vis-à-vis regular endpoint assays of cytotoxicity. The study analyzed whether fluctuations in the electrical properties of cell-covered microelectrodes reflected dynamic changes in cell morphology on exposure to diesel exhaust particles. Exposure of A549 monolayers in 8 well microarrays to DEP caused significant changes in microelectrode resistance (ohm @4 kHz) as compared to controls within 24 h. Variations in impedance were found to have a dose-dependent effect. We compared our results from ECIS with classic cytotoxicity analyses

like MTT, LDH, and NRU assays and observed corroborative endpoint results. Reactive oxygen species production by DCFHDA assay showed an increase in relative fluorescence indicating ROS to be a possible cause of dose-dependent cytotoxicity.

Our findings indicate that ECIS provides many benefits as an alternative method to quantify, automate, and measure the effect of pollutants or particles in real-time when compared to traditional endpoint methods.

Keywords: ECIS; Diesel exhaust nanoparticles; Cytotoxicity; Label-free; Real-time

1. Introduction

Electric cell-substrate impedance sensing (ECIS) is a real-time label-free method for analyzing cellular behavior to an external injury or stimuli using in vitro cell cultures. The system measures changes in impedance/resistance in cell monolayers in real-time and thus provides information faster vis-à-vis endpoint or labelled assays. Most conventional analyses are invasive, use multiple labels, are labor-intensive and provide only endpoint results. Examples of label-free methods include techniques like optical light spectroscopy, quartz microbalance, and electric cell-substrate impedance sensing (ECIS). Among them, ECIS is a powerful tool to assess cellular properties and physiology. This method has attracted wide attention as it overcomes the limitations of conventional endpoint analyses. Ever since Giaever and Keese (1984) invention, ECIS has been used to monitor cell motion, attachment, and spreading and assess cell migration in wound healing assays [1].

In ECIS cells are grown in arrays with golden electrodes at the bottom. A small alternating current (AC) is applied across electrodes patterned at the bottom of arrays, resulting in potential differences across electrodes measured by the ECIS instrument. As cells attach to electrodes and proliferate, resistance increases to the current flow corresponding to morphology and the number of cells covering the electrode. The results are plotted as an impedance versus time graph.

AC frequencies are important in ECIS. Current flow always takes a path of low resistance. At low frequencies, membrane impedance is higher, so most of the current flows in the solution channels under and between cells, whereas at higher frequencies (>40,000Hz) current flows mostly through the insulating cell membranes. Thus, high-frequency impedance is affected by cell coverage and give details about cell spreading and establishment of confluent layer and low frequency will give details about barrier integrity. In the more advanced Zθ equipment, the impedance will be broken down to resistance and capacitance, allowing for more accurate data of the cell behavior, making it an advanced form of cellular impedance-based assays.

Air pollution has been linked to increased morbidity and mortality of pulmonary diseases. Exposure to airborne particulate matter has a strong correlation with adverse outcomes like reduced lung function, premature death [2, 3, 4]. Diesel exhaust nanoparticles (DEP) are a major component of particulate matter in air pollution. DEP results from incomplete combustion of diesel fuel. It is composed of a central core of elemental carbon and adsorbed

organic compounds including Polyaromatic hydrocarbons (PAHs) and nitro-PAHs, and small amounts of sulfate, nitrate, metals, and other trace elements [5] differing in composition depending on the source of collection. These particles having large surface area are highly respirable and are in the nanosize range, reaching the deep portions of the lungs -like the gas exchange regions or alveoli. Airway epithelial cells form an innate line of defense to inhaled allergens, particulates, and pathogens, affected through a combination of secreted mucus and apical junctional complexes (AJC). Our study demonstrates ECIS as an effective tool to understand the effect of nano aerosolized pollutants on the alveolar epithelial cells vis-à-vis regular endpoint analysis.

2. Materials and Method

2.1 Cell culture

Kaighn's modification of Ham's F12 (F12K), Trypsin EDTA, Gentamycin, Amphotericin B solutions were purchased from Hi-media Pvt. Ltd. (Mumbai, India). Fetal bovine serum (FBS) was purchased from Gibco (Grand Island, NY, USA). 3-(4,5-Dimethylthiazol-2-yl)- 2,5-diphenyltetrazolium bromide (MTT), trypan blue, Neutral red dye was purchased from Sigma Chemicals Co. Ltd. (St. Louis, MO, USA). LDH assay was done by using CytoTox96® Non-Radioactive Cytotoxicity Assay kit from Promega. DCFHDA was purchased from Thermo fisher scientific (Waltham, Massachusetts).

2.2 Diesel exhaust nanoparticle preparation and characterization

The diesel exhaust particles (DEP) were collected from a diesel car engine exhaust. The exhaust particles were collected into a membrane filter made of cellulose ester as total suspended particulates. Particles were collected by sonicating the filter for 45mins in 5ml of ultrapure water using a bath sonicator. The suspension was then centrifuged at 10,000rpm for 15mins and lyophilized (Lyolab). Stock solution of diesel exhaust nanoparticles was prepared in complete cell culture medium and sonicated prior to exposure. This was used as DEP in the study. DEP was characterized by Transmission electron microscopy. (JEOL JEM TEM).

2.3 Impedance measurement with ECIS

ECIS was used to study the effect of diesel exhaust particles in A549 cells. The array type used was 8W10E+ (Applied Biophysics, NY, USA), consisting of eight wells, each with two sets of 20 circular active electrodes with 250 μm diameter located on inter-digitated fingers to provide measurements upon 40 electrodes in total. Each well has a substrate area of 0.8cm2 and volume of 600 μL.

The 10E+ arrays used for the study were designed to monitor a large number of cells, sampling over the entire bottom of the well. Arrays were attached to the ECIS system (Model ECIS Zθ, Applied Biophysics, NY, USA), and alternative current (I) of 4000 Hz was applied to the sensing electrodes. Low frequencies were used to assess cellular barrier function, as at higher frequencies, current flows capacitively through the cell membrane, whereas at low frequencies, the membrane impedance increases, and current flows through the cellular junctions, which offer lesser resistance (Figure 1).

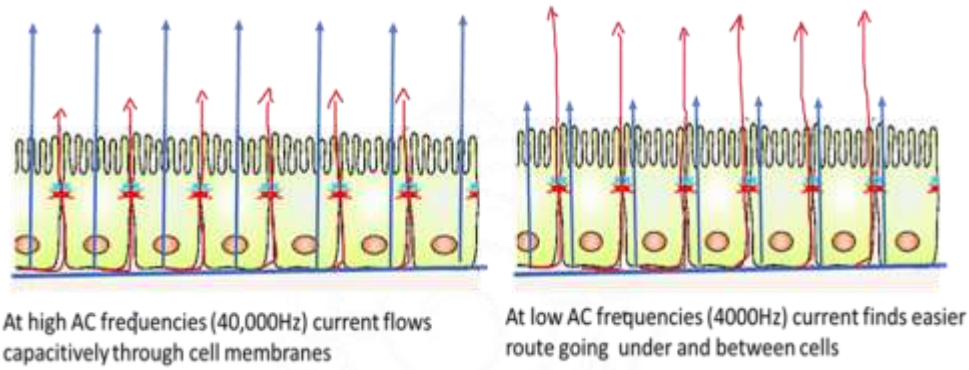

Figure 1: Is a pictogram depicting the cross-section of a confluent cell monolayer inside the ECIS well array and the probable path of current flow at different frequencies is indicated by the arrows.

Prior to the experiment, the array holder was warmed to 37ºC in the incubator [6]. Before seeding the cells, 400µl of complete cell culture medium was added to the 8Well. The arrays were placed on the array holder, such that the gold-plated electrode pads were aligned with the spring-loaded pogo pins and the screws were tightened. The connectivity and impedance were checked. After stabilization of electrodes cell-free impedance was measured. After 1hr the impedance measurement was paused and arrays were removed. The media in the wells were replaced with fresh F12K medium. A549 cells were seeded at a density of 10^4 cells/electrode. The electrodes were placed on the array holder, the connectivity to each well was checked and impedance measurement resumed. As the cells adhered and spread on the electrode, the impedance increased. Once complete electrode coverage was attained by the formation of a monolayer, the impedance measurement plateaued.

2.3.1 Post- exposure measurement: Impedance measurement was carried out till confluence by the method as previously described. Following confluence, impedance measurement was paused and the medium in the wells was replaced by DEP in F12K medium was added in varying concentrations. The impedance measurement was continued for the duration of the experiment. The data was analyzed using Zθ ECIS analysis software. After normalization, the data was plotted against time.

2.4 Classic cytotoxicity analyses

2.4.1 Assessment of cell viability: The MTT assay, assesses metabolic reduction of 3-(4,5-dimethylthiazol-2-yl)-2,5-diphenyl-tetrazolium bromide reagent to formazan crystals. In brief, A549 cells (1×10^4) were seeded into each well of a 96 well plate. Cells were treated with different concentrations of DEP (1, 10, 20, 40, 80, 160, 320 µgm/ml) for 24 h. Following exposure, the medium was removed and cells were washed with PBS. 50 µg/well MTT solution in PBS was added to the wells and incubated for 4hrs. Precipitated formazan crystals were dissolved with 100µl DMSO. Absorbance was read at 540 nm (Bio-Tek Instruments Inc). The percentage of cell viability was calculated as

Viability% = A exp−A bl/A con−A bl*100 where A exp is the absorbance of the experimental group, A bl is the absorbance of the blank group, and A con is the absorbance of the control group.

2.4.2 Assessment of plasma membrane integrity by lactate dehydrogenase assay (LDH): LDH assay helps in plasma membrane integrity assessment by evaluating released Lactate dehydrogenase. In brief, 1 × 10^4 cells were seeded into each well of a 96 well plate. Cells were treated with different concentrations of DEP (1, 10 20, 40, 80,160,320 µgm/ml)) for 24 h. One set of cells treated with complete lysis solution for 45mins served as cell control for maximum LDH release. 50µl of culture supernatant from all wells were transferred to a new 96 well plate. 50 µl of enzyme-substrate solution was added to each well and incubated for 30 mins. LDH was assessed using Promega cytotox96 ®non-radioactive kit. Stop Solution was added, and the absorbance signals were measured at 490nm.

2.4.3 Lysosomal integrity by Neutral red uptake assay: Neutral red assay measures the lysosome integrity based on the vital dye Neutral red uptake by live cells. Borenfreund and Puerner [7] originally developed this simple and accurate method. Cells were seeded in a 96 well plate with a density of 1 × 10^4cells/well and incubated at 37^0 C overnight. Meanwhile, 1% neutral red reagent was also prepared and incubated separately at 37^0 C overnight. Next day, A549 cells were treated with different concentration of DEP 1, 10, 20, 40,80,160,320 µgm/ml for 24h. After treatment, 10 µl of 1% neutral red was added to each well and incubated for 3 h at 37◦C with 5% CO_2. At the end of the incubation period, dye was removed and the wells were washed with PBS. The dye entrapped inside the cell was solubilized using acid alcohol desorbing agent (1% glacial acetic acid and 90% ethanol, and V/V) and the plates were incubated in dark for 30 min. Absorbance was read spectrophotometrically at 540 nm in a microplate reader.

2.5 Assessment of mechanism of cytotoxicity

2.5.1 Intracellular reactive oxygen species (ROS) generation assessment by DCFH-DA: The production of intracellular ROS was determined by DCFH-DA (Dichloro dihydro fluorescein diacetate), a fluorometric probe that passively enters the cell. The resultant compound dichlorofluorescein (DCF) formed from reaction with intracellular ROS is highly fluorescent. For the assay, cells were seeded at a density of 1× 10^4 cells/well and cultured for 24 h. Cells were exposed to different concentration of DEP (1, 10 20, 40, 80,160,320 µgm/ml) and ROS was assessed after 3hrs and 24hrs. 0.09% hydrogen peroxide (H_2O_2) treated cells were used as the positive control (pc). Untreated cells served as negative control. After treatment, cells were washed with PBS and incubated with 100 µl of DCFH-DA (1µM) for 45 min in dark and excess DCFH-DA was removed and replaced with 200µl PBS. Fluorescence was measured using a microplate reader (Synergy Biotek) with excitation and emission at wavelength 485 and 535 nm, respectively.

2.6 Statistical analysis

Graph pad prism 6 and MS Excel was used for statistical analysis. All experiments were done three times (n=5). The results of each assay are expressed as mean ± standard deviation. Differences between

groups were assessed by one-way ANOVA; Statistical significance was accepted at $p < 0.05$ or 0.001.

3. Results

3.1 Characterization of DEP

The DEP was suspended in distilled water, sonicated for 25mins and analyzed by Transmission electron microscope. TEM analysis showed the morphology of collected DEP to be of diffused spheres having average nanoparticle size of 30±4nm (Figure 2).

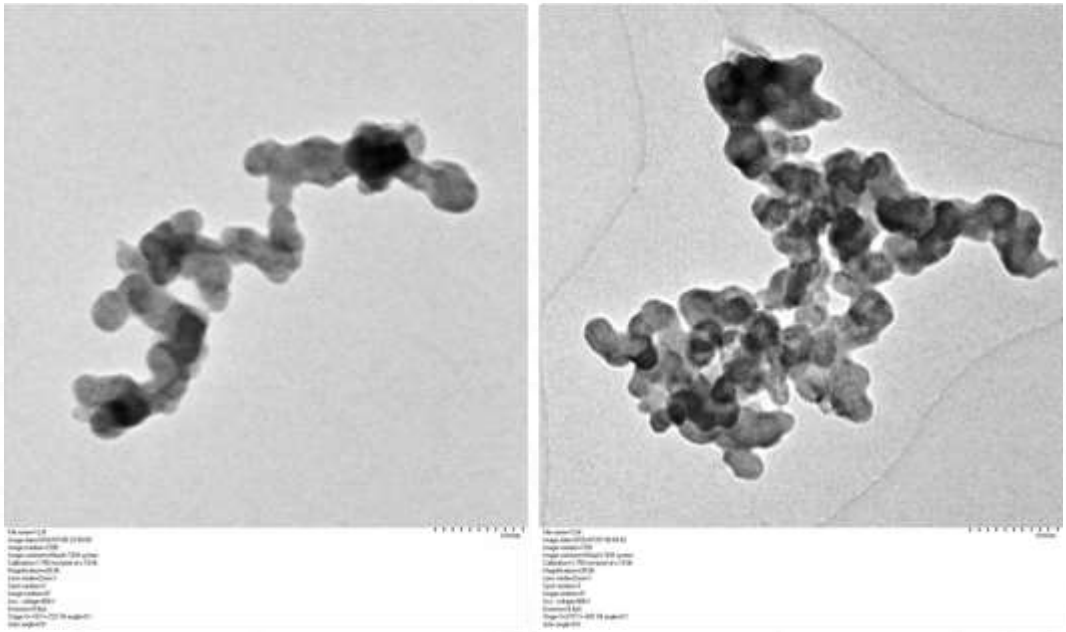

Figure 2: Transmission electron micrographs of the DEP collected from diesel engine showed the morphology of the particle to be diffused spheres.

3.2 Diesel exhaust nanoparticles reduce alveolar epithelial barrier integrity

ECIS was used to study the changes in epithelial morphology on challenge with varying concentrations of DEP by sensing the variations in impedance/resistance offered by A549 monolayer to an AC at 4000Hz. ECIS, the non-invasive biophysical approach showed a drop in impedance on exposure to DEP in a dose-dependent manner (Figure 3).

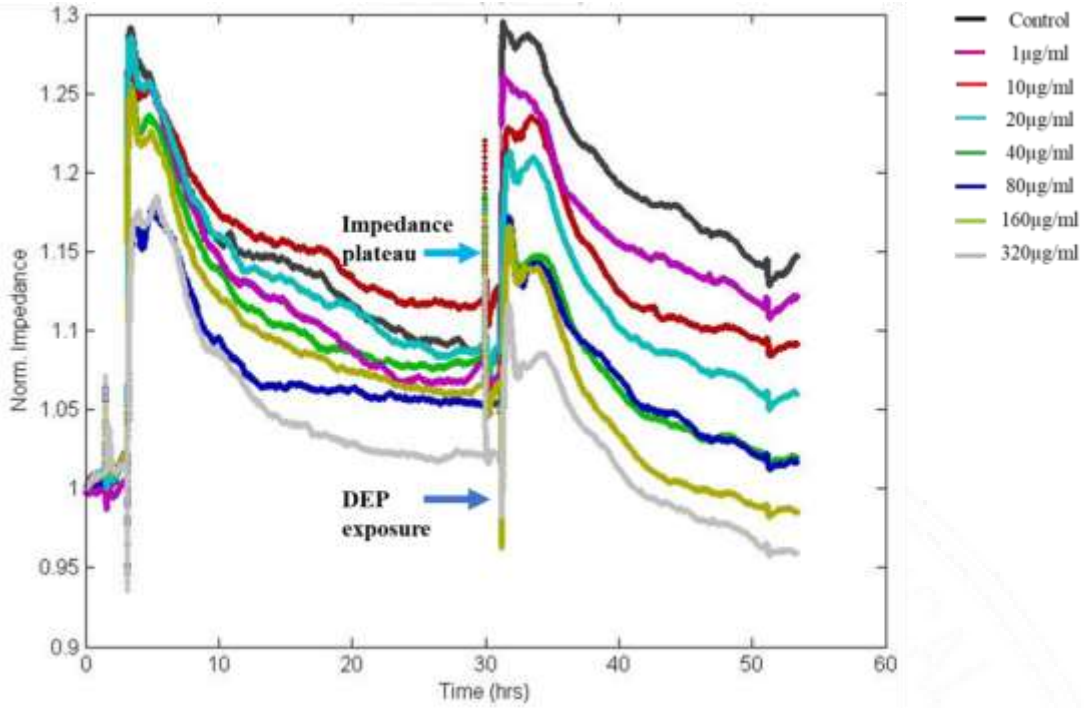

Figure 3: The Normalized impedance v/s time graph of ECIS shows a drop in resistance on exposure to DEP, which was dose-dependent. Impedance after 24hrs of DEP exposure showed values nearly equivalent to initial seeding indicating loss of cell-cell adhesion via intercellular junctional proteins and disruption of the monolayer with loss of barrier integrity at high doses. Colour palettes represent the doses of exposure.

In this study, fluctuations in the electrical properties of cell-covered microelectrodes reflected dynamic changes in cell morphology resulting from disrupted cell monolayers following exposure to DEP. The resistance value reached as low as initial seeding resistance 950Ω for the highest dose of DEP after 24hrs of exposure whereas the resistance of untreated control wells reached more than 1200Ω. Decreased resistance to current flow indicates loss of cell-cell adhesion via intercellular junctional proteins and the disruption of the monolayer with loss of barrier integrity. The impedance was converted into its components, resistance (Figure 4) and capacitance (Figure 5). We observed dose and time-dependent reduction in barrier integrity post-exposure.

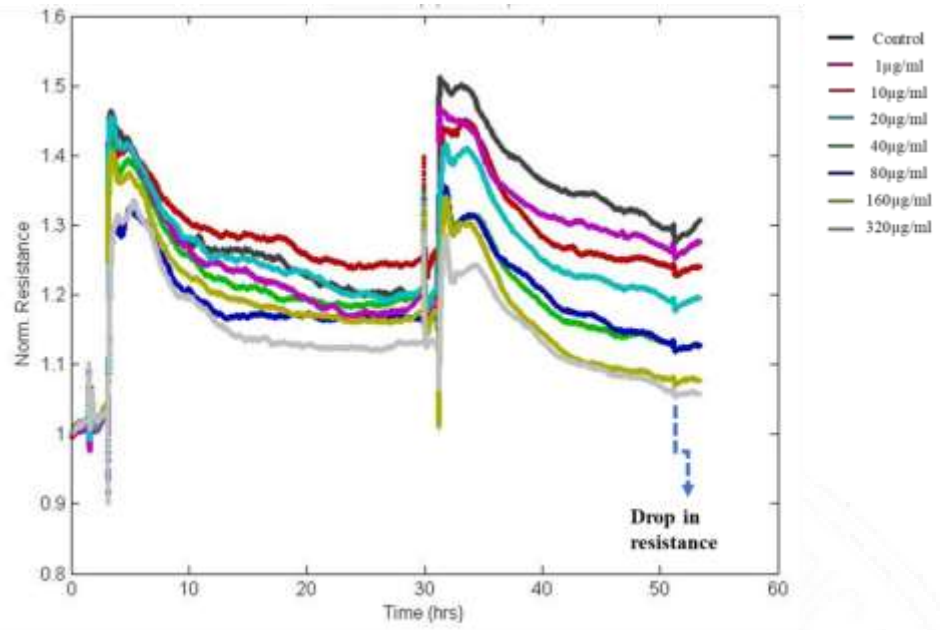

Figure 4: The Normalized resistance of DEP exposed A549 cells. Resistance is decreasing in a dose and time-dependent manner after the exposure to DEP indicating a reduction in resistance to current flow through the junctions.

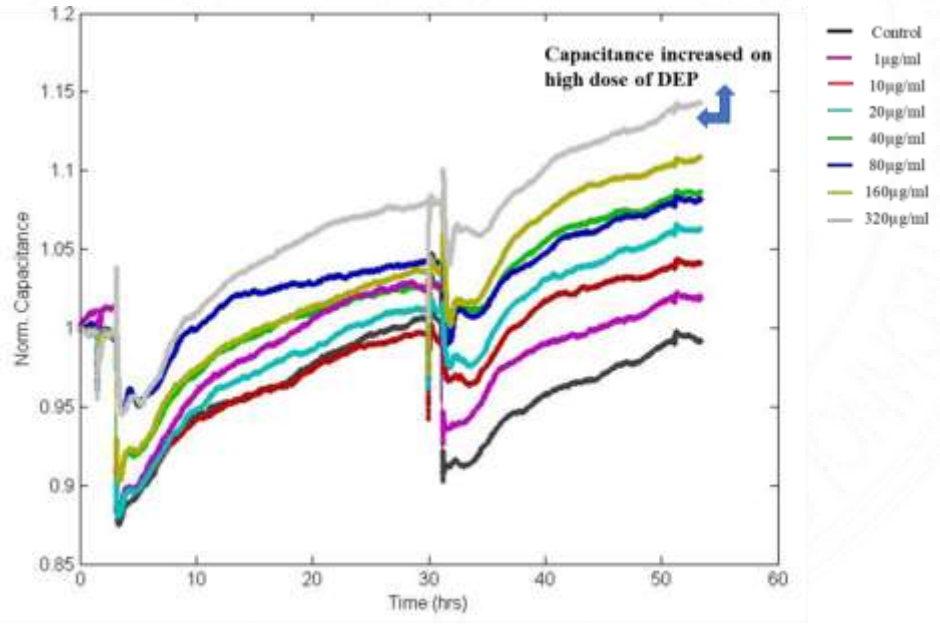

Figure 5: Shows Normalized Capacitance to DEP exposed A549 cells. Capacitance is increasing in a dose and time-dependent manner after the exposure DEP.

3.3 Classical cytotoxicity analyses

3.3.1 Exposure to DEP induced a dose-dependent reduction in cell viability: The viability of A549 was measured by MTT assay after exposure to different concentrations of DEP for 24hrs (Figure 6a). A dose-dependent reduction in viability was observed after exposure. The lowest concentration of 1 µg/ml was not cytotoxic. More than 50% loss of viability was observed when cells were exposed to 40 µg/ml DEP. 23.05% viability was observed in the highest dose (320µg/ml) exposure.

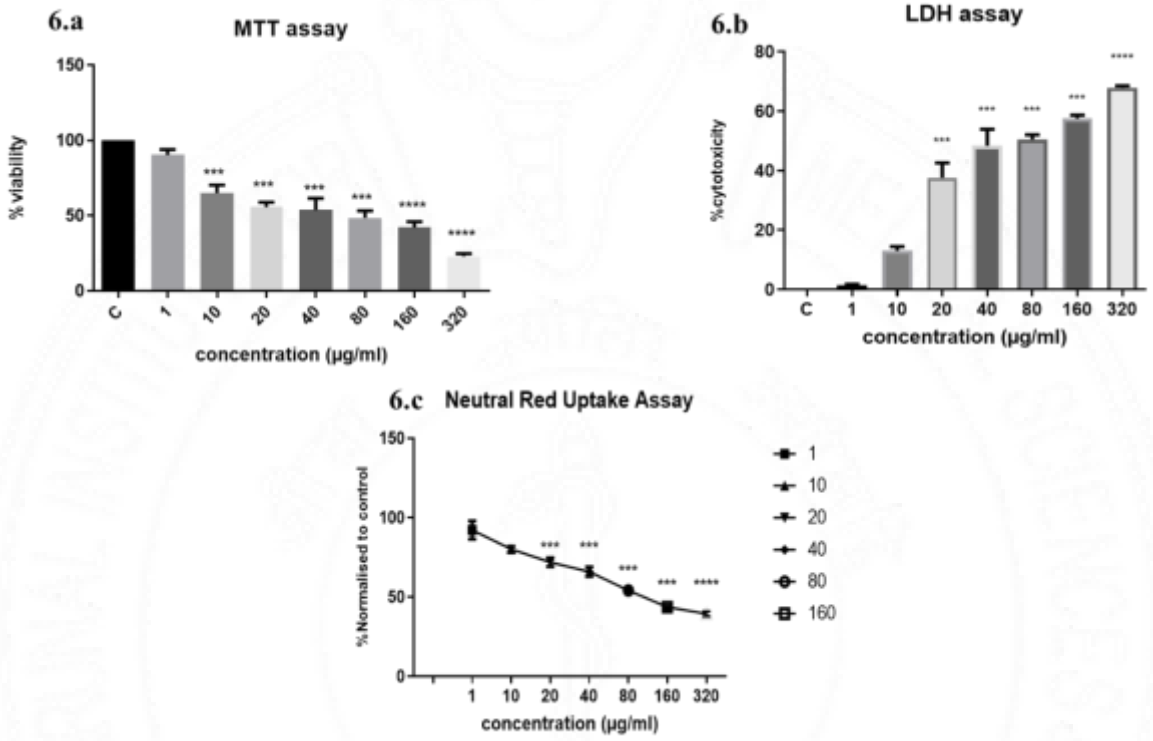

Figure 6: Classic endpoint cytotoxicity analyses. (6a) MTT assay of A549 cells exposed to DEP implied a dose-dependent increase in cytotoxicity; (6b) LDH cytotoxicity assay on DEP exposure. The substrate to LDH enzyme was added to culture media of A549 grown in 96 well plates after exposure to DEP. Complete lysis of A549 cells with lysis solution provided max. LDH released to the supernatant. Percentage cytotoxicity was calculated as a ratio of experimental absorbance/ Max. LDH release x 100; (6c) Neutral Red retention in DEP exposed cells. At the higher concentrations which proved to be cytotoxic, lysosome integrity was affected and less than 30% of cells were retaining the dye. The results are expressed as the mean ±SD of 3 independent experiments. ***p<0.001, ****p<0.0001 were found to be significant. Control wells were not treated with DEP.

3.3.2 Higher concentrations of DEP reduced the plasma membrane integrity: Lactate dehydrogenase is a stable cytosolic enzyme released into the culture medium only on the damage of the plasma membrane.

In the presence of diaphorase enzyme, released LDH from damaged cells could be measured by supplying lactate, NAD+ and **INT** as substrates. The generation of a red formazan product is proportional to the amount of LDH released and thereby the number of lysed cells. We observed a significant increase in LDH release at doses of 40 ug and above of DEP. Loss of plasma membrane integrity is indicative of cell death. At 20µg/ml concentration 40% cytotoxicity was observed and more than 50% cytotoxicity was observed above 40ug doses indicating that increasing concentrations were increasingly cytotoxic (Figure 6b).

3.3.3 DEP exposure induces lysosomal disruption in alveolar epithelial cells: The neutral red uptake assay uses the weak cationic dye neutral red (3-amino-7-dimethylamino-2-methylphenazine hydrochloride), which is preferentially absorbed into lysosomes. Intact lysosomal processes are only maintained in viable cells, so the degree of reduction of viability on a challenge with the test compounds indicates the toxicity of the test substance. The retention of the dye was found to be dose-dependent (Figure 6c). At higher concentrations, DEP is cytotoxic and causes lysosomal destabilization.

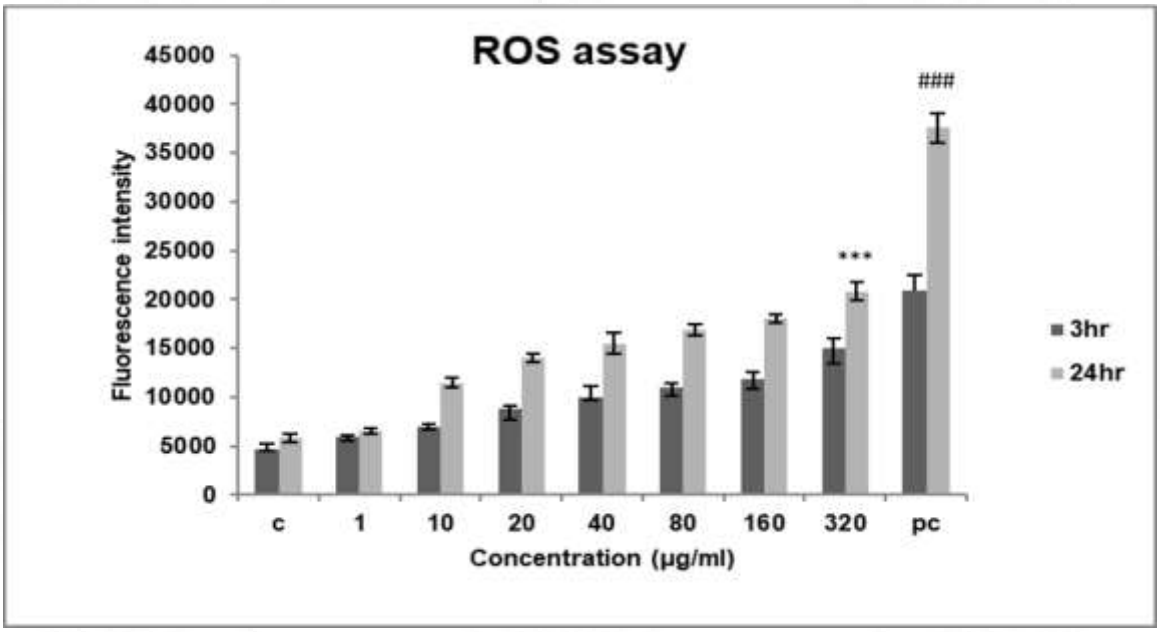

Figure 7: Represents ROS measurement of A549 cells exposed to DEP at varying concentrations and time points. The assay showed an increase in ROS production in a dose and time-dependent manner. The results are expressed as the mean ±SD of 3 independent experiments. ***p<0.001 against control,(###p<0.001 against 3hr)found to be significant.

3.4 DEP induces ROS production in alveolar epithelial cells

To determine the mechanism of cytotoxicity of DEP we assessed intracellular ROS production in A549 cells with a fluorescence probe DCFHDA. Since ROS production is an early response to any cellular insult, we assessed ROS production at two different time points 3hrs and 24hrs.

After exposure to DEP, we found that ROS production increased in a dose and time-dependent manner (Figure 7) in each group. The fluorescent intensity increased by nearly 20000**RFU** after 24hrs at high concentrations of exposure to DEP.

4. Discussion

We have utilized the real-time, non – destructive label-free ECIS method to understand cellular behaviour to external stimuli or injury. Here the epithelial barrier integrity was assessed on DEP exposure. Epithelial cells form monolayers with tight junctional proteins forming an intact barrier to prevent agents from entering circulation. Our study demonstrates that exposure to DEP can reduce the epithelial barrier integrity in a dose-dependent manner. The label-free, continuous measurements obtained in real-time with the Electrical cell-substrate Impedance Sensing (ECIS), outranks traditional label-based methods for cellular assays. The ECIS system is a convenient, rapid, and highly sensitive tool to non-destructively monitor cellular behaviour by analyzing the cell-substrate impedance, which is determined by cellular morphology and distribution on the sensing electrode [8]. The method can be effectively utilized for studies evaluating the effect of particles in barrier integrity and is an effective tool for high throughput toxicity assays. The advantage of this technique is the frequent and repeated measurements of electrical resistance, allowing for the assessment of rapid changes in barrier function. A stimulus that induces rapid disruption followed by recovery may be missed using methods that use a single time point assessment which rely on transcellular passage of molecules like dextrans that can be detected at discrete time points. On the other hand using ECIS method, the electrical resistance is a continuous variable measured in real-time simultaneously along with the stimuli and allows for more precise quantification of barrier disruption [9]. The cytotoxic effects of superparamagnetic iron oxide nanoparticles (SPION) on endothelial cells was investigated using ECIS [10]. Despite the active use of SPION in biomedicine and MRI diagnostics due to its low cytotoxicity, ECIS analysis demonstrated a decrease in cell impedance depending on the concentration of nanoparticles used for treatment, resulting in adverse effects on endothelial integrity, a fact that could be used in defining safe strategies or protocols for clinical application. Likewise, even the slightest morphological variation in adherent cells could be assessed in terms of change in resistance by ECIS. We observed a dose-dependent drop in resistance measurements and the values even reached the range of initial seeding i.e complete absence of adherent cells on exposure at a high dose. This implied a loss in barrier integrity upon DEP exposure at high doses.

Caraballo et al demonstrated that DEP induced transepithelial conductance, loosening of tight junction in alveolar epithelial cells [11]. Lehman et al., also observed disruption of occludin arrangement in epithelial cells when exposed to the high dose of

DEP (125 µg/ml) [12]. These findings suggested that DEP can induce structural changes [13] but they have used standard reference material (NIST) for exposure, which they considered as a surrogate for fresh DEP. Also, they have utilized FITC-Dextran labelling and ERS milli cell volt-ohmmeter to study barrier integrity which has all the limitations mentioned earlier.

We compared our results with classic endpoint cytotoxicity methods like MTT and LDH. The endpoint results were comparable but these results take longer to manifest whereas in ECIS cytotoxicity could be estimated in real time and early on. Lysosomes formally considered as cellular incinerators have now emerged as critical sites for plasma membrane repair, signaling and energy metabolism [14]. Lysosomes also participate in the digestion of endocytosed and autophagocytosed material and are involved in maintaining intracellular Ca2+ homeostasis [15]. Nanomaterials entering the endo-lysosomal system can lead to dysfunction of lysosomes which in turn leads to several diseases [16, 17]. Previous studies with TiO2 reported lysosomal destabilization as a cytotoxicity mechanism in human bronchial epithelial cells and murine fibroblast cells [18, 19]. Our results also show that DEP induces loss of lysosomal integrity and the destabilization is dose-dependent, as indicated by the Neutral red uptake (NRU) assay results. The NRU assay relies upon the weakly cationic vital dye neutral red (NR) uptake, which accumulates in the lysosomes and endosomes of living cells, but not in dead or dying cells, by non-ionic passive diffusion [20, 21]. The quantity of dye retention by the cells is assumed to be proportional to the total number of viable cells present [22]. We observed a dose-dependent reduction in dye retention indicative of loss of lysosome integrity and its destabilization. Cudazzo et al., reported a reduction in NRU as an indication of the lysosomotropic potential of E-cigarettes [23]. They reported nicotine-induced changes in the acidic compartments of multiple mammalian cell lines. Our observations also point to a reduction in dye retention which could be attributed to changes in the acidic compartments. A previous study had indicated that the disruption of epithelial tight junctions and the resulting loss of barrier function play a crucial role in the pathogenesis of a variety of gastrointestinal, hepatic, pulmonary, kidney and ocular diseases, so it is imperative that the barrier function be analysed in real-time to get a realistic idea of cytotoxicity.

We assessed the possible mechanism of cytotoxicity induction also. Increased ROS production disrupts the epithelial and endothelial barrier function by destabilizing tight junctions [24]. The delicate balance between the rate and amount of ROS production and the rate of oxidant elimination maintains normal cellular homeostasis. When the production of ROS overwhelms the cellular antioxidant capacity, the result will be “Oxidative stress”. ROS are generally cleared from the cell by the action of catalase, superoxide dismutase (SOD) or glutathione (GSH) peroxidase. Overproduction of ROS damages cells by altering macromolecules such as polyunsaturated fatty acids in membrane lipids, protein denaturation, and ultimately DNA. Oxidative stress, induced by various reactive oxygen species such as hydrogen peroxide, nitric oxide, peroxynitrite and hypochlorous acid is known to disrupt epithelial and endothelial tight junctions. The mechanisms involved in the oxidative

stress-induced disruption of tight junction include protein modification such as thiol oxidation, phosphorylation, nitration and carbonylation. In our study we assessed ROS production in line with the increased cytotoxic responses and observed a dose and time-dependent increase in ROS production.

5. Conclusion

The present study illustrates that Diesel exhaust nanoparticles collected directly from vehicle emission induce loss of barrier integrity and cytotoxicity in a dose-dependent manner. The likely mechanism of DEP mediated cytotoxicity could be the formation of intracellular ROS and changes in acidic compartments of lysosomes.

Our study clearly shows that ECIS will be a simple, high throughput, valuable tool in understanding the effects of external stimuli on cell monolayers vis-à-vis labour-intensive endpoint analyses, proving to be an easy tool for cytotoxicity assays. It is to be noted that ECIS provided more sensitive results compared to other assays.

Acknowledgement

The authors thank Director SCTIMST & Head BMT wing for providing infrastructure to carry out the study, DST INSPIRE for fellowship and DBT for funding part of the project.

Conflict of Interest

The authors declare that they have no conflict of interest and no affiliation with or involvement in any organization or entity with any financial interest related to this study.

References

1. Giaever I, Keese CR. Monitoring fibroblast behavior in tissue culture with an applied electric field. Proc Natl Acad Sci USA (1984) : 3761-3764.
2. Gauderman WJ, et al. Childhood asthma and exposure to traffic and nitrogen dioxide. Epidemiology (2005): 737-43.
3. Laden F, et al. Reduction in fine particulate air pollution and mortality: extended follow-up of the Harvard six cities study. Am J Respir Crit Care Med (2006): 667-72.
4. Wichmann HE. Diesel exhaust particles. Inhal Toxicol 19 (2007): 241-244.
5. Szulcek R, Bogaard HJ, van Nieuw Amerongen GP. Electric cell-substrate impedance sensing for the quantification of endothelial proliferation, barrier function, and motility. J Vis Exp 28 (2014): 51300.
6. Borenfreund E, Puerner JA. Toxicity determined in vitro by morphological alterations and neutral red absorption. Toxicol Lett (1985): 119-124.
7. Ngoc Le HT, Kim J, Park J, et al. A Review of Electrical Impedance Characterization of Cells for Label-Free and Real-Time Assays. BioChip J (2019): 295-305.
8. Suresh K, Servinsky L, Johnston L, et al. Comparison of polynomial fitting versus single time point analysis of ECIS data for barrier assessment. Physiological reports 9 (2021): e14983.
9. Astanina, Ksenia, Simon, et al. Superparamagnetic iron oxide nanoparticles impair endothelial integrity and inhibit nitric

oxide production. Acta Biomaterialia (2014): 4896-4911.

10. Caraballo JC, Ishii C, Westphal W, et al. Ambient particulate matter affects occludin distribution and increases alveolar transepithelial electrical conductance. Respirology (2011): 340-349.
11. Lehmann AD, Blank F, Baum O, et al. Rothen-Rutishauser: Diesel exhaust particles modulate the tight junction protein occludin in lung cells in vitro. Particle and Fibre Toxicology 6 (2009).
12. Schwarze PE, Totlandsdal AI, Låg M, et al. Inflammation-related effects of diesel engine exhaust particles: studies on lung cells in vitro. Biomed Res Int (2013): 685142.
13. Settembre C, Fraldi A, Medina DL, et al. Signals from the lysosome: a control centre for cellular clearance and energy metabolism. Nat Rev Mol Cell Biol (2013): 283-296.
14. Brini M, Calì T, Ottolini D, et al. Intracellular calcium homeostasis and signaling. In Metallomics and the Cell; Springer (2013): 119-168.
15. Platt FM, Boland B, vander Spoel AC. Lysosomal storage disorders: The cellular impact of lysosomal dysfunction. J. Cell Biol (2012): 723-734.
16. Kong H, Xia K, Pan L, et al. Autophagy and lysosomal dysfunction: A new insight into mechanism of synergistic pulmonary toxicity of carbon black-metal ions co-exposure. Carbon (2017): 322-333.
17. Jin C, Zhu B, Wang X, et al. Cytotoxicity of Titanium Dioxide Nanoparticles in Mouse Fibroblast Cells Cytotoxicity of Titanium Dioxide Nanoparticles in Mouse Fibroblast. Chem. Res. Toxicol (2008): 1871-1877.
18. Hussain S, Thomassen LCJ, Ferecatu I, et al. Carbon black and titanium dioxide nanoparticles elicit distinct apoptotic pathways in bronchial epithelial cells. Part. Fibre Toxicol (2010): 1-17.
19. Winckler J. Vitalfärbung von Lysosomen und anderen Zellorganellen der Ratte mit Neutralrot [Vital staining of lysosomes and other cell organelles of the rat with neutral red (author's transl)]. Prog Histochem Cytochem 6 (1974): 1-91.
20. Filman DJ, Brawn RJ, Dandliker WB. Intracellular supravital stain delocalization as an assay for antibody-dependent complement-mediated cell damage, Journal of Immunological Methods (1975): 189-207.
21. Repetto G, del Peso A, Zurita J. Neutral red uptake assay for the estimation of cell viability/cytotoxicity. Nat Protoc 3 (2008): 1125-1131.
22. Cudazzo, Gianluca, Smart, et al. Lysosomotropic-related limitations of the BALB/c 3T3 cell-based neutral red uptake assay and an alternative testing approach for assessing e-liquid cytotoxicity. Toxicology inVitro (2019): 104647.
23. Radhakrishna Rao Oxidative stress-induced disruption of epithelial and endothelial tight junction Frontiers in Bioscience (2008): 7210-7226

24. Hellawell B, Gutteridge JMC. Free radicals in biology and medicine. Oxford: Oxford Univ Pr (1999).